

140723

# INVESTIGATION OF DYNAMIC BEHAVIOR OF TETHERED BALLOON SYSTEMS

Jerome J. Vorachek  
James W. Burlick  
George R. Doyle, Jr.

Goodyear Aerospace Corporation  
Akron, Ohio 44315

Contract No. F19623-71-C-4021

Project No. 1639

Task No. 765906

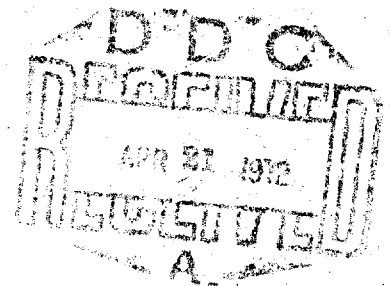
Work Unit No. 76590601

Final Report

1 January 1971 through 31 January 1972

Contract Monitor: Don E. Jackson, Capt., USAF  
Aerospace Instrumentation Laboratory

Approved for public release; distribution unlimited



Best Available Copy

Prepared for

Produced by  
NATIONAL TECHNICAL  
INFORMATION SERVICE  
Springfield, Va. 22161

AIR FORCE CAMBRIDGE RESEARCH LABORATORIES  
AIR FORCE SYSTEMS COMMAND  
UNITED STATES AIR FORCE  
WETMORE, MASSACHUSETTS 01730

**Best  
Available  
Copy**

NAME	UNIT NUMBER
AGE	BOY NUMBER
ADDRESS	
TELEPHONE	
PARENTS' SIGNATURE	
DATE	

Qualified requesters may obtain additional copies from the Defense Documentation Center. All others should apply to the National Technical Information Service.

Best Available Copy

Unclassified

Security Classification

## DOCUMENT CONTROL DATA - R &amp; D

(Security classification of title, body of abstract and indexing annotation must be entered when the overall report is classified)

1. ORIGINATING ACTIVITY (Corporate author) <b>Goodyear Aerospace Corporation 1210 Massillon Road Akron, Ohio 44315</b>		2a. REPORT SECURITY CLASSIFICATION <b>Unclassified</b>	
		2b. GROUP	
3. REPORT TITLE  <b>INVESTIGATION OF DYNAMIC BEHAVIOR OF TETHERED BALLOON SYSTEMS</b>			
4. DESCRIPTIVE NOTES (Type of report and inclusive dates) <b>Scientific. Final. 1 January 1971 through 31 January 1972</b> <b>Approved 29 Feb. 1972</b>			
5. AUTHOR(S) (First name, middle initial, last name) <b>Jerome J. Vorachek James W. Burbick George R. Doyle Jr.</b>			
6. REPORT DATE <b>31 January, 1972</b>		7a. TOTAL NO. OF PAGES <b>164</b>	7b. NO. OF REFS <b>4</b>
8a. CONTRACT OR GRANT NO <b>F-49268-71-C-0091</b>		9a. ORIGINATOR'S REPORT NUMBER(S) <b>GER-15325 15497</b> <b>AFCRL-72-0113</b>	
b. <b>19028</b> <b>7659-06-01</b>		9b. OTHER REPORT NO(S) (Any other numbers that may be assigned this report)	
c. DoD Element: <b>62101F</b>			
d. DoD Subelement: <b>687659</b>			
10. DISTRIBUTION STATEMENT <b>A - Approved for public release; distribution unlimited</b>			
11. SUPPLEMENTARY NOTES <b>TECH OTHER</b>		12. SPONSORING MILITARY ACTIVITY <b>Air Force Cambridge Research Laboratories(LC) L. G. Hanscom Field Bedford, Massachusetts 01730</b>	
13. ABSTRACT <p>An analytical investigation of the dynamic behavior of tethered balloons was conducted. This report covers definition of tethered balloon systems and a study of stability characteristics and dynamic response to wind gusts of tethered balloon systems. Balloon systems which are investigated use the British BJ Barrage Balloon, the Vee Balloon and a Goodyear Aerospace Model No. 1649 Single-Hull Balloon. The major tether construction is Columbian Rope Company's NOLARO utilizing prestretched polyester filaments. Three design altitudes, 5,000, 10,000 and 20,000 feet, are considered.</p> <p>The model for the tethered balloon system consists of the streamlined balloon and a tether made up of three discrete links. The derivation of nonlinear equations of motion for this system in three dimensions is presented. The equations are linearized for stability analysis and treated as uncoupled in the longitudinal and lateral degrees of freedom. Characteristic equations which incorporate the physical, aerodynamic, and mass characteristics of the system are developed and solved for the roots which represent the frequency and damping qualities. The nonlinear equations of motion are programmed for solution on a digital computer.</p> <p>An exploratory investigation to establish the trends of dynamic characteristics for various design parameters is reported. Design parameters considered include balloon shape and altitude, trim angle of attack, vertical location of the bridle confluence point, net static lift, tail size, reduced wind profiles, varying altitude as encountered in launch and retrieval, payload location, and wind location above mean sea level.</p>			

DD FORM 1 NOV 65 1473

Unclassified

Security Classification

Unclassified

Security Classification

14	KEY WORDS	LINK A		LINK B		LINK C	
		ROLE	WT	ROLE	WT	ROLE	WT
	Aerostats						
	Balloons						
	Balloon Aerodynamics						
	Balloon Dynamics						
	Balloon Behavior						
	Balloon Flying Qualities						
	Balloon Mass Characteristics						
	Balloon Stability						
	Balloon Systems						
	Cables						
	Cable Dynamics						
	Captive Balloons						
	Dynamic Simulation Analysis						
	Kite Balloons						
	Stability Analysis						
	Tethered Balloons						
	Tethered LTA Vehicles						
	Tethers						

Unclassified

Security Classification

AFGL - 72 -0113

INVESTIGATION OF DYNAMIC BEHAVIOR  
OF TETHERED BALLOON SYSTEMS

Jerome J. Vorachek  
James W. Burbick  
George R. Doyle, Jr.

Goodyear Aerospace Corporation  
Akron, Ohio 44315

Contract No. F19628-71-C-0091

Project No. 7659

Task No. 765906

Work Unit No. 76590601

Final Report

1 January 1971 through 31 January 1972

Contract Monitor: Don E. Jackson, Capt., USAF  
Aerospace Instrumentation Laboratory

Approved for public release; distribution unlimited

Prepared for

AIR FORCE CAMBRIDGE RESEARCH LABORATORIES  
AIR FORCE SYSTEMS COMMAND  
UNITED STATES AIR FORCE  
BEDFORD, MASSACHUSETTS 01730

## ABSTRACT

An analytical investigation of the dynamic behavior of tethered balloons was conducted. This report covers definition of tethered balloon systems and a study of stability characteristics and dynamic response to wind gusts of tethered balloon systems. Balloon systems which are investigated use the British BJ Barrage Balloon, the Vee Balloon and a Goodyear Aerospace Model No. 1649 Single-Hull Balloon. The major tether construction is Columbian Rope Company's NOLARO utilizing prestretched polyester filaments. Three design altitudes, 5,000, 10,000 and 20,000 feet, are considered.

The model for the tethered balloon system consists of the streamlined balloon and a tether made up of three discrete links. The derivation of nonlinear equations of motion for this system in three dimensions is presented. The equations are linearized for stability analysis and treated as uncoupled in the longitudinal and lateral degrees of freedom. Characteristic equations which incorporate the physical, aerodynamic, and mass characteristics of the system are developed and solved for the roots which represent the frequency and damping qualities. The nonlinear equations of motion are programmed for solution on a digital computer.

An exploratory investigation to establish the trends of dynamic characteristics for various design parameters is reported. Design parameters considered include balloon shape and altitude, trim angle of attack, vertical location of the bridle confluence point, net static lift, tail size, reduced wind profiles, varying altitude as encountered in launch and retrieval, payload location, and wind location above mean sea level.

## FOREWORD

This research was supported by the Air Force Systems Command, USAF, DON, and was under the technical cognizance of the Air Force Cambridge Research Laboratories under Contract No. F 19628-71-C-0091.

The project is being carried out under the direction of Captain Don Jackson as Contract Monitor for the Air Force Cambridge Research Laboratories. Mr. Jerome Vorachek is the Goodyear Aerospace Corporation Project Engineer. Technical effort has been provided by Mr. George Doyle for derivation of the equations of motion and characteristic equations of the tethered balloon systems, programming of equations for solution of stability and dynamic response. Mr. James Burbick generated dynamic response data and evaluation of dynamic response results with the IBM 360 computer. Mr. William Ebert developed the aerodynamic characteristics for the balloon system, and mass characteristics were generated by Mr. Walt Stricker. Technical assistance was also provided by Mr. Philip Myers and Mr. Louis Handler.

The contractor's number for this report is GER-15497.

## TABLE OF CONTENTS

Section	Page
I INTRODUCTION . . . . .	1
II BALLOON DESCRIPTION. . . . .	3
III TECHNIQUES FOR STUDY OF DYNAMIC BEHAVIOR OF TETHERED BALLOONS. . . . .	7
1. Mathematical Models. . . . .	7
2. General Stability Theory . . . . .	9
3. Stability Analysis . . . . .	11
4. Dynamic Response Analysis. . . . .	12
IV DYNAMIC RESPONSE OF TETHERED BALLOONS. . . . .	15
1. Design Conditions Investigated . . . . .	15
2. General Discussion of Dynamic Response of Tethered Balloon Systems . . . . .	17
3. Effects of Design Parameters on Tethered Balloon Design . . . . .	29
V CONCLUSIONS AND RECOMMENDATIONS ON TETHERED BALLOON DYNAMIC BEHAVIOR . . . . .	44
1. Gust Effects on Nominal BJ Balloon . . . . .	44
2. Comparison of Balloon Types. . . . .	45
3. Influence of Trim Angle on Longitudinal and Lateral Dynamic Behavior . . . . .	45
4. Effect of Tail Size on Longitudinal and Lateral Dynamic Behavior . . . . .	46
5. Effect of Altitudes Intermediate to the Design Altitude on Behavior of the BJ Tethered Balloon System . . . . .	46
6. Effects of Reduced Wind on the Behavior of the BJ Tethered Balloon System . . . . .	47
7. Nolaro vs Amgai Tethers. . . . .	47
8. Effect of Payload Location . . . . .	47
9. Effect of Winch Altitude Location. . . . .	47
10. BJ Tethered Balloon Systems Designed for Various Altitudes. . . . .	48
REFERENCES . . . . .	49
APPENLICES	
A Equations of Motion for Dynamic Simulation . . .	A-1
B Dynamic Response Input and Output Data . . . .	B-1

# LIST OF FIGURES

Figure		Page
1	BJ Configuration. . . . .	4
2	Vee-Balloon Configuration . . . . .	4
3	GAC No. 1649 Balloon Configuration. . . . .	6
4	Balloon Tether Model in Longitudinal Plane. . . . .	7
5	Balloon Tether Model in Lateral Plane . . . . .	8
6	Balloon Geometry and Applied Forces . . . . .	9
7	Longitudinal Dynamics of Tethered Balloon - BJ Nominal	13
8	Longitudinal Dynamics of Tethered Balloon - BJ Nominal	13
9	Lateral Wind Gusts. . . . .	17
10	Lateral Stability Characteristics of Nominal BJ Tethered Balloon at 10,000 Feet Altitude. . . . .	20
11	Lateral Case 28, Coordinates Response . . . . .	21
12	Lateral Case 28, Power Spectral Density . . . . .	22
13	Longitudinal Stability Characteristics of Nominal BJ Tethered Balloon at 10,000 Feet Altitude. . . . .	25
14	Lateral Case 4, Coordinates Response. . . . .	26
15	Lateral Case 4, Power Spectral Density. . . . .	27

# LIST OF TABLES

Table		Page
I	Summary of Balloon/Cable Systems. . . . .	5
II	Summary of Cable Solutions. . . . .	6
III	A. Comparison of Longitudinal Dynamic Cases . . . . .	16
	B. Comparison of Lateral Dynamic Cases. . . . .	16
IV	Summary of Lateral Stability Case 1 . . . . .	19
V	Peak Amplitudes for Lateral Dynamics Case 28. . . . .	23
VI	Summary of Longitudinal Stability Case 1 (Reference 2) . . . . .	24
VII	Wind Gust Duration Effects on BJ Nominal Balloon in Longitudinal Plane. . . . .	29
VIII	Wind Gust Ramp Rise Time Effects on BJ Nominal Balloon in Lateral Plane . . . . .	30
IX	Effect of Increase in Gust Velocity on BJ Nominal Balloon in Lateral Plane. . . . .	31
X	Effect of Trim Angle of Attack on Longitudinal Response of Three Balloon Types . . . . .	32
XI	Effect of Lateral Wind Gusts on the Lateral Response of the Three Balloon Types. . . . .	32
XII	Longitudinal Response of BJ Balloon with Tail Size Variation . . . . .	34
XIII	Lateral Response of BJ and Vee Balloons with Tail Size Variation. . . . .	34
XIV	Effect of Intermediate Altitudes on Longitudinal Response of the BJ Balloon. . . . .	35
XV	Effect of Intermediate Altitudes on Lateral Response of the BJ Balloon . . . . .	35
XVI	Effect of Reducing Winds on Longitudinal and Lateral Response. . . . .	37
XVII	Effect of Nolaro and Amgal Tethers on Longitudinal Response. . . . .	38

Table		Page
XVIII	Effect of Nolaro and Amgal Tethers on Lateral Response	38
XIX	Effect of Payload Location on Longitudinal Response .	39
XX	Effect of Winch Altitude Location on Longitudinal Response. . . . .	39
XXI	Effect of Various Design Operational Altitudes. . . .	40
XXII	Structural Design Parameters. . . . .	41
XXIII	Instrumentation Design Parameters . . . . .	41
XXIV	Maximum Variations of Structural and Instrumentation Design Performance Parameters - Longitudinal Cases. .	42
XXV	Maximum Variations of Structural and Instrumentation Design Performance Parameters - Lateral Cases . . . .	43

## SECTION I

### INTRODUCTION

The objective of this program is to investigate the dynamic behavior of tethered balloons and in so doing to establish design criteria for tethered balloons, tethers and payloads. The program is organized into three steps:

- (1) Definition of balloon systems for dynamic analysis
- (2) A study of stability characteristics of tethered balloon systems
- (3) A study of dynamic response of tethered balloon systems to wind gusts

Reference 1 presents a definition of tethered balloon systems to be used for dynamic studies. These systems are summarized in this report. Reference 2 presents a development of the study of stability characteristics of the tethered balloon systems. This report presents further development of the equations of motion and solutions for the dynamic response of the tethered balloon system. Recommendations for the design of tethered balloon systems are presented in this report.

The system is defined as a balloon tethered at the end of a cable which is fixed to a stationary winch. The tether is represented by 3 straight links, each of the same length. The links are considered rigid and connected to each other by frictionless hinges. Goodyear Aerospace Corporation has employed this method of representation of the tethered system for other studies such as that described in Reference 3.

For design purposes in the subject investigation the following design parameters were specified by AFCRL.

#### Payload and Design Altitude

<u>Payload (lb)</u> P	<u>Float Altitude (ft above MSL)</u> h
1500	5,000
1000	10,000
600	20,000

#### Tethers

Two specific tether constructions are to be considered, NOLARO by Columbian Rope Company, and Amgal-Monitor AA wire rope by United States Steel.

A safety factor of 2.0 will be used with NOLARO; 1.5 for Amgal-Monitor. Tether design load will be based on a survival wind of 1.3 times the operational wind at balloon altitude.

#### Wind Profile

The wind profile as specified is tabulated below:

<u>Altitude</u> (ft above MSL)	<u>Operational</u> <u>Wind Speed</u> (knots)	<u>Survival</u> <u>Wind Speed</u> (knots)
Sea Level	10	13.
5,000	31	40.3
10,000	40	52.
20,000	54	70.2

## SECTION II

### BALLOON DESCRIPTION

The balloon systems evaluated in this stability investigation have been described in Reference 1. The three balloon types in these systems are the British BJ Balloon, the Vee-Balloon\* and the GAC No. 1649 Single Hull Balloon as depicted in Figures 1, 2, and 3. The nominal tethered systems characteristics defined in Reference 1 are summarized in Tables I and II.

Static and dynamic aerodynamic characteristics for the balloons have been determined from experimental data where available and by analytical techniques otherwise. The aerodynamic characteristics are presented and discussed in Reference 2 along with additional mass and suspension system geometries which were not included in Reference 1.

Design parameters varied in the stability investigation include the trim angle of attack, vertical location of the suspension system confluence point below the balloons, the free-static lift, and the tail size.

The trim angle of attack can be controlled by locating the confluence point of the suspension system. The location of this point is established by the two coordinates as shown in Figure 1. The fuselage station from the nose and the waterline below the centerline of the balloon defines this point. The trim angle of attack change as a function of bridle apex point location has been calculated and is given in Reference 2.

The free-static lift as used in this report is the excess buoyant lift provided by the balloon after the balloon physical weight and the weight of the tether in no wind is supported.

Nominal tail sizes for each balloon are depicted in Figures 1, 2, and 3. For the British BJ Balloon, tail size is increased and decreased about the nominal by changing the linear dimensions of each of the three tails and maintaining similar proportions. The intersection of the trailing edge of the tails and the hull is maintained at the same point for all tail sizes. For the Vee-Balloon the horizontal tail geometry is maintained. The vertical tails are increased in size in two steps for tails below the hulls. Also investigated are the conditions where vertical tails are located symmetrically above and below the hulls. In addition to establishing aerodynamic characteristics for these tail configurations as noted in Reference 2, the increase in physical mass and additional mass was computed and used in the determination of stability characteristics.

Ascent and descent studies for a specific balloon also incorporate the change in mass characteristics due to air density changes with altitude.

---

\* Trademark, Goodyear Aerospace Corporation, Akron, Ohio 44315

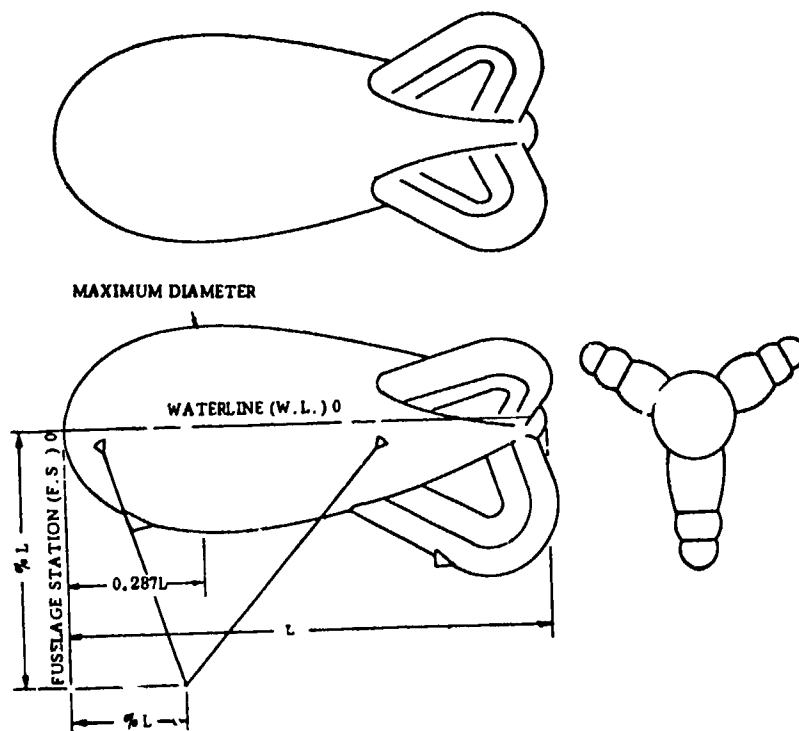


Figure 1. BJ Configuration

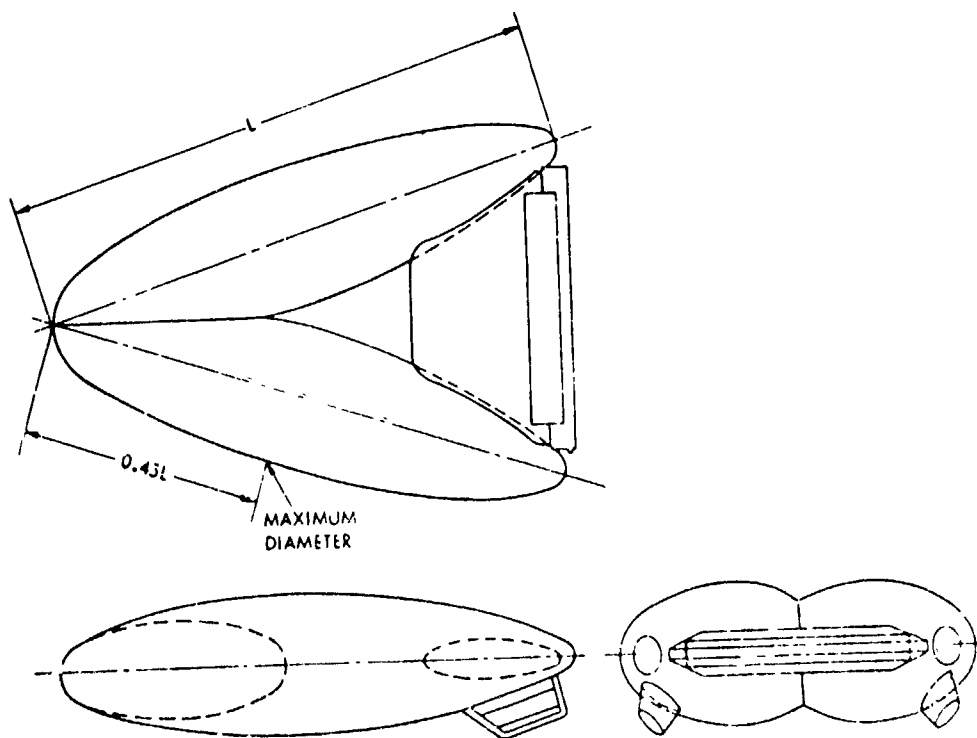


Figure 2. Vee-Balloon Configuration

Table I. Summary of Balloon/Cable Systems

Balloon Type	h	Ball Volume (ft <sup>3</sup> )	Gross Static Lift (lb)	W <sub>B1</sub> (lb)	P (lb)	L <sub>B</sub> (lb)	Survival				Operational				Tether *				
							$\alpha_{Trim}$	L <sub>a</sub> (lb)	D (lb)	L <sub>m</sub> (lb)	T (lb)	$\alpha_{Trim}$	L <sub>a</sub> (lb)	D (lb)	L <sub>m</sub> (lb)	T (lb)	Type	O.D. (in)	B.S. (lb)
BJ	5,000	46,000	2,534	635	1,500	399	8.7	1,391	656	1,790	1,906	7.0	659	351	1,058	1,115	MOLANO	0.321	3,813
	10,000	80,000 (85,263) <sup>1</sup>	4,029	1,541	1,000	1,488	5.7	6,427	2,422	7,916	8,278	6.9	4,437	1,514	9,925	6,116	MOLANO	0.585	16,600
Vee-Balloon		144,000 (153,654) <sup>1</sup>	7,253	2,712	1,000	3,541	5.7	9,509	3,583	13,050	13,533	6.9	6,564	2,239	10,105	10,350	ANGAL	7/16	20,000
	BJ	60,000	2,832	1,031	1,000	801	10.2	2,706	1,219	3,507	3,713	8.2	1,391	651	2,192	2,287	MOLANO	0.410	7,540
75,000		3,540	1,276	1,000	1,264	10.2	3,140	1,414	4,405	4,626	8.2	1,614	755	2,878	2,975	ANGAL	1/4	6,750	
#1649 w/ Thin Film	80,000	3,776	1,548	1,000	1,228	10.2	4,963	1,346	6,191	6,336	8.7	2,508	757	3,736	3,812	MOLANO	0.520	12,700	
	133,000	6,278	2,511	1,000	2,767	10.2	6,965	1,887	9,732	9,913	8.2	3,519	1,061	6,286	6,376	ANGAL	3/8	14,800	
BJ	20,000	500,000	17,737	8,933	600	7,504	8.7	15,420	6,785	22,924	23,907	7.0	7,571	3,577	15,075	15,494	MOLANO	0.993	47,814

W<sub>B1</sub> Total balloon and suspension weight (no gas, payload or tether)

L<sub>S1</sub> Net static lift (Gross static lift - W<sub>B1</sub>)

\* See Table II for detail cable description

\*\* Trim angle of attack  $\alpha_{TRIM}$  is as defined by Table VI of Reference 1

Table II. Summary of Cable Solutions

Balloon Type	Altitude (ft)	Hull Volume (ft <sup>3</sup> )	Tether Type	B.S. (lb)	O.D. (ft)	Wt/Ft (lb/ft)	X (ft)	θ (deg)	T (lb)	Length (ft)	Total Tether Weight (lb)
BJ h = 5,000 ft P = 1,500 lb	5,000	46,000	NOLARO	3,813	0.02679	0.03211	0	161.6	1,115	0	--
	S.L.						2,672	144.2	956	,692	183
Vee-Balloon h = 10,000 ft P = 1,000 lb	10,000	80,000	NOLARO	16,600	0.04875	0.11400	0	165.7	6,115	0	--
	5,000						1,775	154.7	5,552	5,314	606
	S.L.	144,000	AMGAL	20,000	0.03642	0.30400	4,594	146.6	4,991	11,060	1,260
	10,000						0	157.5	10,350	0	--
BJ h = 10,000 ft P = 1,000 lb	5,000	75,000	AMGAL	6,750	0.02083	0.09970	1,389	160.8	8,836	5,193	1,280
	S.L.						3,452	153.9	7,300	10,605	3,230
	10,000	60,000	NOLARO	7,540	0.03420	0.05600	0	163.4	2,287	0	--
	5,000						2,456	143.6	2,036	5,600	374
#1649 w/Thin Fins h = 10,000 ft P = 1,000 lb	S.L.	133,000	AMGAL	14,800	0.03125	0.22000	7,377	127.7	1,761	12,639	708
	10,000						0	165.3	2,975	0	--
	5,000	80,000	NOLARO	12,700	0.04330	0.0900	1,843	153.2	2,482	5,340	532
	S.L.						5,072	140.3	1,989	11,305	1,128
BJ h = 20,000 ft P = 600 lb	10,000	500,000	NOLARO	47,814	0.08281	0.32427	0	168.5	3,812	0	--
	5,000						1,702	153.0	3,374	5,298	476
	S.L.	133,000	AMGAL	14,800	0.03125	0.22000	4,950	141.1	2,930	11,274	1,015
	10,000						0	170.4	6,375	0	--
BJ h = 20,000 ft P = 600 lb	5,000	500,000	NOLARO	47,814	0.08281	0.32427	1,193	161.8	5,281	5,145	1,132
	S.L.						3,275	152.7	4,187	10,559	2,325
	20,000	500,000	NOLARO	47,814	0.08281	0.32427	0	166.7	15,494	0	--
	15,000						1,646	155.9	13,897	5,272	1,710
BJ h = 20,000 ft P = 600 lb	10,000	500,000	NOLARO	47,814	0.08281	0.32427	4,495	143.7	12,171	11,039	3,580
	5,000						9,106	130.2	10,702	17,856	5,790
	S.L.						17,231	112.0	9,107	27,436	8,900

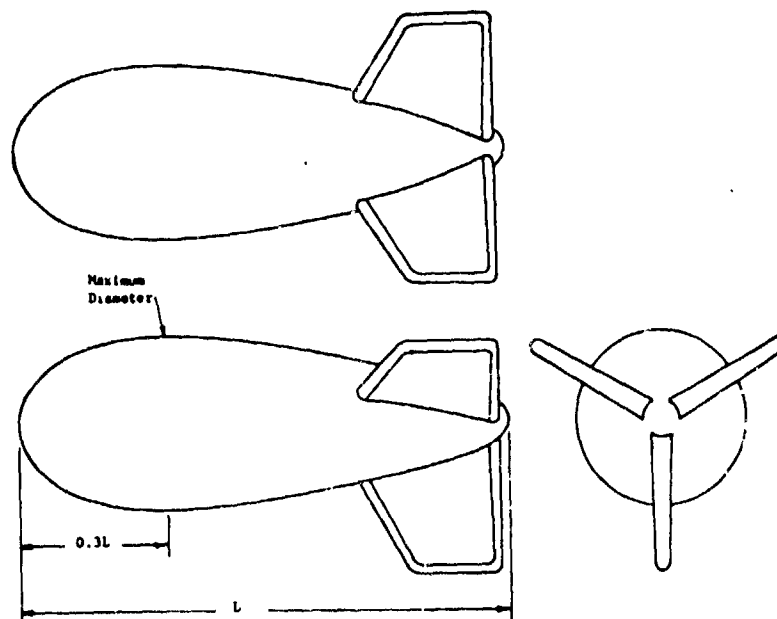


Figure 3. GAC No. 1649 Balloon Configuration

### SECTION III

#### TECHNIQUES FOR STUDY OF DYNAMIC BEHAVIOR OF TETHERED BALLOONS

##### 1. MATHEMATICAL MODELS

A system of differential equations was developed (Reference 2 and Appendix A of this report) that describes the motion of the tethered balloon in three dimensions. The degrees of freedom associated with the motion are yaw, pitch and roll of the balloon about its dynamic mass center, and pitch and yaw (lateral rotation) of the tether. There are a total of  $3 + 2N$  degrees of freedom where  $N$  is the number of links used to simulate the tether.

First consider the longitudinal degrees of freedom. The dependent variables shown in Figure 4 are  $\theta$  (pitch of the balloon) and  $\zeta_r$  (pitch of the "r"th link), where  $r$  is a particular link. All angles are shown positive.

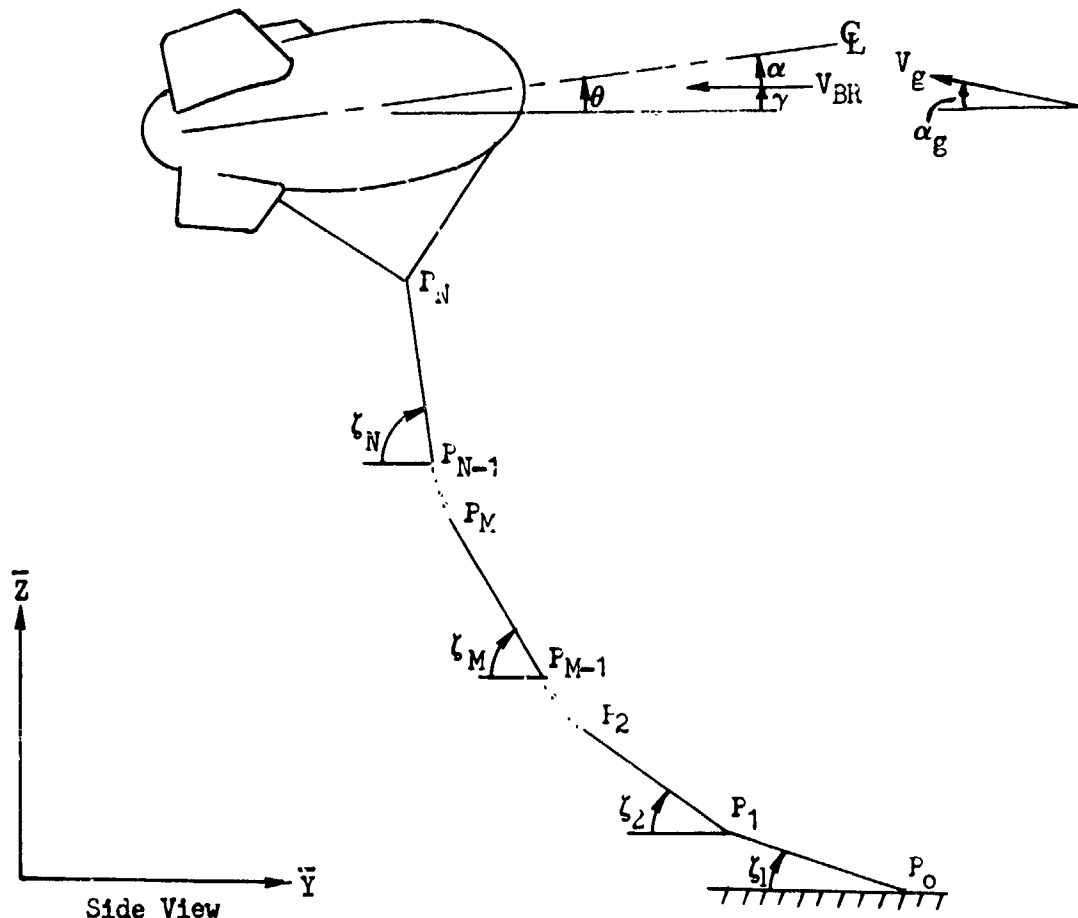


Figure 4 . Balloon Tether Model in Longitudinal Plane

In Figure 4  $V_{BR}$  is the relative velocity of the balloon's center of gravity with respect to the air and is the resultant of the steady wind, the wind gust, the balloon translational motion and the velocity due to rotation of the balloon about its center of mass. The angle of attack ( $\alpha$ ) is the angle that the relative wind forms with the longitudinal axis of the balloon.

The lateral degrees of freedom are displayed in Figure 5 which gives the front and top views of the tethered balloon. The lateral degrees of freedom are:  $\Psi$  (yaw of balloon),  $\phi$  (roll of balloon), and  $\sigma_r$  (yaw of  $r$ th link). All angles are shown positive.

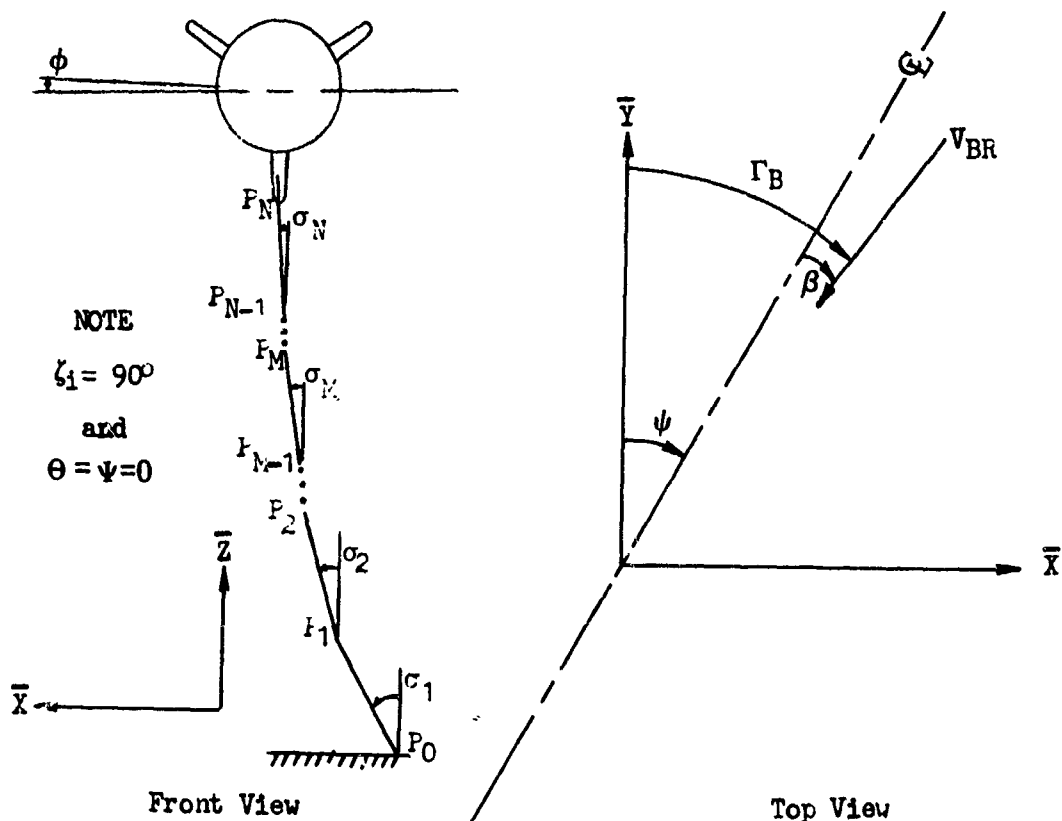
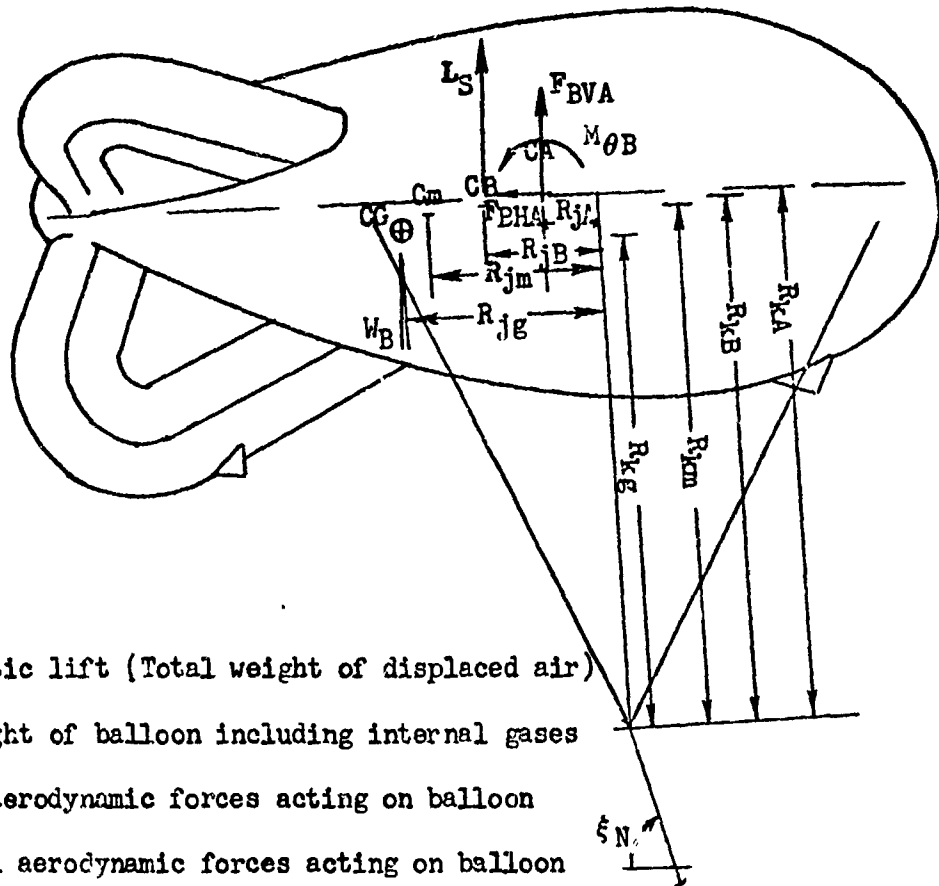


Figure 5. Balloon Tether Model in Lateral Plane

Pertinent geometry of the tethered balloon and applied forces are identified in Figure 6.

In order to separate the equations of motion into a longitudinal response and a lateral response, it was further assumed that the system was near equilibrium. This resulted in a set of equations describing the longitudinal motion which is coupled only in the pitching variables of the balloon and the pitching variables of the tether. However, the second set of equations for the lateral motion does not completely uncouple from the



- $L_S$  - Gross static lift (Total weight of displaced air)
- $W_B$  - Total weight of balloon including internal gases
- $F_{BVA}$  - Vertical aerodynamic forces acting on balloon
- $F_{BHA}$  - Horizontal aerodynamic forces acting on balloon
- $M_{\theta B}$  - Aerodynamic pitching moment acting on balloon
- CA - Aerodynamic reference center (at center of hull volume)
- CB - Center of buoyancy of total displaced volume
- $C_m$  - Apparent mass center and dynamic center in pitch (and yaw)
- CG - Center of gravity of total weight of balloon

Figure 6. Balloon Geometry and Applied Forces

longitudinal degrees of freedom because the equilibrium angles in the longitudinal plane are not zero. Therefore, when solving the lateral degrees of freedom, it must be assumed that the longitudinal variables remain constant and equal to their equilibrium values. In both the longitudinal and lateral cases, the tether is simulated by three rigid links. The number of uncoupled dynamic equations is four for the longitudinal response and five for the lateral response.

## 2. GENERAL STABILITY THEORY

The equilibrium configuration of a tethered balloon can be defined as that position which demands that the summation of all applied moments equals zero. The equilibrium is said to be stable if, for any small disturbance,

the system ultimately returns to its equilibrium conditions. Two types of stability are of interest. In the first (statically stable), a small displacement of the system will create forces which tend to return the system to its equilibrium position. The second (dynamically stable) produces a motion which eventually restores equilibrium. If the motion is periodic, it is characterized by a damped frequency and a damping ratio. Similar definitions apply for statically and dynamically unstable motions. A third possibility is for the system to be neutrally stable during which the motion neither diverges nor converges.

It was necessary during this study to develop techniques to investigate and understand the stability of the system. To this end, characteristic equations are derived. The general approach is as follows:

- (1) Derive the nonlinear equations of motion in three dimensions for each degree-of-freedom
- (2) Assume the motion is near equilibrium so that the equations can be linearized and separated into a longitudinal motion and a lateral motion
- (3) Laplace transform the linear equations from the time domain to the "S" domain assuming that the initial conditions are zero. This establishes a matrix equation of the following form:

$$[A] \{X(S)\} = \{0\} \quad (1)$$

where  $\{X(S)\}$  is the eigenvector and  $[A]$  is a square matrix whose elements are quadratics in  $S$  containing the physical properties of the system.

- (4) Expand the determinant of  $[A]$  such that the characteristics polynomial is obtained.

Each root of the characteristic equation represents a term in the general solution of the form,  $A_i e^{S_i t}$ , where  $S_i$  is the "i"th root and  $A_i$  is an amplitude, dependent on the initial conditions of the system. Both real and complex roots may appear where the complex roots occur in conjugate pairs. In general for "n" degrees of freedom, the characteristic equation will yield "2n" roots. Each pair of complex conjugate roots represents one oscillatory motion, while each real root represents one aperiodic motion.

First consider an oscillatory system. This motion is characterized by two roots of the form  $S_i = X \pm i Y$ , where  $X$  and  $Y$  are real numbers and  $i = \sqrt{-1}$ . Several important quantities can be found from the root. The natural frequency associated with this motion is  $\omega_n = \sqrt{X^2 + Y^2}$ . The damping ratio is  $\zeta = \frac{-X}{\omega_n}$ . The damping frequency is  $\omega_d = \omega_n \sqrt{1 - \zeta^2} = Y$ . It is also of interest to know the time to half amplitude for a stable root or the time to double amplitude for an unstable root. This quantity can easily be found by considering one oscillatory motion. The general solution for free vibration is

$$Z = Ce^{-\zeta \omega_n t} \sin(\omega_d t + \phi) \quad (2)$$

where  $\phi$  is the phase angle dependent upon initial conditions

C is a constant dependent upon initial conditions

The second possibility is an aperiodic motion given by the expression

$$Z = Ce^{Xt} \quad (3)$$

where X is the real part of one root and the imaginary part (Y) is zero

If X is negative, Z approaches zero as time increases indefinitely and the motion is said to be overdamped. Like the oscillatory motion, roots which give overdamped motions will also occur in pairs. However, unlike the complex conjugate roots which result in one oscillatory motion, each real root is a distinct motion. Therefore, it is possible for an "n" degree-of-freedom system to have "2n" distinct motions if the system is so heavily damped that all the roots to the characteristic equation are real.

There is a third possible motion which is a borderline case. If two roots are real and equal, the system is said to be critically damped. The motion will be aperiodic and both roots will give the same motion.

The general solution to the motion of the system is a linear combination of all the motions defined by the roots to the characteristic equation. Associated with each root is a mode shape which gives the relative amplitudes of each degree of freedom when the system is responding to one particular root. It is of interest to establish these mode shapes so that each stability curve can be associated with a definite motion of the whole system. For example, one mode shape may show that the pitching motion of the balloon is very large compared to the motion of the tether.

### 3. STABILITY ANALYSIS

Derivations of the equations of motion of the tethered balloon system and development of the characteristic equations for a tethered balloon system approximated with a three-link tether are given in Reference 2.

The four linearized longitudinal equations are Laplace transformed, and an eighth order characteristic equation generated which specifies stability characteristics of the system. In like manner, the five linearized lateral equations can be reduced to a tenth order equation which gives stability information in the lateral degrees-of-freedom. The roots of these characteristic equations identify the natural frequencies, damped frequencies and damping ratios.

Results of characteristic equations analysis can be displayed in the form of plots in a complex plane typically as shown in Figure 10 of this report. In these plots, the abscissa is the real part of the roots to the characteristic equation, the ordinate is the imaginary part. A negative real part means that mode of oscillation is converging or stable; a positive real part is a diverging mode. Only the first and second quadrants are displayed because the roots are complex conjugates which are symmetric to the real axes, except in the case of overdamped roots which lie on the real axes. In general, the following information is easily available for each root directly from the plots. The natural frequency is measured in rad/sec as the distance from the origin to the root; the damped frequency (rad/sec) is the value of the imaginary part of the root; the damping ratio is equal to the absolute value of the real part of the root divided by the natural frequency.

#### 4. DYNAMIC RESPONSE ANALYSIS

The calculation of the balloon system response to specific disturbances is the subject of the dynamic response analysis. The most general motion the system can have is a linear superposition of the normal modes.

Each aperiodic or nonoscillatory normal mode has one arbitrary constant (the initial value of any one of the variables) associated with it; and each periodic or oscillatory normal mode has two arbitrary constants (the amplitude and phase angle of any one of the variables) associated with it. The total number of arbitrary constants is then equal to the number of aperiodic modes plus twice the number of periodic modes; i.e. to the degree of the characteristic equation, or the order of the system. A specific disturbance will excite the normal modes in varying degrees and establish the values of the arbitrary constants.

The dynamic response of tethered balloon systems to various wind disturbances is obtained by integrating numerically the longitudinal and lateral equations of motion to produce a time history of the dynamics. The start conditions, or equilibrium conditions for the dynamic response computer programs are obtained from the linearized stability computer programs (Reference 2). This approach to analysis has the advantage that wind gusts can be produced and the actual motion of the system can be observed. The major disadvantage is that a greater amount of computer time is required when compared to evaluation of stability by investigating the roots of the characteristic equations.

The equations of motion for the longitudinal dynamics of a tethered balloon system were initially derived in two forms (see Appendix A):

- 1) inertia terms which contain products of angular velocities are neglected,
- 2) inertia terms which contain products of angular velocities are included.

The concept of neglecting products of angular velocities is associated with the assumption that angular velocities are small; and therefore, products of angular velocities are negligible.

Numerical integrations were made with the computer to determine the effect of neglecting the inertia terms containing products of angular velocities. Although the effect is obviously present (Figures 7 and 8), the overall differences between the results of the two sets of equations is small.

# LONGITUDINAL DYNAMICS OF TETHERED BALLOON

8J NOMINAL

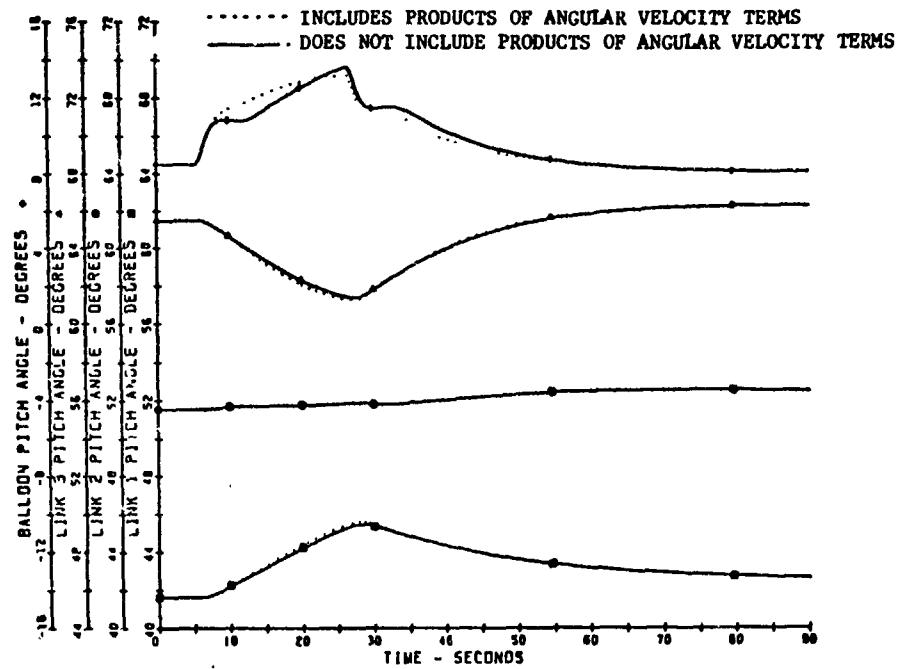


Figure 7

# LONGITUDINAL DYNAMICS OF TETHERED BALLOON

9J NOMINAL

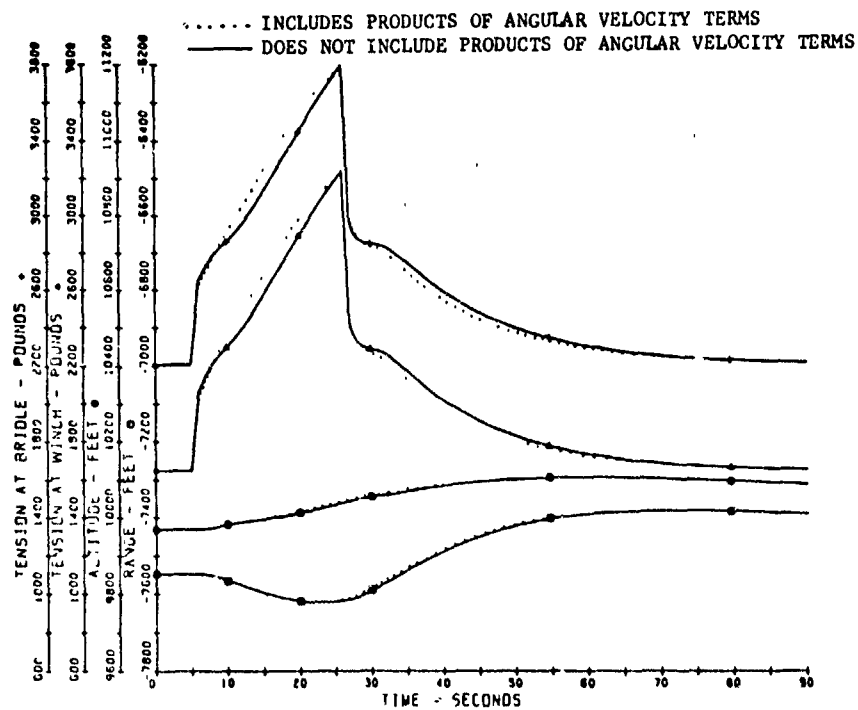


Figure 8

Figure 7 shows the time history of the four generalized coordinates  $\xi_1$ ,  $\xi_2$ ,  $\xi_3$ , and  $\theta$ . A horizontal gust of 20 feet per second with a duration of 20 seconds was applied. The dotted lines represent the angular displacement when the products of angular velocities are included in the inertia terms. Figure 8 presents the range and altitude of the balloon as a function of time and also the variation in tether tension at the winch and at the bridle confluence point. Since this gust velocity is considered to be high, it is concluded that the difference between the solid lines and the dotted lines is maximum.

It was decided that dynamic simulation studies would be conducted with a model which neglects products of angular velocities for three reasons. First, the equations containing products of angular velocities are shown to give only slightly different results. Second, it is desirable to keep the dynamic equations compatible to the equations used in the stability study (the stability study used linearized equations). Third, it is desirable to keep the longitudinal equations compatible to the lateral equations (to derive the lateral equations of motion containing products of angular velocities in the inertia terms would be a very difficult task because of the number of terms involved.)

## SECTION IV

### DYNAMIC RESPONSE OF TETHERED BALLOONS

#### 1. DESIGN CONDITIONS INVESTIGATED

The parametric study conditions found in Appendix B, Tables B-I and B-II and Reference 2 are the source of information for the results and recommendations of this report. Each parametric dynamic response study condition has a computer drawn plot of various balloon parameters versus time. These plots are found in Appendix B.

The parameters chosen for investigation during this study are placed in three major categories:

- (1) "Balloon on Station" performance parameters
- (2) "Structural Design" performance parameters
- (3) "On Board Instrumentation" Design parameters

The "Balloon on Station" performance parameters are defined as balloon displacements from equilibrium and, specifically, are changes in balloon range, altitude, pitch angle, roll angle, yaw angle, and lateral displacement induced by a parameter variation, such as a change in trim angle.

The "Structural Design" performance parameters of interest are the cable tension at winch and bridle, and the balloon translational and rotational accelerations.

The "On Board Instrumentation" design parameters are defined as the balloon angular displacements and rates.

The effects of gusts, trim angle, altitude, tail size, and other parameters on balloon performance parameters are reviewed in detail later in this section of the report. Table III lists the cases compared and the reason for comparison for the longitudinal and lateral cases.

The operational winds used for the investigation, as a function of altitude, are listed in the Introduction to this report. Gusts used for dynamic response are added to the operational winds and are applied to the balloon. The gusts used in analysis are discussed next.

Consider the nominal altitude condition of 10,000 feet where the operational design wind was 67.5 feet per second. Longitudinal gusts were applied where the horizontal wind increased by 30 percent, for a discrete time, to a value of  $1.3 \times 67.5 = 87.6$  fps. Gusts of 2, 10, and 20 seconds and infinite time durations were investigated with various rise times. A case was also investigated where the 30 percent gust increment was applied vertically upward.

Table III

## A. Comparison of Longitudinal Dynamic Cases

<u>Cases Compared</u>	<u>Balloon Type</u>	<u>Reason for Comparison</u>
1,2,3,4,5	BJ Nominal	Gusts and Wind Effects
3,21,18	All	Comparison of Balloon Types
3,6,7	BJ Nominal	Trim Angle Effects *
18,19,20	VEE Balloon	Trim Angle Effects *
21,22,23	GAC Balloon	Trim Angle Effects *
11,3,12	BJ Nominal	Tail Size Effect
3,14,15	BJ Nominal	Winching Effects
13,3	BJ Nominal	Reduced Wind (40%) Effect
10,3	BJ Nominal	Amgal vs NOLARO
16,3	BJ Nominal	Effect of Payload on Underside of Balloon
17,3	BJ Nominal	Winch at 5000 ft, and 0.0 Ft.
8,3,9	BJ	Operational Altitude Effects

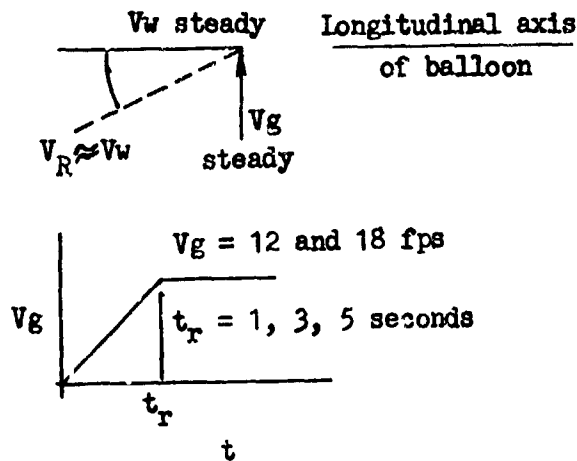
\* Trim angle changed by varying fore and aft location of bridle confluence point

## B. Comparison of Lateral Dynamic Cases

<u>Cases Compared</u>	<u>Balloon Type</u>	<u>Reason for Comparison</u>
24,25,26	BJ Nominal	Effects of Gust Ramp Time
27,26	BJ Nominal	Effects of 50% Increase in Gust Velocity
40,37,25	BJ, VEE, GAC	Comparison of Balloon Types
32,25,33	BJ	Tail Size Effect
37,38,39	VEE Balloon	Tail Size Effect
35,36	BJ Nominal	Winch Effects
34,25	BJ Nominal	Reduced Wind Effect (100%→40%)
31,25	BJ Nominal	Effects of Amgal vs NOLARO
29,25,30	BJ	Operational Altitude Effects

The lateral gusts applied to the tethered balloon systems to investigate dynamic response may be generally interpreted in two ways as shown in Figure 9 which depicts the wind in a horizontal plane.

Condition A - Build-up  
of wind from side



Condition B - Shift  
in wind direction

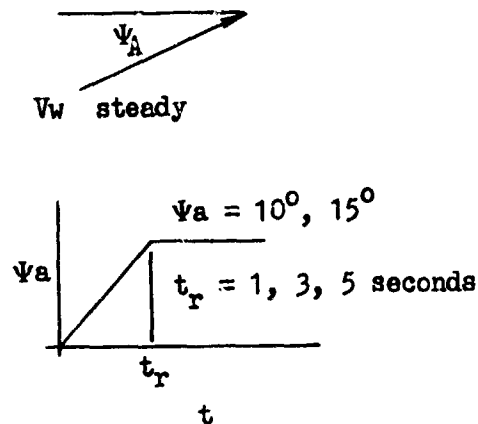


Figure 9 . Lateral Wind Gusts

In Condition A the wind gust from the side builds up with time. This is approximately equivalent to the Condition B where the wind remains constant in magnitude and changes heading direction with time.

## 2. GENERAL DISCUSSION OF DYNAMIC RESPONSE OF TETHERED BALLOON SYSTEMS

The non-linear differential equations defining the motion of a tethered balloon system and the linearized equations used in studying the stability characteristics of the balloon system are given in Reference 2 together with the results of the stability analysis of various balloon systems. Appendix A of this report expands the equations of motion of Reference 2 to include wind gusts. The response of the non-linear balloon system when subjected to wind gusts has been programmed for computer solution using numerical integration methods. Various balloon systems, subjected to different types of gusts, have been studied using this computer program and the results are found in Appendix B.

The response plots shown in Appendix B reveal that the balloon systems are highly damped. This agrees with the stability analyses of the balloon systems given in Reference 2. In fact, the motion is so highly damped that the lower frequency response modes are, in general, damped out within two cycles or less of motion. Thus, the high aerodynamic damping involved in the balloon systems, makes it very difficult to evaluate the response plots with regard to phase relationships between coordinates, damping characteristics, and the frequencies involved in the motion. It becomes evident after looking at the

response plots that only the amplitude and direction of the response can be obtained. A mathematical tool will be required to obtain information regarding phase relationships, natural frequencies, and damping characteristics of the modal motions involved. Such a tool would be very valuable for evaluating flight data from tethered balloons.

What then, is this mathematical tool? The response of a highly damped multidegree of freedom system to a known disturbance can be represented mathematically as the sum of the system's modal responses. Assuming the system follows the response of a viscously damped system, a modal response definition is given by the following equation.

$$z_i = \left( c_i e^{-\zeta_i \omega_{n_i} t} \right) \sin(\omega_{d_i} t + \phi_i)$$

The total response  $Z_T$  of a particular coordinate is then given by

$$Z_T = \sum_{i=1}^{i=N} \left( c_i e^{-\zeta_i \omega_{n_i} t} \right) \sin(\omega_{d_i} t + \phi_i) \quad (1)$$

$N$  represents the number of frequencies involved in the response

$\zeta$  represents the damping ratio

$\omega_n$  represents the natural frequency

$\omega_d$  represents the damped frequency

$\phi_i$  represents the phase angle

$C$  represents an amplitude constant

Each modal response  $Z_i$  has 4 unknowns, since  $\omega_d$  is related to  $\omega_n$  by  $\omega_d = \omega_n \sqrt{1 - \zeta^2}$ .

Thus any response curve which is defined by a sufficient number of points can be mathematically represented by Equation (1) and solved for the unknown constants using numerical curve fitting methods. No curve fitting program is presently available to the project for use with Equation (1); however, there is a curve fitting program available which uses a Fourier Transform and performs a power spectral density (P.S.D.) analysis of the Fourier Transformation. This program is only valid for analyzing systems with no damping. The program still gives a general overall view of the frequencies involved in the motion and it is thought worthwhile to analyze the response of two dynamic cases and to compare the frequencies found with the frequencies obtained from the stability analysis of the same balloon configurations given in Reference 2. The dynamic cases chosen for frequency comparison are lateral dynamic response Case 28 and longitudinal dynamic response Case 4. The cases represent a nominal BJ balloon at 10,000 feet. Lateral response is for a 10 second duration step side gust and longitudinal response is for a 20 second duration step horizontal gust.

## a. COMPARISON OF THE NON-LINEAR LATERAL DYNAMICS CASE 28, WITH THE LINEARIZED STABILITY CASE 1

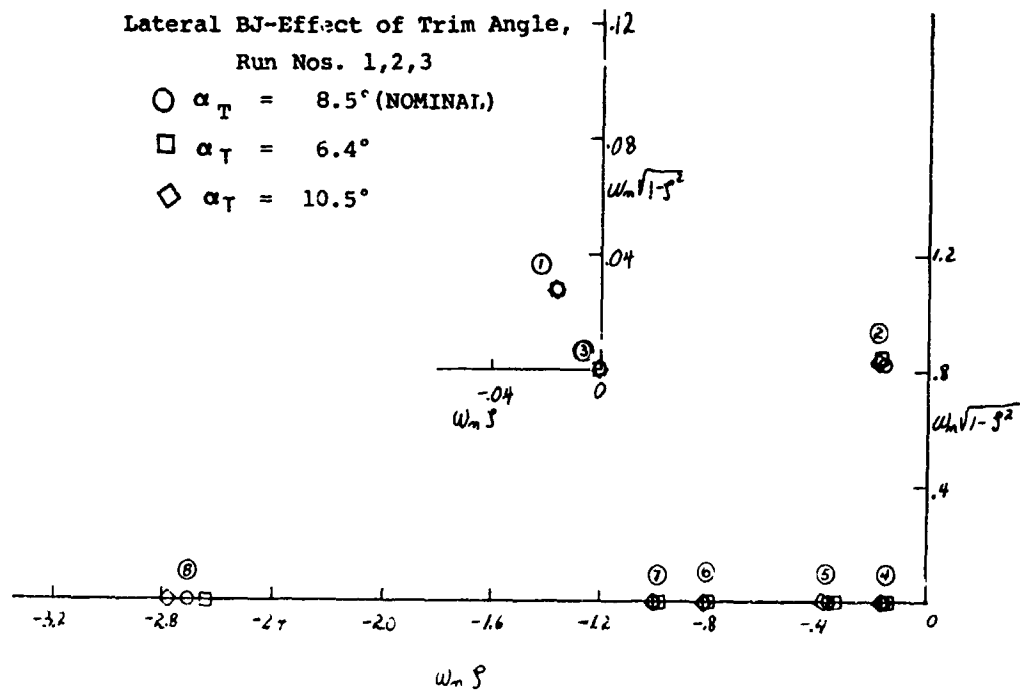
The small displacement motion of a forced non-linear system, in the time era after the forcing function is removed, should result in system motions similar to the sum of the mode shape times participation factor for each mode found in the linearized stability analysis of the system. To verify this, Lateral Dynamics Case 28 and Lateral Stability Case 1 (Reference 2) were chosen for comparison. A complete description of Lateral Dynamics Case 28 is found in Appendix B, and the Lateral Stability Case 1 description is found in Reference 2. For convenience the results of Lateral Stability Case 1 are summarized in Table IV and Figure 10 of this report. In order to analyze the coordinate motions of Case 28, a power spectral density analysis with Fourier Transform was performed on each of the lateral coordinate degrees of freedom;  $\psi$ ,  $\phi$ ,  $\sigma_1$ ,  $\sigma_2$ ,  $\sigma_3$ . The input coordinate waveforms and PSD plots for each degree of freedom are given in Figures 11 and 12.

The PSD plots reveal that there are two predominate modes involved in the system motion. These are underdamped oscillatory modes 1 and 2 with natural frequencies and damping ratios of  $f_{n1} = 0.0051$  Hz and  $\zeta_1 = 0.511$  for mode 1 and  $f_{n2} = 0.136$  Hz and  $\zeta_2 = 0.207$  for mode 2. Mode one (0.0051 Hz) is the predominate mode with mode 2 (0.136 Hz) of smaller amplitude superimposed on mode 1. The lateral wind gust disturbance in Case 28 is removed after  $T = 11$  seconds, therefore all comparisons should be made after the first peak is reached beyond 11 seconds. It should be noted that mode 2 is predominately a  $\phi$  or roll mode, and this is evident from the plots of the coordinates, since only the  $\phi$  coordinate plot has evidence of a 0.136 Hz mode. On the  $\phi$  plot mode 2 appears damped out of the  $\phi$  motion by the time  $T = 37$  sec.

Table IV. Summary of Lateral Stability Case 1

### Normalized Modes

Mode Number	Frequency Hz	Damping Ratio	$\psi$		$\phi$		$\sigma_1$		$\sigma_2$		$\sigma_3$	
			Ampl.	$\chi^0$	Ampl.	$\chi^0$	Ampl.	$\chi^0$	Ampl.	$\chi^0$	Ampl.	$\chi^0$
1	0.0051	0.511	1.0	0.0	0.195	301	0.342	83.3	0.429	222	0.483	275
2	0.1363	0.207	1.0	0.0	9.12	252	0.016	17.7	0.051	215	0.102	58.9
3	0.000215	1.0	1.0	0.0	0.0082	0	8.86	180	2.51	180	0.487	180
4	0.0252	1.0	1.0	0.0	0.927	0	1.22	360	2.27	180	0.957	360
5	0.0578	1.0	1.0	0.0	1.58	0	2.02	360	3.59	180	1.54	360
6	0.1295	1.0	1.0	0.0	23.1	180	0.345	180	0.147	360	0.513	360
7	0.1608	1.0	1.0	0.0	60.7	360	7.34	180	6.09	180	12.7	360
8	0.4320	1.0	1.0	0.0	0.988	360	0.00007	180	0.0006	360	0.0051	180



Lateral BJ-Nominal, Run No. 1

Mode Shapes

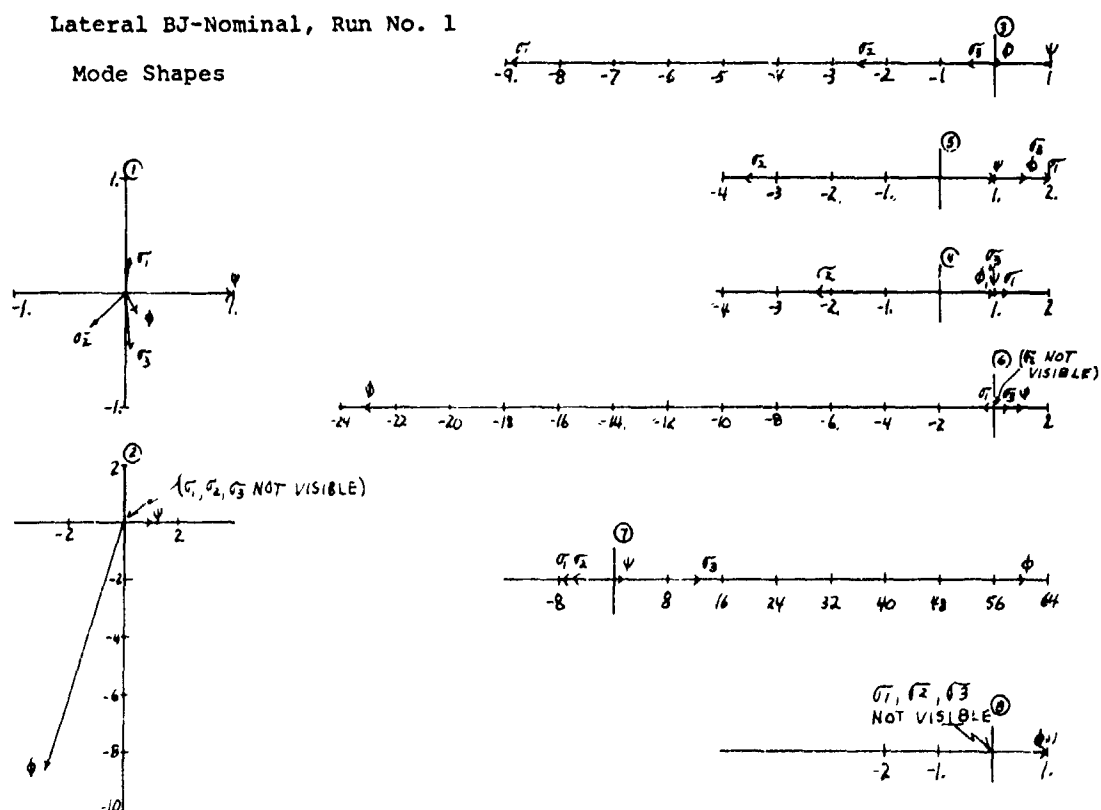


Figure 10. Lateral Stability Characteristics of Nominal BJ Tethered Balloon at 10,000 Feet Altitude

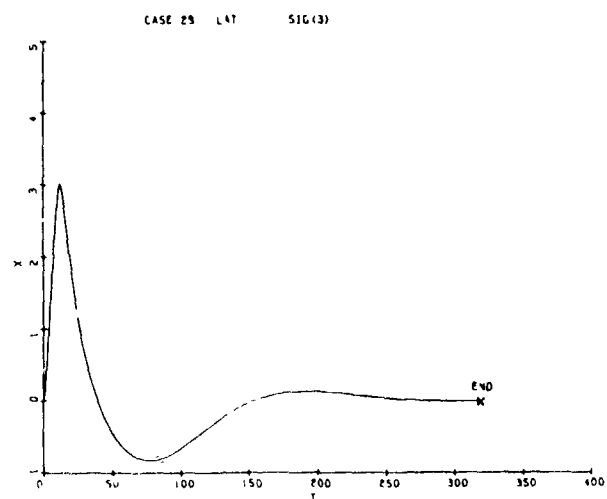
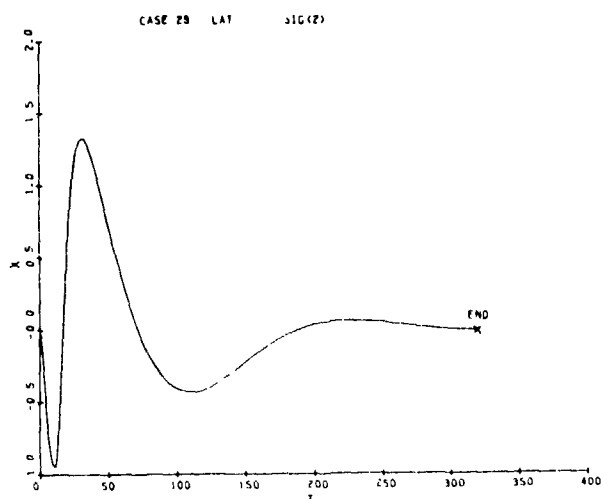
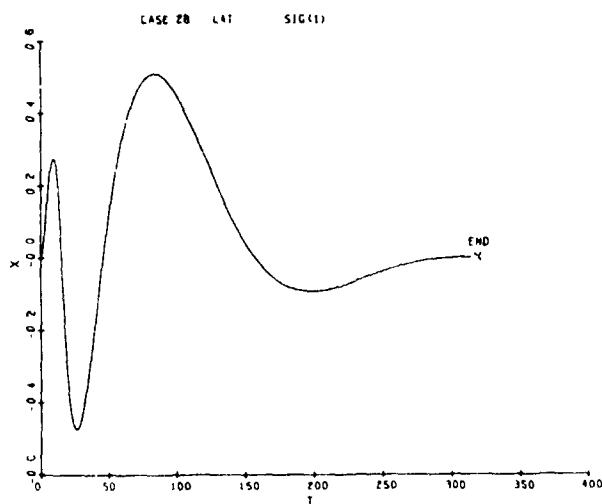
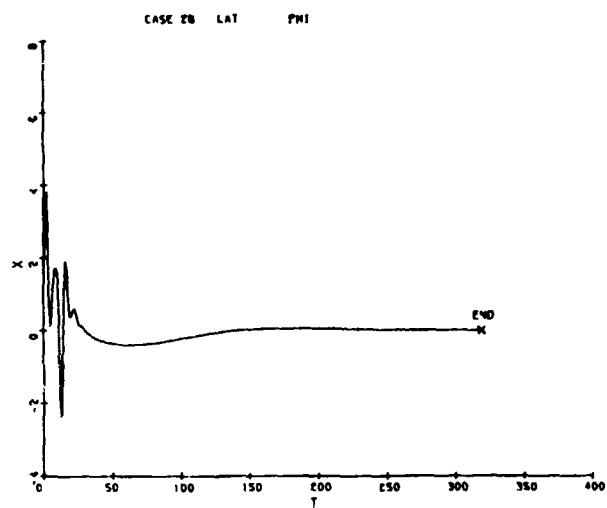
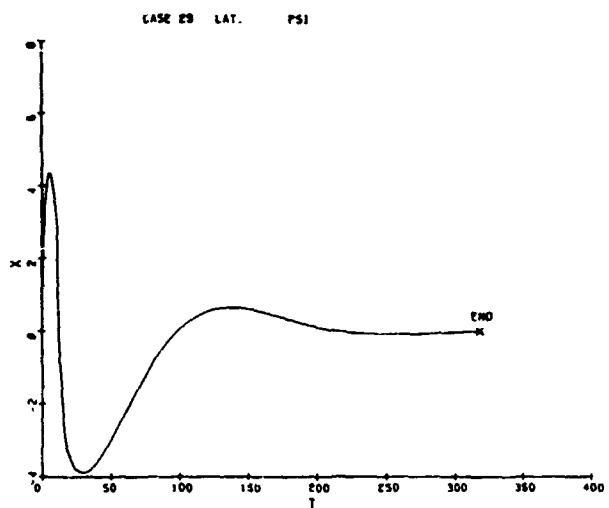


Figure 11. Lateral Case 28, Coordinates Response  
21

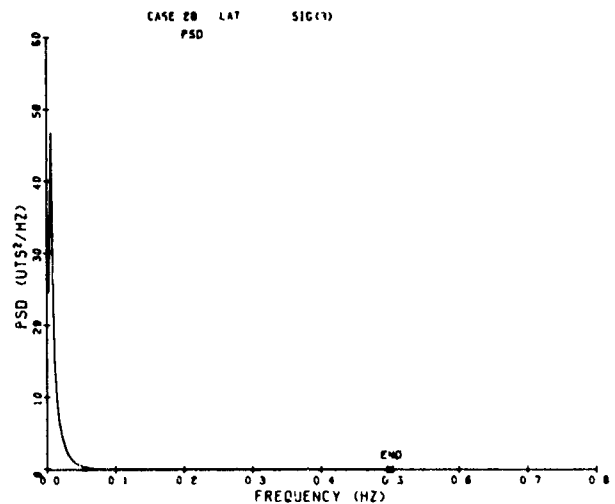
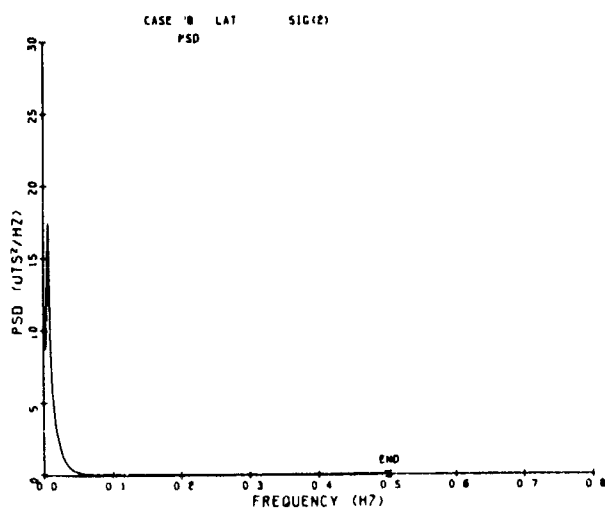
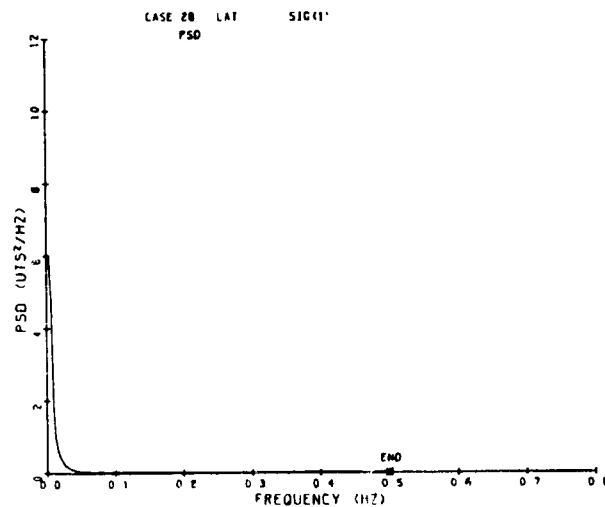
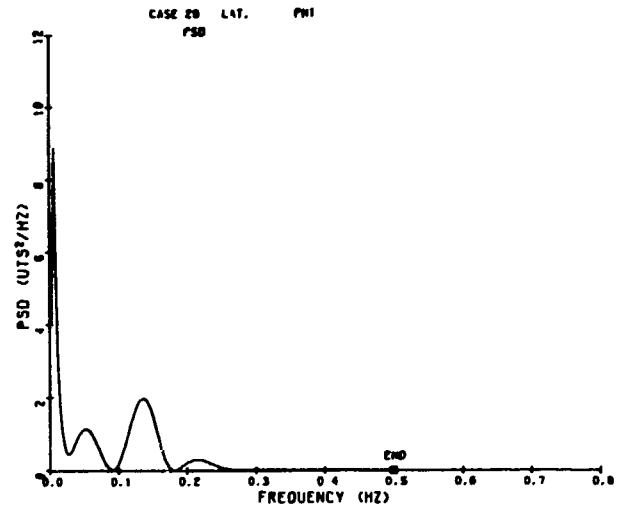
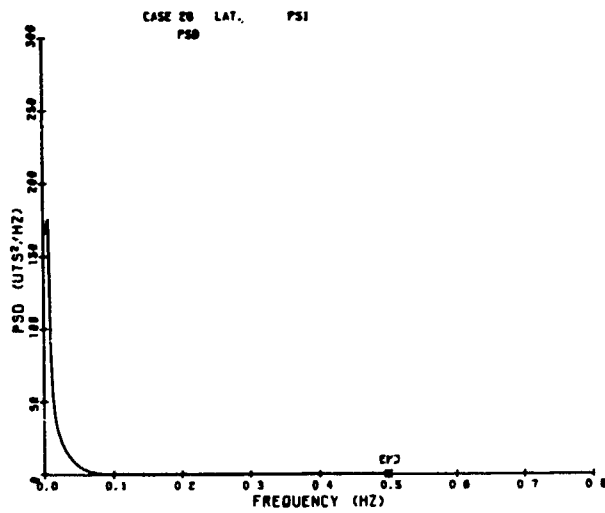


Figure 12. Lateral Case 28, Power Spectral Density

The aerodynamic damping characteristics of the system appear viscous in nature for the 0.0051 Hz mode.

Table V lists, for Case 28, the time and amplitude of the various coordinates for the first and second peaks after the gust is removed. Included in Table V is the period, amplitude ratio, and frequency as calculated from the coordinate data of Case 28.

The period and amplitude ratio for the coordinates  $\psi$ ,  $\phi$ , and  $\sigma_3$  show very good agreement with a 0.0051 Hz viscously damped ( $\zeta = 0.51$ ) system. The period between peaks of a 0.0051 Hz viscously damped system with  $\zeta = 0.51$  is given by

$$T = \frac{1}{f \sqrt{1 - \zeta^2}} = \frac{1}{0.0051 \sqrt{1 - 0.51^2}} = 228 \text{ sec.}$$

The amplitude ratio between successive peaks is given by

$$\frac{x_{n+1}}{x_n} = e^{\left[ \frac{-2\pi\zeta}{\sqrt{1 - \zeta^2}} \right]} = e^{\left[ \frac{-2\pi(0.51)}{\sqrt{1 - 0.51^2}} \right]} = 0.025$$

Table V. Peak Amplitudes for Lateral Dynamics Case 28

Coordinate	First Peak After Gust		Second Peak After Gust		Period T Sec.	Frequency $\frac{1}{T}$	Ampl. Ratio $\frac{x_{n+1}}{x_n}$
	Time	Ampl.	Time	Ampl.			
$\psi$	29	-3.905	250	-0.099	221	0.0045	0.0253
$\phi$	61	-0.404	289	-0.00973	228	0.0044	0.0241
$\sigma_1$	26	-0.475	197	0.0943	171	0.0059	0.199
$\sigma_2$	31	1.33	224	0.0630	193	0.0052	0.0474
$\sigma_3$	76	-0.834	304	-0.0207	228	0.0044	0.0248

b. COMPARISON OF NON LINEAR LONGITUDINAL DYNAMICS, CASE 4, WITH LINEARIZED LONGITUDINAL STABILITY, CASE 1

A description of Longitudinal Dynamics, Case 4, is found in Appendix B and Linearized Longitudinal Stability, Case 1, is defined in Reference 2. A summary of the Longitudinal Stability, Case 1, is given in Table VI and Figure 13 of this report.

A Fourier and PSD analysis is performed on each of the Longitudinal Dynamics, Case 4, coordinate degrees of freedom  $\theta$ ,  $\xi_1$ ,  $\xi_2$ , and  $\xi_3$ . The input coordinate waveform and PSD plot for each degree of freedom is given in Figures 14 and 15 respectively.

The need of a mathematical tool for analyzing a highly damped response is very evident in Longitudinal Dynamics, Case 4. The response of every coordinate is damped out, or nearly so, in less than one cycle. The Fourier and PSD non-damped harmonic analysis of this motion is not too meaningful. However, it does indicate that the motion is comprised of frequencies below 0.05 Hz with the most power below 0.01 Hz.

Table VI. Summary of Longitudinal Stability Case 1  
(Reference 2)

Normalized Modes

Mode Number	Frequency Hz	Damping Ratio	$\theta$		$\xi_1$		$\xi_2$		$\xi_3$	
			Ampl.	$\angle^\circ$	Ampl.	$\angle^\circ$	Ampl.	$\angle^\circ$	Ampl.	$\angle^\circ$
1	0.00554	-0.037	1.0	0.0	2.14	281.	1.27	238.	1.28	194.0
2	0.0728	0.653	1.0	0.0	0.131	197.	0.080	353.	0.058	39.7
3	0.0986	0.51	1.0	0.0	0.0747	9.6	0.214	188.	0.145	7.4
4	0.0156	1.0	1.0	0.0	0.888	0.0	0.800	0.0	0.363	180.
5	0.1715	1.0	1.0	0.0	0.00033	0.0	0.0123	0.0	0.0066	180.

c. YAW-ROLL COUPLING IN LATERAL DYNAMIC CASES

Yaw-roll coupling for BJ and GAC single hull balloons subjected to lateral wind is evident when the  $\psi$  response plots are reviewed. The Vee balloon appears to have negligible coupling. As an example, observe the motion of coordinate  $\psi$  (Reference Appendix B) for Lateral Case 28. One would think that, when a balloon is in equilibrium with a steady head wind and then is subjected to a side gust from the left, the balloon would yaw into the resultant wind. This would be a negative yaw angle, however, Lateral Case 28 shows the balloons first yaw motion is positive or away from the resultant wind for a time of approximately 7 seconds and to  $\psi = +4^\circ$  before the balloon starts yawing toward the resultant wind.

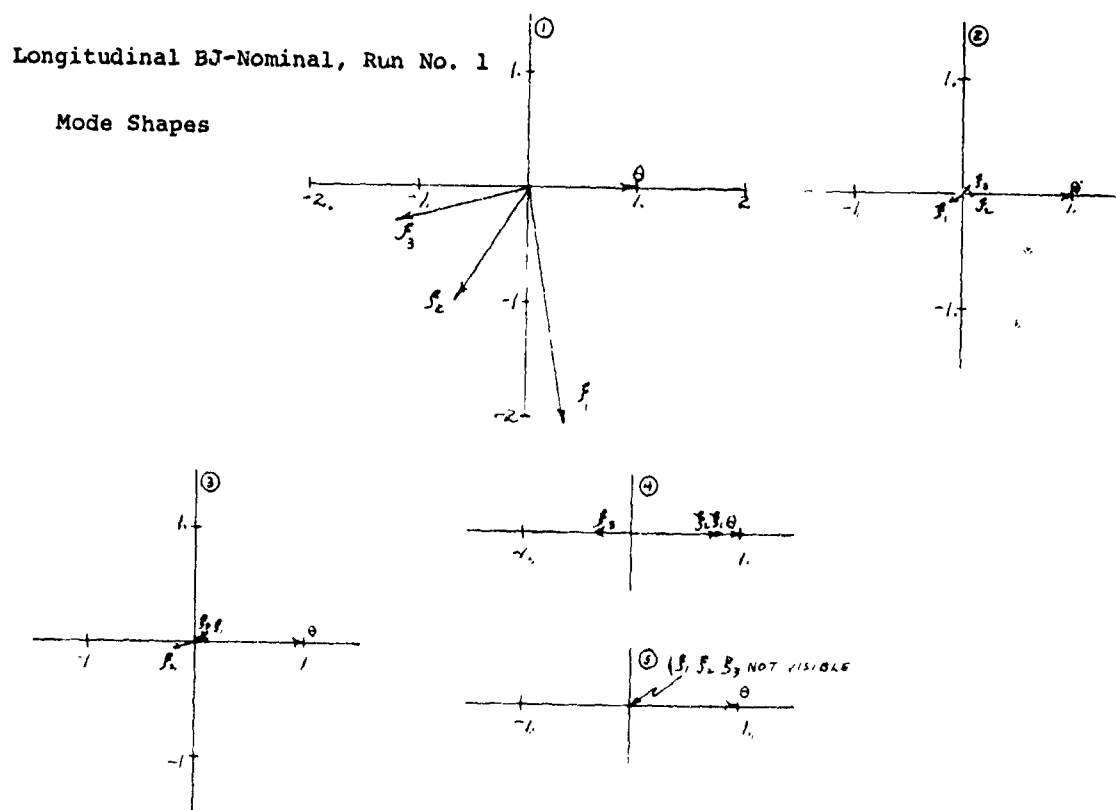
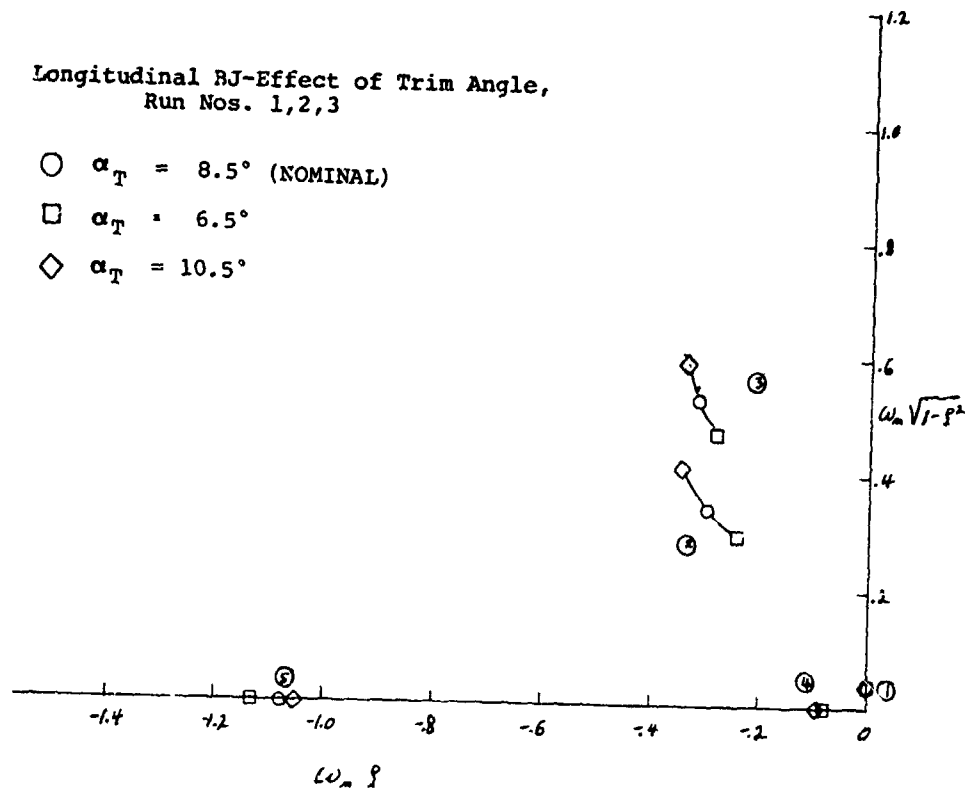


Figure 13. Longitudinal Stability Characteristics of Nominal BJ Tethered Balloon at 10,000 Feet Altitude

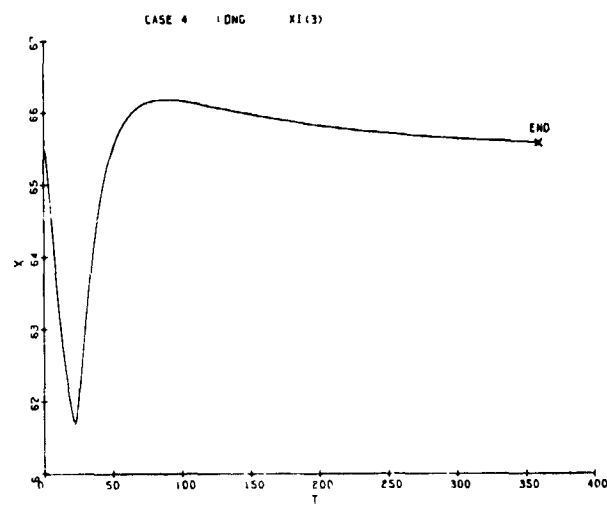
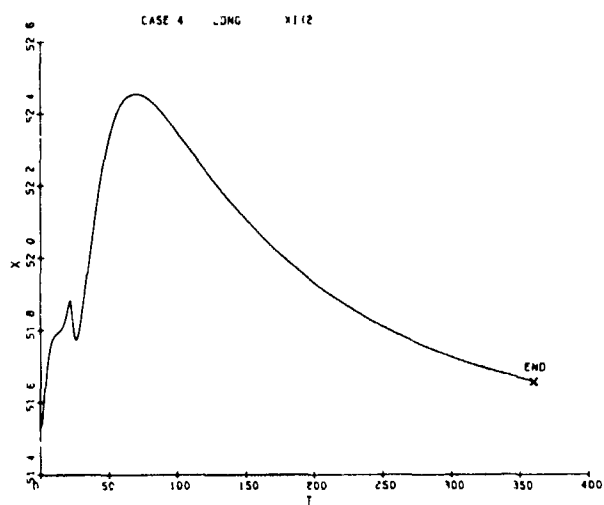
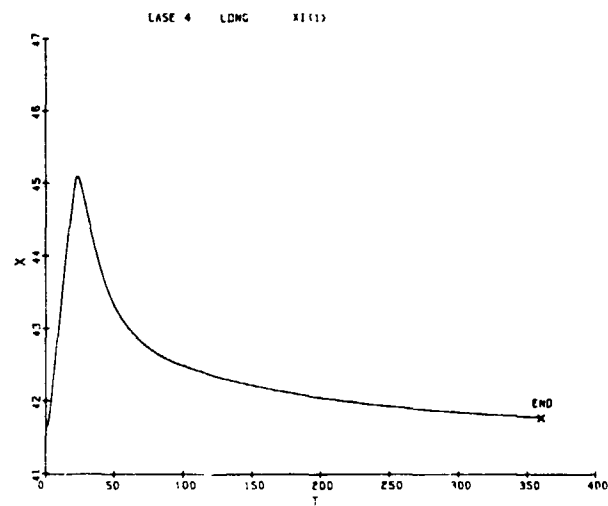
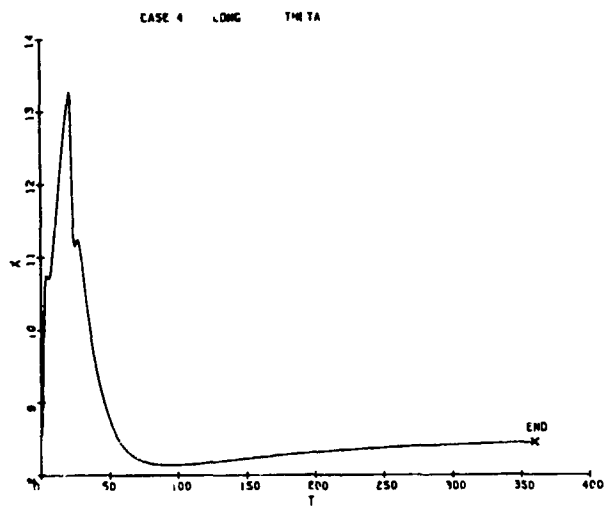


Figure 14. Lateral Case 4, Coordinates Response

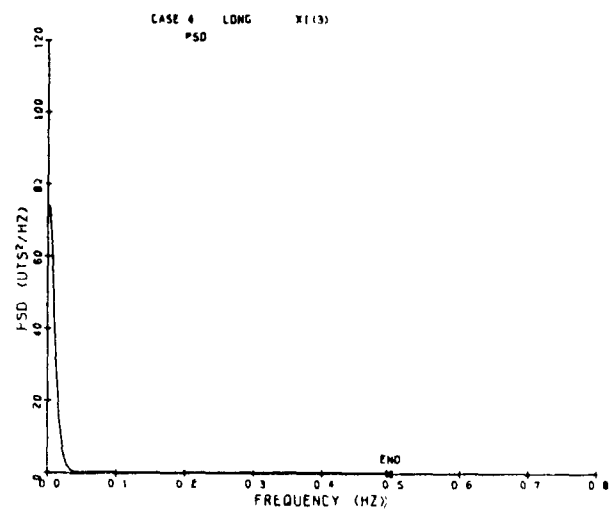
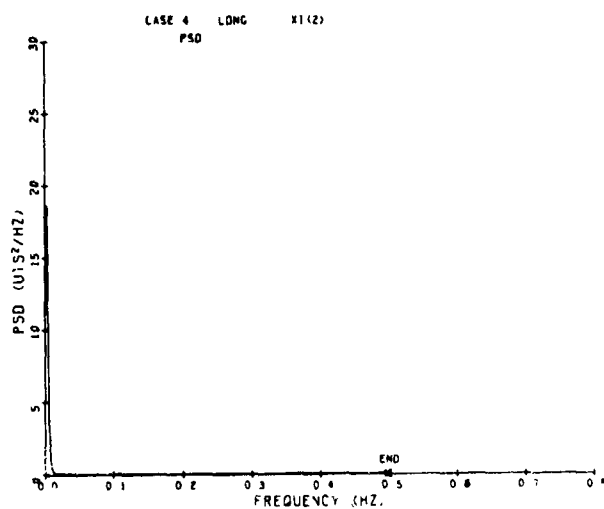
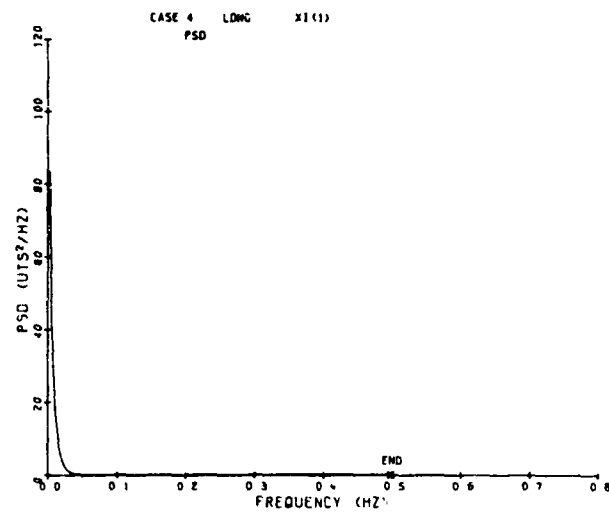
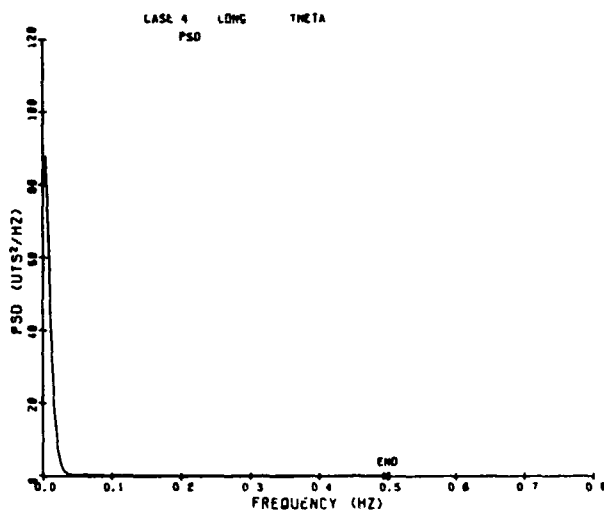


Figure 15. Lateral Case 4, Power Spectral Density

To explain this motion refer to Equation 86 in Appendix A. Neglecting link acceleration terms results in the following equation.

$$F_{\psi} = \left\{ M_S \left[ -R_{jm} \epsilon_{33} + R_{km} \epsilon_{23} \right] \left[ -R_{km} \right] - I_{YB} S\theta + I_{YZB} C\theta C\phi \right\} \ddot{\phi} \\ + \left\{ M_S \left[ -R_{jm} \epsilon_{33} + R_{km} \epsilon_{23} \right]^2 + \left[ M_L - R_{km} \epsilon_{13} \right]^2 \right. \\ + \left[ M_V + R_{jm} \epsilon_{13} \right]^2 + C^2 \theta \left[ I_{XB} S^2 \phi + I_{ZB} C^2 \phi \right] \\ \left. + S^2 \theta I_{YB} - S^2 \theta C\phi I_{YZB} \right\} \ddot{\psi}$$

Substituting a and b for the coefficients of  $\ddot{\phi}$  and  $\ddot{\psi}$  results in the following equation.

$$F_{\psi} = a \ddot{\phi} + b \ddot{\psi}$$

The equation is solved for

$$\ddot{\psi} = \frac{F_{\psi} - a \ddot{\phi}}{b}$$

where  $F_{\psi}$  is the total externally applied balloon y oment.

Case 28 parameters have the following values at  $T = 5.5$  seconds (from digital printout of Case 28).

$F_{\psi} = -40039 \text{ ft-lb}$	$\ddot{\phi} = 3.060^\circ/\text{sec}^2$	$\ddot{\psi} = 1.207^\circ/\text{sec}^2$
$I_{XB} = 116,000 \text{ Slug Ft}^2$	$\dot{\phi} = 2.373^\circ/\text{sec}$	$\dot{\psi} = 1.989^\circ/\text{sec}$
$I_{YB} = 26,000 \text{ Slug Ft}^2$	$\phi = 0.531^\circ$	$\psi = 0.426^\circ$
$I_{ZB} = 119,000 \text{ Slug Ft}^2$		
$I_{YZB} = 12,500 \text{ Slug Ft}^2$		

Inspection of the  $\ddot{\psi}$  coefficient,  $b$ , reveals it to be positive. Since  $F\psi = -40039$  ft-lb and will tend to turn the balloon into the resultant wind, the only term left to cause  $\ddot{\psi}$  to be positive is the roll coupling term  $a\dot{\phi}$ . In conclusion the initial  $\psi$  motion away from the resultant wind is caused by roll ( $\phi$ ) inertia coupling.

### 3. EFFECTS OF DESIGN PARAMETERS ON TETHERED BALLOON DESIGN

#### a. Balloon on Station Performance Parameters

(1) General. As listed in Part 1 of this section a number of tethered balloon design parameters and flight conditions were varied to establish their influence on a tethered balloon design. This subsection summarizes some of the major effects on tethered balloon dynamic behavior as established from the dynamic response calculations presented in Appendix B and an evaluation of these data.

(2) Wind Gust Effects. The response data in Table VII shows the effect of increasing the duration of a horizontal gust on the longitudinal motions of the nominal BJ balloon design for 10,000 foot altitude. It is apparent from an examination of these data that the longer duration of the gust the greater the angle of attack of the balloon becomes. A new equilibrium condition is reached when the gust is left on indefinitely. As a consequence of the increased angle of attack and wind velocity the aerodynamic lift increases and a somewhat more favorable aerodynamic lift to drag ratio is obtained. This serves to increase the altitude of the balloon and reduce the downwind displacement of the balloon. A substantial increase in tether tension is also evident.

A nominal BJ balloon operating at 10,000 feet is subjected to a 20.2 ft/sec, 20 second duration, horizontal gust in Longitudinal Case 4 and to a 20.2 ft/sec, 20 second duration, vertical gust in Longitudinal Case 4A. Table VII also summarizes the results of these two cases.

Table VII. Wind Gust Duration Effects on BJ Nominal Balloon in Longitudinal Plane

Altitude = 10,000 Ft.  
Payload Weight = 1,000 Lb.  
Trim Angle = 8.5°

Gust Velocity = 20.2 Ft/Sec  
Gust Duration =  $t_G$

Case No.	$t_G$ Sec.	Balloon Displacements From Equilibrium			Cable Tensions At Equilibrium		Maximum Cable Tensions	
		$\Delta$ Range Down/Up Ft.	$\Delta$ Altitude Ft.	$\Delta$ Pitch Deg.	Winch Lb.	Bridle Lb.	Winch Lb.	Bridle Lb.
1	$\infty$	-65/800	690	5.7	1650	2210	3630	4200
2	2	-12/16	15	1.9	1650	2210	2250	2830
3	10	-52/73	82	2.9	1650	2210	2650	3210
4	20	-68/146	121	4.7	1650	2210	3180	3740
4A	20	0/451	345	1.25	1650	2210	3582	3947

Specific comments for this comparison are:

- (1) The vertical gust displaced the balloon up range approximately three times the horizontal gust up range displacement.
- (2) The vertical gust caused the balloon to rise three times higher than the horizontal gust.
- (3) The pitch angle change from a vertical gust is only 1/4 the pitch angle change due to a horizontal gust of equal magnitude.
- (4) Maximum cable tension increased by 400 pounds due to the vertical gust. It is noted that equilibrium cable tension is slightly different from that listed in Table I. This is a result of different balloon trim angles and number of cable links used in the two analyses.

The effects of gust ramp rise time on the response of a nominal BJ balloon is given in Table VIII. These cases represent BJ nominal balloons at 10,000 feet that are subjected to a steady lateral gust with ramp rise times of 1, 3 and 5 seconds.

Table VIII reveals that gust linear ramp rise times of 1, 3, and 5 seconds have little effect on balloon response, except for balloon roll where the 1 second rise time is 1.8 times larger than the 5 second rise time response.

Table VIII. Wind Gust Ramp Rise Time Effects on BJ Nominal Balloon in Lateral Plane

Case No.	Ramp Rise Time	Gust Velocity Ft/Sec	Balloon Displacements from Initial Equilibrium			Cable Tension At Equilibrium		Maximum Cable Tension	
			Yaw +/- Deg.	Roll +/- Deg.	Lat. Displ. Ft.	At Winch Lb.	At Bridle Lb.	At Winch Lb.	At Bridle Lb.
24	1 sec	12	4 /-13.6	3.9/-0.4	460	1650	2210	1686	2258
25	3 sec	12	4.3/-13.8	3.1/-0.35	460	1650	2210	1680	2250
26	5 sec	12	4 /-13.6	2.2/-0.4	460	1650	2210	1675	2244

The effects of a 50 percent increase in lateral gust velocity on the response of a nominal BJ balloon is given in Table IX. The balloon is operating at 10,000 feet in a steady head wind when subjected to steady lateral gusts of 12 ft/sec and 18 ft/sec. Each gust has a ramp rise time of five seconds. Table IX reveals that a 50 percent increase in steady lateral gust velocity results in approximately a 50 percent increase in balloon lateral displacement, roll, and yaw response.

Table IX. Effect of Increase in Gust Velocity on BJ Nominal Balloon in Lateral Plane

Case No.	Balloon Displacements from Initial Equilibrium			Cable Tension At Equilibrium		Maximum Cable Tension	
	Yaw +/- Deg.	Roll +/- Deg.	Lat. Displ.	At Winch Lb.	At Bridle Lb.	At Winch Lb.	At Bridle Lb.
26	4.0/-13.6	2.2/-0.4	460	1650	2210	1675	2244
27	6.0/-20.0	3.2/-0.6	710	1650	2210	1708	2285

(3) Comparison of Balloon Types. The effects of trim angle on the longitudinal response of BJ nominal, VEE, and GAC single hull balloons is given in Table X. The balloons, in equilibrium with a steady head wind at 10,000 feet, are subjected to a horizontal longitudinal gust of 20.2 feet/second for ten seconds. Table X reveals that:

- (1) the down range displacements from equilibrium decreases with an increase in trim angle of attack
- (2) the GAC single hull balloon has the smallest displacement from equilibrium of the three balloons
- (3) the BJ nominal balloon has the smallest cable tension of the three balloon types
- (4) cable tension increases with an increase in trim angle
- (5) changes in trim angle have a negligible effect on pitch response to gusts.

The effects of lateral steady wind gusts on the lateral response of BJ nominal, VEE, and GAC single hull balloons are given in Table XI. The balloons are in equilibrium at 10,000 feet with a steady head wind and then subjected to a steady lateral horizontal gust of 12 ft/sec with a three second ramp rise time. Table XI reveals that:

- (1) the response of the three balloons is approximately the same in both yaw and roll response
- (2) the VEE balloon has 1/3 the lateral displacement of the other balloons
- (3) the VEE balloon has 2.5 times more tether load than the BJ balloon as a result of the larger aerodynamic lift of this balloon.

Table X. Effect of Trim Angle of Attack on Longitudinal Response of Three Balloon Types

Type Balloon	Case No.	Trim Angle	Balloon Displacements from Equilibrium			Cable Tensions At Equilibrium		Maximum Cable Tensions	
			$\Delta$ Range Down/Up Ft.	$\Delta$ Alt. Ft.	$\Delta$ Pitch Degree	At Winch Lb.	At Bridle Lb.	At Winch Lb.	At Bridle Lb.
BJ Nom.	6	6.5	-65/65	65	2.8	1350	1880	2070	2610
	3	8.5	-52/73	82	2.9	1650	2210	2650	3210
	7	10.5	-50/75	55	2.9	1950	2525	3220	3800
VEE	19	5.0	-35/135	80	4.2	3450	4500	7500	8600
	18	7.0	-22/119	60	3.7	4620	5802	10100	11300
	20	9.1	-19/105	40	3.3	6000	7200	12900	14000
CAC Single Hull	22	6.0	-60/30	20	0.70	2200	3070	3150	4000
	21	7.9	-48/38	20	0.75	2696	3596	3940	4830
	23	10.0	-40/42	25	0.40	3230	4150	4850	5770

Table XI. Effect of Lateral Wind Gusts on the Lateral Response of the Three Balloon Types

Type Balloon	Case No.	Balloon Displacements from Equilibrium			Cable Tensions At Equilibrium		Maximum Cable Tensions	
		Yaw +/- Deg.	Roll +/- Deg.	Lat. Displ. Ft.	At Winch Lb.	At Bridle Lb.	At Winch Lb.	At Bridle Lb.
BJ	25	4.3/-13.8	3.1/-0.35	460	1650	2210	1680	2250
VEE	37	0.5/-15.5	3.1/-0.4	178	4620	5802	4683	5822
CAC	40	5.5/-14.5	2.7/-0.5	510	2696	3596	2734	3645

(4) Effect of Tail Size. The effect of tail size on the response of nominal BJ balloons subjected to longitudinal gusts is given in Table XII. The effects of tail size on the response of BJ nominal and VEE balloons subjected to lateral gusts are given in Table XIII. The longitudinal cases of Table XII are in equilibrium with a steady headwind and then subjected to 20.2 ft/sec step gust of 10-second duration. The tail sizes investigated were 81%, 100% and 144% of nominal tail area. Table XII reveals that:

- (1) both up and down range displacements decrease with increasing tail size
- (2) pitch angle response decreases with increasing tail size
- (3) the maximum tether load at bridle and winch decrease with increasing tail size.

The lateral cases of Table XIII are in equilibrium with a steady head wind and then subjected to a lateral steady gust of 12 ft/sec with a ramp rise time of three seconds. Table XIII reveals that:

- (1) the BJ balloon has larger lateral displacement response and less roll response with increasing tail size
- (2) the VEE balloon has smaller response in yaw, roll, and lateral displacement with increasing tail size
- (3) tether loads for both types of balloons increase with an increase in tail size.

(5) Effects on Balloon Behavior of Intermediate Altitudes. The effects of intermediate altitude operation on a nominal BJ balloon designed for 10,000 feet are given in Table XIV. The altitudes investigated are 1,000, 4,000 and 10,000 feet. The balloon is in equilibrium with a steady head wind and then is subjected to longitudinal gusts of 10-second duration with varying velocities of 20.2 ft/sec, 13.6 ft/sec, and 7.1 ft/sec for longitudinal dynamics cases 3, 14, and 15, respectively. The wind gust velocities are reduced proportional to the steady wind velocity reductions with altitude. Table XIV reveals the longitudinal responses all decrease with a decrease in altitude and the maximum tether load at bridle is proportional to the gust velocity.

The effects of intermediate altitude operation on the lateral response of a BJ balloon designed for 10,000 feet are given in Table XV. The balloon is in equilibrium with a steady head wind and then is subjected to lateral steady gusts of 12 ft/sec, 8 ft/sec, and 1 ft/sec corresponding to altitudes of 10,000, 4,000, and 1,000 feet. Table XV reveals that:

- (1) the lateral responses of the nominal BJ balloon subjected to lateral steady gusts increase with decreasing altitude
- (2) a review of the computer plots of Case 36 (1000 feet) in Appendix B indicates the response is unstable.

A detailed discussion of Lateral Case 36 follows.

Table XII. Longitudinal Response of BJ Balloon With Tail Size Variation

Trim Angle Deg.	Tail Size	Case No.	Balloon Displacements From Equilibrium			Cable Tensions At Equilibrium		Maximum Cable Tensions	
			Range Down/Up Ft.	Alt. Ft.	Pitch Deg.	At Winch Lb.	At Bridle Lb.	At Winch Lb.	At Bridle Lb.
11.0	81%	11	-61/88	70	4.6	1730	1880	3000	3550
8.5	100%	3	-52/73	82	2.9	1650	2210	2650	3210
7.4	144%	12	-50/55	40	1.3	1750	2320	2600	3170

Table XIII. Lateral Response of BJ and VEE Balloons With Tail Size Variation

Type Balloon	Tail Size	Trim Angle	Case No.	Balloon Displacements from Equilibrium			Cable Tensions at Equilibrium		Maximum Cable Tensions	
				Yaw +/- Deg.	Roll +/- Deg.	Lat. Displ. Ft.	At Winch Lb.	At Bridle Lb.	At Winch Lb.	At Bridle Lb.
BJ	81%	10.98°	32	3.4/-13.5	11/-1	420	1700	2283	1818	2400
	100%	8.5°	25	4.3/-13.8	3.1/-0.35	460	1650	2210	1680	2250
	144%	7.37°	33	6.1/-13.3	2.3/-0.6	480	2383	2901	2435	2972
VEE	100%	6.96°	37	0.5/-15	3.1/-0.4	177	4650	4805	4683	4855
	200%	7.23°	38	0 /-11	1.9/-0.2	78	4763	5904	4771	5909
	300%	7.5°	39	0 /-11	0.7/-0.1	72	4874	6017	4883	6021

Table XIV. Effect of Intermediate Altitudes on Longitudinal Response of the BJ Balloon

Case No.	Altitude Feet	Gust Velocity Ft/Sec	Balloon Displacements from Equilibrium			Cable Tensions at Equilibrium		Maximum Cable Tension	
			Range Down/Up	Alt.	Pitch	At Winch	At Bridle	At Winch	At Bridle
			Ft.	Ft.	Deg.	Lb.	Lb.	Lb.	Lb.
3	10,000	20.2	-52/73	82	2.9	1656	2210	2650	3210
14	4,000	13.6	-30/0	-10	0.6	1420	1650	2040	2260
15	1,000	7.1	-25/10	-3	0.45	980	1020	1110	1160

Table XV. Effect of Intermediate Altitudes on Lateral Response of the BJ Balloon

Case No.	Gust Velocity Ft/Sec	Alt. Ft.	Balloon Displacements from Equilibrium			Cable Tensions at Equilibrium		Maximum Cable Tensions	
			Yaw +/-	Roll +/-	Lat. Displ.	At Winch	At Bridle	At Winch	At Bridle
			Deg.	Deg.	Ft.	Lb.	Lb.	Lb.	Lb.
25	12.0	10,000	4.3/-13.8	3.1/-0.35	460	1650	2210	1680	2250
35	8.0	4,000	13.1/-27.0	2.1/-1.26	490	1422	1645	1449	1667
36	1.0	1,000	52.7/-63.3	10.2/-5.5	570	977	1031	1961	1988

Case 36 represents a nominal BJ Balloon designed for a 10,000-foot operational altitude and operating at 1,000 feet altitude. The balloon is in equilibrium with a steady headwind and then is subjected to a 1 foot/second steady lateral wind.

A lateral stability analysis of this condition is found in Reference 2 Run No. 22. Reference 2 (Figure 42) reveals an unstable mode with a frequency of 0.011 Hz. The shape of this mode is also found in Reference 2 (Figure 11) and has the following relationships between amplitudes and phase angles when the mode is normalized on the balloon yaw angle,

Coordinate	Relative * Amplitude	Phase Angle * Degree
Balloon Yaw $\psi$	1.000	0.0
Balloon Roll $\phi$	0.253	101.3
Link 1 Yaw $\sigma_1$	0.340	82.4
Link 2 Yaw $\sigma_2$	0.332	81.9
Link 3 Yaw $\sigma_3$	0.324	80.9

\* Data is taken from computer digital printout of Run 22 (this data not included in Reference 2).

The stability analyses also reveals this mode has a rise time to double amplitude of 86.2 seconds.

Turning to the computer plots for lateral case 36 (see Appendix B), the following observations are made:

- (1) Tether links are in phase and of approximately equal amplitude.
- (2) The balloon roll angle is approximately  $90^\circ$  out of phase with respect to the balloon yaw angle.
- (3) The three links are approximately 83 degrees out of phase with respect to the balloon yaw angle.
- (4) The rise time to double amplitude for the balloon yaw angle is approximately 85 seconds.
- (5) The oscillation has a period of 93 seconds (0.0108 Hz).
- (6) Observations (1) through (5) indicate that lateral case 36 is predominantly the unstable 0.011 Hz mode found in the stability analysis run 22.
- (7) It should be noted also that the oscillations appear to be diverging, as would be expected, since the 0.011 Hz mode is predominate.

In conclusion lateral case 36 indicates a nominal BJ Balloon designed for a 10,000-foot operating altitude will have lateral instability problems, if it is operated at 1,000 feet. Lateral cases 35 and 37 fly the same balloon at 4,000 and 10,000 feet and reveal no diverging motion. GAC has investigated this type of instability problems in Reference 4. In this Reference the formulation of a method of analysis to predict the instability of short tethered balloons exposed to wind was derived and experimental tests were performed on towed models to verify the analysis. As a result of this work, it can be stated that lateral instability occurs when the inverted pendulum frequency of the balloon on the tether coincides with the balloon yaw frequency. Since the pendulum frequency is inversely proportional to the square root of the tether length, it is obvious that for a certain wind velocity a critical tether length exists. It should also be mentioned that Case 36 is not a winching condition, since the cable was a fixed length in the analysis. However, it does suggest that a possible stability problem will occur when the balloon is winched through the 1,000 foot altitude level.

(6) Effects of Reduced Winds (40 Percent of Nominal Winds). The effects of reducing the steady equilibrium wind and gusts to 40 percent of nominal on response in the longitudinal and lateral planes are summarized in Table XVI. In comparing the effects of a 40 percent reduction in winds, it should be noted that the equilibrium trim angle decreased from 8.5 degrees at 100 percent of nominal wind to 2.96 degrees at 40 percent of nominal wind. The yaw response reveals no change in response, while the other responses are reduced as expected.

Table XVI. Effect of Reducing Winds on Longitudinal and Lateral Response

a) Longitudinal Response

Case No.	Wind And Gusts	Trim Angle Deg.	Balloon Displacements from Equilibrium			Cable Tensions at Equilibrium		Maximum Cable Tensions	
			Range Down/Up Ft.	Alt. Ft.	Pitch Deg.	At Winch Lb.	A Bridle Lb.	At Winch Lb.	At Bridle Lb.
3	Nominal	8.5°	-52/73	82	2.9	1650	2210	2650	3210
13	40% Nom.	2.96°	-38/0.0	8	0.63	315	875	355	910

b) Lateral Response

Case No.	Wind And Gusts	Trim Angle Deg.	Balloon Displacements from Initial Equilibrium			Cable Tension at Equilibrium		Maximum Cable Tension	
			Yaw +/- Deg.	Roll +/- Deg.	Lat. Displ. Ft.	At Winch Lb.	At Bridle Lb.	At Winch Lb.	At Bridle Lb.
25	Nominal	8.5	4.3/-13.8	3.1/-0.35	460	1650	2210	1680	2250
34	40% Nom.	2.96	4.9/-13.8	0.91/-0.07	322	316.5	871.6	321.2	874.7

(7) Effects of Nolaro versus Amgal Tethers. The effects of Nolaro and Amgal tethers on the longitudinal response of BJ type balloons are given in Table XVII. The BJ type balloons are at 10,000 feet in equilibrium with a steady head wind and then are subjected to a 20.2 ft/sec horizontal longitudinal gust of 10 seconds duration. The balloon using the Nolaro tether has a volume of 60,000 cu. ft., while the balloon using the Amgal tether has a volume of 75,000 cu. ft. The larger balloon is required because the Amgal tether is heavier than the Nolaro tether. The trim angle for both cases is 8.5°. Table XVII reveals the Nolaro system has slightly more response and smaller tether loads than the Amgal system.

Table XVII. Effect of Nolaro and Amgal Tethers on Longitudinal Response

Cable Type	Case No.	Balloon Displacements From Equilibrium			Cable Tensions At Equilibrium		Max Cable Tensions	
		Range Up/Down Ft	Alt Ft.	Pitch Deg.	Winch Lb	Bridle Lb	Winch Lb	Bridle Lb
Nolaro	3	-52/13	82	2.9	1650	2210	2650	3210
Amgal	10	-60/50	28	2.1	1880	2870	3190	4180

The effects of Nolaro and Amgal tethers on the lateral response of 60 K. Ft<sup>3</sup> and 75K. Ft<sup>3</sup> BJ type balloon systems are given in Table XVIII. The balloon systems are in equilibrium with a steady head wind and then subjected to a steady lateral horizontal gust of 12 ft/sec with a ramp rise time of three seconds. Table XVIII reveals that

- (1) Yaw and roll response of the Nolaro system are slightly larger than the response of the Amgal system
- (2) The lateral displacement of the Amgal system is 1.2 times the response of the Nolaro system
- (3) The Amgal system has larger tether loads as expected since the Amgal tether is heavier.

Table XVIII. Effect of Nolaro and Amgal Tethers on Lateral Response

Case No.	Cable Type	Trim Angle Deg.	Balloon Displacements From Initial Equilibrium			Cable Tension At Equilibrium		Max Cable Tension	
			Yaw +/- Deg.	Roll +/- Deg.	Lat Displ. Ft.	At Winch Lb	At Bridle Lb	At Winch Lb	At Bridle Lb
25	Nolaro	8.5	4.3/-14	3.1/- .35	460	1650	2210	1680	2250
31	Amgal	8.3	4 /-13	2.1/ -.4	560	1880	2872	1905	2905

(8) Effects of Payload Location. The effects of payload location on the longitudinal response of a nominal BJ balloon at 10,000 ft are given in Table XIX. Case three has the 1,000 pound payload located on the confluence point of the bridle while case sixteen has the payload mounted on the underside of the balloon. The balloons are in equilibrium with a steady head wind and then subjected to a head gust of 20.2 ft/sec with a duration of 10 seconds. Table XIX reveals the configuration with the payload at the bridle confluence point (case 3) has approximately 40 percent more longitudinal response than the payload mounted on the balloon bottom configuration. The tether loads are approximately the same for both configurations.

Table XIX. Effect of Payload Location on Longitudinal Response

Case No.	Payload Location	Balloon Displacements From Equilibrium			Cable Tension At Equilibrium		Max Cable Tension	
		Range Down/Up Ft.	Alt Ft.	Pitch Deg.	At Winch Lb.	At Bridle Lb.	At Winch Lb.	At Bridle Lb.
3	Confl.	-52 /73	82	2.9	1650	2210	2650	3210
16	Underside	-49 /56	48	2.1	1650	2210	2540	3100

(9) Effect of Winch Altitude Location. The effect of winch altitude location on the longitudinal response of a nominal BJ balloon remaining at 10,000 feet MSL is given in Table XX. The winch is located at 0.0 ft and 5,000 ft for cases 3 and 17 respectively. The balloons are in equilibrium with a steady head wind and subjected to a 20.2 ft/sec gust of 10 seconds duration. Table XX reveals that,

- (1) the range and altitude responses are reduced when the winch is at 5,000 feet,
- (2) the pitching response is slightly larger with the winch at 5,000 feet,
- (3) the tether load is maximum when the winch is at 5,000 feet.

Table XX. Effect of Winch Altitude Location on Longitudinal Response

Case No.	Winch Alt. Ft.	Balloon Displacements From Equilibrium			Cable Tension At Equilibrium		Max Cable Tension	
		Range Down/Up Ft.	Alt. Ft.	Pitch Deg.	At Winch Lb.	At Bridle Lb.	At Winch Lb.	At Bridle Lb.
3	0.0	-52 /73	82	2.9	1650	2210	2650	3210
17	5000	-20 /47	24	3.1	1940	2210	3670	3940

(10) Effects of Different Operational Altitudes. The effects of three different operational altitudes on the response of BJ type balloons are given in Table XXII. The design operational altitudes and corresponding balloon volumes are 5,000 ft. and 46,000 cu. ft., 10,000 ft. and 60,000 cu. ft., and 20,000 ft. and 500,000 cu. ft. The balloons are in equilibrium with steady head winds which vary according to wind velocity altitude profile. Longitudinal ten second duration gusts of 15.7 ft/sec, 20.2 ft/sec, and 27.3 ft/sec are applied respectively to the 5,000, 10,000, and 20,000 ft. operational altitude configurations in the longitudinal cases. Lateral three second ramp rise time steady gusts of 9 ft/sec, 12 ft/sec, and 16 ft/sec are applied respectively to the 5,000, 10,000, and 20,000 ft. operational altitude configurations in the lateral cases. Table XXI reveals that

- (1) the range displacements from equilibrium increase with an increase in operational altitude
- (2) pitch displacements from equilibrium decreases with an increase in operational altitude
- (3) the lateral responses show little change due to operational altitude
- (4) the tether load increases with altitude as expected.

Table XXI. Effect of Various Design Operational Altitudes

Case No.	Balloon Volume Ft <sup>3</sup>	Equil. Alt. Ft.	Gust* Vel. Ft/Sec	Balloon Displacement From Equilibrium			Cable Tensions At Equilibrium		Max Cable Tensions	
				Range Down/Up Ft.	Alt. Ft.	Pitch Deg.	Winch Lb.	Bridle Lb.	Winch Lb.	Bridle Lb.
8	46000	5000	15.7	-12 / 38	17	3.8	800	960	1290	1840
3	60000	10000	20.2	-52 / 73	82	2.9	1650	2210	2650	3210
9	500000	20000	27.3	-127 / 70	80	1.45	8600	15030	10820	17300

Case No.	Trim Angle Deg.	Balloon Displacements From Initial Equilibrium			Cable Tension At Equilibrium		Max Cable Tension	
		Yaw +/- Deg.	Roll +/- Deg.	Lat Displ. Ft.	At Winch Lb.	At Bridle Lb.	At Winch Lb.	At Bridle Lb.
29	5.25	3. / -14.5	3.8 / - .5	560	803	845	829	866
25	8.50	4.3 / -13.8	3.1 / - .35	460	1650	2210	1680	2250
30	8.43	5.7 / -14	3.6 / -1	670	9612	15033	9735	15217

## B. Balloon Structural Design Performance Parameters

The balloon structural design performance parameters of interest are the tensions at the winch and bridle and the translational and rotational accelerations of the balloon center of gravity. Tables XXIV and XXV list the maximum variation of these parameters from equilibrium for selected longitudinal and lateral cases. From a design limit load point of view, the values found in Table XXII represent the structural design parameters for the three balloon types subjected to longitudinal gusts of 20.2 ft/sec and 10 second duration and lateral steady gusts of 12 ft/sec.

Table XXII. Structural Design Parameters

Item Balloon Type	Translational Accelerations ~ Ft/sec <sup>2</sup>			Rotational Accelerations ~ Deg/Sec <sup>2</sup>			Cable Max. Tensions Lbs.	
	Hor.	Vert.	Lat.	Pitch	Yaw	Roll	Winch	Bridle
BJ Nom	3.8	2.6	8.3	3.4	1.9	2.8	3630	4200
VEE	3.5	2.9	3.0	5.6	1.4	1.2	12900	14000
GAC	3.1	3.8	5.0	.4	.7	.5	4850	5770

## C. Balloon Instrumentation Design Performance Parameters

The balloon instrumentation design performance parameters of interest in designing an "on-board" instrumentation package are as follows:

- (1) displacements (horizontal, vertical, and lateral)
- (2) velocities (horizontal, vertical, and lateral)
- (3) angular displacements (pitch, yaw, and roll)
- (4) angular velocities (pitch, yaw, and roll)

Tables XXIV and XXV list the maximum variation of these parameters from equilibrium for selected longitudinal and lateral cases.

From an instrumentation design point of view, the values found in Table XXIII represent the instrumentation design parameters for the three balloon types subjected to longitudinal gusts of 20.2 ft/sec and 10 second duration and lateral steady gusts of 12 ft/sec.

Table XXIII. Instrumentation Design Parameters

Item Balloon Type	Displacements Ft.			Velocity Ft/Sec			Angular Displ. Degree			Angular Velocities Deg/Sec		
	Hor.	Vert.	Lat.	Hor.	Vert.	Lat.	Pitch	Yaw	Roll	Pitch	Yaw	Roll
BJ Nom	73	82	560	6.2	3.5	16.9	2.2	13.8	3.9	1.14	1.74	2.2
VEE	135	80	177	9.3	4.1	11.5	4.3	15.4	3.2	1.73	2.4	1.2
GAC	60	25	506	6.6	2.1	18.5	.8	14.3	2.7	10	1.5	.5

TABLE XXIV  
MAXIMUM VARIATIONS OF STRUCTURAL AND INSTRUMENTATION DESIGN PERFORMANCE PARAMETERS  
LONGITUDINAL CASES

EFFECT		DESCRIPTION: TYPE BALLOON	GUST	CASE NUMBER	CHANGE IN PITCH DEG	PITCH VELOCITY DEG/SEC	PITCH ACC. DEG/SEC <sup>2</sup>	HOR. DISP. FT.	HOR. VEL. FT/SEC	HOR. ACC. FT/SEC <sup>2</sup>	VERT. DISP. FT.	VERT. VEL. FT/SEC	VERT. ACC. FT/SEC <sup>2</sup>	MAX. TETHER WINCH LB.	LOADS BRIDLE LB.
GUST DURATION	2 Sec.	BJ Nominal	20.2 Ft/Sec	2	1.89	1.14	3.09	16	-4.13	-3.09	15	3.25	2.29	2250	2830
	10 Sec.			3	2.24	1.14	3.09	73	-6.22	-3.09	82	3.47	2.29	2650	3210
	20 Sec.			4	4.73	1.14	3.09	146	9.34	-3.09	121	5.12	2.29	3180	3740
TAIL SIZE	81%	BJ Nominal	20.2 Ft/Sec	11	4.59	2.15	5.18	88	-7.09	-3.80	70	4.13	2.21	3000	3550
	100%			12	2.24	1.14	3.09	73	-6.22	-3.09	82	3.47	2.29	2650	3210
	144%			12	1.29	.63	1.77	55	-5.46	-2.36	40	2.96	2.77	2600	3170
OPER. ALTITUDE	5000 Ft	BJ Type	15.7 Ft/Sec 10 Sec	8	3.79	.93	2.04	38	3.77	-2.06	17	1.18	.78	1290	1840
	1000 Ft			3	4.73	1.14	3.09	73	-6.22	-3.09	82	3.47	2.29	2650	3210
	20,000 Ft			9	1.42	.62	1.31	70	-12.1	-2.53	80	4.88	2.37	10,820	17,300
TRIM ANGLE	$\alpha = 7.0^\circ$	Vec	20.2 Ft/Sec 10 Sec.	18	3.78	1.73	5.59	119	9.32	-3.30	60	3.56	2.92	10,100	11,300
	$\alpha = 5.0^\circ$			19	4.77	1.70	5.50	135	9.10	-3.38	80	4.11	2.65	7500	8600
	$\alpha = 9.1^\circ$			20	3.34	1.62	5.35	105	9.24	-3.51	40	2.98	2.93	12,900	14,000
TRIM ANGLE	$\alpha = 7.9^\circ$	GAC	20.2 Ft/Sec 10 Sec.	21	.68	.097	.31	48	-5.78	-2.04	20	2.00	3.28	3940	4830
	$\alpha = 6.0^\circ$			22	.75	.092	.35	60	-6.58	-2.31	20	1.81	2.74	3150	4000
	$\alpha = 10.0^\circ$			23	.40	.103	.14	40	5.21	-1.88	25	2.10	3.75	4850	5770
TRIM ANGLE	$\alpha = 8.5$	BJ Nominal	20.2 Ft/Sec 10 Sec.	3	2.24	1.14	3.09	73	-6.22	-3.09	82	3.47	2.29	2650	3210
	$\alpha = 6.5$			6	2.8	1.04	2.65	65	-6.85	-3.02	65	3.40	1.87	2070	2610
	$\alpha = 10.5$			7	2.9	1.24	3.44	75	-5.77	-3.11	55	3.42	2.64	3220	3800

TABLE XXV  
MAXIMUM VARIATIONS OF STRUCTURAL AND INSTRUMENTATION DESIGN PERFORMANCE PARAMETERS  
LATERAL CASES

EFFECT	DESCRIPTION TYPE BALLOON	GUST	CASE NUMBER	CHANGE IN YAW DEG.	YAW VELOCITY DEG/SEC	YAW ACC. DEG/SEC. <sup>2</sup>	CHANGE IN ROLL DEG.	ROLL VELOCITY DEG/SEC	ROLL ACC. DEG/SEC. <sup>2</sup>	LATERAL DISPL. FT.	LATERAL VELOCITY FT/SEC	LATERAL ACC. FT/SEC. <sup>2</sup>	MAX. TETHER WINCH LB	LOADS BRIDLE LB
RAMP RISE TIME	1 Sec 3 Sec 5 Sec	12 Ft/Sec Steady	24	-13.8	1.74	1.86	3.88	2.63	2.83	460	16.9	8.29	1186	2258
			25	-13.8	1.19	.62	3.13	1.33	.94	460	16.8	4.83	1680	2258
			26	-13.8	.85	.37	2.10	.80	.57	460	16.6	3.29	1675	2244
TAIL SIZE	81% 100% 141%	12 Ft/Sec Steady	32	-13.5	.74	.70	10.95	4.94	3.63	420	15.9	4.10	1818	2400
			25	-13.8	1.19	.62	3.13	1.33	.94	460	16.8	4.83	1680	2250
			33	-13.4	1.77	.84	2.33	.90	.57	480	20.4	5.96	2435	2972
OPER ALTITUDE	5000 Ft 10,000 Ft 20,000 Ft	9 Ft/Sec Steady 12 Ft/Sec Steady 16 Ft/Sec Steady	29	-19.0	1.00	.66	5.18	2.24	1.68	560	15.8	4.18	829	866
			25	-13.8	1.19	.62	3.13	1.33	.94	460	16.8	4.83	1680	2250
			30	-10.6	1.08	.43	2.78	.59	.41	670	18.6	4.60	9735	15,217
GUST	10 Sec, Step Steady	12 Ft/Sec 18 Ft/Sec	28	4.38	-2.27	1.21	3.99	-3.04	3.07	161	16.9	7.80	1687	2256
			27	-20.4	1.31	.56	3.25	1.20	.85	706	25.1	5.00	1708	2285
TAIL SIZE	100% 200% 300%	12 Ft/Sec	37	-15.4	.80	.132	3.16	1.21	.67	177	11.5	2.94	4683	4855
			38	-11.1	-2.07	-.96	.98	.41	.29	78	5.36	1.97	4771	5909
			39	-10.9	-2.41	-1.35	.70	.31	.23	72	4.71	1.88	4883	6021
GUST	Steady	12 Ft/Sec	40	-14.3	1.49	.65	2.70	.47	.25	506	18.5	4.98	2735	3645

## 2. COMPARISON OF BALLOON TYPES

The BJ balloon, with ram air filled ballonet and fins, provides the smallest size tethered balloon system to fly a 1000-pound payload at 10,000 feet. However, it has the greatest downrange displacement from the ground tether point. Equilibrium tether tensions are the lowest. Longitudinal excursions around equilibrium are moderate, but lateral displacements due to side gusts are substantial as compared to the Vee-type balloon.

Generally the Vee balloon investigated has a somewhat greater angle-of-attack excursion about static equilibrium for a given input, but with the high aerodynamic lift configuration, results in less overall downrange displacement from the tether point. Lateral excursion is a minimum for this balloon type. Overall, the Vee offers the least excursion with wind variation but at the expense of relatively high tether tension. Elastic devices can be built into the suspension system to limit angle of attack and tether tension. However, analysis of elastic suspension is beyond the scope of the reported analysis. The Vee-type balloon then offers a configuration for applications where the tethered system should be nearer vertical with respect to the tether point, and where displacement from the tether point should be minimized.

The GAC single-hull balloon provides a greater aerodynamic lift and aerodynamic lift-to-drag ratio and less downrange displacement from the tether point than the BJ balloon, and not much greater than that for the Vee for the 10,000-foot altitude system (4950 feet as compared to 7377 feet for the BJ and 4594 feet for the Vee). The equilibrium cable tension is moderate (3800 pounds). Longitudinal motions of this balloon are substantially less for given input wind disturbances than for the other types. Lateral displacements are comparable to those for the BJ balloon for an equal disturbance. The first longitudinal and lateral modes of GAC single-hull balloon type are notably more stable (see Figures 31 and 51 of Reference 2) than the other balloon types

Structural and onboard payload design parameters for particular wind gust inputs are listed in Tables XXIV and XXV.

## 3. INFLUENCE OF TRIM ANGLE ON LONGITUDINAL AND LATERAL DYNAMIC BEHAVIOR

Considering the BJ balloon, longitudinal dynamic response data indicates that trim angle-of-attack does not significantly change the response of the balloon in longitudinal translation and rotation.

In view of the lateral dynamic response, analysis indicates that the two lower modes of motion are excited (i.e., pendulum motion of the balloon and tether as a whole, and balloon roll). Trim angle change does not substantially influence these modes for the BJ balloon. However, the vertical location of the confluence point affects the second mode (balloon roll). The apex closer to the balloon results in greater damping of this mode while not greatly affecting the damping of the first mode (Figure 36 of Reference 2).

Longitudinal dynamic response of the Vee balloon is somewhat more sensitive to design trim angle-of-attack. A tethered balloon system, employing the Vee balloon, should be designed to fly at moderate angle-of-attack (say 7 degrees) inasmuch as longitudinal instability tendencies exist at low angle-of-attack. This tendency is indicated in the linearized stability analysis by the lack of damping in the roots of the characteristic equation for the lowest frequency mode of motion. From the stability analysis, first and second longitudinal and lateral modes of motion for the GAC single hull balloon are stable and well damped (Figures 31 and 51 of Reference 2). The first two longitudinal modes are, respectively, a pitching motion of tether and balloon, and a pitching of the balloon. The first two lateral modes are a coupled balloon yaw and lateral link rotation, and a coupled balloon yaw and roll and lateral link rotation. These modes of motion are relatively insensitive to trim angle of attack and vertical location of the bridle confluence point. Dynamic response data also verify that longitudinal linear and angular displacements from equilibrium are relatively insensitive to trim angle-of-attack changes.

#### 4. EFFECT OF TAIL SIZE ON LONGITUDINAL AND LATERAL DYNAMIC BEHAVIOR

Tail size for the BJ balloon was varied by proportionally changing all dimensions to obtain tail area of 81%, 100% and 144% of the nominal design values. Stability analysis indicates that tail size increase to 144% is required to give longitudinal stability for the first oscillatory mode, but that all tail sizes provide lateral stability in the first lateral mode. Also, the tether dynamic load factor reduces with larger tail sizes because of reduced angle-of-attack excursions. However, increased tail sizes increase the side displacements somewhat. It appears that 100% tails should be adequate since near neutral stability is present about the equilibrium point for the first longitudinal mode, and dynamic response data does not show displacement divergence for any of the tail sizes for the 180 seconds of response that were calculated.

The Vee balloon investigation was confined to determining the effect of increasing vertical tail area only. Consequently, longitudinal dynamic characteristics are not greatly affected. The vertical tails on the lower side of the two hulls are increased in area from the 100% nominal size to 300%. An examination of the roots of the characteristic equations for lateral stability (Figure 49 of Reference 2) indicates that the larger tails give somewhat greater damping and lower frequency for the first mode, and an inverse effect for the second mode. The lateral dynamic response data indicate that lateral displacements of yaw, roll, and side motion are all reduced with the larger tail sizes. Tail areas of 200% of nominal then appears to be most desirable.

#### 5. EFFECT OF ALTITUDES INTERMEDIATE TO THE DESIGN ALTITUDE ON BEHAVIOR OF THE BJ TETHERED BALLOON SYSTEM

As the BJ tethered balloon system designed for 10,000 feet is brought to lower and lower altitudes, the wind speed it sees is reduced and the trim angle of attack changes inasmuch as the suspension bridle geometry remains unchanged. Generally, the longitudinal modes of motion become less damped at the lower altitudes. Dynamic response data indicates that longitudinal response is diminished, as might be expected, with the lower steady winds and gusts used in the analysis.

The lateral stability analysis reveals an unstable lateral first mode consisting of coupled balloon yaw and lateral displacement of the 1000-foot altitude. Generally, damping of all lateral modes is reduced substantially at the lower altitudes. A divergent lateral motion is revealed in the dynamic response analysis at 1000 feet altitude for the 10,000-foot design. Comparing dynamic response and stability data, it is concluded that the unstable first lateral mode consists of a coupled yaw lateral displacement. This mode oscillates at a frequency which is approximately equal to an inverted pendulum mode where the frequency is established by the pendulum length and the restoring forces consisting of the net buoyancy and the aerodynamic forces. The divergent motion was not revealed at the 4000-foot altitude. Design features which improve the damping of this mode, such as larger tails and/or automatically actuated stabilizing aerodynamic surfaces, are required. A more detailed investigation and analysis is required to make specific recommendations to improve the dynamic characteristics exposed by this exploratory analysis.

#### 6. EFFECTS OF REDUCED WIND ON THE BEHAVIOR OF THE BJ TETHERED BALLOON SYSTEM

The longitudinal and lateral dynamic characteristics consisting of frequencies and damping qualities change considerably as the wind is reduced. The trim angle of attack steadily decreases as wind decreases. Generally, damping of the tethered balloon system also reduces substantially as wind is reduced. As steady winds and wind gusts reduce yaw response is unchanged but other balloon motion responses reduce as might be expected.

#### 7. NOLARO VS AMGAL TETHERS

The BJ balloon system employing a NOLARO type tether offers the advantage of a smaller balloon to meet the requirements of supporting a 1000-pound payload at 10,000 feet. Dynamic response of the balloon longitudinal and lateral degrees of freedom are not greatly influenced by the different tethers with the exception of lateral displacements. Greater lateral displacements result with the system employing AMGAL. This may be attributed to the lesser lateral damping of the smaller diameter AMGAL tether. For 20,000 foot altitude designs, a single balloon tethered system can not be achieved with a reasonable size balloon using AMGAL tether material. Considering these factors, the NOLARO type tether generally will provide a more favorable tethered balloon system.

#### 8. EFFECT OF PAYLOAD LOCATION

The configuration with payload located at the confluence point of the bridle has somewhat greater longitudinal response than that with the payload located at the underside of the balloon. However, longitudinal response changes are relatively minor and need not influence a decision on payload location. Lateral dynamic response characteristics were not determined for this design variation.

#### 9. EFFECT OF WINCH ALTITUDE LOCATION

In this comparison the BJ balloon is still flown at 10,000 feet altitude, M.S.L., but the winch is at 5000 feet M.S.L. Dynamic response is somewhat larger in the longitudinal plane with the winch at 5000 feet. Lateral dynamic response characteristics were not determined for this design variation. Lateral stability analysis indicates that one of the overdamped modes becomes oscillatory when the winch is located at 5000 feet.

## 10. BJ TETHERED BALLOON SYSTEMS DESIGNED FOR VARIOUS ALTITUDES

Tethered balloon system designs for altitudes of 5000, 10,000 and 20,000 feet have been defined. As commented elsewhere, it was not possible to obtain a reasonably sized single balloon system with AMGAL tether for the 20,000 foot condition. Dynamic response analysis indicates that longitudinal displacements are somewhat reduced for higher altitude designs and lateral displacements are somewhat increased. However, substantial changes have not been observed. Dynamic load factors for tether cable design are significantly less for the higher altitude design.

Longitudinal stability analysis indicates that the second and third oscillatory modes, which are balloon pitching modes, reduce in frequency for the higher altitude designs. The lower frequencies might be somewhat attributed to the larger pitching inertia associated with the larger balloons.

It is recommended that the mathematical techniques developed be investigated further by comparing analytical predictions of the tools with experimental data. After this correlation has been completed, more comprehensive analysis of tethered balloon systems of specific interest with wind conditions and gusts to be expected in operations can be conducted.

#### REFERENCES

1. Definition of Tethered Balloon Systems, Scientific Report No. 1  
AFCRL-71-0213, 31 March 1971.
2. Investigation of Stability Characteristics of Tethered Balloon Systems,  
Scientific Report No. 2, AFCRL-71-0406, 30 July 1971.
3. Doyle, George R., Jr.: Mathematical Model for the Ascent and  
Descent of a High-Altitude Tethered Balloon; Journal of Aircraft,  
Vol. 6, No. 5, September-October 1969.
4. GER-13668, Prediction of Flight Stability of Tethered Balloons,  
Goodyear Aerospace Corporation, Akron, Ohio, February 1968

APPENDIX A

EQUATIONS OF MOTION  
FOR DYNAMIC SIMULATION

## TABLE OF CONTENTS

Section		Page
I	INTRODUCTION . . . . .	A -3
II	LONGITUDINAL EQUATIONS OF MOTION FOR SMALL ANGULAR VELOCITIES. . . . .	A -20
III	NON LINEAR LONGITUDINAL EQUATIONS OF MOTION . . . . .	A -30
IV	LATERAL EQUATIONS OF MOTION FOR SMALL ANGULAR VELOCITIES . . . . .	A -40

## SECTION I

### INTRODUCTION

In Appendix A of the Second Scientific Report\*, the equations of motion of a tethered balloon were derived in three dimensions. The initial derivation assumed that angular velocities were small so that products of angular velocities could be neglected. This assumption reduced the complexity of the equations (especially the lateral equations) by a considerable amount, but each equation remained nonlinear and coupled in each degree of freedom. It is assumed that the reader has read Ref. 2 Appendix A, Section II and has a clear understanding of the derivation of the equation of motion, for this discussion will begin with the results of that section.

Many of the terms used in this derivation are defined in the listing which follows.

\*Reference 2

<u>FORTTRAN</u>	<u>STANDARD</u>	<u>DESCRIPTION</u>	<u>UNITS</u>
AA(4,4)		A four by four array of variables used to define incremental velocities in the numerical integration	rad/sec
AAG(8)		An array of eight variables signifying the angle of the gust to the horizon corresponding to TTG(8)	deg
AALP(16)		An array of sixteen variables signifying the angle-of-attack of the balloon	rad
AALPD(16)		An array of sixteen variables signifying the angle-of-attack of the balloon	deg
AALT(8)		An array of eight variables signifying altitudes of steady state wind velocities	ft
AG	$\alpha_g$	Gust angle off the horizon interpolated from AAG(8) and TTG(8)	deg
AGR	$\alpha_g$	Gust angle off the horizon	rad
ALPB	$\alpha_B$	Angle-of-attack of balloon	rad
ALPBD	$\dot{\alpha}_B$	$d \alpha_B / dt$	rad/sec
ALPBDD	$\ddot{\alpha}_B$	$d^2 \alpha_B / dt^2$	deg/sec
ALPBDE	$\alpha_B$	Angle-of-attack of balloon	deg
ALPSL		A ratio of two angle-of-attack differences used in interpolation of aerodynamic coefficients of the balloon at some $\alpha$	
ALTSL		A ratio of two altitude differences used in interpolation of steady state wind velocities	
AXB	$a_{XB}$	The inertial force acting on the balloon along the lateral axis of the balloon	slug-ft/ sec <sup>2</sup>
AYB	$u_{YB}$	The inertial force acting on the balloon along the longitudinal axis of the balloon	slug-ft/ sec <sup>2</sup>

<u>FORTTRAN</u>	<u>STANDARD</u>	<u>DESCRIPTION</u>	<u>UNITS</u>
AZB	$a_{ZB}$	The inertial force acting on the balloon along the vertical axis of the balloon	slug-ft/sec <sup>2</sup>
BBET(8)		An array of eight variables signifying the sideslip angle of the balloon	rad
BBETD(8)		An array of eight variables signifying the sideslip angle of the balloon	deg
BETJ	$\beta$	Sideslip angle of balloon (positive-wind to the right of balloon's centerline)	rad
BETBD	$\dot{\beta}$	$d \beta / dt$	rad/sec
BETBDD	$\ddot{\beta}$	$d^2 \beta / dt^2$	deg/sec
BETBDE	$\beta$	Sideslip angle of balloon (positive-wind to the right of balloon's centerline)	deg
BETSL		A ratio of two sideslip angle differences used in interpolation of aerodynamic coefficients of the balloon at some $\beta$	
C(3)	$C_r$	Non-dimensional center-of-pressure of "r" th link	
CCDB(16)		An array of sixteen variables signifying drag coefficients of the balloon corresponding to AALPD(16)	
CCLB(16)		An array of sixteen variables signifying lift coefficients of the balloon in the longitudinal program corresponding to AALPD(16)	
CCLB(8)		An array of eight variables signifying roll moment coefficients of the balloon in the lateral program corresponding to BBETD(8)	
CCLIS(16)		An array of sixteen variables signifying lift coefficients of the balloon in the lateral program corresponding to AALPD(16)	

<u>FORTTRAN</u>	<u>STANDARD</u>	<u>DESCRIPTION</u>	<u>UNITS</u>
CCMB(16)		An array of sixteen variables signifying pitch moment coefficients of the balloon corresponding to AALPD(16)	
CCNB(8)		An array of eight variables signifying yaw moment coefficients of the balloon corresponding to BBETD(8)	
CDB	$C_{DB}$	Drag coefficients of balloon	
CDC	$C_{DC}$	Drag coefficient of link (infinite cylinder)	
CDTDB	$C_{D\dot{\theta}B}$	Balloon drag coefficient due to pitch velocity	$\text{rad}^{-1}$
CGAMB	$C \gamma_B$	$\cos \gamma_B$	
CLB	$C_{LB}$	Lift coefficient of balloon in longitudinal program	
CLB	$C_{lB}$	Balloon roll moment coefficient in lateral program	
CLLB	$C_{LB}$	Lift coefficient of balloon in lateral program	
CLPHDB	$C_{l\dot{\phi}B}$	Balloon roll moment coefficient due to roll velocity	$\text{rad}^{-1}$
CLPSDB	$C_{l\dot{\psi}B}$	Balloon roll moment coefficient due to yaw velocity	$\text{rad}^{-1}$
CLTDB	$C_{L\dot{\theta}B}$	Balloon lift coefficient due to pitch velocity	$\text{rad}^{-1}$
CME	$C_{mB}$	Balloon pitch moment coefficient	
CMTDB	$C_{m\dot{\theta}B}$	Balloon pitch moment coefficient due to pitch velocity	$\text{rad}^{-1}$
CNB	$C_{nB}$	Balloon yaw moment coefficient	
CNPHDB	$C_{n\dot{\phi}B}$	Balloon yaw moment coefficient due to roll velocity	$\text{rad}^{-1}$

<u>FORTTRAN</u>	<u>STANDARD</u>	<u>DESCRIPTION</u>	<u>UNITS</u>
CNPSDB	$C_{n\dot{\psi}B}$	Balloon yaw moment coefficient due to yaw velocity	$\text{rad}^{-1}$
COM1		Input data defining computer run	
CPHI	$C\phi$	$\cos \phi$	
CPHI2	$C^2\phi$	$\cos^2 \phi$	
CPSI	$C\psi$	$\cos \psi$	
CSIG(3)	$C\sigma_i$	$\cos \sigma_i, (i = 1, 2, 3)$	
CSIG2(3)	$C^2\sigma_i$	$\cos^2 \sigma_i, (i = 1, 2, 3)$	
CTHE	$C\theta$	$\cos \theta$	
CTHE2	$C^2\theta$	$\cos^2 \theta$	
CTPX(3)	$C(\theta + \xi_i)$	$\cos(\theta + \xi_i), (i = 1, 2, 3)$	
CTPX2(3)	$C^2(\theta + \xi_i)$	$\cos^2(\theta + \xi_i), (i = 1, 2, 3)$	
CXI(3)	$C\xi_i$	$\cos \xi_i, (i = 1, 2, 3)$	
CXI2(3)	$C^2\xi_i$	$\cos^2 \xi_i, (i = 1, 2, 3)$	
CXMX(3,3)	$C(\xi_i - \xi_j)$	$\cos(\xi_i - \xi_j), (i = 1, 2, 3; j = 1, 2, 3)$	
CYB	$C_{YB}$	Side force coefficient	
CYPHDB	$C_{y\dot{\phi}B}$	Side force coefficient of balloon due to roll velocity	$\text{rad}^{-1}$
CYPSDB	$C_{y\dot{\psi}B}$	Side force coefficient of balloon due to yaw velocity	$\text{rad}^{-1}$
DB	$d_B$	Aerodynamic reference length of balloon ( $V^{1/3}$ )	ft
DC		Diameter of tether	ft
DCH(3)	$D_{C,i}$	Horizontal aerodynamic force acting on the center-of-pressure of the "i"th link, $(i = 1, 2, 3)$	$\text{lb}_f$

<u>FORTTRAN</u>	<u>STANDARD</u>	<u>DESCRIPTION</u>	<u>UNITS</u>
DCS (3)	$D_{Csi}$	Lateral aerodynamic force acting on the center-of-pressure of the "i"th link, (i = 1,2,3)	$lb_f$
DCV (3)	$D_{CVi}$	Vertical aerodynamic force acting on the center-of-pressure of the "i"th link, (i = 1,2,3)	$lb_f$
DD (4,4)		A four by four array of variables signifying the coefficients of the second derivatives in the equations of motion	$slug-ft^2$
DRAGB	DRAGB	Aerodynamic drag acting on balloon	
DT		Integration time increment	sec
DTP		Number of integrations between data printouts	
DTP1		Number of integrations between data printouts when $DT = DT1$	
DTP2		Number of integrations between data printouts when $DT = DT2$	
DT1		Integration time increment when $T < TDTC$	sec
DT2		Integration time increment when $T \geq TDTC$	sec
DYPRB	$q_B$	Effective dynamic pressure acting on c.g. of balloon	$lb_f/ft^2$
DYPRH (4)	$q_{Hi}$	Effective dynamic pressure acting on the "i"th link hinge, (i = 1,2,3,4). The first hinge is at the winch	$lb_f/ft^2$

<u>FORTTRAN</u>	<u>STANDARD</u>	<u>DESCRIPTION</u>	<u>UNITS</u>
EE(4)		An array of four variables signifying the generalized forces plus terms containing products of angular velocities if this option is chosen. See FF	ft-lb <sub>f</sub>
EEPS(3,3)	$\epsilon_{ij}$	A three by three array representing the transformation matrix between the balloon body unit vectors and the inertia frame unit vectors	
FBHA	$F_{BHA}$	Horizontal aerodynamic forces acting on balloon	lb <sub>f</sub>
FBSA	$F_{BSA}$	Lateral aerodynamic forces acting on balloon	lb <sub>f</sub>
FBVA	$F_{BVA}$	Vertical aerodynamic forces acting on balloon	lb <sub>f</sub>
FCH(3)	$F_{CHi}$	Horizontal component of tension acting on the "i"th link, (i = 1,2,3)	lb <sub>f</sub>
FCN(3)	$F_{CNi}$	Aerodynamic force acting normal to "i"th link, (i = 1,2,3)	lb <sub>f</sub>
FCS(3)	$F_{CSi}$	Lateral component of tension acting on the "i"th link, (i = 1,2,3)	lb <sub>f</sub>
FCV(3)	$F_{CVi}$	Vertical component of tension acting on the "i"th link, (i = 1,2,3)	lb <sub>f</sub>
FF		Input variable which gives the option of including inertia terms containing products of angular velocities in the longitudinal program. If these terms are not wanted set FF = 0. . If the terms are to be included, set FF to any number except "0".	

<u>FORTTRAN</u>	<u>STANDARD</u>	<u>DESCRIPTION</u>	<u>UNITS</u>
FPHI	$F_{\phi}$	Generalized force acting on balloon's roll degree-of-freedom	ft-lb <sub>f</sub>
FPSI	$F_{\psi}$	Generalized force acting on balloon's yaw degree-of-freedom	ft-lb <sub>f</sub>
FSIG(3)	$F_{\bar{\sigma}i}$	Generalized force acting on the "i"th link's yaw degree-of-freedom, (i = 1,2,3)	ft-lb <sub>f</sub>
FTHE	$F_{\theta}$	Generalized force acting on balloon's pitch degree-of-freedom	ft-lb <sub>f</sub>
FWH		Horizontal component of tether tension acting at winch	lb <sub>f</sub>
FWS		Lateral component of tether tension acting at winch	lb <sub>f</sub>
FWV		Vertical component of tether tension acting at winch	lb <sub>f</sub>
FXI(3)	$F_{\xi i}$	Generalized force acting on the "i"th link's pitch degree-of-freedom, (i = 1,2,3)	ft-lb <sub>f</sub>
G	g	Acceleration <sub>2</sub> of gravity = 32.17 ft/sec <sup>2</sup>	ft/sec <sup>2</sup>
GAMB	$\gamma_B, \Gamma_B$	In the longitudinal program $\gamma_B$ is the relative flight path angle of the balloon in the longitudinal plane; in the lateral program $\Gamma_B$ is the relative flight path angle of the balloon in the horizontal plane	rad
GAMBD	$\dot{\gamma}_B, \dot{\Gamma}_B$	d $\gamma_B$ /dt or d $\Gamma_B$ /dt	rad/sec
GAMBDE	$\gamma_B, \Gamma_B$	See GAMB	deg
GAMBDD	$\dot{\gamma}_B, \dot{\Gamma}_B$	d $\gamma_B$ /dt or d $\Gamma_B$ /dt	deg/sec
IXB	$I_{XB}$	Apparent pitch moment of inertia of balloon	slug-ft <sup>2</sup>

<u>FORTTRAN</u>	<u>STANDARD</u>	<u>DESCRIPTION</u>	<u>UNITS</u>
IYB	$I_{YB}$	Apparent roll moment of inertia of balloon	slug-ft <sup>2</sup>
IYZB	$I_{YZB}$	Apparent product of inertia of balloon with respect to roll and yaw body axis	slug-ft <sup>2</sup>
IZB	$I_{ZB}$	Apparent yaw moment of inertia of balloon	slug-ft <sup>2</sup>
L	$\ell$	Length of one tether link	ft
LIFTB	LIFTB	Aerodynamic lift acting on balloon	lb <sub>f</sub>
LS	$L_S$	Buoyant lift of balloon = weight of displaced air	lb <sub>f</sub>
M	m	Mass of one tether link	slugs
MAL		Added mass of balloon along its longitudinal axis	slugs
MAS		Added mass of balloon along its lateral axis	slugs
MAV		Added mass of balloon along its vertical axis	slugs
ML	$M_L$	Apparent mass of balloon along its longitudinal axis. Apparent mass equals total static mass associated with the balloon plus air mass being accelerated in a particular direction.	slugs
MPHIB	$M_{\phi B}$	Aerodynamic rolling moment acting on balloon	ft-lb <sub>f</sub>
MPL	$m_{PL}$	Mass of payload-located at bridle tether connection	slugs
MPSIB	$M_{\psi B}$	Aerodynamic yawing moment acting on balloon	ft-lb <sub>f</sub>
MS	$M_S$	Apparent mass of balloon along its lateral axis	slugs
MTHB	$M_{\theta B}$	Aerodynamic pitching moment acting on balloon	ft-lb <sub>f</sub>

<u>FORTTRAN</u>	<u>STANDARD</u>	<u>DESCRIPTION</u>	<u>UNITS</u>
MV	$M_V$	Apparent mass of balloon along its vertical axis	slugs
PHI	$\phi$	Roll angle of balloon (positive-right wing down)	rad
PHID	$\dot{\phi}$	$d\phi/dt$	rad/sec
PHIDD	$\ddot{\phi}$	$d^2\phi/dt^2$	rad/sec <sup>2</sup>
PHIDDD	$\ddot{\phi}$	$d^2\phi/dt^2$	deg/sec <sup>2</sup>
PHIDDE	$\dot{\phi}$	$d\phi/dt$	deg/sec
PHIDEG	$\phi$	Roll angle of balloon (positive-right wing down)	deg
PHID2	$\phi^2$	$\phi^2$	rad <sup>2</sup> /sec <sup>2</sup>
PR		Atmospheric pressure (not used in program)	lb/ft <sup>2</sup>
PSI	$\psi$	Yaw angle of balloon (positive-nose to right)	rad
PSID	$\dot{\psi}$	$d\psi/dt$	rad/sec
PSIDD	$\ddot{\psi}$	$d^2\psi/dt^2$	rad/sec <sup>2</sup>
PSIDDD	$\ddot{\psi}$	$d^2\psi/dt^2$	deg/sec <sup>2</sup>
PSIDDE	$\dot{\psi}$	$d\psi/dt$	deg/sec
PSIDEG	$\psi$	Yaw angle of balloon (positive-nose to right)	deg
PSID2	$\psi^2$	$\psi^2$	rad <sup>2</sup> /sec <sup>2</sup>
RHOB	$\rho_B$	Air density at $Z_B$	slug/ft <sup>3</sup>
RHOC(3)	$\rho_{ci}$	Air density at $Z_{ci}$ (i=1,2,3)	slug/ft <sup>3</sup>
RHOCH(3)	$\rho_{Hi}$	Air density at $Z_{chi}$ (i=1,2,3,4)	slug/ft <sup>3</sup>
RJA	$R_{jA}$	Distance along longitudinal axis of balloon from aerodynamic reference center to bridle apex (positive toward nose)	ft

<u>FORTTRAN</u>	<u>STANDARD</u>	<u>DESCRIPTION</u>	<u>UNITS</u>
RJB	$R_{jB}$	Distance along longitudinal axis of balloon from center of buoyancy to bridle apex (positive toward nose)	ft
RJG	$R_{jg}$	Distance along longitudinal axis of balloon from center of gravity to bridle apex (positive toward nose)	ft
RJM	$R_{jm}$	Distance along longitudinal axis of balloon from dynamic mass center to bridle apex (positive toward nose)	ft
RKA	$R_{kA}$	Distance along vertical axis of balloon from aerodynamic reference center to bridle apex (positive up)	ft
RKB	$R_{kB}$	Distance along vertical axis of balloon from center of buoyancy to bridle apex (positive up)	ft
RKG	$R_{kg}$	Distance along vertical axis of balloon from center of gravity to bridle apex (positive up)	ft
RKM	$R_{km}$	Distance along vertical axis of balloon from dynamic mass center to bridle apex (positive up)	ft
SB	$S_B$	Aerodynamic reference area of balloon ( $\frac{V}{V_1}$ )	ft <sup>2</sup>
SC(3)	$S_{ci}$	Aerodynamic reference area of one tether link = $(l)(dc)$ , (i = 1,2,3)	ft <sup>2</sup>
SGAMB	$S_{\gamma_B}$	$\sin \gamma_B$	
SIG(3)	$\sigma_i$	Yaw angle of "i"th link, (i = 1,2,3) (positive-counter-clockwise looking down range)	rad
SIGD(3)	$\dot{\sigma}_i$	$d\sigma_i/dt$ , (i = 1,2,3)	rad/sec

<u>FORTTRAN</u>	<u>STANDARD</u>	<u>DESCRIPTION</u>	<u>UNITS</u>
SIGDD(3)	$\ddot{\sigma}_i$	$d^2\sigma_i/dt^2, (i = 1,2,3)$	rad/sec <sup>2</sup>
SIGDDD(3)	$\ddot{\sigma}_i$	$d^2\sigma_i/dt^2, (i = 1,2,3)$	deg/sec <sup>2</sup>
SIGDDE(3)	$\dot{\sigma}_i$	$d\sigma_i/dt, (i = 1,2,3)$	deg/sec
SIGDEG(3)	$\sigma_i$	Yaw angle of "i"th link, (i = 1,2,3) (positive- counterclockwise looking down range)	deg
SIGD2(3)	$\dot{\sigma}_i^2$	$\dot{\sigma}_i^2, (i = 1,2,3)$	rad <sup>2</sup> /sec <sup>2</sup>
SPHI	$S\phi$	$\sin \phi$	
SPHI2	$S^2\phi$	$\sin^2\phi$	
SPSI	$S\psi$	$\sin \psi$	
SSIG(3)	$S\sigma_i$	$\sin \sigma_i, (i = 1,2,3)$	
STHE	$S\theta$	$\sin \theta$	
STHE2	$S^2\theta$	$\sin^2\theta$	
STPX(3)	$S(\theta + \xi_i)$	$\sin (\theta + \xi_i), (i = 1,2,3)$	
STPX2(3)	$S^2(\theta + \xi_i)$	$\sin^2(\theta + \xi_i), (i = 1,2,3)$	
SXI(3)	$S\xi_i$	$\sin \xi_i, (i = 1,2,3)$	
SXI2(3)	$S^2\xi_i$	$\sin^2\xi_i, (i = 1,2,3)$	
SXMX(3,3)	$S(\xi_i - \xi_j)$	$\sin(\xi_i - \xi_j), (i=1,2,3; j=1,2,3)$	
S2THE	$S2\theta$	$\sin 2\theta$	
T	t	Flight time	sec
TDTC		Flight time at which DT is changed from DT1 to DT2 and DTP is changed from DTP1 to DTP2	sec
TENS(3)	$T_i$	Tension in tether at top of "i"th link, (i = 1,2,3)	lb <sub>f</sub>
TENSW	$T_w$	Tension in tether at winch	lb <sub>f</sub>

<u>FORTTRAN</u>	<u>STANDARD</u>	<u>DESCRIPTION</u>	<u>UNITS</u>
TETH		Total length of tether	ft
THE	$\theta$	Pitch angle of balloon (positive-nose up)	rad
THED	$\dot{\theta}$	$d\theta/dt$	rad/sec
THEDD	$\ddot{\theta}$	$d^2\theta/dt$	rad/sec <sup>2</sup>
THEDDD	$\ddot{\theta}$	$d^2\theta/dt$	deg/sec <sup>2</sup>
THEDDE	$\dot{\theta}$	$d\theta/dt$	deg/sec
THEDEG	$\theta$	Pitch angle of balloon (positive-nose up)	deg
THED2	$\dot{\theta}^2$	$\dot{\theta}^2$	rad <sup>2</sup> /sec <sup>2</sup>
THEODE	$\theta_o$	Equilibrium pitch angle of balloon	deg
TSL		A ratio of two time differences used in inter- polation of gust velocities and gust angles	
TTG(8)		An array of eight variables signifying the time history of the gust	sec
TTT		Flight time at which computer simulation ends	sec
VBR	$V_{BR}$	Relative velocity of balloon's c.g. with respect to the air	ft/sec
VC(3)	$V_{ci}$	Relative velocity of the c.p. of the "i"th link with re- spect to the air, (i=1,2,3)	ft/sec
VG	$V_g$	Gust velocity	ft/sec
VGH	$V_{gH}$	Component of gust in $Y_B$ direction	ft/sec
VGS	$V_{gs}$	Component of gust in $X_B$ direction	ft/sec

<u>FORTTRAN</u>	<u>STANDARD</u>	<u>DESCRIPTION</u>	<u>UNITS</u>
VGW	$V_{gv}$	Component of gust in $Z_B$ direction	ft/sec
VHR(4)	$V_{Hri}$	Relative wind velocity of "i"th link hinge in the $Y_B$ direction, (i=1,2,3,4). The first hinge is at the winch.	ft/sec
VS		Speed of sound (not used in program)	ft/sec
VVG(8)		An array of eight variables signifying gust velocity acting on balloon and corresponding to TTG(8)	ft/sec
VVW(8)		An array of eight variables signifying steady state wind profile and corresponding to AALT(8)	ft/sec
VW	$V_w$	Steady state wind velocity at $Z_B$	ft/sec
VWC(3)	$V_{wci}$	Steady state wind velocity at $Z_{ci}$ , (i = 1,2,3)	ft/sec
VWH(4)	$V_{wHi}$	Steady state wind velocity at $Z_{cHi}$ , (i = 1,2,3,4)	ft/sec
WB	$W_B$	Total weight of balloon - includes balloon and bridle material, and enclosed gases	lbs
WPL		Weight of payload located at bridle tether connection	lb
WTC		Weight of tether	lb
XB	$X_B$	Lateral displacement of balloon's c.g. in the inertia reference frame	ft
XBD	$\dot{X}_B$	$dx_B/dt$	ft/sec
XEDD	$\ddot{X}_B$	$d^2x_B/dt^2$	ft/sec <sup>2</sup>
XBDDR		Lateral acceleration of balloon's c.g. relative to air	ft/sec <sup>2</sup>

<u>FORTTRAN</u>	<u>STANDARD</u>	<u>DESCRIPTION</u>	<u>UNITS</u>
XBDR		Lateral velocity of balloon's c.g. relative to air	ft/sec
XCD(3)	$\dot{X}_{ci}$	Lateral velocity of c.p. of "i"th link, (i = 1,2,3)	ft/sec
XCDD(3)	$\ddot{X}_{ci}$	Lateral acceleration of c.g. of "i"th link, (i = 1,2,3)	ft/sec <sup>2</sup>
XCHD(4)	$\dot{X}_{cHi}$	Lateral velocity of "i"th link hinge, (i = 1,2,3,4). The first hinge is at the winch	ft/sec
XI(3)	$\xi_i$	Pitch angle of "i"th link, (i = 1,2,3) (positive-rotated up from the horizon, clockwise)	rad
XID(3)	$\dot{\xi}_i$	$d\xi_i/dt$ , (i = 1,2,3)	rad/sec
XIDD(3)	$\ddot{\xi}_i$	$d^2\xi_i/dt^2$ , (i = 1,2,3)	rad/sec <sup>2</sup>
XIDDDE(3)	$\ddot{\xi}_i$	$d^2\xi_i/dt^2$ , (i = 1,2,3)	deg/sec <sup>2</sup>
XIDDEG(3)	$\dot{\xi}_i$	$d\xi_i/dt$ , (i = 1,2,3)	deg/sec
XIDEG(3)	$\xi_i$	Pitch angle of "i"th link, (i = 1,2,3) (positive-rotated up from the horizon, clockwise)	deg
XID2(3)	$\dot{\xi}_i^2$	$\dot{\xi}_i^2$ (i = 1,2,3)	rad <sup>2</sup> /sec <sup>2</sup>
XIODEG(3)	$\xi_{io}$	Equilibrium pitch angle of "i"th link, (i = 1,2,3)	deg
XPLDD	$\ddot{X}_{PL}$	Lateral acceleration of payload	ft/sec <sup>2</sup>
YB	$Y_B$	Down range displacement of balloon's c.g. in the inertia reference frame	ft
YBD	$\dot{Y}_B$	$dY_B/dt$	ft/sec
YBDD	$\ddot{Y}_B$	$d^2Y_B/dt^2$	ft/sec <sup>2</sup>

<u>FORTTRAN</u>	<u>STANDARD</u>	<u>DESCRIPTION</u>	<u>UNITS</u>
YBDDR		Down range acceleration of balloon's c.g. relative to air	ft/sec <sup>2</sup>
YBDR		Down range velocity of balloon's c.g. relative to air	ft/sec
YCD(3)	$\dot{Y}_{ci}$	Down range velocity of C.P. of "i"th link, (i = 1,2,3)	ft/sec
YCDD(3)	$\ddot{Y}_{ci}$	Down range acceleration of c.g. of "i"th link, (i = 1,2,3)	ft/sec
YCHD(4)	$\dot{Y}_{cHi}$	Down range velocity of "i"th link hinge, (i = 1,2,3,4) The first hinge is at the winch	ft/sec
YPLDD	$\ddot{Y}_{PL}$	Down range acceleration of payload	ft/sec <sup>2</sup>
ZB	$Z_B$	Altitude of balloons c.g. in inertia reference frame	ft
ZBD	$\dot{Z}_B$	$dZ_B/dt$	ft/sec
ZBDD	$\ddot{Z}_B$	$d^2Z_B/dt^2$	ft/sec <sup>2</sup>
ZBDDR		Vertical acceleration of balloon's c.g. relative to air	ft/sec <sup>2</sup>
ZBDR		Vertical velocity of balloon's c.g. relative to air	ft/sec
ZC(3)	$Z_{ci}$	Altitude of C.P. of "i"th link, (i = 1,2,3)	ft
ZCD(3)	$\dot{Z}_{ci}$	Vertical velocity of C.P. of "i"th link, (i = 1,2,3)	ft/sec
ZCDD(3)	$\ddot{Z}_{ci}$	Vertical acceleration of c.g. of "i"th link, (i = 1,2,3)	ft/sec <sup>2</sup>
ZCH(4)	$Z_{cHi}$	Altitude of "i"th link hinge, (i = 1,2,3,4) The first hinge is at the winch	ft

<u>FORTTRAN</u>	<u>STANDARD</u>	<u>DESCRIPTION</u>	<u>UNITS</u>
ZCHD(4)	$\dot{z}_{chi}$	Vertical velocity of "i"th link hinge, (i = 1,2,3,4) The first hinge is at the winch	ft/sec
ZPLDD	$\ddot{z}_{PL}$	Vertical acceleration of payload	ft/sec <sup>2</sup>

## SECTION II

### LONGITUDINAL EQUATIONS OF MOTION FOR SMALL ANGULAR VELOCITIES

First consider the longitudinal equation of motion. The dependent variables (see Figure 1) are  $\theta$  (pitch of the balloon) and  $\xi_r$  (pitch of the "r" th link), where r is a particular link.

The appropriate equations of motion in the Second Scientific Report, Appendix A, Section II are (80) and (97). Since these equations were derived in three dimensions, they contain the lateral degrees-of-freedom,  $\psi$  (yaw of balloon),  $\phi$  (roll of balloon), and  $\sigma_r$  (yaw of "r" th link). It will be assumed that the balloon remains in equilibrium in the lateral degrees-of-freedom. Therefore,  $\psi \equiv \phi \equiv \sigma_r \equiv 0$ . With this assumption Equation (80) and (97) are rewritten as follows:

$$M_L \langle \ell R_{Lm} \sum_{i=1}^N \{ \ddot{\xi}_i [S \xi_i C \theta + C \xi_i S \theta] \} + R_{Lm}^2 \ddot{\theta} \rangle + M_V \langle \ell R_{Vm} \sum_{i=1}^N \{ -\ddot{\xi}_i [-S \xi_i S \theta + C \xi_i C \theta] \} + R_{Vm}^2 \ddot{\theta} \rangle + I_{XB} \ddot{\theta} = F_\theta \quad (1)$$

$$\begin{aligned} & \sum_{n=1}^N m \ell^2 \left\{ \sum_{i=1}^{n-1} \ddot{\xi}_i C(\xi_n - \xi_i) + \frac{1}{2} \ddot{\xi}_n C(\xi_n - \xi_n) \right\} + \frac{m}{2} \ell^2 \sum_{i=1}^{n-1} \ddot{\xi}_i C(\xi_n - \xi_i) + \frac{m}{3} \ell^2 \ddot{\xi}_n \\ & + m_{PL} \ell^2 \sum_{i=1}^N \ddot{\xi}_i C(\xi_n - \xi_i) + M_L \langle \ell^2 \sum_{i=1}^N \ddot{\xi}_i [S \xi_i C \theta + C \xi_i S \theta] [S \xi_n C \theta + C \xi_n S \theta] \\ & + R_{Lm} \ell \ddot{\theta} [S \xi_n C \theta + C \xi_n S \theta] \rangle + M_V \langle \ell^2 \sum_{i=1}^N \ddot{\xi}_i [-S \xi_i S \theta + C \xi_i C \theta] [-S \xi_n S \theta + C \xi_n C \theta] \\ & - R_{Vm} \ell \ddot{\theta} [-S \xi_n S \theta + C \xi_n C \theta] \rangle = F_{\xi_n} \end{aligned} \quad (2)$$

where  $S \theta = \sin \theta$  and  $C \theta = \cos \theta$ , etc.

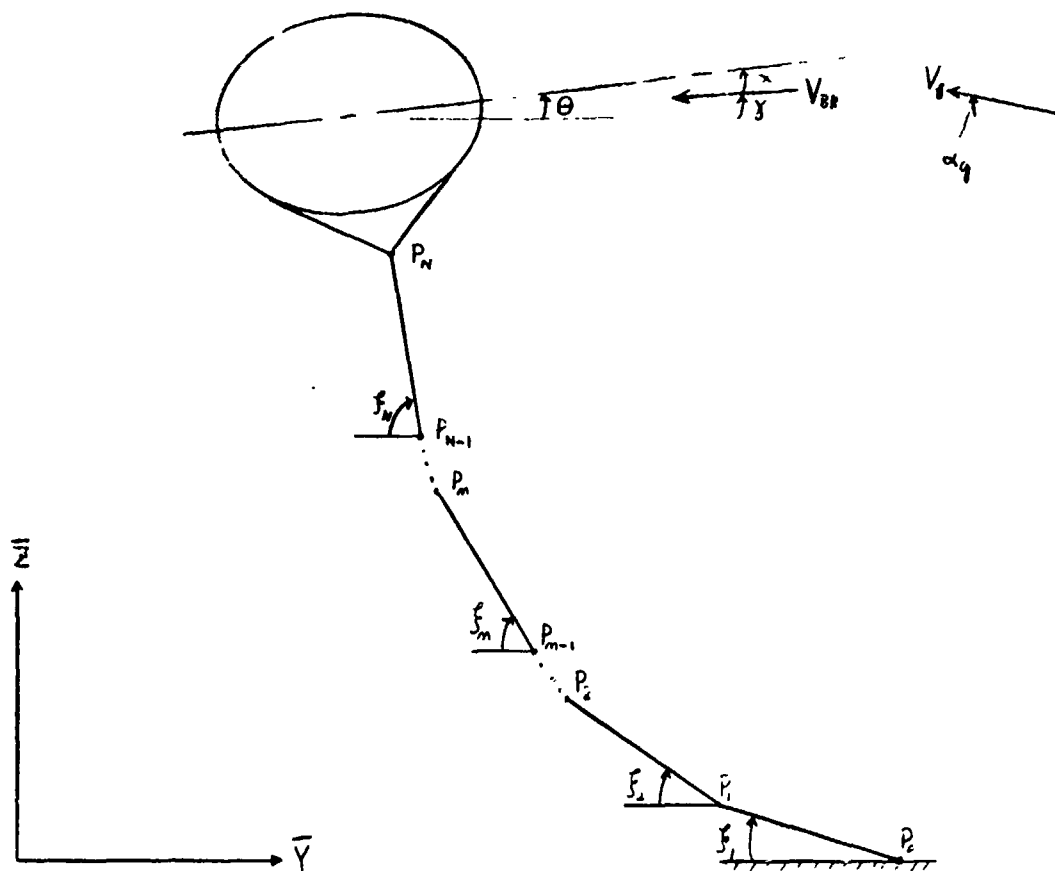


FIGURE 1 - BALLOON TETHER MODEL IN LONGITUDINAL PLANE

In order to solve Equations (1) and (2), it will be assumed that  $N = 3$ . Rewrite Equations (1) and (2) with this assumption and substitute in the trigometric identities for the sums of angles.

$$\begin{aligned}
 & [M_L R_{Lm}^2 + M_V R_{Vm}^2 + I_{V0}] \ddot{\theta} + [M_L L R_{Lm} s(\beta_1 + \theta) - M_V L R_{Vm} c(\beta_1 + \theta)] \ddot{\beta}_1 \\
 & + [M_L L R_{Lm} s(\beta_2 + \theta) - M_V L R_{Vm} c(\beta_2 + \theta)] \ddot{\beta}_2 \\
 & + [M_L L R_{Lm} s(\beta_3 + \theta) - M_V L R_{Vm} c(\beta_3 + \theta)] \ddot{\beta}_3 = F_\theta
 \end{aligned} \tag{3}$$

For  $r = 1$ ,

$$\begin{aligned}
 & [M_L \ell R_{Lm} s(\beta_1 + \theta) - M_V \ell R_{Vm} c(\beta_1 + \theta)] \ddot{\theta} \\
 & + \ell^2 \left[ \frac{7m}{3} + m_{pL} + M_L s^2(\beta_1 + \theta) + M_V c^2(\beta_1 + \theta) \right] \ddot{\beta}_1 \\
 & + \ell^2 \left[ \left( \frac{3m}{2} + m_{pL} \right) c(\beta_1 - \beta_2) + M_L s(\beta_1 + \theta) s(\beta_2 + \theta) + M_V c(\beta_1 + \theta) c(\beta_2 + \theta) \right] \ddot{\beta}_2 \\
 & + \ell^2 \left[ \left( \frac{m}{2} + m_{pL} \right) c(\beta_1 - \beta_3) + M_L s(\beta_1 + \theta) s(\beta_3 + \theta) + M_V c(\beta_1 + \theta) c(\beta_3 + \theta) \right] \ddot{\beta}_3 = F_{\beta_1} \quad (4)
 \end{aligned}$$

For  $r = 2$ ,

$$\begin{aligned}
 & [M_L \ell R_{Lm} s(\beta_2 + \theta) - M_V \ell R_{Vm} c(\beta_2 + \theta)] \ddot{\theta} \\
 & + \ell^2 \left[ \left( \frac{3m}{2} + m_{pL} \right) c(\beta_1 - \beta_2) + M_L s(\beta_1 + \theta) s(\beta_2 + \theta) + M_V c(\beta_1 + \theta) c(\beta_2 + \theta) \right] \ddot{\beta}_1 \\
 & + \ell^2 \left[ \frac{4m}{3} + m_{pL} + M_L s^2(\beta_2 + \theta) + M_V c^2(\beta_2 + \theta) \right] \ddot{\beta}_2 \\
 & + \ell^2 \left[ \left( \frac{m}{2} + m_{pL} \right) c(\beta_2 - \beta_3) + M_L s(\beta_2 + \theta) s(\beta_3 + \theta) + M_V c(\beta_2 + \theta) c(\beta_3 + \theta) \right] \ddot{\beta}_3 = F_{\beta_2} \quad (5)
 \end{aligned}$$

For  $r = 3$ ,

$$[M_L \ell R_{Lm} s(\beta_3 + \theta) - M_V \ell R_{Vm} c(\beta_3 + \theta)] \ddot{\theta}$$

$$\begin{aligned}
& l^2 \left[ \left( \frac{m}{2} + m_{PL} \right) c(\beta_1 - \beta_3) + M_L s(\beta_1 + \theta) s(\beta_3 + \theta) + M_V c(\beta_1 + \theta) c(\beta_3 + \theta) \right] \ddot{\beta}_1 \\
& l^2 \left[ \left( \frac{m}{2} + m_{PL} \right) c(\beta_2 - \beta_3) + M_L s(\beta_2 + \theta) s(\beta_3 + \theta) + M_V c(\beta_2 + \theta) c(\beta_3 + \theta) \right] \ddot{\beta}_2 \\
& + l^2 \left[ \frac{m}{3} + m_{PL} + M_L s^2(\beta_3 + \theta) + M_V c^2(\beta_3 + \theta) \right] \ddot{\beta}_3 = F_{\beta_3}
\end{aligned} \tag{6}$$

The generalized forces ( $F_\theta$ ,  $F_{\beta_1}$ ,  $F_{\beta_2}$ ,  $F_{\beta_3}$ ) were derived in Section III, Appendix A of the Second Scientific Report\*. The following necessary equations are taken from that section.

$$\begin{aligned}
F_\theta = & [L_S R_{LB} - W_B R_{Lg} + F_{BVA} R_{LA} - F_{BHA} R_{JA}] S\theta \\
& + [-L_S R_{JB} + W_B R_{Jg} - F_{BVA} R_{JA} - F_{BHA} R_{JA}] C\theta + M_{\theta B}
\end{aligned} \tag{7}$$

$$\begin{aligned}
F_{\beta_1} = & [L_S - W_B + F_{BVA} - m_{PL} g - D_{PLV} - \frac{5}{2} mg] l C \beta_1 \\
& + [-F_{BHA} - D_{PLH}] l S \beta_1 - l C_1 [D_{CH1} S^2 \beta_1 + D_{CV1} C^2 \beta_1] \\
& - l [(D_{CH2} S^2 \beta_2 + D_{CV2} C^2 \beta_2) c(\beta_1 - \beta_2) + (D_{CH3} S^2 \beta_3 \\
& + D_{CV3} C^2 \beta_3) c(\beta_1 - \beta_3)]
\end{aligned} \tag{8}$$

$$F_{P_2} = \left[ L_2 - W_B + F_{BVA} - m_{PL} g - D_{PLV} - \frac{3m}{2} g \right] \ell C \beta_2 + \left[ -F_{BHA} - D_{PLH} \right] \ell S \beta_2 \\ - \ell \left\{ C_2 \left[ D_{CH2} S^2 \beta_2 + D_{CV2} C^2 \beta_2 \right] + \left[ D_{CH3} S^2 \beta_3 + D_{CV3} C^2 \beta_3 \right] C (\beta_2 - \beta_3) \right\} \quad (9)$$

$$F_{P_3} = \left[ L_3 - W_B + F_{BVA} - m_{PL} g - D_{PLV} - \frac{m}{2} g \right] \ell C \beta_3 \\ + \left[ -F_{BHA} - D_{PLH} \right] \ell S \beta_3 - \ell C_3 \left[ D_{CH2} S^2 \beta_2 + D_{CV2} C^2 \beta_2 \right] \quad (10)$$

$$F_{BHA} = \text{DRAGB} (C \delta_B) + \text{LIFTB} (S \delta_B) \quad (11)$$

$$F_{BVA} = \text{LIFTB} (C \delta_B) - \text{DRAGB} (S \delta_B) \quad (12)$$

$$\text{DRAGB} = q_B S_B \left[ C_{LB} + C_{L\dot{\theta}_B} \left( \frac{d_B}{V_{BR}} \right) \dot{\theta} \right] \quad (13)$$

$$\text{LIFTB} = q_B S_B \left[ C_{DB} + C_{D\dot{\theta}_B} \left( \frac{d_B}{V_{BR}} \right) \dot{\theta} \right] \quad (14)$$

$$M_{BB} = q_B S_B d_B \left[ C_{m\theta} + C_{m\dot{\theta}_B} \left( \frac{d_B}{V_{BR}} \right) \dot{\theta} \right] \quad (15)$$

$$D_{CHi} = \frac{1}{2} \rho_{ci} S_{ci} C_{DC} V_{ci} (\dot{V}_{Wci} + \dot{Y}_{ci}) \quad (16)$$

$$D_{CVi} = \frac{1}{2} \rho_{ci} S_{ci} C_{DC} V_{ci} (\dot{Z}_{ci}) \quad (17)$$

The drag on the payload is neglected.

$$D_{PLH} = D_{PLV} = 0 \quad (18)$$

$$C_n = \frac{1}{3} \left( \frac{g_{Hn} + 2g_{Hn+1}}{g_{Hn} + g_{Hn+1}} \right) \quad (19)$$

$$g_B = \frac{1}{2} \rho_B V_{BR}^2 \quad (20)$$

$$V_{BR}^2 = (\dot{y}_B + V_w + V_{gH})^2 + (\dot{z}_B - V_{gV})^2 \quad (21)$$

$$\gamma_B = \tan^{-1} [(\dot{z}_B - V_{gV}) / (\dot{y}_B + V_w + V_{gH})] \quad (22)$$

$$\alpha_B = \theta - \gamma_B \quad (23)$$

See Figure 1

In order to show the load distribution along the tether at any time, the tension in the tether is calculated at the end of each link. This is done by summing forces in the vertical and horizontal directions at each hinge. Before summing forces, consider the inertia forces acting on the balloon. Figure 2 shows the balloon and with the apparent inertia forces acting along and normal to the centerline.

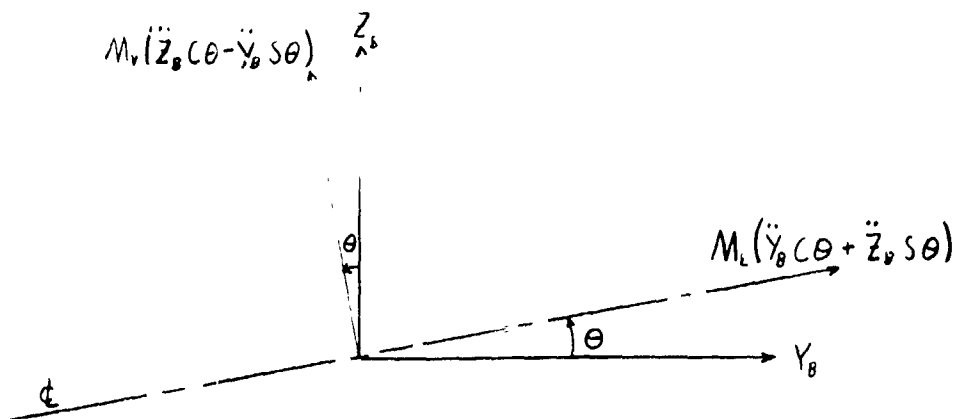


FIGURE 2 INERTIA FORCES ACTING ON BALLOON IN LONGITUDINAL PLANE

$$\begin{aligned}\sum F_x &= M_v (\ddot{z}_B \cos \theta - \ddot{y}_B \sin \theta) \cos \theta + M_L (\dot{y}_B \cos \theta + \dot{z}_B \sin \theta) \sin \theta \\ &= \ddot{z}_B [M_v \cos^2 \theta + M_L \sin^2 \theta] + \ddot{y}_B [M_L - M_v] \sin \theta \cos \theta\end{aligned}\quad (24)$$

$$\begin{aligned}\sum F_y &= M_L (\ddot{y}_B \cos \theta + \ddot{z}_B \sin \theta) \cos \theta - M_v (\ddot{z}_B \cos \theta - \ddot{y}_B \sin \theta) \sin \theta \\ &= \ddot{z}_B [M_L - M_v] \sin \theta \cos \theta + \ddot{y}_B [M_v \sin^2 \theta + M_L \cos^2 \theta]\end{aligned}\quad (25)$$

The summation of forces acting on the balloon are:

$$\sum F_z = L_s + F_{BVA} - W_B - T_{BV}\quad (26)$$

$$\sum F_y = T_{BH} - F_{BHA}\quad (27)$$

where:  $T_{BV}$  and  $T_{BH}$  are the vertical and horizontal tension forces at the bridle-tether confluence point respectively.

Note that the payload forces are not included in these summations, but will be included shortly. Equating Equations (24) and (26), and Equations (25) and (27) gives the following expressions for  $T_{BV}$  and  $T_{BH}$ .

$$T_{BV} = L_s + F_{BVA} - W_B - \ddot{z}_B [M_v \cos^2 \theta + M_L \sin^2 \theta] - \ddot{y}_B [M_L - M_v] \sin \theta \cos \theta\quad (28)$$

$$T_{BH} = F_{BHA} + \ddot{z}_B [M_L - M_v] \sin \theta \cos \theta + \ddot{y}_B [M_v \sin^2 \theta + M_L \cos^2 \theta]\quad (29)$$

Equations (28) and (29) give the tensions on the tether at a point just above the payload. Figure 3 shows the payload with all forces acting on it.

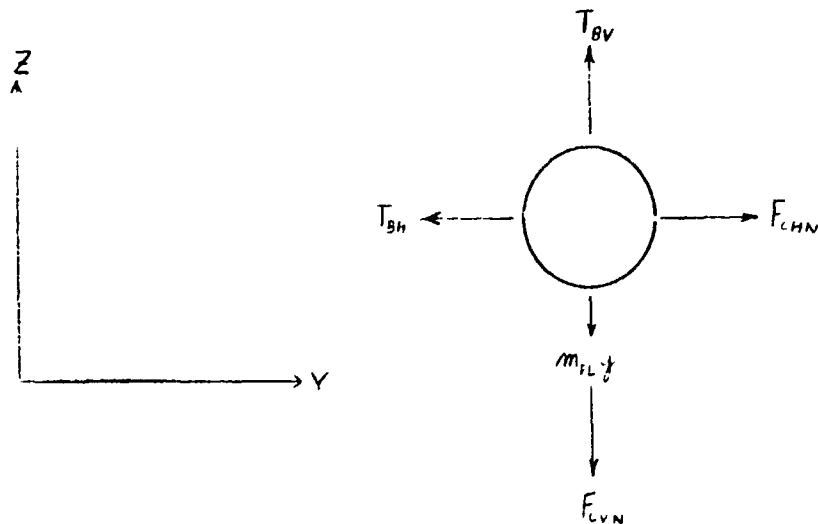


FIGURE 3 APPLIED FORCES ACTING ON PAYLOAD IN LONGITUDINAL PLANE

Summing forces in the vertical and horizontal directions gives:

$$\sum F_z = m_{PL} \ddot{z}_{PL} = T_{BV} - m_{PL} g - F_{CVN} \quad (30)$$

$$\sum F_y = m_{PL} \ddot{y}_{PL} = F_{CHN} - T_{BH} \quad (31)$$

where  $F_{CVN}$  and  $F_{CHN}$  are the vertical and horizontal components of tension at the top of the tether below the payload. Substituting Equation (28) into (30) and (29) into (31) and solving for the vertical and horizontal components of tension at the top of the tether results in the following equations.

$$F_{CVN} = L_S + F_{BVA} - W_B - \ddot{z}_B [M_V C^2 \theta + M_L S^2 \theta]$$

$$-\ddot{y}_B [M_L - M_V] S \theta C \theta - m_{PL} g - m_{PL} \ddot{z}_{PL} \quad (32)$$

$$F_{CHN} = F_{BHA} + \ddot{z}_B [M_L - M_V] S \theta C \theta + \ddot{y}_B [M_V S^2 \theta + M_L C^2 \theta] + m_{PL} \ddot{y}_{PL} \quad (33)$$

The total tension at the top of the tether is:

$$T_N = \sqrt{F_{CHN}^2 + F_{CVN}^2} \quad (34)$$

Figure 4 shows the applied forces acting on the "N"th link

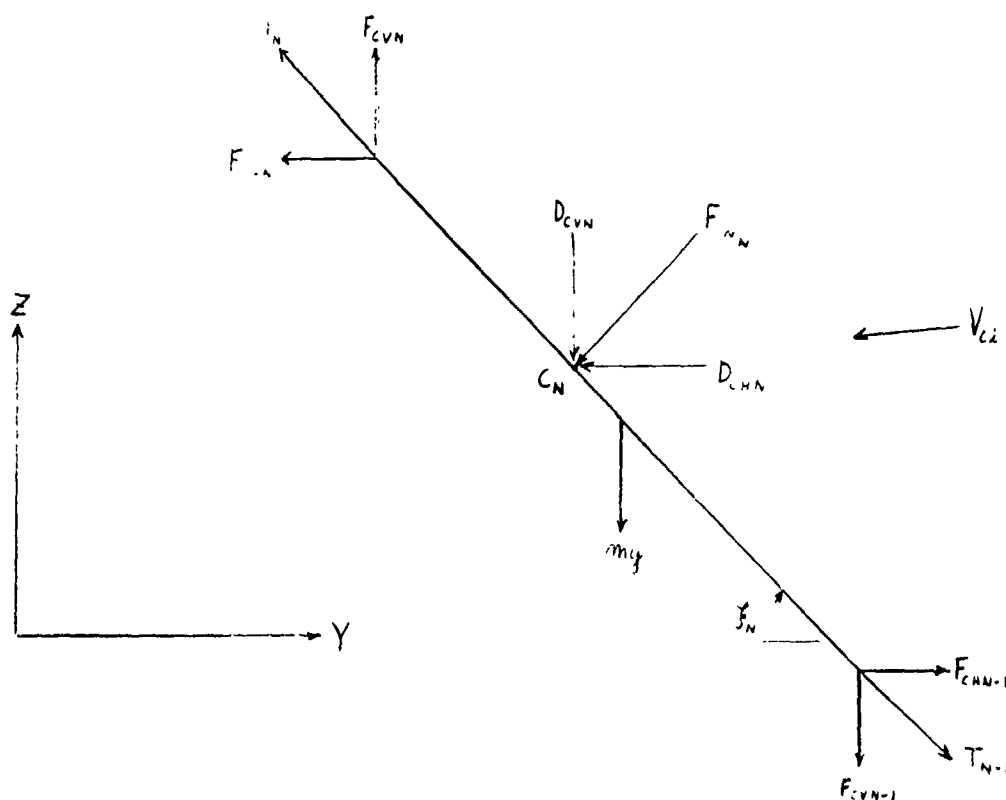


FIGURE 4 APPLIED FORCES ACTING ON "N"TH LINK IN LONGITUDINAL PLANE

The aerodynamic forces  $D_{CHN}$  and  $D_{CVN}$  are the horizontal and vertical components respectively of the normal aerodynamic force ( $F_{CN_N}$ ) acting at the c.p. of the "N"th link due to the relative motion of the "N"th link with respect to the air. This relative motion takes into account both the steady state wind and the horizontal and vertical inertial velocities of the link. Expressions for  $D_{CHN}$  and  $D_{CVN}$  are given in Equations (16) and (17). The normal force acting on the link is given by:

$$F_{CN_N} = D_{CHN} S^2 \beta_N + D_{CVN} C^2 \beta_N \quad (35)$$

Summing vertical and horizontal forces on the "N" link:

$$\Sigma F_z = m \ddot{z}_{CN} = F_{CVN} - F_{CN_N} C \beta_N - mg - F_{CVN-1} \quad (36)$$

$$\Sigma F_y = m \ddot{y}_{CN} = -F_{CHN} - F_{CN_N} S \beta_N + F_{CHN-1} \quad (37)$$

Solving for the tension forces at the bottom of the "N"th link gives the following equations.

$$F_{CVN-1} = F_{CVN} - F_{CN_N} C \beta_N - mg - m \ddot{z}_{CN} \quad (38)$$

$$F_{CHN-1} = F_{CHN} + F_{CN_N} S \beta_N + m \ddot{y}_{CN} \quad (39)$$

$$F_{CVN-1} = F_{CVN} - F_{CN_N} C \beta_N - m(g + \ddot{z}_{CN}) \quad (40)$$

$$F_{CHN-1} = F_{CHN} + F_{CN_N} S \beta_N + m \ddot{y}_{CN} \quad (41)$$

$$T_{N-1} = \sqrt{F_{CVN-1}^2 + F_{CHN-1}^2} \quad (42)$$

The tension at the winch is found by setting  $n = 1$ .

### SECTION III

#### NON LINEAR LONGITUDINAL EQUATIONS OF MOTION

Section II of this Appendix contains the longitudinal equations of motion of a tethered balloon if angular velocities are small and products of angular velocities are negligible. This assumption was made in the derivation in Appendix A of the Second Scientific Report\*. It is now desirable to examine the equations of motion when large angular velocities are allowed. As in Section II, appropriate equations will be extracted from Appendix A of the Second Scientific Report\*. These equations are (41), (79) and (96). Equation (41) is the total kinetic energy of the system: Equation (79) and (96) are terms that are needed for Lagrange's equations. However, these equations are functions of both the longitudinal and lateral degrees-of-freedom. Therefore, before rewriting Equations (41), (79) and (96) of Appendix A\* set all lateral degrees-of-freedom equal to zero ( $\psi \equiv \phi \equiv \sigma_r \equiv 0$ ).

The total kinetic energy of the system in the longitudinal plane is:

$$\begin{aligned} T = & \sum_{n=1}^N \left[ \frac{1}{2} m (\vec{V}^{\rho_n})^2 + \frac{1}{2} m \ell^2 \dot{\xi}_n^2 \right] + \frac{1}{2} m_{\rho_L} (\vec{V}^{\rho_L})^2 \\ & + \frac{1}{2} M_L (\vec{V}^{\rho_L} \cdot \vec{j}_0)^2 + \frac{1}{2} M_V (\vec{V}^{\rho_L} \cdot \vec{k}_0)^2 + \frac{1}{2} I_{x_0} \dot{\theta}^2 \end{aligned} \quad (43)$$

where

$$\vec{V}^{\rho_n} = \ell \left[ \sum_{i=1}^{n-1} \dot{\xi}_i \vec{e}_i + \frac{1}{2} \dot{\xi}_n \vec{e}_n \right] \quad (44)$$

\*Reference 2

$$\vec{V}^{PL} = \ell \sum_{i=1}^N \dot{\beta}_i \vec{e}_i \quad (45)$$

$$\vec{V}^G = \ell \sum_{i=1}^N \dot{\beta}_i \vec{e}_i + [R_{km} \vec{j}_k - R_{jm} \vec{k}_k] \dot{\theta} \quad (46)$$

Now write Equation (79) of Appendix A\*

$$\begin{aligned} \frac{\partial \bar{T}}{\partial \dot{\theta}} = & M_L \left\{ \ell \sum_{i=1}^N \dot{\beta}_i s(\theta + \beta_i) + R_{km} \dot{\theta} \right\} R_{km} \\ & + M_V \left\{ \ell \sum_{i=1}^N \dot{\beta}_i c(\theta + \beta_i) - R_{jm} \dot{\theta} \right\} \{-R_{jm}\} + I_{s0} \dot{\theta} \end{aligned} \quad (47)$$

Rewriting Equation (96) of Appendix A\*:

$$\begin{aligned} \frac{\partial \bar{T}}{\partial \dot{\beta}_n} = & \sum_{n=1}^N m \ell^2 \left\{ \sum_{i=1}^{n-1} \dot{\beta}_i c(\beta_n - \beta_i) + \frac{1}{2} \dot{\beta}_n c(\beta_n - \beta_n) \right\} \\ & + m \ell^2 \left\{ \frac{1}{2} \sum_{i=1}^{n-1} \dot{\beta}_i c(\beta_n - \beta_i) + \frac{1}{2} \dot{\beta}_n \right\} + m_{P_n} \ell^2 \left\{ \sum_{i=1}^N \dot{\beta}_i c(\beta_n - \beta_i) \right\} \\ & + M_L \left\{ \ell^2 \sum_{i=1}^N \dot{\beta}_i s(\theta + \beta_i) + \ell R_{km} \dot{\theta} \right\} s(\theta + \beta_n) \\ & + M_V \left\{ \ell^2 \sum_{i=1}^N \dot{\beta}_i c(\theta + \beta_i) - \ell R_{jm} \dot{\theta} \right\} c(\theta + \beta_n) \end{aligned} \quad (48)$$

Langrange's equations for the system are:

$$\frac{d}{dt} \left( \frac{\partial \bar{T}}{\partial \dot{\theta}} \right) - \frac{\partial \bar{T}}{\partial \theta} = F_\theta \quad (49)$$

$$\frac{d}{dt} \left( \frac{\partial \bar{T}}{\partial \dot{\beta}_n} \right) - \frac{\partial \bar{T}}{\partial \beta_n} = F_{\beta_n} \quad (50)$$

\*Reference 2

First derive the terms in Equation (49). Using Equation (47) the following term is formed.

$$\begin{aligned} \frac{d}{dt} \left( \frac{\partial \bar{T}}{\partial \dot{\theta}} \right) = & M_L \left\{ \ell \left[ \sum_{i=1}^N \ddot{\theta}_i s(\theta + \theta_i) + \sum_{i=1}^N \dot{\theta}_i (\dot{\theta} + \dot{\theta}_i) c(\theta + \theta_i) \right] + R_{k,m} \ddot{\theta} \right\} R_{k,n} \\ & + M_V \left\{ \ell \left[ \sum_{i=1}^N \ddot{\theta}_i c(\theta + \theta_i) - \sum_{i=1}^N \dot{\theta}_i (\dot{\theta} + \dot{\theta}_i) s(\theta + \theta_i) \right] - R_{j,m} \ddot{\theta} \right\} R_{j,n} \\ & + I_{x0} \ddot{\theta} \end{aligned} \quad (51)$$

From Equation (43)

$$\begin{aligned} \frac{\partial \bar{T}}{\partial \theta} = & M_L (\bar{V}^a \cdot \bar{j}_B) \left[ \frac{\partial \bar{V}^a}{\partial \theta} \bar{j}_B + \bar{V}^a \cdot \frac{\partial \bar{j}_B}{\partial \theta} \right] \\ & + M_V (\bar{V}^a \cdot \bar{k}_B) \left[ \frac{\partial \bar{V}^a}{\partial \theta} \bar{k}_B + \bar{V}^a \cdot \frac{\partial \bar{k}_B}{\partial \theta} \right] \end{aligned} \quad (52)$$

From Equation (46)

$$\bar{V}^a \cdot \bar{j}_B = \ell \sum_{i=1}^N \dot{\theta}_i \bar{e}_i \cdot \bar{j}_B + R_{k,m} \dot{\theta} \quad (53)$$

$$\bar{V}^a \cdot \bar{j}_B = \ell \sum_{i=1}^N \dot{\theta}_i s(\theta + \theta_i) + R_{k,m} \dot{\theta} \quad (54)$$

$$\bar{V}^a \cdot \bar{k}_B = \ell \sum_{i=1}^N \dot{\theta}_i c(\theta + \theta_i) - R_{j,m} \dot{\theta} \quad (55)$$

$$\frac{\partial \bar{V}^a}{\partial \theta} = \left[ R_{k,m} \frac{\partial \bar{j}_B}{\partial \theta} - R_{j,m} \frac{\partial \bar{k}_B}{\partial \theta} \right] \dot{\theta} = \left[ R_{k,m} \bar{k}_B + R_{j,m} \bar{j}_B \right] \dot{\theta} \quad (56)$$

$$\frac{\partial \bar{V}^a}{\partial \theta} \cdot \bar{j}_B = R_{j,m} \dot{\theta} \quad (57)$$

$$\frac{\partial \vec{V}^a}{\partial \theta} \cdot \vec{k}_a = R_{km} \dot{\theta} \quad (58)$$

$$\vec{V}^a \cdot \frac{\partial \vec{k}_a}{\partial \theta} = \mathcal{L} \sum_{i=1}^N \dot{\xi}_i c(\theta + \xi_i) - R_{jm} \dot{\theta} \quad (59)$$

$$\vec{V}^a \cdot \frac{\partial \vec{k}_a}{\partial \theta} = \mathcal{L} \sum_{i=1}^N -\dot{\xi}_i s(\theta + \xi_i) - R_{km} \dot{\theta} \quad (60)$$

Substitute Equations (53) to (60) into (52):

$$\begin{aligned} \frac{\partial \bar{T}}{\partial \theta} = & M_L \left[ \mathcal{L} \sum_{i=1}^N \dot{\xi}_i s(\theta + \xi_i) + R_{km} \dot{\theta} \right] \left[ R_{jm} \dot{\theta} + \mathcal{L} \sum_{i=1}^N \dot{\xi}_i c(\theta + \xi_i) - R_{jm} \dot{\theta} \right] \\ & + M_V \left[ \mathcal{L} \sum_{i=1}^N \dot{\xi}_i c(\theta + \xi_i) - R_{jm} \dot{\theta} \right] \left[ R_{km} \dot{\theta} - \mathcal{L} \sum_{i=1}^N \dot{\xi}_i s(\theta + \xi_i) - R_{km} \dot{\theta} \right] \end{aligned} \quad (61)$$

$$\begin{aligned} \frac{\partial \bar{T}}{\partial \theta} = & [M_L - M_V] \left[ \mathcal{L}^2 \sum_{i=1}^N \dot{\xi}_i s(\theta + \xi_i) \sum_{i=1}^N \dot{\xi}_i c(\theta + \xi_i) \right] \\ & + M_L \mathcal{L} R_{km} \dot{\theta} \sum_{i=1}^N \dot{\xi}_i c(\theta + \xi_i) + M_V \mathcal{L} R_{jm} \dot{\theta} \sum_{i=1}^N \dot{\xi}_i s(\theta + \xi_i) \end{aligned} \quad (62)$$

Substituting Equations (51) and (62) into Equation (49) yields the final nonlinear balloon pitching equation. Note,  $F_\theta$  is the same for both the nonlinear equation that follows, and Equation (1) which assumed small angular velocities. The expression for  $F_\theta$  is given by Equation (7),

$$\begin{aligned} & M_L \mathcal{L} R_{km} \sum_{i=1}^N \ddot{\xi}_i s(\theta + \xi_i) - M_V \mathcal{L} R_{jm} \sum_{i=1}^N \ddot{\xi}_i c(\theta + \xi_i) + [M_L R_{km}^2 + M_V R_{jm}^2 + I_{x0}] \ddot{\theta} \\ & = [M_L - M_V] \left[ \mathcal{L}^2 \sum_{i=1}^N \ddot{\xi}_i s(\theta + \xi_i) \sum_{i=1}^N \dot{\xi}_i c(\theta + \xi_i) \right] \\ & \quad - M_L \mathcal{L} R_{km} \sum_{i=1}^N \dot{\xi}_i^2 c(\theta + \xi_i) - M_V \mathcal{L} R_{jm} \sum_{i=1}^N \dot{\xi}_i^2 s(\theta + \xi_i) + F_\theta \end{aligned} \quad (63)$$

Now consider the tether equation of motion (50). From Equation (48) it follows:

$$\begin{aligned}
 \frac{d}{dt} \left( \frac{\partial \bar{T}}{\partial \dot{\mathbf{p}}_n} \right) = & \sum_{n=1}^N m \ell^2 \left\{ \sum_{i=1}^{n-1} \ddot{\mathbf{p}}_i c(\mathbf{p}_n - \mathbf{p}_i) - \sum_{i=1}^{n-1} \dot{\mathbf{p}}_i (\dot{\mathbf{p}}_n - \dot{\mathbf{p}}_i) s(\mathbf{p}_n - \mathbf{p}_i) \right. \\
 & + \frac{1}{2} \ddot{\mathbf{p}}_n c(\mathbf{p}_n - \mathbf{p}_n) - \frac{1}{2} \dot{\mathbf{p}}_n (\dot{\mathbf{p}}_n - \dot{\mathbf{p}}_n) s(\mathbf{p}_n - \mathbf{p}_n) \left. \right\} + m \ell^2 \left\{ \frac{1}{2} \sum_{i=1}^{n-1} \ddot{\mathbf{p}}_i c(\mathbf{p}_i - \mathbf{p}_i) \right. \\
 & - \frac{1}{2} \sum_{i=1}^{n-1} \dot{\mathbf{p}}_i (\dot{\mathbf{p}}_n - \dot{\mathbf{p}}_i) s(\mathbf{p}_n - \mathbf{p}_i) + \frac{1}{3} \ddot{\mathbf{p}}_n \left. \right\} + m_{p_2} \ell^2 \left\{ \sum_{i=1}^N \ddot{\mathbf{p}}_i c(\mathbf{p}_n - \mathbf{p}_i) \right. \\
 & - \sum_{i=1}^N \dot{\mathbf{p}}_i (\dot{\mathbf{p}}_n - \dot{\mathbf{p}}_i) s(\mathbf{p}_n - \mathbf{p}_i) \left. \right\} \\
 & + M_2 \left\{ \left[ \ell^2 \sum_{i=1}^N \ddot{\mathbf{p}}_i s(\theta + \mathbf{p}_i) + \ell^2 \sum_{i=1}^N \dot{\mathbf{p}}_i (\dot{\theta} + \dot{\mathbf{p}}_i) c(\theta + \mathbf{p}_i) + \ell R_{km} \ddot{\theta} \right] s(\theta + \mathbf{p}_n) \right. \\
 & + \left. \left[ \ell^2 \sum_{i=1}^N \dot{\mathbf{p}}_i s(\theta + \mathbf{p}_i) + \ell R_{km} \dot{\theta} \right] [\dot{\theta} + \dot{\mathbf{p}}_n] c(\theta + \mathbf{p}_n) \right\} \\
 & + M_V \left\{ \left[ \ell^2 \sum_{i=1}^N \ddot{\mathbf{p}}_i c(\theta + \mathbf{p}_i) - \ell^2 \sum_{i=1}^N \dot{\mathbf{p}}_i (\dot{\theta} + \dot{\mathbf{p}}_i) s(\theta + \mathbf{p}_i) - \ell R_{jm} \ddot{\theta} \right] c(\theta + \mathbf{p}_n) \right. \\
 & - \left. \left[ \ell^2 \sum_{i=1}^N \dot{\mathbf{p}}_i c(\theta + \mathbf{p}_i) - \ell R_{jm} \dot{\theta} \right] [\dot{\theta} + \dot{\mathbf{p}}_n] s(\theta + \mathbf{p}_n) \right\} \quad (64)
 \end{aligned}$$

From Equation (43):

$$\begin{aligned}
 \frac{\partial \bar{T}}{\partial \mathbf{p}_n} = & \sum_{n=1}^N m \left( \vec{V}^{p_n} \cdot \frac{\partial \vec{V}^{p_n}}{\partial \mathbf{p}_n} \right) + m_{p_2} \left( \vec{V}^{p_2} \cdot \frac{\partial \vec{V}^{p_2}}{\partial \mathbf{p}_n} \right) \\
 & + M_2 \left( \vec{V}^{\theta} \cdot \vec{j}_{\theta} \right) \left( \frac{\partial \vec{V}^{\theta}}{\partial \mathbf{p}_n} \cdot \vec{j}_{\theta} \right) + M_V \left( \vec{V}^{\psi} \cdot \vec{k}_{\psi} \right) \left( \frac{\partial \vec{V}^{\psi}}{\partial \mathbf{p}_n} \cdot \vec{k}_{\psi} \right) \quad (65)
 \end{aligned}$$

From Equation (44):

$$\frac{\partial \vec{V}^{\rho_n}}{\partial \dot{\theta}_n} = \begin{cases} -l \dot{\theta}_n \vec{e}_n & n > n \\ -\frac{1}{2} l \dot{\theta}_n \vec{e}_n & n = n \\ 0 & n < n \end{cases} \quad (66)$$

$$\sum_{n=1}^N \vec{V}^{\rho_n} \cdot \frac{\partial \vec{V}^{\rho_n}}{\partial \dot{\theta}_n} = -l^2 \sum_{n=1}^N \left[ \sum_{i=1}^{n-1} \dot{\theta}_i \dot{\theta}_n \vec{e}_i \cdot \vec{e}_n + \frac{1}{2} \dot{\theta}_n \dot{\theta}_n \vec{e}_n \cdot \vec{e}_n \right. \\ \left. - l^2 \left[ \frac{1}{2} \sum_{i=1}^{n-1} \dot{\theta}_i \dot{\theta}_n \vec{e}_i \cdot \vec{e}_n - \frac{1}{4} \dot{\theta}_n^2 \vec{e}_n \cdot \vec{e}_n \right] \right] \quad (67)$$

From Equation (45):

$$\frac{\partial \vec{V}^{\rho_n}}{\partial \dot{\theta}_n} = -l \dot{\theta}_n \vec{e}_n \quad (68)$$

$$\vec{V}^{\rho_n} \cdot \frac{\partial \vec{V}^{\rho_n}}{\partial \dot{\theta}_n} = -l^2 \sum_{i=1}^N \dot{\theta}_i \dot{\theta}_n \vec{e}_i \cdot \vec{e}_n \quad (69)$$

From Equation (46):

$$\frac{\partial \vec{V}^{\rho_n}}{\partial \dot{\theta}_n} = -l \dot{\theta}_n \vec{e}_n \quad (70)$$

$$\frac{\partial \vec{V}^{\rho_n}}{\partial \dot{\theta}_n} \cdot \vec{j}_0 = -l \dot{\theta}_n [-c \dot{\theta}_n \cos \theta + s \dot{\theta}_n \sin \theta] \quad (71)$$

$$\frac{\partial \vec{V}^{\rho_n}}{\partial \dot{\theta}_n} \cdot \vec{k}_0 = -l \dot{\theta}_n [c \dot{\theta}_n \sin \theta + s \dot{\theta}_n \cos \theta] \quad (72)$$

Substituting Equations (67), (69), (71), (72), (54), and (55) into Equation (65) yields.

$$\begin{aligned}
 \frac{\partial \bar{T}}{\partial \dot{\theta}_n} = & \ell^2 m \left\{ \sum_{n=N+1}^N \left[ \sum_{i=1}^{n-1} \dot{\theta}_i \dot{\theta}_n s(\theta_i - \theta_n) + \frac{1}{2} \dot{\theta}_n \dot{\theta}_n s(\theta_n - \theta_n) \right] \right. \\
 & + \frac{1}{2} \sum_{i=1}^{n-1} \dot{\theta}_i \dot{\theta}_n s(\theta_i - \theta_n) \left. \right\} + m_{pL} \ell^2 \sum_{i=1}^N \dot{\theta}_i \dot{\theta}_n s(\theta_i - \theta_n) \\
 & + M_L \ell \dot{\theta}_n c(\theta + \theta_n) \left[ \ell \sum_{i=1}^N \dot{\theta}_i s(\theta + \theta_i) + R_{Lm} \dot{\theta} \right] \\
 & - M_V \ell \dot{\theta}_n s(\theta + \theta_n) \left[ \ell \sum_{i=1}^N \dot{\theta}_i c(\theta + \theta_i) - R_{j,m} \dot{\theta} \right]
 \end{aligned} \tag{73}$$

Substitute Equations (64) and (73) into Equation (50) to give the final nonlinear tether pitching equation.  $F_{\theta_n}$  has already been found in Equations (8), (9) and (10).

$$\begin{aligned}
 & \sum_{n=N+1}^N m \ell^2 \left\{ \sum_{i=1}^{n-1} \ddot{\theta}_i c(\theta_i - \theta_n) + \frac{1}{2} \ddot{\theta}_n c(\theta_n - \theta_n) \right\} + m \ell^2 \left\{ \frac{1}{2} \sum_{i=1}^{n-1} \ddot{\theta}_i c(\theta_i - \theta_n) + \frac{1}{3} \ddot{\theta}_n \right\} \\
 & + m_{pL} \ell^2 \sum_{i=1}^N \ddot{\theta}_i c(\theta_i - \theta_n) + M_L \left[ \ell^2 \sum_{i=1}^N \ddot{\theta}_i s(\theta + \theta_i) + \ell R_{Lm} \ddot{\theta} \right] s(\theta + \theta_n) \\
 & + M_V \left[ \ell^2 \sum_{i=1}^N \ddot{\theta}_i c(\theta + \theta_i) - \ell R_{j,m} \ddot{\theta} \right] c(\theta + \theta_n) \\
 & = \sum_{n=N+1}^N m \ell^2 \left\{ \sum_{i=1}^{n-1} \dot{\theta}_i^2 s(\theta_i - \theta_n) + \frac{1}{2} \dot{\theta}_n^2 s(\theta_n - \theta_n) \right\} + \frac{m \ell^2}{2} \sum_{i=1}^{n-1} \dot{\theta}_i^2 s(\theta_i - \theta_n) \\
 & + m_{pL} \ell^2 \sum_{i=1}^N \dot{\theta}_i^2 s(\theta_i - \theta_n) + M_L \left\{ \ell^2 \left[ \sum_{i=1}^N \dot{\theta}_i (\dot{\theta} + \dot{\theta}_i) c(\theta + \theta_i) s(\theta + \theta_n) \right. \right. \\
 & \left. \left. - \sum_{i=1}^N \dot{\theta}_i \dot{\theta} s(\theta + \theta_i) c(\theta + \theta_n) \right] - \ell R_{Lm} \dot{\theta}^2 c(\theta + \theta_n) \right\}
 \end{aligned}$$

$$\begin{aligned}
& + M_v \left\{ \ell^2 \left[ \sum_{i=1}^N \ddot{\theta}_i (\dot{\theta} + \dot{\theta}_i) s(\theta + \theta_i) c(\theta + \theta_i) \right. \right. \\
& \left. \left. + \sum_{i=1}^N \ddot{\theta}_i \dot{\theta} c(\theta + \theta_i) s(\theta + \theta_i) - \ell R_{jm} \dot{\theta}^2 s(\theta + \theta_i) \right] + F_{\theta} \right\} \quad (74)
\end{aligned}$$

Now assume the tether is composed of three links ( $N = 3$ ).  
 Rewriting the balloon pitching Equation (63) gives:

$$\begin{aligned}
& \{ I_{XB} + M_L R_{Lm}^2 + M_v R_{jm}^2 \} \ddot{\theta} \\
& + \ell \{ M_L R_{Lm} s(\theta + \theta_1) - M_v R_{jm} c(\theta + \theta_1) \} \ddot{\theta}_1 \\
& + \ell \{ M_L R_{Lm} s(\theta + \theta_2) - M_v R_{jm} c(\theta + \theta_2) \} \ddot{\theta}_2 \\
& + \ell \{ M_L R_{Lm} s(\theta + \theta_3) - M_v R_{jm} c(\theta + \theta_3) \} \ddot{\theta}_3 \\
& = [M_L - M_v] \left[ \ell^2 \sum_{i=1}^3 \ddot{\theta}_i s(\theta + \theta_i) \sum_{j=1}^3 \ddot{\theta}_j c(\theta + \theta_j) \right] \\
& - M_L \ell R_{Lm} \sum_{i=1}^3 \ddot{\theta}_i^2 c(\theta + \theta_i) - M_v \ell R_{jm} \sum_{i=1}^3 \ddot{\theta}_i^2 s(\theta + \theta_i) + F_{\theta} \quad (75)
\end{aligned}$$

For  $N = 3$  and  $r = 1$ , Equation (74) becomes:

$$\begin{aligned}
& \{ M_L \ell R_{Lm} s(\theta + \theta_1) - M_v \ell R_{jm} c(\theta + \theta_1) \} \ddot{\theta} \\
& + \ell^2 \left\{ \frac{7m}{3} + m_{p1} + M_L s^2(\theta + \theta_1) + M_v c^2(\theta + \theta_1) \right\} \ddot{\theta}_1 \\
& + \ell^2 \left\{ \left[ \frac{3m}{2} + m_{p1} \right] c(\theta_1 - \theta_2) + M_L s(\theta + \theta_1) s(\theta + \theta_2) + M_v c(\theta + \theta_1) c(\theta + \theta_2) \right\} \ddot{\theta}_2
\end{aligned}$$

$$\begin{aligned}
& + \ell^2 \left\{ \left[ \frac{m}{2} + m_{pk} \right] c(\theta_1 - \theta_2) + M_L s(\theta + \theta_1) s(\theta + \theta_2) + M_V c(\theta + \theta_1) c(\theta + \theta_2) \right\} \ddot{\theta}_1 \\
& = m \ell^2 \left\{ \frac{3}{2} \dot{\theta}_1^2 s(\theta_1 - \theta_2) + \frac{1}{2} \dot{\theta}_2^2 s(\theta_1 - \theta_2) \right\} + m_{pk} \ell^2 \sum_{i=2}^3 \dot{\theta}_i^2 s(\theta_i - \theta_1) \\
& + [M_V - M_L] \ell^2 \left\{ s(\theta + \theta_1) \sum_{i=1}^3 \dot{\theta}_i \dot{\theta} c(\theta + \theta_i) + c(\theta + \theta_1) \sum_{i=1}^3 \dot{\theta}_i \dot{\theta} s(\theta + \theta_i) \right\} \\
& + M_V \ell^2 c(\theta + \theta_1) \sum_{i=1}^3 \dot{\theta}_i^2 s(\theta + \theta_i) - M_L \ell^2 s(\theta + \theta_1) \sum_{i=1}^3 \dot{\theta}_i^2 c(\theta + \theta_i) \\
& - \ell \left[ M_L R_{km} c(\theta + \theta_1) + M_V R_{jm} s(\theta + \theta_1) \right] \dot{\theta}^2 + F_{\theta_1}
\end{aligned} \tag{76}$$

For  $N = 3$  and  $r = 2$ , Equation (74) becomes:

$$\begin{aligned}
& \{ M_L \ell R_{km} s(\theta + \theta_2) - M_V \ell R_{jm} c(\theta + \theta_2) \} \ddot{\theta} \\
& + \ell^2 \left\{ \left[ \frac{3m}{2} + m_{pk} \right] c(\theta_1 - \theta_2) + M_L s(\theta + \theta_1) s(\theta + \theta_2) + M_V c(\theta + \theta_1) c(\theta + \theta_2) \right\} \ddot{\theta}_1 \\
& + \ell^2 \left\{ \frac{4m}{3} + m_{pk} + M_L s^2(\theta + \theta_2) + M_V c^2(\theta + \theta_2) \right\} \ddot{\theta}_2 \\
& + \ell^2 \left\{ \left[ \frac{m}{2} + m_{pk} \right] c(\theta_2 - \theta_3) + M_L s(\theta + \theta_2) s(\theta + \theta_3) + M_V c(\theta + \theta_2) c(\theta + \theta_3) \right\} \ddot{\theta}_3 \\
& = m \ell^2 \left\{ \frac{3}{2} \dot{\theta}_1^2 s(\theta_1 - \theta_2) + \frac{1}{2} \dot{\theta}_2^2 s(\theta_1 - \theta_2) \right\} + m_{pk} \ell^2 \sum_{i=1}^3 \dot{\theta}_i^2 s(\theta_i - \theta_2) \\
& + [M_V - M_L] \ell^2 \left\{ s(\theta + \theta_2) \sum_{i=1}^3 \dot{\theta}_i \dot{\theta} c(\theta + \theta_i) + c(\theta + \theta_2) \sum_{i=1}^3 \dot{\theta}_i \dot{\theta} s(\theta + \theta_i) \right\} \\
& + M_V \ell^2 c(\theta + \theta_2) \sum_{i=1}^3 \dot{\theta}_i^2 s(\theta + \theta_i) - M_L \ell^2 s(\theta + \theta_2) \sum_{i=1}^3 \dot{\theta}_i^2 c(\theta + \theta_i) \\
& - \ell \left[ M_L R_{km} c(\theta + \theta_2) + M_V R_{jm} s(\theta + \theta_2) \right] \dot{\theta}^2 + F_{\theta_2}
\end{aligned} \tag{77}$$

For  $N = 3$  and  $r = 3$ , Equation (74) becomes:

$$\begin{aligned}
 & \{M_L \ell R_{Lm} s(\theta + \varphi_3) - M_V \ell R_{Vm} c(\theta + \varphi_3)\} \ddot{\theta} \\
 & + \ell^2 \left\{ \left[ \frac{m}{2} + m_{pL} \right] c(\varphi_1 - \varphi_3) + M_L s(\theta + \varphi_1) s(\theta + \varphi_3) + M_V c(\theta + \varphi_1) c(\theta + \varphi_3) \right\} \ddot{\varphi}_1 \\
 & + \ell^2 \left\{ \left[ \frac{m}{2} + m_{pL} \right] c(\varphi_2 - \varphi_3) + M_L s(\theta + \varphi_2) s(\theta + \varphi_3) + M_V c(\theta + \varphi_2) c(\theta + \varphi_3) \right\} \ddot{\varphi}_2 \\
 & + \ell^2 \left\{ \frac{m}{3} + m_{pL} + M_L s^2(\theta + \varphi_3) + M_V c^2(\theta + \varphi_3) \right\} \ddot{\varphi}_3 \\
 & = \ell^2 \left[ \frac{m}{2} + m_{pL} \right] \sum_{i=1}^3 \dot{\varphi}_i^2 s(\varphi_i - \varphi_3) \\
 & + [M_V - M_L] \ell^2 \left\{ s(\theta + \varphi_3) \sum_{i=1}^3 \dot{\varphi}_i \dot{\theta} c(\theta + \varphi_i) + c(\theta + \varphi_3) \sum_{i=1}^3 \dot{\varphi}_i \dot{\theta} s(\theta + \varphi_i) \right\} \\
 & + M_V \ell^2 c(\theta + \varphi_3) \sum_{i=1}^3 \dot{\varphi}_i^2 s(\theta + \varphi_i) - M_L \ell^2 s(\theta + \varphi_3) \sum_{i=1}^3 \dot{\varphi}_i^2 c(\theta + \varphi_i) \\
 & - \ell [M_L R_{Lm} c(\theta + \varphi_3) + M_V R_{Vm} s(\theta + \varphi_3)] \dot{\theta}^2 + F_{\varphi_3}
 \end{aligned} \tag{78}$$

## LATERAL EQUATIONS OF MOTION FOR SMALL ANGULAR VELOCITIES

FRONT VIEW

TOP VIEW

A - 40

The appropriate equations of motion are Equations (73), (86), and (108) of Appendix A of the Second Scientific Report\*. These three equations will be rewritten below remembering that  $\theta$  (pitch of balloon) and  $\zeta_r$  (pitch of "r" link) are constants. The first equation is the balloon yaw equation of motion.

$$\begin{aligned}
 M_s \{ & l \sum_{i=1}^N \ddot{\sigma}_i [C\sigma_i (s\phi s\theta s\psi + c\phi c\psi) + S\sigma_i C\beta_i (s\phi s\theta c\psi - c\phi s\psi) - S\sigma_i S\beta_i (-s\phi c\theta)] \\
 & + [R_{jm} (-\ddot{\psi} c\theta c\phi) - R_{km} (-\ddot{\psi} s\theta + \dot{\phi})] \} \{ -R_{jm} c\theta c\phi + R_{km} s\theta \} \\
 & + M_L \{ l \sum_{i=1}^N \ddot{\sigma}_i [C\sigma_i (c\theta s\psi) + S\sigma_i C\beta_i (c\theta c\psi) - S\sigma_i S\beta_i (s\theta)] + [R_{km} (\ddot{\psi} s\phi c\theta)] \} \{ R_{km} s\phi c\theta \} \\
 & + M_V \{ l \sum_{i=1}^N \ddot{\sigma}_i [C\sigma_i (-c\phi s\theta s\psi + s\phi c\psi) + S\sigma_i C\beta_i (-c\phi s\theta c\psi - s\phi s\psi) - S\sigma_i S\beta_i (c\phi c\theta)] \\
 & + [-R_{jm} (\ddot{\psi} s\phi c\theta)] \} \{ -R_{jm} s\phi c\theta \} + \dot{\phi} [-I_{YB} s\theta + I_{YZB} c\theta c\phi] \\
 & + [c^2\theta (I_{XB} s^2\phi + I_{ZB} c^2\phi) + s^2\theta I_{YB} - s2\theta c\phi I_{YZB}] = F_\psi \quad (79)
 \end{aligned}$$

The second equation is the balloon roll equation.

$$\begin{aligned}
 M_s \{ & l \sum_{i=1}^N \ddot{\sigma}_i [C\sigma_i (s\phi s\theta s\psi + c\phi c\psi) + S\sigma_i C\beta_i (s\phi s\theta c\psi - c\phi s\psi) - S\sigma_i S\beta_i (-s\phi c\theta)] \\
 & + [R_{jm} (-\ddot{\psi} c\theta c\phi) - R_{km} (-\ddot{\psi} s\theta + \dot{\phi})] \} \{ -R_{km} \} \\
 & + \dot{\phi} [I_{YB}] + \ddot{\psi} [-I_{YB} s\theta + I_{YZB} c\theta c\phi] = F_\phi \quad (80)
 \end{aligned}$$

The equation for the tether link yaw equation of motion is given as follows:

$$\begin{aligned}
 & \sum_{n=n+1}^N m \ell^2 \left\{ \sum_{i=1}^{n-1} \ddot{\sigma}_i \left[ c\sigma_i c\sigma_n + s\sigma_i s\sigma_n c(\beta_n - \beta_i) \right] + \frac{1}{2} \ddot{\sigma}_n \left[ c\sigma_n c\sigma_n + s\sigma_n s\sigma_n c(\beta_n - \beta_n) \right] \right\} \\
 & + \frac{m}{2} \ell^2 \sum_{i=1}^{n-1} \ddot{\sigma}_i \left[ c\sigma_i c\sigma_n + s\sigma_i s\sigma_n c(\beta_n - \beta_i) \right] + \frac{m}{3} \ell^2 \ddot{\sigma}_n \\
 & + m_{pL} \ell^2 \sum_{i=1}^N \ddot{\sigma}_i \left[ c\sigma_i c\sigma_n + s\sigma_i s\sigma_n c(\beta_n - \beta_i) \right] \\
 & + M_s \left\{ \ell \sum_{i=1}^N \ddot{\sigma}_i \left[ c\sigma_i (s\phi s\theta s\psi + c\phi c\psi) + s\sigma_i c\beta_i (s\phi s\theta c\psi - c\phi s\psi) - s\sigma_i s\beta_i (-s\phi c\theta) \right] \right. \\
 & + \left. \left[ R_{jm} (-\ddot{\psi} c\theta c\phi) - R_{km} (-\ddot{\psi} s\theta + \ddot{\phi}) \right] \right\} \ell \left\{ c\sigma_n (s\phi s\theta s\psi + c\phi c\psi) \right. \\
 & + \left. s\sigma_n c\beta_n (s\phi s\theta c\psi - c\phi s\psi) - s\sigma_n s\beta_n (-s\phi c\theta) \right\} \\
 & + M_L \left\{ \ell \sum_{i=1}^N \ddot{\sigma}_i \left[ c\sigma_i (c\theta s\psi) + s\sigma_i c\beta_i (c\theta c\psi) - s\sigma_i s\beta_i (s\theta) \right] \right. \\
 & + \left. \left[ R_{km} (\ddot{\psi} s\phi c\theta) \right] \right\} \ell \left\{ c\sigma_n (c\theta s\psi) + s\sigma_n c\beta_n (c\theta c\psi) - s\sigma_n s\beta_n (s\theta) \right\} \\
 & + M_v \left\{ \ell \sum_{i=1}^N \ddot{\sigma}_i \left[ c\sigma_i (-c\phi s\theta s\psi + s\phi c\psi) + s\sigma_i c\beta_i (-c\phi s\theta c\psi - s\phi s\psi) \right. \right. \\
 & + \left. \left. -s\sigma_i s\beta_i (c\phi c\theta) \right] + \left[ -R_{jm} (\ddot{\psi} s\phi c\theta) \right] \right\} \ell \left\{ c\sigma_n (-c\phi s\theta s\psi + s\phi c\psi) \right. \\
 & + \left. s\sigma_n c\beta_n (-c\phi s\theta c\psi - s\phi s\psi) - s\sigma_n s\beta_n (c\phi c\theta) \right\} = F_{\sigma_n}
 \end{aligned}
 \tag{81}$$

In Equations (79), (80), and (81), there are several trigonometric combinations of the balloon angles  $\psi$ ,  $\theta$ ,  $\phi$ . These terms are the elements of a matrix (Equation (51)) given in Appendix A of the Second Scientific Report\*. The matrix  $(E_{ij})$  gives the relation between the balloon unit vectors and the inertia frame.

$$E_{ij} = \begin{bmatrix} s\phi s\theta s\psi + c\phi c\psi & s\phi s\theta c\psi - c\phi s\psi & -s\phi c\theta \\ c\theta s\psi & c\theta c\psi & s\theta \\ -c\phi s\theta s\psi + s\phi c\psi & -c\phi s\theta c\psi - s\phi s\psi & c\phi c\theta \end{bmatrix} \quad (82)$$

The balloon yaw Equation (79) is rewritten as:

$$\begin{aligned} & M_S \left\{ \ell \sum_{i=1}^N \ddot{\sigma}_i [c\sigma_i E_{11} + s\sigma_i c\beta_i E_{12} - s\sigma_i s\beta_i E_{13}] - R_{j,m} E_{33} + R_{h,m} E_{23} \right\} \\ & + M_L \left\{ \ell \sum_{i=1}^N \ddot{\sigma}_i [c\sigma_i E_{21} + s\sigma_i c\beta_i E_{22} - s\sigma_i s\beta_i E_{23}] - R_{h,m} E_{13} \right\} \\ & + M_V \left\{ \ell \sum_{i=1}^N \ddot{\sigma}_i [c\sigma_i E_{31} + s\sigma_i c\beta_i E_{32} - s\sigma_i s\beta_i E_{33}] - R_{j,m} E_{13} \right\} \\ & + \dot{\psi} \left\{ [-R_{j,m} E_{33} + R_{h,m} E_{23}]^2 M_S + [-R_{h,m} E_{13}]^2 M_L + [R_{j,m} E_{13}]^2 M_V \right. \\ & \left. + c^2 \theta [I_{x\theta} s^2 \phi + I_{z\theta} c^2 \phi] + s^2 \theta I_{y\theta} - s 2\theta c\phi I_{yz\theta} \right\} \\ & + \dot{\phi} \left\{ -R_{h,m} [-R_{j,m} E_{33} + R_{h,m} E_{23}] M_S - I_{y\theta} s\theta + I_{yz\theta} c\theta c\phi \right\} = F_\psi \end{aligned} \quad (83)$$

The balloon roll Equation (80) is rewritten as:

\*Reference 2

$$\begin{aligned}
& M_S \left\{ \ell^2 \sum_{i=1}^N \ddot{\theta}_i [C\sigma_i E_{11} + S\sigma_i C\beta_i E_{12} - S\sigma_i S\beta_i E_{13}] [-R_{km}] \right\} \\
& + \dot{\psi} \{ [-R_{jm} E_{33} + R_{km} E_{23}] [-R_{km}] M_S - I_{y0} S\theta + I_{yz0} C\theta C\phi \} \\
& + \ddot{\phi} \{ M_S [R_{km}]^2 + I_{y0} \} = F_\phi \quad (34)
\end{aligned}$$

The tether yaw Equation (81) is rewritten as:

$$\begin{aligned}
& \sum_{n=1}^N m \ell^2 \left\{ \sum_{i=1}^{n-1} \ddot{\theta}_i [C\sigma_i C\sigma_n + S\sigma_i S\sigma_n C(\beta_n - \beta_i)] + \frac{1}{2} \ddot{\theta}_n [C\sigma_n C\sigma_n + S\sigma_n S\sigma_n C(\beta_n - \beta_n)] \right\} \\
& + \frac{m}{2} \ell^2 \sum_{i=1}^{n-1} \ddot{\theta}_i [C\sigma_i C\sigma_n + S\sigma_i S\sigma_n C(\beta_n - \beta_i)] + \frac{m}{3} \ell^2 \ddot{\theta}_n \\
& + m \rho_L \ell^2 \sum_{i=1}^N \ddot{\theta}_i [C\sigma_i C\sigma_n + S\sigma_i S\sigma_n C(\beta_n - \beta_i)] \\
& + M_S \left\{ \ell^2 \sum_{i=1}^N \ddot{\theta}_i [C\sigma_i E_{11} + S\sigma_i C\beta_i E_{12} - S\sigma_i S\beta_i E_{13}] [C\sigma_n E_{11} + S\sigma_n C\beta_n E_{12} - S\sigma_n S\beta_n E_{13}] \right\} \\
& + M_L \left\{ \ell^2 \sum_{i=1}^N \ddot{\theta}_i [C\sigma_i E_{21} + S\sigma_i C\beta_i E_{22} - S\sigma_i S\beta_i E_{23}] [C\sigma_n E_{21} + S\sigma_n C\beta_n E_{22} - S\sigma_n S\beta_n E_{23}] \right\} \\
& + M_V \left\{ \ell^2 \sum_{i=1}^N \ddot{\theta}_i [C\sigma_i E_{31} + S\sigma_i C\beta_i E_{32} - S\sigma_i S\beta_i E_{33}] [C\sigma_n E_{31} + S\sigma_n C\beta_n E_{32} - S\sigma_n S\beta_n E_{33}] \right\} \\
& + \dot{\psi} \{ \ell M_S [-R_{jm} E_{33} + R_{km} E_{13}] [C\sigma_n E_{11} + S\sigma_n C\beta_n E_{12} - S\sigma_n S\beta_n E_{13}] \\
& + \ell M_L [-R_{km} E_{13}] [C\sigma_n E_{21} + S\sigma_n C\beta_n E_{22} - S\sigma_n S\beta_n E_{23}] + \ell M_V [R_{jm} E_{13}] [C\sigma_n E_{31} \\
& + S\sigma_n C\beta_n E_{32} - S\sigma_n S\beta_n E_{33}] \} + \ddot{\phi} \{ \ell M_S [-R_{km}] [C\sigma_n E_{11} + S\sigma_n C\beta_n E_{12} - S\sigma_n S\beta_n E_{13}] \} = F_{\sigma_n} \quad (85)
\end{aligned}$$

In order to solve Equations (83), (84), and (85), assume  $N = 3$ . The balloon yaw equation is:

$$\begin{aligned}
 & \ell \{ M_s [C\sigma_1 \epsilon_{11} + S\sigma_1 C\beta_1 \epsilon_{12} - S\sigma_1 S\beta_1 \epsilon_{13}] [-R_{j,m} \epsilon_{32} + R_{k,m} \epsilon_{23}] \\
 & + M_k [C\sigma_1 \epsilon_{21} + S\sigma_1 C\beta_1 \epsilon_{22} - S\sigma_1 S\beta_1 \epsilon_{23}] [-R_{k,m} \epsilon_{13}] \\
 & + M_v [C\sigma_1 \epsilon_{31} + S\sigma_1 C\beta_1 \epsilon_{32} - S\sigma_1 S\beta_1 \epsilon_{33}] [R_{j,m} \epsilon_{12}] \} \ddot{\sigma}_1 \\
 & + \ell \{ M_s [C\sigma_2 \epsilon_{11} + S\sigma_2 C\beta_2 \epsilon_{12} - S\sigma_2 S\beta_2 \epsilon_{13}] [-R_{j,m} \epsilon_{32} + R_{k,m} \epsilon_{23}] \\
 & + M_k [C\sigma_2 \epsilon_{21} + S\sigma_2 C\beta_2 \epsilon_{22} - S\sigma_2 S\beta_2 \epsilon_{23}] [-R_{k,m} \epsilon_{13}] \\
 & + M_v [C\sigma_2 \epsilon_{31} + S\sigma_2 C\beta_2 \epsilon_{32} - S\sigma_2 S\beta_2 \epsilon_{33}] [R_{j,m} \epsilon_{12}] \} \ddot{\sigma}_2 \\
 & + \ell \{ M_s [C\sigma_3 \epsilon_{11} + S\sigma_3 C\beta_3 \epsilon_{12} - S\sigma_3 S\beta_3 \epsilon_{13}] [-R_{j,m} \epsilon_{32} + R_{k,m} \epsilon_{23}] \\
 & + M_k [C\sigma_3 \epsilon_{21} + S\sigma_3 C\beta_3 \epsilon_{22} - S\sigma_3 S\beta_3 \epsilon_{23}] [-R_{k,m} \epsilon_{13}] \\
 & + M_v [C\sigma_3 \epsilon_{31} + S\sigma_3 C\beta_3 \epsilon_{32} - S\sigma_3 S\beta_3 \epsilon_{33}] [R_{j,m} \epsilon_{12}] \} \ddot{\sigma}_3 \\
 & + \{ M_s [-R_{j,m} \epsilon_{32} + R_{k,m} \epsilon_{23}]^2 + M_k [-R_{k,m} \epsilon_{13}]^2 + M_v [R_{j,m} \epsilon_{12}]^2 \\
 & + C^2 \theta [I_{x\theta} S^2 \phi + I_{z\theta} C^2 \phi] + S^2 \theta I_{y\theta} - S^2 \theta C \phi I_{y z \theta} \} \ddot{\psi} \\
 & + \{ M_s [-R_{j,m} \epsilon_{32} + R_{k,m} \epsilon_{23}] [-R_{k,m}] - I_{y\theta} S \theta + I_{y z \theta} C \theta C \phi \} \ddot{\phi} = F_\psi
 \end{aligned}
 \tag{86}$$

The balloon roll equation is

$$\begin{aligned}
 & \ell \{ M_s [C\sigma_1 \epsilon_{11} + S\sigma_1 C\beta_1 \epsilon_{12} - S\sigma_1 S\beta_1 \epsilon_{13}] [-R_{km}] \} \ddot{\sigma}_1 \\
 & + \ell \{ M_s [C\sigma_2 \epsilon_{11} + S\sigma_2 C\beta_2 \epsilon_{12} - S\sigma_2 S\beta_2 \epsilon_{13}] [-R_{km}] \} \ddot{\sigma}_2 \\
 & + \ell \{ M_s [C\sigma_3 \epsilon_{11} + S\sigma_3 C\beta_3 \epsilon_{12} - S\sigma_3 S\beta_3 \epsilon_{13}] [-R_{km}] \} \ddot{\sigma}_3 \\
 & + \{ M_s [-R_{j,m} \epsilon_{33} + R_{k,m} \epsilon_{33}] [-R_{km}] - I_{yB} S\theta + I_{y2B} C\theta C\phi \} \ddot{\psi} \\
 & + \{ M_s [R_{km}]^2 + I_{yB} \} \ddot{\phi} = F_\phi
 \end{aligned} \tag{87}$$

From Equation (85), three equations will be generated (one for each link) by assuming  $r = 1$ ,  $r = 2$ ,  $r = 3$  consecutively.

For  $r = 1$ ,

$$\begin{aligned}
 & \ell^2 \left\{ \frac{7m}{3} + m_{pL} + M_s [C\sigma_1 \epsilon_{11} + S\sigma_1 C\beta_1 \epsilon_{12} - S\sigma_1 S\beta_1 \epsilon_{13}]^2 \right. \\
 & + M_L [C\sigma_1 \epsilon_{21} + S\sigma_1 C\beta_1 \epsilon_{22} - S\sigma_1 S\beta_1 \epsilon_{23}]^2 + M_V [C\sigma_1 \epsilon_{31} + S\sigma_1 C\beta_1 \epsilon_{32} - S\sigma_1 S\beta_1 \epsilon_{33}]^2 \left. \right\} \dot{\sigma}_1 \\
 & + \ell^2 \left\{ [C\sigma_2 C\sigma_1 + S\sigma_2 S\sigma_1 C(\beta_1 - \beta_2)] \left[ \frac{3m}{2} + m_{pL} \right] \right. \\
 & + M_s [C\sigma_2 \epsilon_{11} + S\sigma_2 C\beta_2 \epsilon_{12} - S\sigma_2 S\beta_2 \epsilon_{13}] [C\sigma_1 \epsilon_{11} + S\sigma_1 C\beta_1 \epsilon_{12} - S\sigma_1 S\beta_1 \epsilon_{13}] \\
 & + M_L [C\sigma_2 \epsilon_{21} + S\sigma_2 C\beta_2 \epsilon_{22} - S\sigma_2 S\beta_2 \epsilon_{23}] [C\sigma_1 \epsilon_{21} + S\sigma_1 C\beta_1 \epsilon_{22} - S\sigma_1 S\beta_1 \epsilon_{23}]
 \end{aligned}$$

$$\begin{aligned}
& +M_V [C\sigma_2 E_{31} + S\sigma_2 C\beta_2 E_{32} - S\sigma_2 S\beta_2 E_{33}] [C\sigma_1 E_{11} + S\sigma_1 C\beta_1 E_{12} - S\sigma_1 S\beta_1 E_{13}] \ddot{\sigma}_2 \\
& + \ell^2 \{ [C\sigma_3 C\sigma_1 + S\sigma_3 S\sigma_1 C(\beta_1 - \beta_3)] \left[ \frac{m}{2} + m_{\rho_L} \right] \\
& + M_S [C\sigma_3 E_{11} + S\sigma_3 C\beta_3 E_{12} - S\sigma_3 S\beta_3 E_{13}] [C\sigma_1 E_{11} + S\sigma_1 C\beta_1 E_{12} - S\sigma_1 S\beta_1 E_{13}] \\
& + M_L [C\sigma_3 E_{21} + S\sigma_3 C\beta_3 E_{22} - S\sigma_3 S\beta_3 E_{23}] [C\sigma_1 E_{21} + S\sigma_1 C\beta_1 E_{12} - S\sigma_1 S\beta_1 E_{23}] \\
& + M_V [C\sigma_3 E_{31} + S\sigma_3 C\beta_3 E_{32} - S\sigma_3 S\beta_3 E_{33}] [C\sigma_1 E_{31} + S\sigma_1 C\beta_1 E_{32} - S\sigma_1 S\beta_1 E_{33}] \ddot{\sigma}_3 \\
& + \ell \{ M_S [-R_{j,m} E_{33} + R_{k,m} E_{23}] [C\sigma_1 E_{11} + S\sigma_1 C\beta_1 E_{12} - S\sigma_1 S\beta_1 E_{13}] \\
& + M_L [-R_{k,m} E_{13}] [C\sigma_1 E_{21} + S\sigma_1 C\beta_1 E_{22} - S\sigma_1 S\beta_1 E_{23}] \\
& + M_V [R_{j,m} E_{13}] [C\sigma_1 E_{31} + S\sigma_1 C\beta_1 E_{32} - S\sigma_1 S\beta_1 E_{33}] \} \ddot{\psi} \\
& + \ell \{ M_S [-R_{k,m}] [C\sigma_1 E_{11} + S\sigma_1 C\beta_1 E_{12} - S\sigma_1 S\beta_1 E_{13}] \} \ddot{\phi} = F_{\sigma}, \quad (88)
\end{aligned}$$

For  $r = 2$ ,

$$\begin{aligned}
& \ell^2 \{ [C\sigma_1 C\sigma_2 + S\sigma_1 S\sigma_2 C(\beta_1 - \beta_2)] \left[ \frac{3m}{2} + m_{\rho_L} \right] \\
& + M_S [C\sigma_1 E_{11} + S\sigma_1 C\beta_1 E_{12} - S\sigma_1 S\beta_1 E_{13}] [C\sigma_2 E_{11} + S\sigma_2 C\beta_2 E_{12} - S\sigma_2 S\beta_2 E_{13}]
\end{aligned}$$

$$\begin{aligned}
& +M_L [C\sigma_1 \epsilon_{21} + S\sigma_1 C\beta_1 \epsilon_{22} - S\sigma_1 S\beta_1 \epsilon_{23}] [C\sigma_2 \epsilon_{21} + S\sigma_2 C\beta_2 \epsilon_{22} - S\sigma_2 S\beta_2 \epsilon_{23}] \\
& +M_V [C\sigma_1 \epsilon_{31} + S\sigma_1 C\beta_1 \epsilon_{32} - S\sigma_1 S\beta_1 \epsilon_{33}] [C\sigma_2 \epsilon_{31} + S\sigma_2 C\beta_2 \epsilon_{32} - S\sigma_2 S\beta_2 \epsilon_{33}] \ddot{\sigma}_1 \\
& +\mathcal{L}^2 \left\{ \frac{4m}{3} + m\rho_L + M_S [C\sigma_2 \epsilon_{11} + S\sigma_2 C\beta_2 \epsilon_{12} - S\sigma_2 S\beta_2 \epsilon_{13}]^2 \right. \\
& +M_L [C\sigma_3 \epsilon_{21} + S\sigma_3 C\beta_3 \epsilon_{22} - S\sigma_3 S\beta_3 \epsilon_{23}]^2 + M_V [C\sigma_3 \epsilon_{31} + S\sigma_3 C\beta_3 \epsilon_{32} - S\sigma_3 S\beta_3 \epsilon_{33}]^2 \left. \right\} \ddot{\sigma}_2 \\
& +\mathcal{L}^2 \left\{ [C\sigma_3 C\sigma_2 + S\sigma_3 S\sigma_2 C(\beta_2 - \beta_3)] \left[ \frac{m}{2} + m\rho_L \right] \right. \\
& +M_S [C\sigma_3 \epsilon_{11} + S\sigma_3 C\beta_3 \epsilon_{12} - S\sigma_3 S\beta_3 \epsilon_{13}] [C\sigma_2 \epsilon_{11} + S\sigma_2 C\beta_2 \epsilon_{12} - S\sigma_2 S\beta_2 \epsilon_{13}] \\
& +M_L [C\sigma_3 \epsilon_{21} + S\sigma_3 C\beta_3 \epsilon_{22} - S\sigma_3 S\beta_3 \epsilon_{23}] [C\sigma_2 \epsilon_{21} + S\sigma_2 C\beta_2 \epsilon_{22} - S\sigma_2 S\beta_2 \epsilon_{23}] \\
& +M_V [C\sigma_3 \epsilon_{31} + S\sigma_3 C\beta_3 \epsilon_{32} - S\sigma_3 S\beta_3 \epsilon_{33}] [C\sigma_2 \epsilon_{31} + S\sigma_2 C\beta_2 \epsilon_{32} - S\sigma_2 S\beta_2 \epsilon_{33}] \left. \right\} \ddot{\sigma}_3 \\
& +\mathcal{L} \{ M_S [-R_{j,m} \epsilon_{33} + R_{k,m} \epsilon_{23}] [C\sigma_2 \epsilon_{11} + S\sigma_2 C\beta_2 \epsilon_{12} - S\sigma_2 S\beta_2 \epsilon_{13}] \\
& +M_L [-R_{k,m} \epsilon_{13}] [C\sigma_2 \epsilon_{21} + S\sigma_2 C\beta_2 \epsilon_{22} - S\sigma_2 S\beta_2 \epsilon_{23}] \\
& +M_V [R_{j,m} \epsilon_{13}] [C\sigma_2 \epsilon_{31} + S\sigma_2 C\beta_2 \epsilon_{32} - S\sigma_2 S\beta_2 \epsilon_{33}] \} \ddot{\psi} \\
& +\mathcal{L} \{ M_S [-R_{k,m}] [C\sigma_2 \epsilon_{11} + S\sigma_2 C\beta_2 \epsilon_{12} - S\sigma_2 S\beta_2 \epsilon_{13}] \} \dot{\phi} = F_{\sigma_2}
\end{aligned}$$

(89)

For  $r = 3$ ,

$$\begin{aligned}
 & \mathcal{L}^2 \left\{ [C\sigma_1 C\sigma_3 + S\sigma_1 S\sigma_3 C(\beta_3 - \beta_1)] \left[ \frac{m}{2} + m\rho_1 \right] \right. \\
 & + M_5 [C\sigma_1 \epsilon_{11} + S\sigma_1 C\beta_1 \epsilon_{12} - S\sigma_1 S\beta_1 \epsilon_{13}] [C\sigma_3 \epsilon_{11} + S\sigma_3 C\beta_3 \epsilon_{12} - S\sigma_3 S\beta_3 \epsilon_{13}] \\
 & + M_6 [C\sigma_1 \epsilon_{21} + S\sigma_1 C\beta_1 \epsilon_{22} - S\sigma_1 S\beta_1 \epsilon_{23}] [C\sigma_3 \epsilon_{21} + S\sigma_3 C\beta_3 \epsilon_{22} - S\sigma_3 S\beta_3 \epsilon_{23}] \\
 & \left. + M_7 [C\sigma_1 \epsilon_{31} + S\sigma_1 C\beta_1 \epsilon_{32} - S\sigma_1 S\beta_1 \epsilon_{33}] [C\sigma_3 \epsilon_{31} + S\sigma_3 C\beta_3 \epsilon_{32} - S\sigma_3 S\beta_3 \epsilon_{33}] \right\} \ddot{\sigma}_1 \\
 & + \mathcal{L}^2 \left\{ [C\sigma_2 C\sigma_3 + S\sigma_2 S\sigma_3 C(\beta_3 - \beta_2)] \left[ \frac{m}{2} + m\rho_1 \right] \right. \\
 & + M_5 [C\sigma_2 \epsilon_{11} + S\sigma_2 C\beta_2 \epsilon_{12} - S\sigma_2 S\beta_2 \epsilon_{13}] [C\sigma_3 \epsilon_{11} + S\sigma_3 C\beta_3 \epsilon_{12} - S\sigma_3 S\beta_3 \epsilon_{13}] \\
 & + M_6 [C\sigma_2 \epsilon_{21} + S\sigma_2 C\beta_2 \epsilon_{22} - S\sigma_2 S\beta_2 \epsilon_{23}] [C\sigma_3 \epsilon_{21} + S\sigma_3 C\beta_3 \epsilon_{22} - S\sigma_3 S\beta_3 \epsilon_{23}] \\
 & \left. + M_7 [C\sigma_2 \epsilon_{31} + S\sigma_2 C\beta_2 \epsilon_{32} - S\sigma_2 S\beta_2 \epsilon_{33}] [C\sigma_3 \epsilon_{31} + S\sigma_3 C\beta_3 \epsilon_{32} - S\sigma_3 S\beta_3 \epsilon_{33}] \right\} \ddot{\sigma}_2 \\
 & + \mathcal{L}^2 \left\{ \frac{m}{3} + m\rho_1 + M_5 [C\sigma_3 \epsilon_{11} + S\sigma_3 C\beta_3 \epsilon_{12} - S\sigma_3 S\beta_3 \epsilon_{13}]^2 \right. \\
 & + M_6 [C\sigma_3 \epsilon_{21} + S\sigma_3 C\beta_3 \epsilon_{22} - S\sigma_3 S\beta_3 \epsilon_{23}]^2 + M_7 [C\sigma_3 \epsilon_{31} + S\sigma_3 C\beta_3 \epsilon_{32} - S\sigma_3 S\beta_3 \epsilon_{33}]^2 \left. \right\} \ddot{\sigma}_3 \\
 & + \mathcal{L} \left\{ M_5 [-R_{j,m} \epsilon_{32} + R_{k,m} \epsilon_{23}] [C\sigma_3 \epsilon_{11} + S\sigma_3 C\beta_3 \epsilon_{12} - S\sigma_3 S\beta_3 \epsilon_{13}] \right. \\
 & \left. + M_6 [-R_{k,m} \epsilon_{13}] [C\sigma_3 \epsilon_{21} + S\sigma_3 C\beta_3 \epsilon_{22} - S\sigma_3 S\beta_3 \epsilon_{23}] \right.
 \end{aligned}$$

$$+M_r [R_{j_m} \epsilon_{13}] [C\sigma_3 \epsilon_{31} + S\sigma_3 C\beta_3 \epsilon_{32} - S\sigma_3 S\beta_3 \epsilon_{33}] \ddot{\psi} \\ + \mathcal{L} \{ M_s [-R_{k_m}] [C\sigma_3 \epsilon_{11} + S\sigma_3 C\beta_3 \epsilon_{12} - S\sigma_3 S\beta_3 \epsilon_{13}] \} \ddot{\phi} = F_{\sigma_3} \quad (90)$$

The generalized forces ( $F_\psi$ ,  $F_\phi$ ,  $F_{\sigma_1}$ ,  $F_{\sigma_2}$ ,  $F_{\sigma_3}$ ) were derived in Section V, Appendix A of the Second Scientific Report\*. The following equations are taken from that section.

$$F_\psi = F_{BSA} [(-R_{j_A} \epsilon_{33} + R_{k_A} \epsilon_{23}) \epsilon_{11} + (R_{k_A} \epsilon_{13}) \epsilon_{12} + (R_{j_A} \epsilon_{13}) \epsilon_{31}] + M_{\psi_0} \quad (91)$$

$$F_\phi = [W_B R_{k_B} - L_S R_{B_B}] \epsilon_{13} + [-F_{BSA} R_{k_A}] \epsilon_{11} + M_{\phi_0} \quad (92)$$

$$F_{\sigma_1} = \mathcal{L} \{ [L_S - W_B - (m_{p_k} + \frac{3m}{2}) g] [-S\sigma_1 S\beta_1] + [F_{BSA}] [C\sigma_1] \\ + [D_{CS1}] [C_1 C^2\sigma_1] + [D_{CS2}] [C^2\sigma_2 (C\sigma_2 C\sigma_1 + S\sigma_2 S\sigma_1 C(\beta_1 - \beta_2))] \\ + [D_{CS3}] [C^2\sigma_3 (C\sigma_3 C\sigma_1 + S\sigma_3 S\sigma_1 C(\beta_1 - \beta_3))] \} \quad (93)$$

$$F_{\sigma_2} = \mathcal{L} \{ [L_S - W_B - (m_{p_k} + \frac{3m}{2}) g] [-S\sigma_2 S\beta_2] + [F_{BSA}] [C\sigma_2] \\ + [D_{CS2}] [C_2 C^2\sigma_2] + [D_{CS3}] [C^2\sigma_3 (C\sigma_3 C\sigma_2 + S\sigma_3 S\sigma_2 C(\beta_2 - \beta_3))] \} \quad (94)$$

$$F_{\sigma_3} = \mathcal{L} \{ [L_S - W_B - (m_{p_k} + \frac{3m}{2}) g] [-S\sigma_3 S\beta_3] + [F_{BSA}] [C\sigma_3] + [D_{CS3}] [C_3 C^2\sigma_3] \} \quad (95)$$

The aerodynamic forces and moments are:

$$F_{BSA} = q_B S_B [C_{YB} + C_{Y\psi_B} \left( \frac{d_B}{V_{BR}} \right) \dot{\psi} + C_{Y\dot{\phi}_B} \left( \frac{d_B}{V_{BR}} \right) \dot{\phi}] \quad (96)$$

\*Reference 2

$$M_{\psi B} = g_B S_B d_B \left[ C_{mB} + C_{m\dot{\psi}B} \left( \frac{d_B}{V_{BR}} \right) \dot{\psi} + C_{m\dot{\phi}B} \left( \frac{d_B}{V_{BR}} \right) \dot{\phi} \right] \quad (97)$$

$$M_{\phi B} = g_B S_B d_B \left[ C_{L\phi B} + C_{L\dot{\psi}B} \left( \frac{d_B}{V_{BR}} \right) \dot{\psi} + C_{L\dot{\phi}B} \left( \frac{d_B}{V_{BR}} \right) \dot{\phi} \right] \quad (98)$$

$$D_{CSi} = -\frac{1}{2} \rho_{CL} S_{CL} C_{DC} V_{CL} \dot{X}_{CL} \quad (99)$$

$$g_B = \frac{1}{2} \rho_B V_{BR}^2 \quad (100)$$

$$V_{BR}^2 = (\dot{X}_B - V_{gs})^2 + (\dot{Y}_B + V_w)^2 + (\dot{Z}_B - V_{gv})^2 \quad (101)$$

$$\Gamma_B = \tan^{-1} (\dot{X}_{BR} / \dot{Y}_{BR}) \quad (102)$$

$$\beta = \Gamma_B - \psi \quad (103)$$

$$C_n = \frac{1}{3} \left( \frac{g_{nn} + 2g_{nn+1}}{g_{nn} + g_{nn+1}} \right) \quad (104)$$

As in the longitudinal dynamics, it is desirable to know the tension in the tether. This is done by summing forces at each hinge point. First consider the apparent inertia forces acting on the balloon along and normal to the centerline.

$$A_{XB} = M_S [\ddot{X}_B \epsilon_{11} + \ddot{Y}_B \epsilon_{12} + \ddot{Z}_B \epsilon_{13}] \quad (105)$$

$$A_{YB} = M_L [\ddot{X}_B \epsilon_{21} + \ddot{Y}_B \epsilon_{22} + \ddot{Z}_B \epsilon_{23}] \quad (106)$$

$$A_{ZB} = M_V [\ddot{X}_B \epsilon_{31} + \ddot{Y}_B \epsilon_{32} + \ddot{Z}_B \epsilon_{33}] \quad (107)$$

In Equations (105), (106), and (107),  $\ddot{X}_B$ ,  $\ddot{Y}_B$  and  $\ddot{Z}_B$  are inertia accelerations of the balloon:  $a_{XB}$ ,  $a_{YB}$ , and  $a_{ZB}$  are inertia forces in the positive direction of the balloon's lateral, longitudinal, and vertical axes.  $\epsilon_{ij}$  are elements of the matrix defined in Equation (82). Summing the apparent inertia forces in the lateral, longitudinal, and vertical directions gives:

$$\sum F_x = \epsilon_{11}a_{XB} + \epsilon_{21}a_{YB} + \epsilon_{31}a_{ZB} \quad (108)$$

$$\sum F_y = \epsilon_{12}a_{XB} + \epsilon_{22}a_{YB} + \epsilon_{32}a_{ZB} \quad (109)$$

$$\sum F_z = \epsilon_{13}a_{XB} + \epsilon_{23}a_{YB} + \epsilon_{33}a_{ZB} \quad (110)$$

The forces acting on the balloon above the payload are:

$$\sum F_x = F_{BSA} - T_{BS} \quad (111)$$

$$\sum F_y = T_{BH} - F_{BHA} \quad (112)$$

$$\sum F_z = L_S - W_B + F_{BVA} - T_{BV} \quad (113)$$

Now equate Equations (108), (109), and (110) with Equations (111), (112), and (113) respectively, and the following expressions for  $T_{BS}$ ,  $T_{BH}$ , and  $T_{BV}$  are found.

$$T_{BS} = F_{BSA} - (\epsilon_{11}a_{XB} + \epsilon_{21}a_{YB} + \epsilon_{31}a_{ZB}) \quad (114)$$

$$T_{BN} = F_{BNA} + (\epsilon_{11} a_{XB} + \epsilon_{22} a_{YB} + \epsilon_{33} a_{ZB}) \quad (115)$$

$$T_{BV} = F_{BVA} + L_S - W_B - (\epsilon_{13} a_{XB} + \epsilon_{23} a_{YB} + \epsilon_{33} a_{ZB}) \quad (116)$$

If forces are summed at the payload location, the components of tension at the top of the tether results.

$$F_{CSN} = F_{BSA} - (\epsilon_{11} a_{XB} + \epsilon_{21} a_{YB} + \epsilon_{31} a_{ZB}) - m_{PL} \ddot{x}_{PL} \quad (117)$$

$$F_{CHN} = F_{BNA} + (\epsilon_{12} a_{XB} + \epsilon_{22} a_{YB} + \epsilon_{32} a_{ZB}) + m_{PL} \ddot{y}_{PL} \quad (118)$$

$$F_{CVN} = F_{BVA} + L_S - W_B - (\epsilon_{13} a_{XB} + \epsilon_{23} a_{YB} + \epsilon_{33} a_{ZB}) - m_{PL} g - m_{PL} \ddot{z}_{PL} \quad (119)$$

The vertical and horizontal forces on the "N"th link are the same as they were in the longitudinal dynamics program. The force in the lateral direction is given in Equation (99). In general for the "r"th link.

$$F_{CSr-1} = F_{CSr} - D_{CSr} - m \ddot{x}_{Cr} \quad (120)$$

$$F_{CHr-1} = F_{CHr} + F_{CNr} \delta \theta_r + m \ddot{y}_{Cr} \quad (121)$$

$$F_{CVr-1} = F_{CVr} - F_{CNr} c \theta_r - m g - m \ddot{z}_{Cr} \quad (122)$$

$$T_{r-1} = \sqrt{(F_{CSr-1})^2 + (F_{CHr-1})^2 + (F_{CVr-1})^2} \quad (123)$$

The tension at the winch is found by setting  $r = 1$ .

APPENDIX B

DYNAMIC RESPONSE INPUT AND OUTPUT DATA  
LONGITUDINAL AND LATERAL DYNAMIC SIMULATIONS  
CASES 1 THROUGH 40

## SECTION I

### INTRODUCTION

Appendix B consists of the input data used in making the computer run cases 1 through 40, and computer constructed plots of selected output variables for these cases.

Table B-I lists input data for the longitudinal dynamic cases 1 through 23, and Table B-II lists the input data for the lateral dynamic cases 24 through 40. Tables B-III and B-IV list the balloon longitudinal and lateral static aerodynamic coefficients respectively.

Computer constructed plots (3 plots per case are included on each page) for cases 1 through 40 follow Table B-IV. The parameters plotted with respect to time are listed below.

#### Longitudinal Cases 1 through 23

Balloon pitch angle	
Link 3 pitch angle	Plot
Link 2 pitch angle	1
Link 1 pitch angle	
Tension at bridle	
Tension at winch	Plot
Balloon altitude	2
Balloon range	
Wind gust velocity	
Pitching velocity of balloon	Plot
Wind angle of attack	3
Relative velocity of balloon	

#### Lateral Cases 24 through 40

Balloon roll angle	
Balloon yaw angle	Plot
Balloon yaw rate	1
Balloon sideslip angle	
Balloon lateral displacement	
Link 3 yaw angle	Plot
Link 2 yaw angle	2
Link 1 yaw angle	
Wind gust velocity	
Relative velocity of Balloon	Plot
Tension at bridle	3
Tension at winch	

Table B-1. Input Data for Longitudinal Cases

Run No	Balloon Type	Altitude Feet	Tether Type	Tail Config	Volume Ft <sup>3</sup>	Wind Profile	WB Lb	LS Lb	MPL Slugs	WTC Lb	IRB Slug-Ft <sup>2</sup>	MAL Slugs	MAV Slugs	FF	SB- $\frac{2}{3}$ Ft <sup>2</sup>	DB- $\frac{1}{3}$ Ft <sup>2</sup>	CDC	DC Ft	Teth Ft	CMTDB Rad-l	CLTDB Rad-l
1	BJ	10,000	Nolard	Nominal	60K	100%	2157	3942	31.06	708	116,000	15.7	110.0	0	1533	39.15	1.1	0.0342	12,639	-2.01	1.68
2																					
3																					
4 *																					
5																					
6																					
7		10,000			60K		2157	3942	31.06	708	116,000	15.7	110.0		1533	39.15	1.1	0.0342	12,639		
8		5,000			46K		1627	3526	46.58	183	75,000	12.0	86.0		1284	35.83		0.0248	5,692		
9		20,000	Nolard		500K		15624	23715	18.63	8900	3,204,000	95.0	666.0		6300	79.37		0.0828	27,436		
10.		10,000	Angal	Nominal	75K		2665	4928	31.06	1128	167,000	20.0	138.0		1778	42.17		0.0208	11,305	-2.01	1.68
11			Nolard	81%	60K		1970	3811		708	104,100	14.7	103.0		1533	39.15		0.0342	12,639	-1.58	1.25
12				144%		100%	2680	4340			142,000	18.8	131.0							-2.61	2.14
13		10,000		Nominal		40%	2157	3942		708	116,000	15.7	110.0						12,639	-2.01	1.68
14		4,000				100%	2877	4720		234	142,000	31.7	222.0						4,170		
15		1,000					3358	5190		54.0	159,400	35.5	249.0						970		
16 (Payload on Underside)		10,000					3157	942		708	171,300	15.7	110.0						12,639		
17 (Winch at 5000 Feet)	BJ				60K		2157	3942		314	116,000	15.7	110.0		1533	39.15		0.0342	5,600	-2.01	1.68
18	Vee				80K		2334	4822		1260	166,300	47.0	189.0		1856.7	43.09		0.0488	11,060	-2.483	2.495
19																					
20	Vee						2334	4822		1260	166,300	47.0	189.0					0.0488	11,060	-2.483	2.495
21	CAC						2788	5016		1015	249,400	14.7	169.4					0.0433	11,274	-2.07	1.49
22																					
23	CAC	10,000	Nolard	Nominal	80K	100%	2788	5016	31.06	1015	249,400	14.7	169.4	0	1856.7	43.09	1.1	0.0433	11,274	-2.07	1.49

\* Case 4A is identical to Case 4 except gust is applied vertically up in Case 4A rather than horizontally aft

Table B-I. (Continued)

Run No.	RJM Ft	RKM Ft	RJA Ft	RKA Ft	RJB Ft	RKG Ft	RJB Ft	RKB Ft	THE DEG DEG	XIDEG (1) DEG	XIDEG (2) DEG	XIDEG (3) DEG	THEDDE DEG	XIDEG (1) DEG	DT1 Sec	DT2 Sec	DTP1	DTP2	TDTC Sec	TTT Sec	T Sec
1	19.6	-44.6	6.7	-46.0	23.7	-42.3	12.6	-45.4	8.5030	41.6466	51.5297	65.4682	0.0	0.0	.5	1.	1.	5.	60.	180.	0.0
2																					
3																					
4																					
5																					
6	21.4	-44.6	8.5	-46.0	25.5	-42.3	14.4	-45.4	6.4289	36.9724	48.2677	64.0386			.5	1.	1.	5.	60.	180.	
7	17.9	-44.6	5.0	-46.0	22.0	-42.3	10.9	-45.4	10.4826	45.0979	53.9550	66.5133									
8	16.9	-41.1	4.9	-42.1	24.7	-39.2	10.3	-41.5	5.2536	55.3565	60.0976	66.8154									
9	45.6	80.7	19.9	-03.3	51.4	-84.7	31.9	-92.0	8.4342	30.0426	48.4859	67.6940									
10	20.7	-48.4	6.8	-40.6	25.1	-45.6	13.2	-48.9	8.3106	53.9520	62.2320	70.9677									
11	19.5	-44.6	8.9	-46.0	23.8	-42.5	13.4	-45.6	10.9832	41.6777	51.1670	64.5175									
12	21.5	-44.4	4.5	-46.0	25.4	-42.0	13.3	-44.9	7.3693	43.4984	53.1029	66.6907									
13	19.6	-44.6	6.7	-46.0	23.7	-42.3	12.6	-45.4	2.9646	57.3521	71.4708	81.0848									
14	21.4	-44.2	2.7	-46.0	23.8	-41.4	12.6	-45.4	8.7908	69.8457	72.2866	75.5869									
15	20.9	-44.1	6.7	-46.0	22.5	-41.5	12.6	-45.4	7.3067	83.2441	83.6630	84.1377			.25	.5	2.	10.			
16 (Payload on Underside)	20.7	-38.0	9.7	-46.0	21.3	-28.9	15.6	-45.4	6.5076	41.6310	51.5191	55.4645			.5	.1	1.	5.			
17 (Winch at 5000 Feet)	19.6	-44.6	6.7	-46.0	23.7	-42.3	12.6	-45.4	8.5103	56.4410	62.6544	69.4930									
18	21.3	-37.5	9.4	-38.6	17.0	-34.5	11.7	-38.5	6.9577	58.5433	64.1700	71.7230									
19	24.2	-37.5	12.3	-38.6	19.9	-34.5	14.6	-38.5	4.9941	52.7234	59.9523	69.3939									
20	18.6	-37.5	6.7	-38.6	14.3	-34.5	9.0	-38.5	9.1072	62.8254	67.3040	73.4503									
21	18.3	-56.6	-5	-57.5	18.4	-54.7	4.7	-57.5	7.9176	53.9442	62.0587	72.9344									
22	22.5	-56.6	3.7	-57.5	22.6	-54.7	8.7	-57.5	5.9761	49.0389	58.4903	70.9483									
23	14.6	-56.6	-4.2	-57.5	14.7	-54.7	.8	-57.5	10.0287	58.0858	65.0961	74.6215									

Table B-I. (Continued)

Run No.	Time (seconds)						Velocity (feet per second)					
	TTG (1)	TTG (2)	TTG (3)	TTG (4)	TTG (5)	TTG (6)	VVG (1)	VVG (2)	VVG (3)	VVG (4)	VVG (5)	VVG (6)
1	0.0	4.99	5.0	1000.			0.0	0.0	20.2	20.2	0.0	0.0
2				7.0	7.01	1000.						
3				15.0	15.01							
4				25.0	25.01							
5												
6				15.0	15.01	1000.			20.2	20.2	0.0	0.0
7									20.2	20.2	0.0	0.0
8									15.7	15.7		
9									27.3	27.3		
10									20.2	20.2		
11												
12												
13									8.0	8.0		
14									13.6	13.6		
15									7.1	7.1		
16									20.2	20.2		
17												
18												
19												
20												
21												
22												
23												

Table B-II. Input Data for Lateral Cases

Run. No.	Balloon Type	Altitude Ft	Tether Type	Tail Conf	Volume Ft <sup>3</sup>	Wind Profile	WB Lb	LS Lb	MPL Slugs	WTC Lb	IZB Slugs-Ft <sup>2</sup>	IYB Slugs-Ft <sup>2</sup>	IYZB Slugs Ft <sup>2</sup>	IXB Slugs Ft <sup>2</sup>
24	BJ	10,000	Nolard	Nominal	60K	100%	2157.	3942.	31.06	708.	119,000.	26,000.	12,500.	116,000.
25														
26														
27														
28														
29		5,000			46K		1627.	3526.	46.58	183.	75,300.	17,000	8,200	75,000.
30		20,000			500K		15624.	23715.	18.63	8900.	3,374,000.	771,000	296,000	3,204,000.
31		10,000	Amgal		75K		2665.	4928	31.06	1128.	172,000.	40,300	18,000	167,000.
32			Nolard	81%	60K		1970.	3211.		708.	106,400.	17,600	10,200	104,100
33				144%			2680.	4340.			145,000.	53,900	18,600	142,000
34				Nominal		40%	2157.	3942.		602.	119,000.	25,000	12,500	116,000
35		4,000				100%	2877.	4740.	31.06	234.	146,800.	35,800	13,400	142,400
36		1,000					3358.	5190.		54.0	164,700.	39,300	14,500	159,400
37		10,000			80K		2334.	4822.		1260.	173,300.	84,000	3,900	166,300
38				200%			2408.	4832.			187,000.	86,200	7,500	167,900
39	GAC			300%			2476.	4842.			198,700.	68,300	10,700	170,000
40				Nominal			2788.	5016.		1015.	228,800.	106,500	10,500	249,400

Table II. (Continued)

Run No.	THEODE DEG	X±0 DEG (1) DEG	XIO DEG (2) DEG	XIO DEG (3) DEG	RJM	RKM	RJA	RKA	RJG	RKG	RJB	RKB
24	8.5030	41.6466	51.5297	65.4682	20.5	-42.6	6.7	-46.0	23.7	-42.3	12.6	-45.4
25		↓	↓	↓	↓	↓	↓	↓	↓	↓	↓	↓
26												
27												
28												
29	5.2536	55.3565	60.0976	66.8153	17.8	-39.1	4.9	-42.1	21.7	-39.2	10.3	-41.5
30	8.4342	30.0426	48.4859	67.6940	47.2	-85.8	19.9	-93.3	51.4	-84.7	31.9	-92.0
31	8.3106	53.9520	62.2320	70.9677	21.7	-45.9	6.8	-49.6	25.1	-45.6	13.2	-48.9
32	10.9832	41.6977	51.1670	64.5175	18.3	-43.2	8.9	-46.0	23.8	-42.5	13.4	-45.6
33	7.3693	43.4984	53.1029	66.6907	24.7	-41.3	4.5	-46.0	25.4	-42.0	13.3	-44.9
34	2.9646	57.3521	71.4708	81.0948	20.5	-42.6	6.7	-46.0	23.7	-42.3	12.6	-45.4
35	8.7908	69.8457	72.2866	75.5869	22.3	-42.2	6.7	-46.0	23.8	-41.4	12.6	-45.4
36	7.3067	83.2441	83.6630	84.1377	21.8	-42.2	6.7	-46.0	22.5	-41.5	12.6	-45.4
37	6.9577	58.5433	64.1700	71.7230	13.7	-36.7	9.4	-38.6	17.0	-34.5	11.7	-38.5
38	7.2273	58.8436	64.3656	71.7906	13.8	-36.0	9.4	-38.6	17.5	-34.3	11.7	-38.5
39	7.5040	59.1800	64.5910	71.8802	14.0	-35.4	9.4	-38.6	18.1	-33.9	11.7	-38.5
40	7.9776	53.9442	62.0587	72.9344	16.2	-55.0	-5	-57.5	18.4	-54.7	4.7	-57.5

Table B-II. (Continued)

R in No	SB = $\psi^{2/3}$ FT	DB = $\psi^{1/3}$ FT	CDC	DC FT	TETH FT	MAL Slugs	MAV Slugs	MAS Slugs	CYPSDB rad <sup>-1</sup>	CYPHDB rad <sup>-1</sup>	CNPSPDB rad <sup>-1</sup>	CNPHDB rad <sup>-1</sup>	CLPSPDB rad <sup>-1</sup>	CLPHDB rad <sup>-1</sup>	DT1 Sec	DT2 Sec	DTP1	DTP2	TDIC Sec	TTT Sec	T Sec
24	1533	39.15	1.1	.0382	12639	15.7	110.0	115.0	1.79	.142	-2.31	-.122	-.347	-.327	.5	1.	1.	5.	30.	360.	0.
25																					
26																					
27																					
28																					
29	1284	35.83		.0268	5692	12.0	86.0	86.0											30.		
30	1300	39.37		.0836	27436	95.0	666.0	690.0											30.		
31	1778	42.17		.0208	11305.	20.0	138.0	143.0											60.		
32	1533	39.15		.0342	12639	14.7	103.0	107.0	1.55	104	-2.08	-.096	-.280	-.210					30.		
33									2.27	224	-2.67	-.170	-.484	-.609							
34					10740	15.7	110.0	115.0	1.79	.142	-2.31	-.122	-.347	-.327							
35					4170.	31.7	222.0	227.0													
36					970	35.5	249.0	255.0							.25	.25	2.	20.	60.	720.	
37	1850.7	43.09		.0488	11060	47.0	189.0	127.0	.43	.054	-.482	-.0505	-.0212	-.3758					120.	360.	
38									.716	.108	-.784	-.1010	-.0494	-.3930					30.		
39									.997	.162	-1.086	-.1615	-.0810	-.4120							
40				.0433	11274.	14.7	169.4	154.4	1.94	0.0	-2.07	0.0	-.298	-.508							

Table B-II. (Continued)

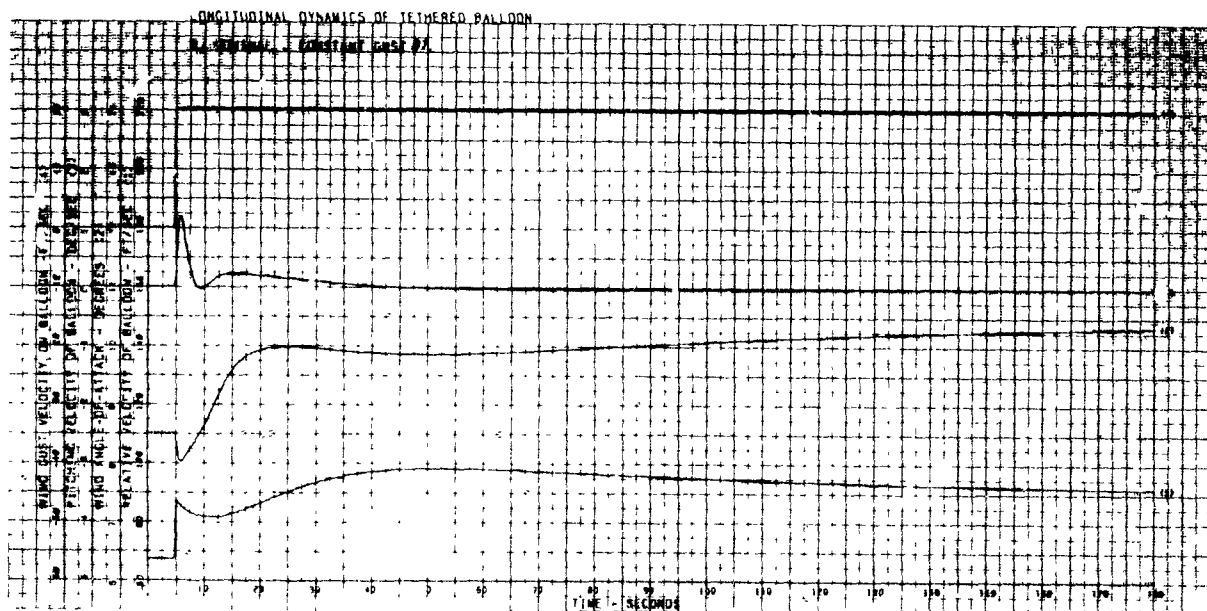
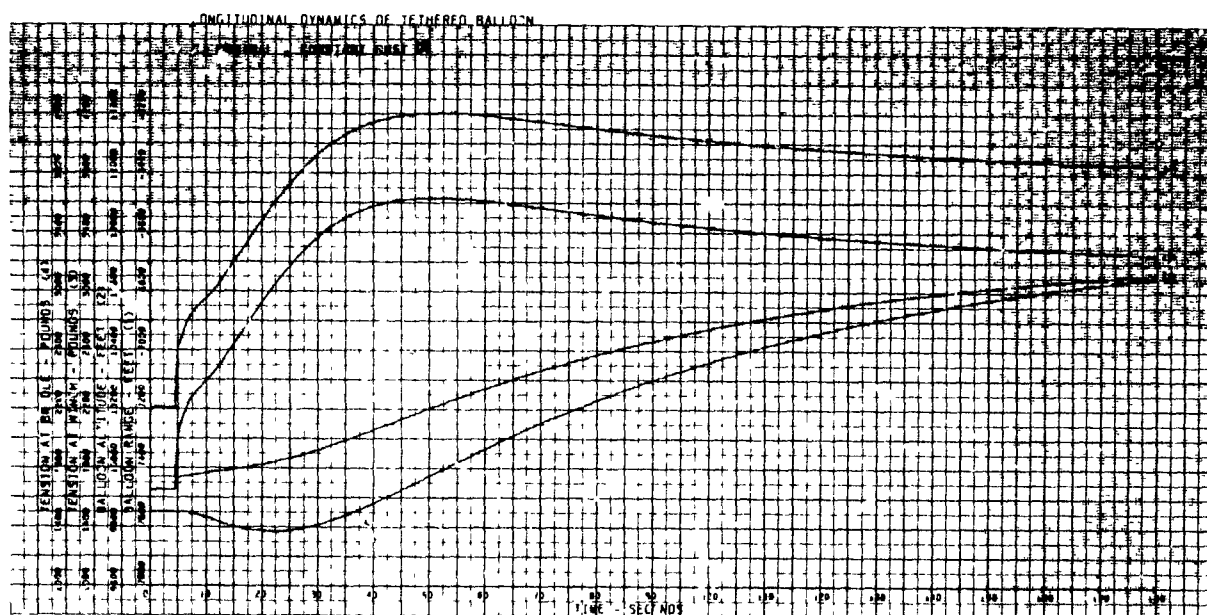
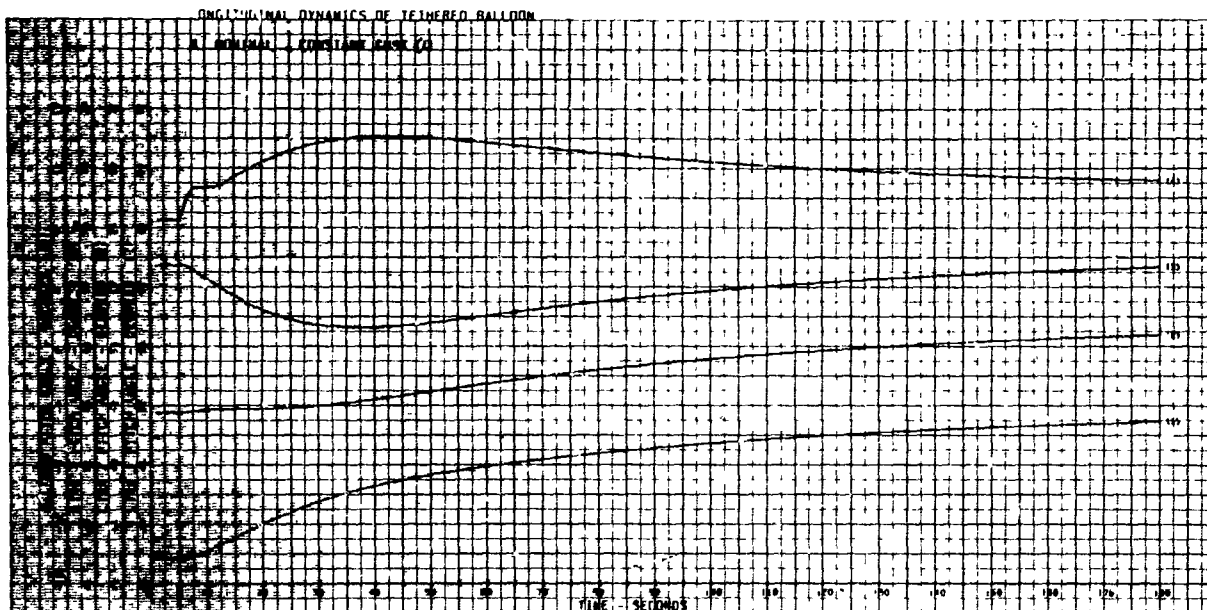
Run No.	Time (seconds)						Velocity (Feet per second)					
	TTG (1)	TTG (2)	TTG (3)	TTG (4)	TTG (5)	TTG (6)	VVG (1)	VVG (2)	VVG (3)	VVG (4)	VVG (5)	VVG (6)
24	9.0			1000.			0.0	0.0		12.0		
25		8.0							↓	↓		
26		10.0										
27		↓							18.0	18.0		
28		5.01		15.0	15.01	1000.			12.0	12.0	0.0	0.0
29		8.0		1000.					9.0	9.0		
30									16.0	16.0		
31									12.0	12.0		
32									↓	↓		
33												
34									4.8	4.8		
35									8.0	8.0		
36									1.0	1.0		
37									12.0	12.0		
38												
39												
40												

TABLE B-III. LONGITUDINAL STATIC AERODYNAMIC COEFFICIENTS

Angle -Of -Attack	-5	0	5	10	12	15	20	25
BJ (Nominal)	$C_m$	.0137	.0103	-.0005	.0044	.0050	-.0075	-.0780
	$C_L$	-.1100	.0063	.1368	.2514	.2991	.5100	.6200
	$C_D$	.1100	.0764	.0865	.1133	.1279	.2200	.3000
BJ (81% Tail)	$C_m$	-.0099	.0103	.0231	.0515	.0615	.0532	.0398
	$C_L$	-.0838	.0063	.1106	.1990	.2363	.4053	.4891
	$C_D$	.1094	.0764	.0857	.1103	.1236	.2077	.2814
BJ (144% Tail)	$C_m$	.0490	.0103	-.0358	-.0663	-.0798	-.1824	-.2547
	$C_L$	-.1528	.0063	.1796	.3369	.4017	.6810	.8338
	$C_D$	.1115	.0764	.0883	.1198	.1372	.2464	.3402
VEE (Nominal)	$C_m$	-.010	.030	.103	.110	.113	.090	.022
	$C_L$	-.400	0.0	.400	.800	.970	1.610	2.030
	$C_D$	.150	.160	.170	.230	.265	.510	.740
GAC (Nominal)	$C_m$	.070	-.010	-.074	-.120	-.170	-.310	-.460
	$C_L$	-.240	0.0	.210	.380	.450	.830	1.080
	$C_D$	.195	.085	.090	.100	.110	.230	.390

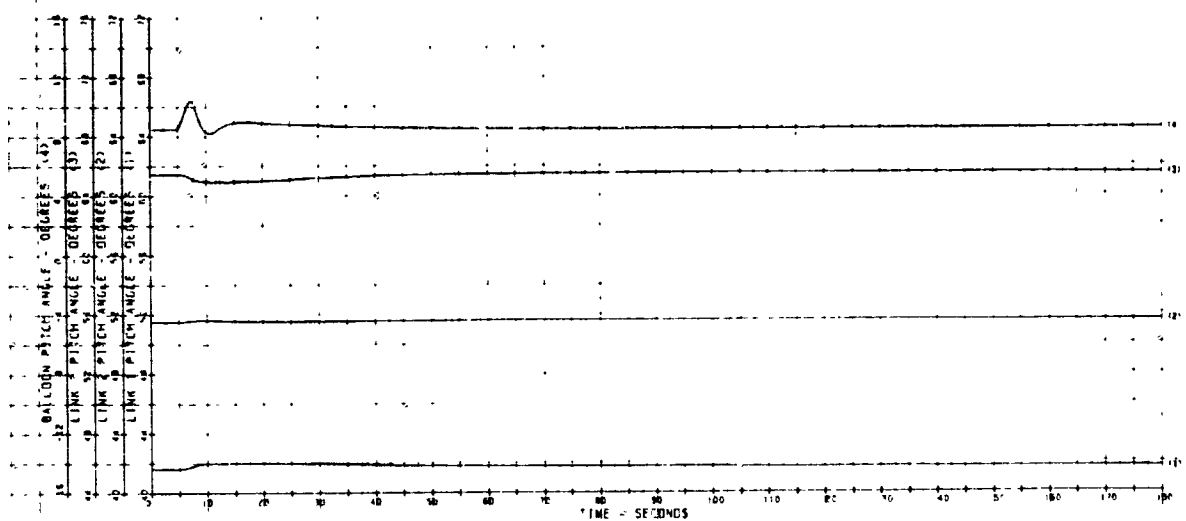
TABLE B-IV. LATERAL STATIC AERODYNAMIC COEFFICIENTS

Sideslip Angle		-20	0	20
BJ (Nominal)	$C_y$	.7260	0.0	-.726
	$C_m$	-.0366	0.0	.0366
	$C_l$	-.1226	0.0	.1226
BJ (81% Tail)	$C_y$	.646	0.0	-.646
	$C_m$	.0279	0.0	-.0279
	$C_l$	.0907	0.0	-.0907
BJ (144% Tail)	$C_y$	.923	0.0	-.923
	$C_m$	-.174	0.0	.174
	$C_l$	-.193	0.0	.193
VEE (Nominal)	$C_y$	.299	0.0	-.299
	$C_m$	-.0014	0.0	.0014
	$C_l$	-.002	0.0	.002
VEE (200% Bottom Tail)	$C_y$	.502	0.0	-.502
	$C_m$	-.154	0.0	.154
	$C_l$	-.0471	0.0	.0741
VEE (300% Bottom Tail)	$C_y$	.706	0.0	-.706
	$C_m$	-.3065	0.0	.3065
	$C_l$	-.0768	0.0	.0768
GAC (Nominal)	$C_y$	.663	0.0	-.663
	$C_m$	-.0768	0.0	.0768
	$C_l$	-.1305	0.0	.1305



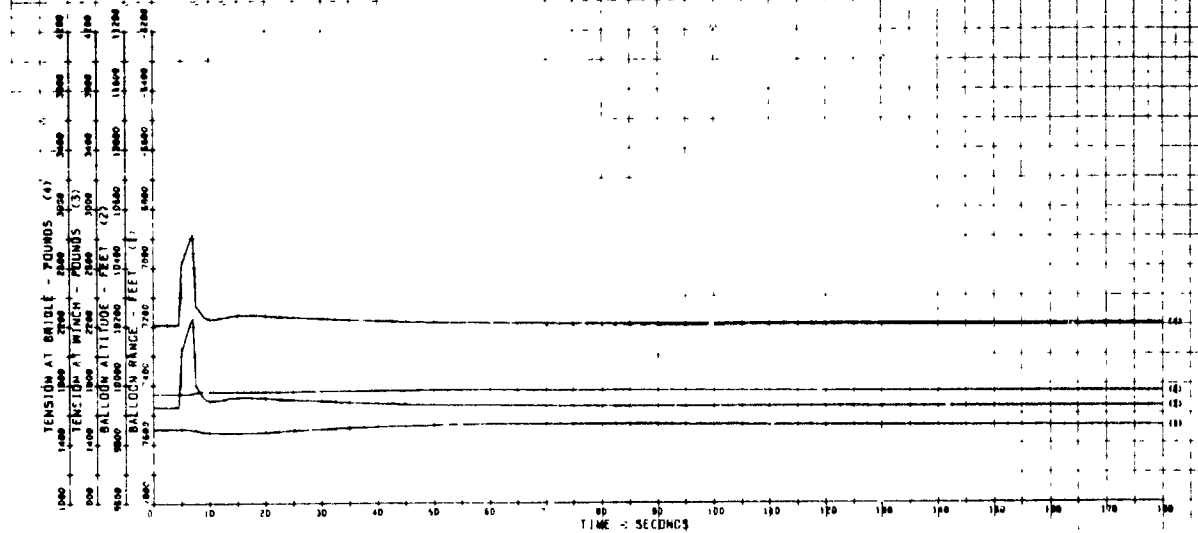
# LONGITUDINAL DYNAMICS OF TETHERED BALLOON

B.1 NOMINAL - 2 SEC. GUST (2)



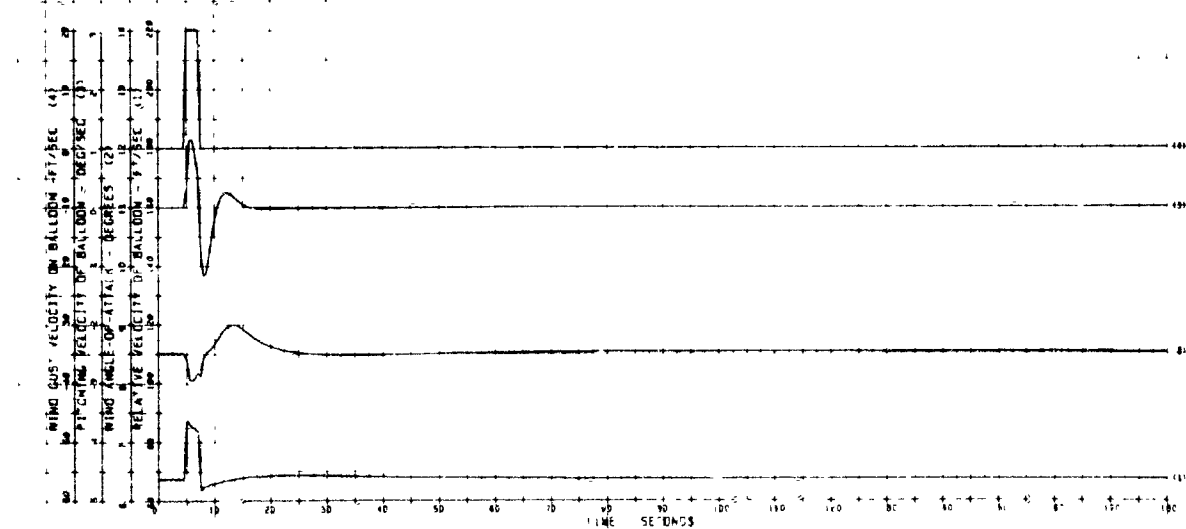
# LONGITUDINAL DYNAMICS OF TETHERED BALLOON

B.1 NOMINAL - 2 SEC. GUST (2)



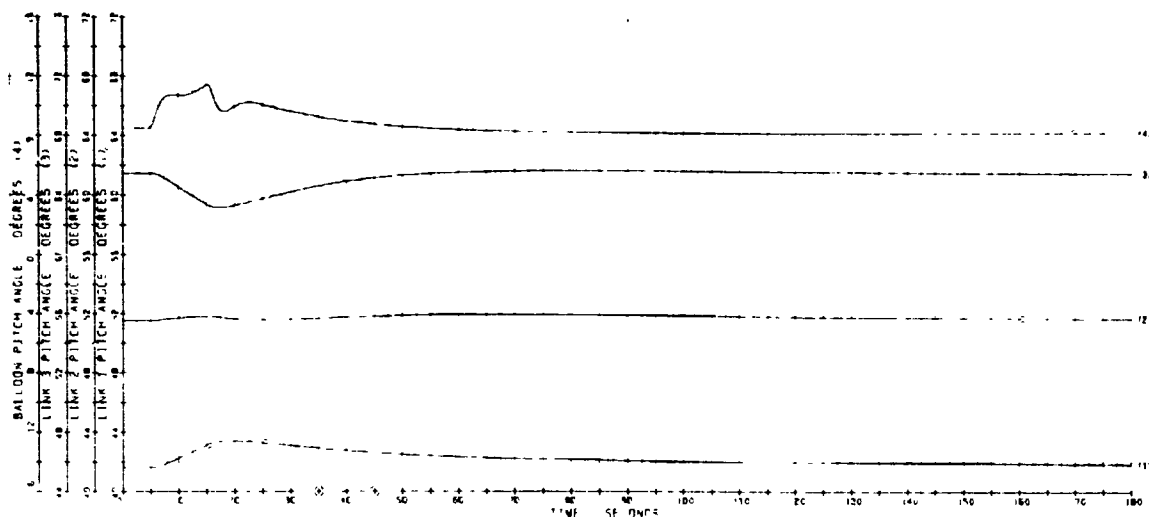
# LONGITUDINAL DYNAMICS OF TETHERED BALLOON

B.1 NOMINAL - 2 SEC. GUST (2)



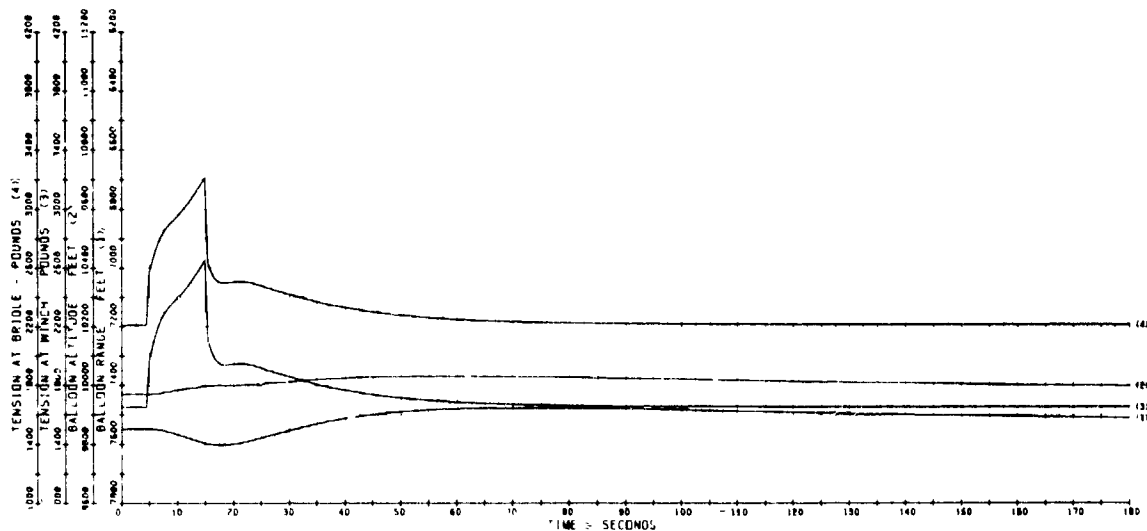
# LONGITUDINAL DYNAMICS OF TETHERED BALLOON

B.J. NOMINAL . 10 SEC. GUST (3)



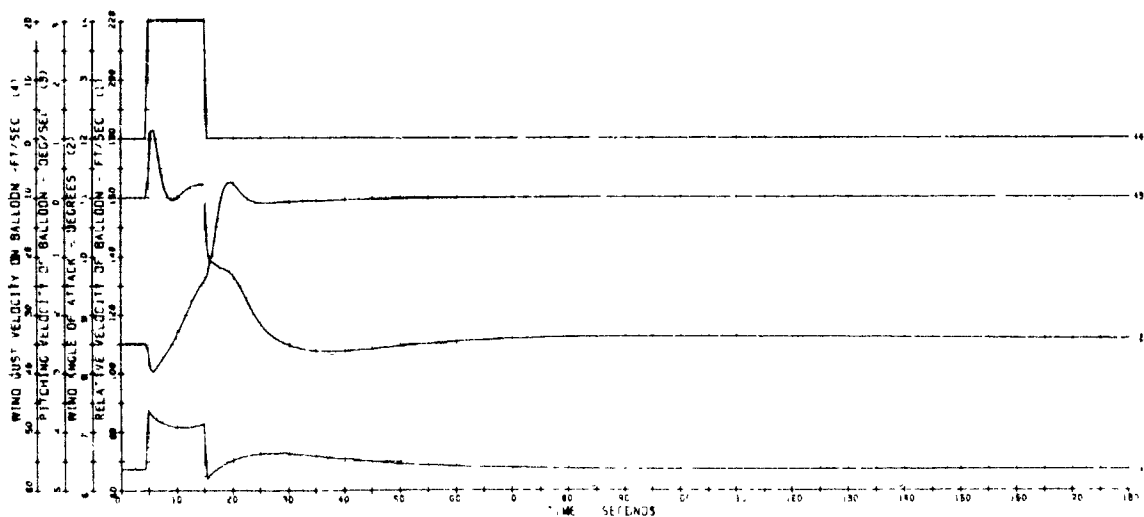
# LONGITUDINAL DYNAMICS OF TETHERED BALLOON

B.J. NOMINAL . 10 SEC. GUST (3)



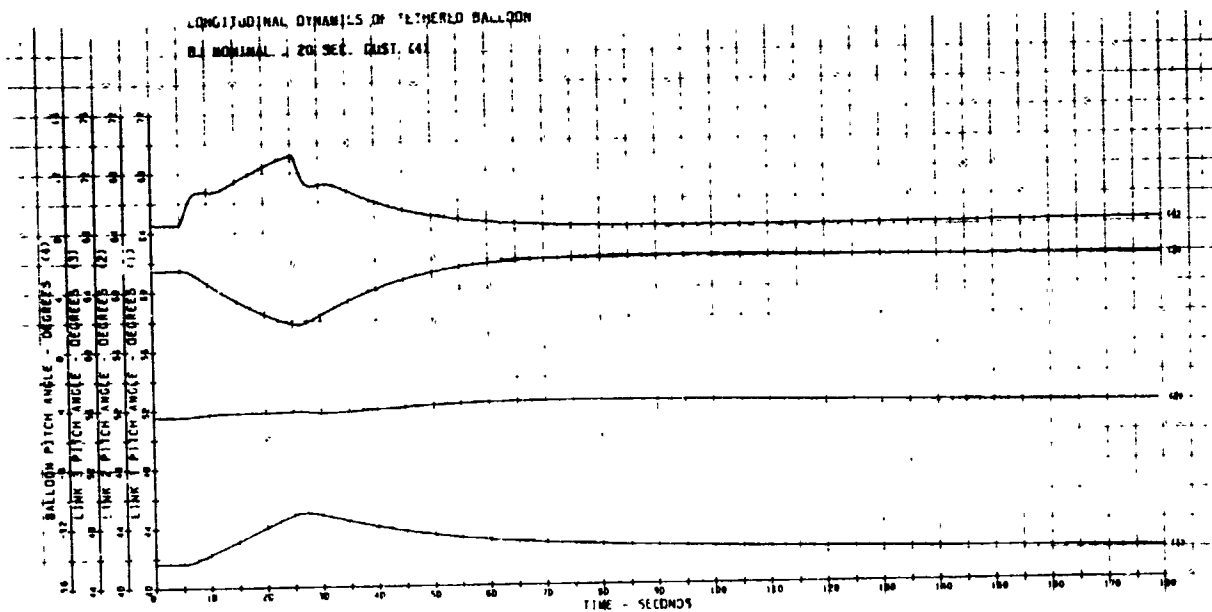
# LONGITUDINAL DYNAMICS OF TETHERED BALLOON

B.J. NOMINAL . 10 SEC. GUST (3)



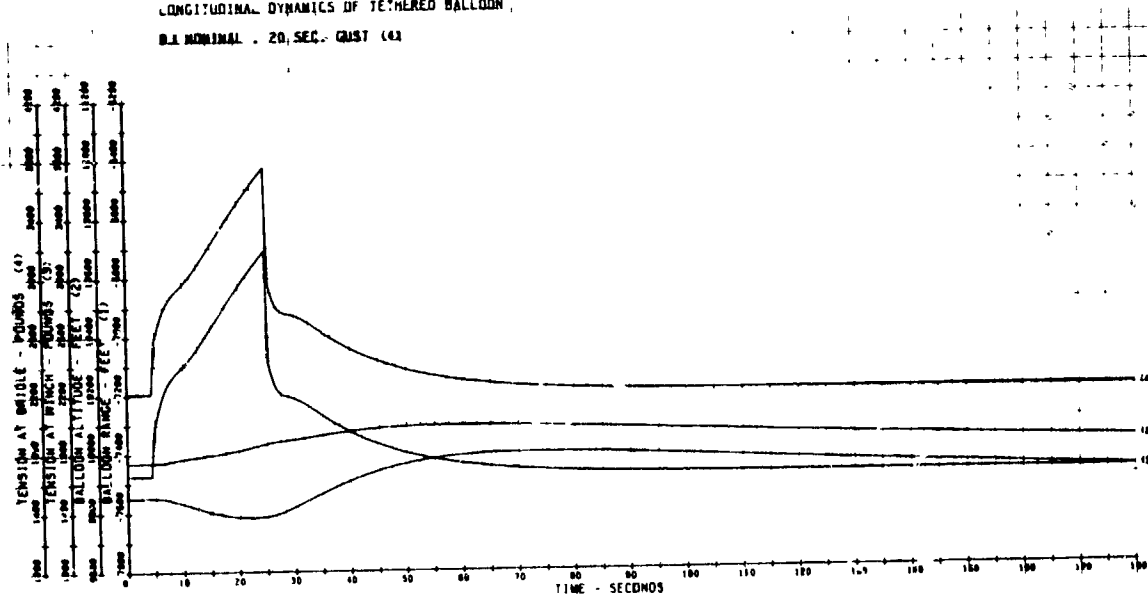
# LONGITUDINAL DYNAMICS OF TETHERED BALLOON

B.I. NOMINAL . 20 SEC. GUST (4)



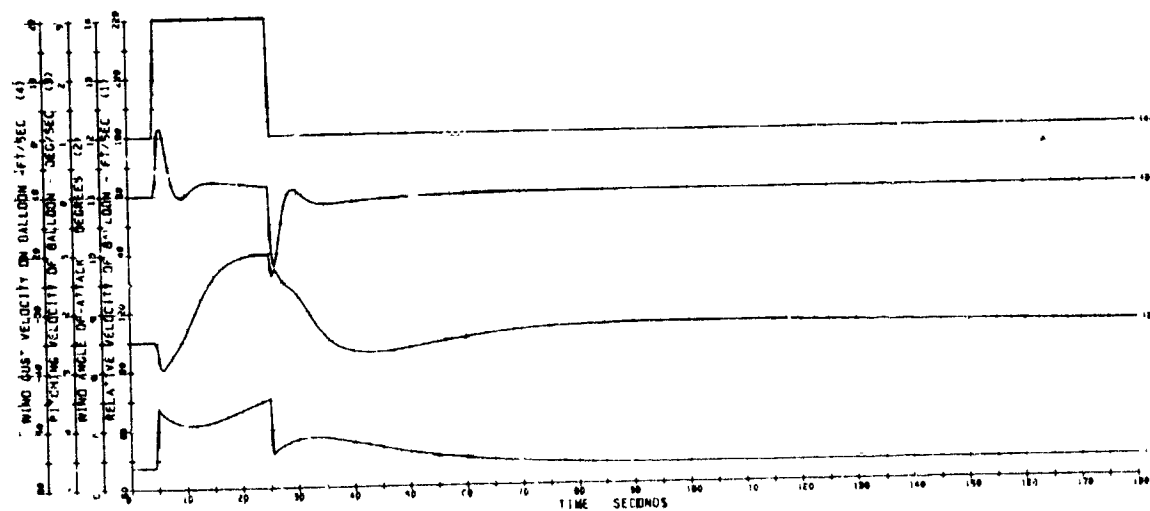
## LONGITUDINAL DYNAMICS OF TETHERED BALLOON

B.I. NOMINAL . 20 SEC. GUST (4)

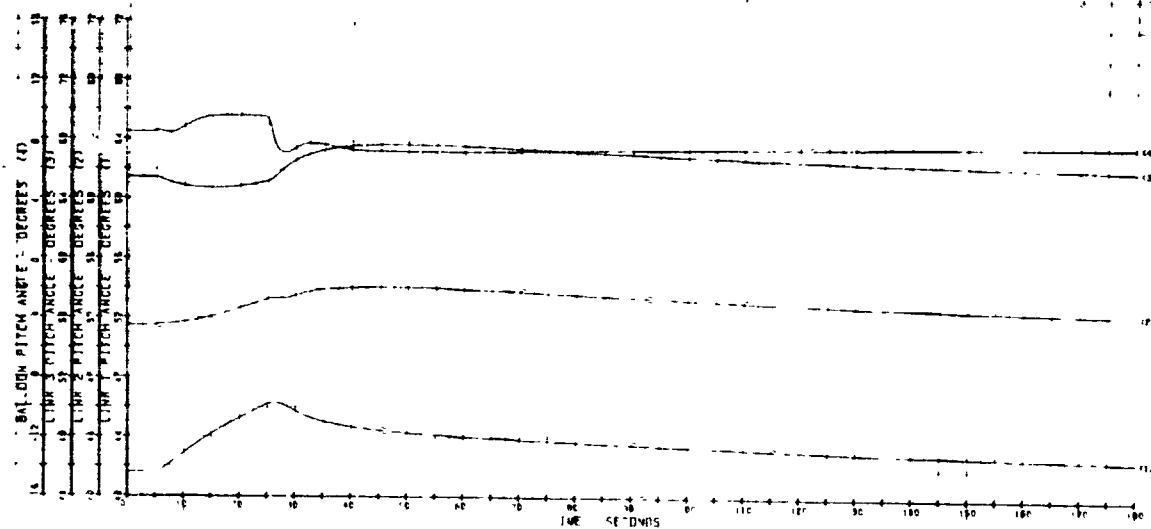


## LONGITUDINAL DYNAMICS OF TETHERED BALLOON

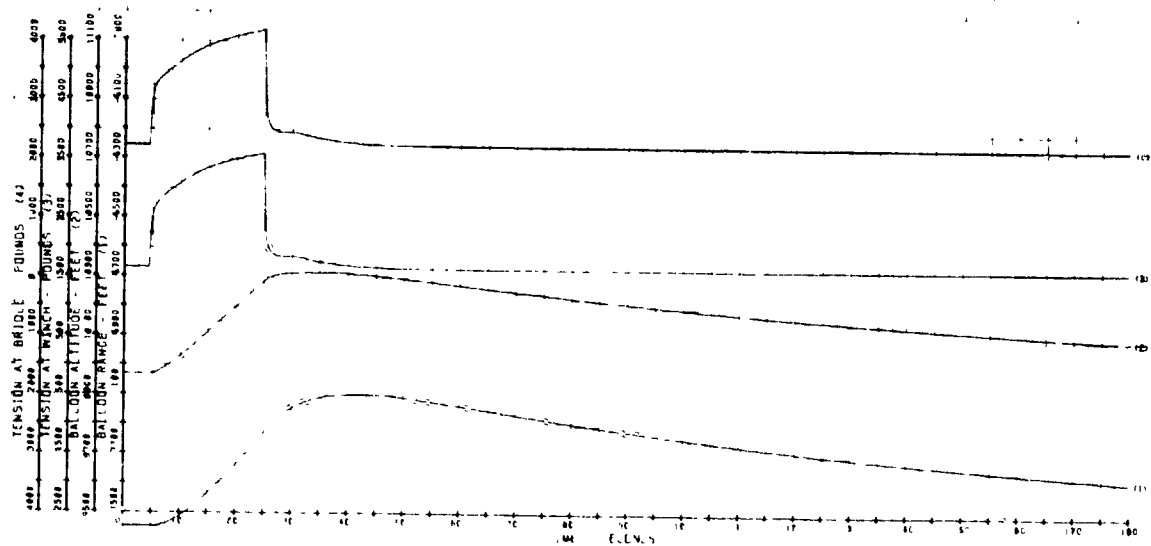
B.I. NOMINAL . 20 SEC. GUST (4)



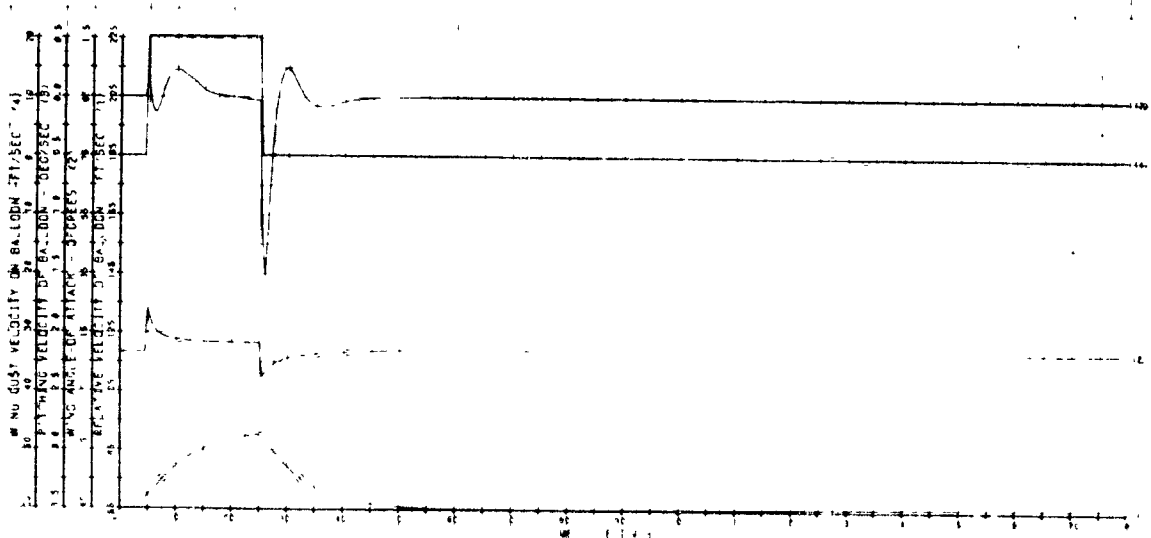
LONGITUDINAL DYNAMICS OF TETHERED BALLOON  
 (B) NOMINAL CASE (4A) (VERTICAL GUST)

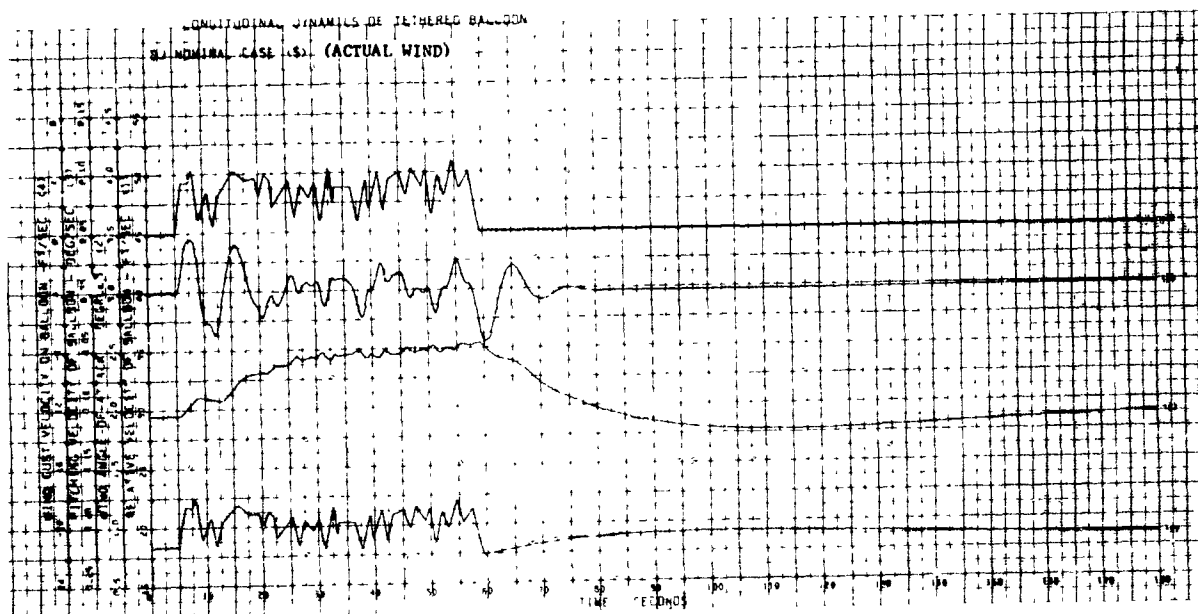
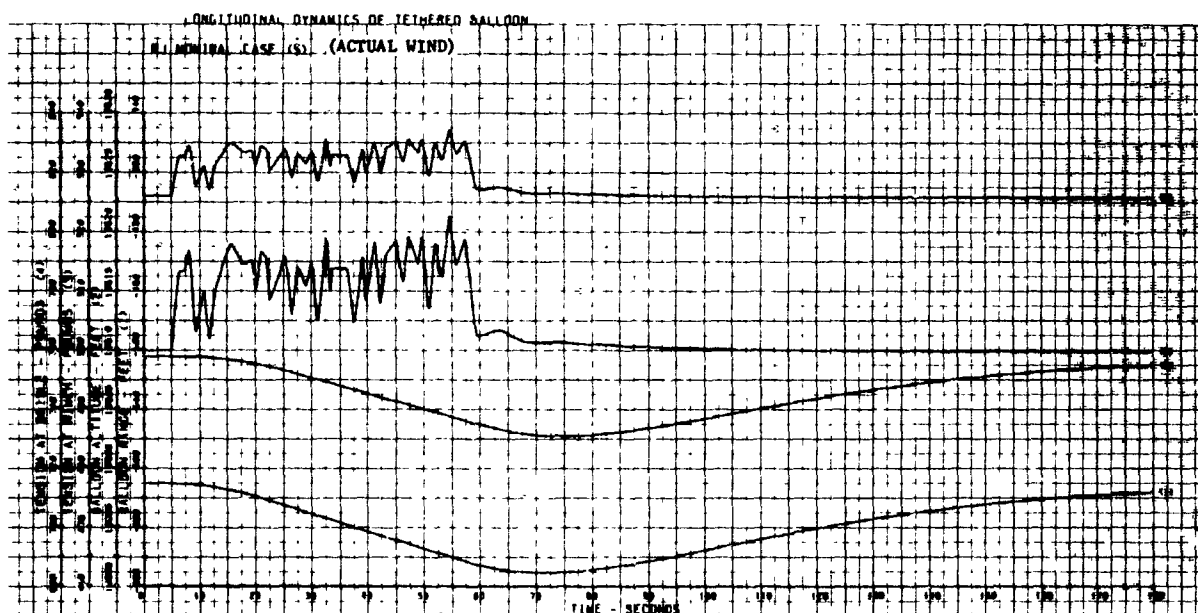
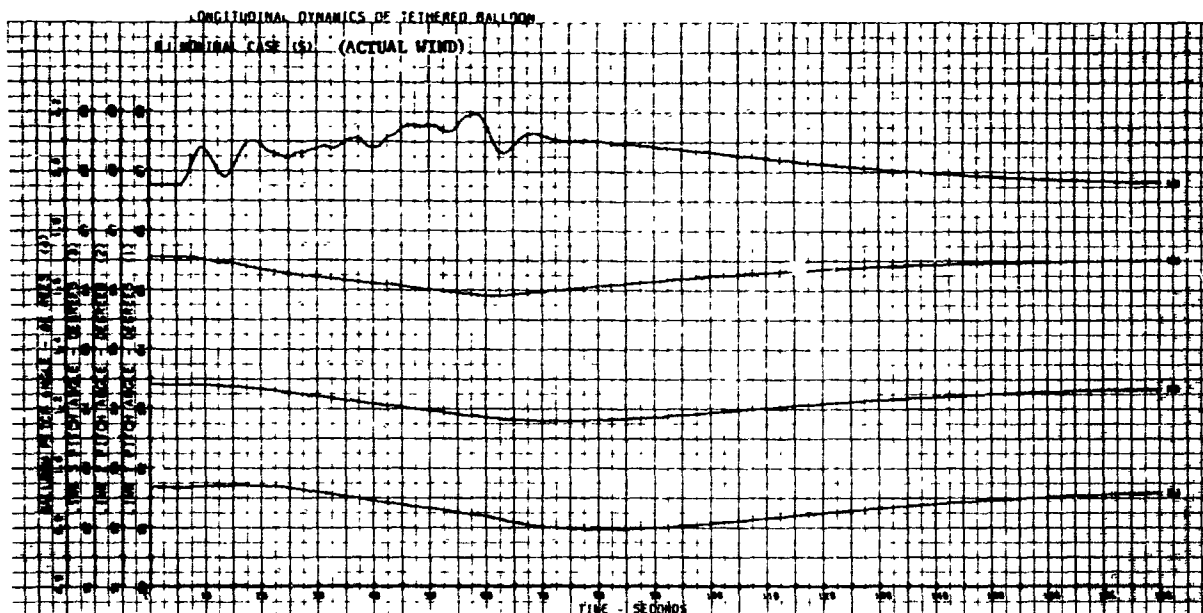


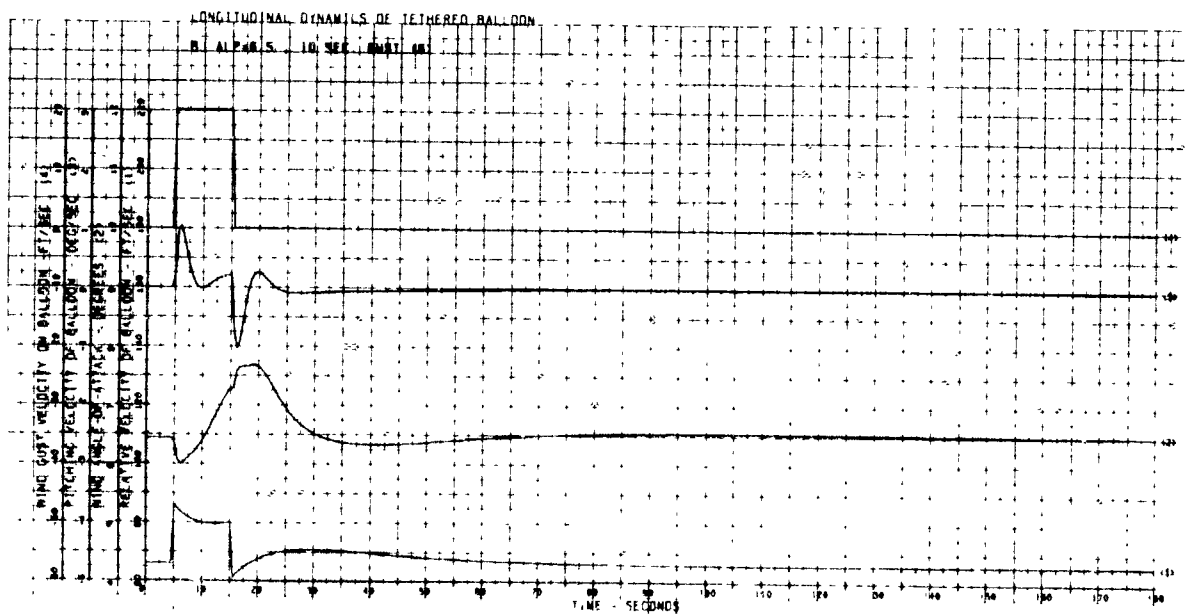
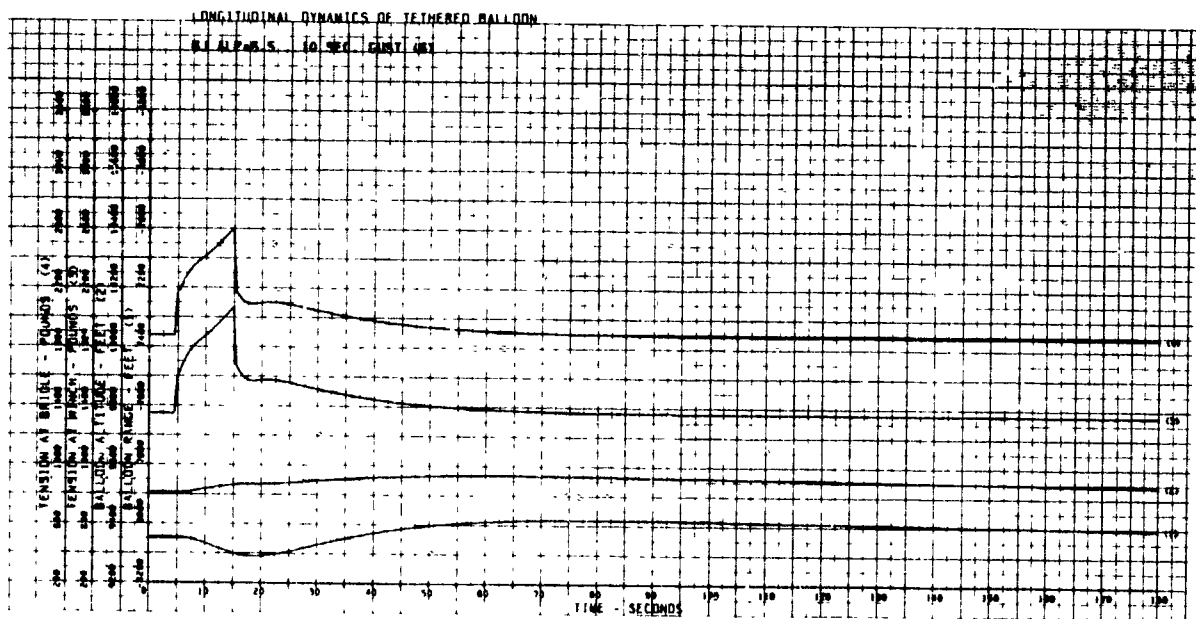
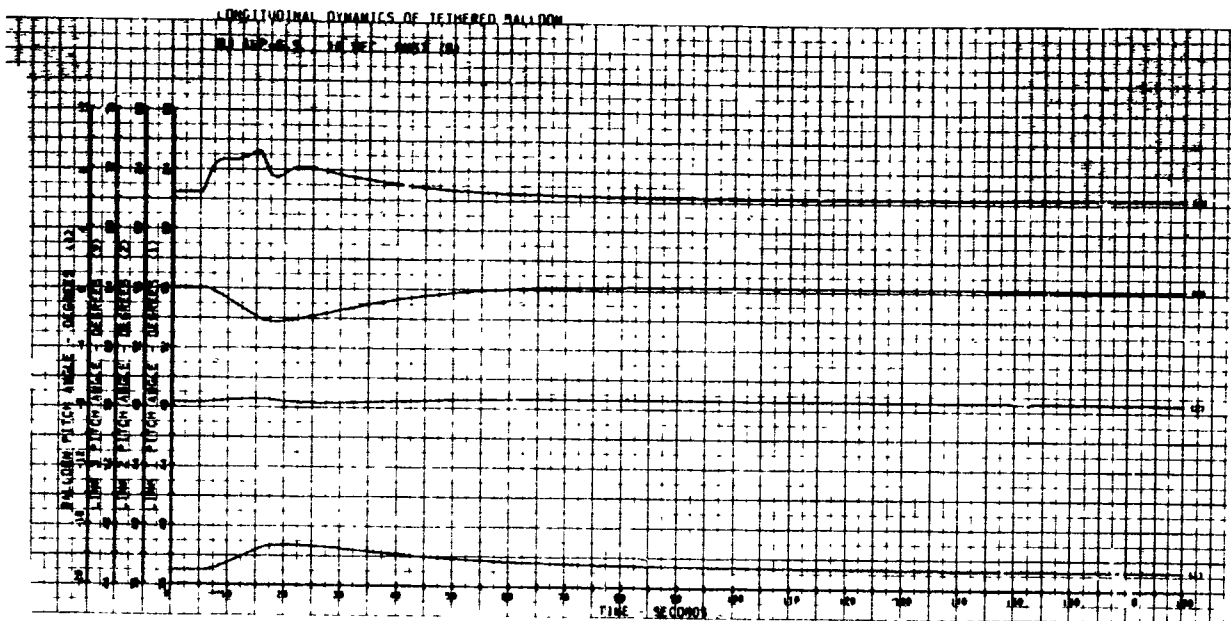
LONGITUDINAL DYNAMICS OF TETHERED BALLOON  
 (B) NOMINAL CASE (4A) (VERTICAL GUST)



LONGITUDINAL DYNAMICS OF TETHERED BALLOON  
 (B) NOMINAL CASE (4A) (VERTICAL GUST)

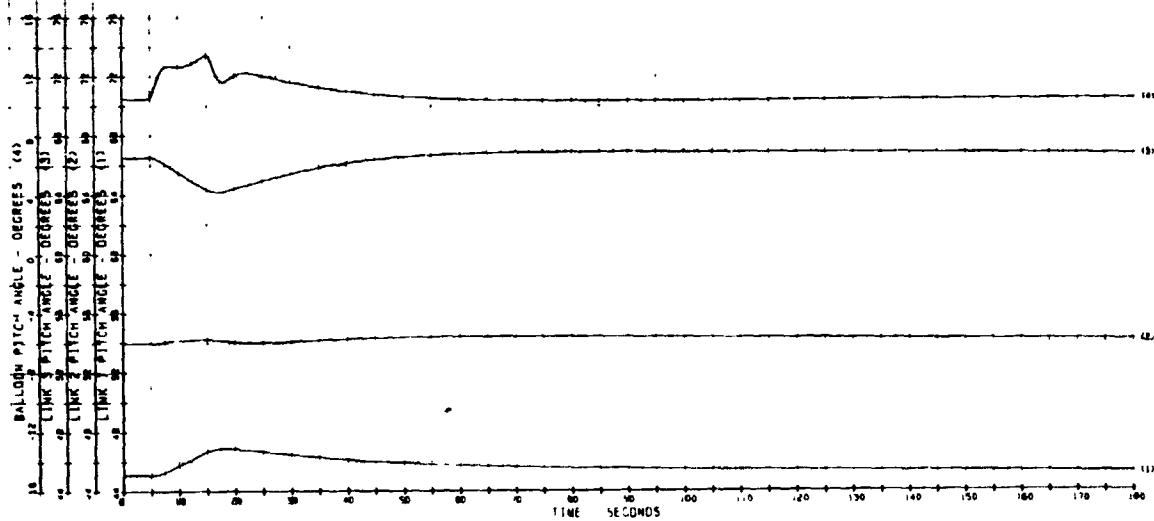






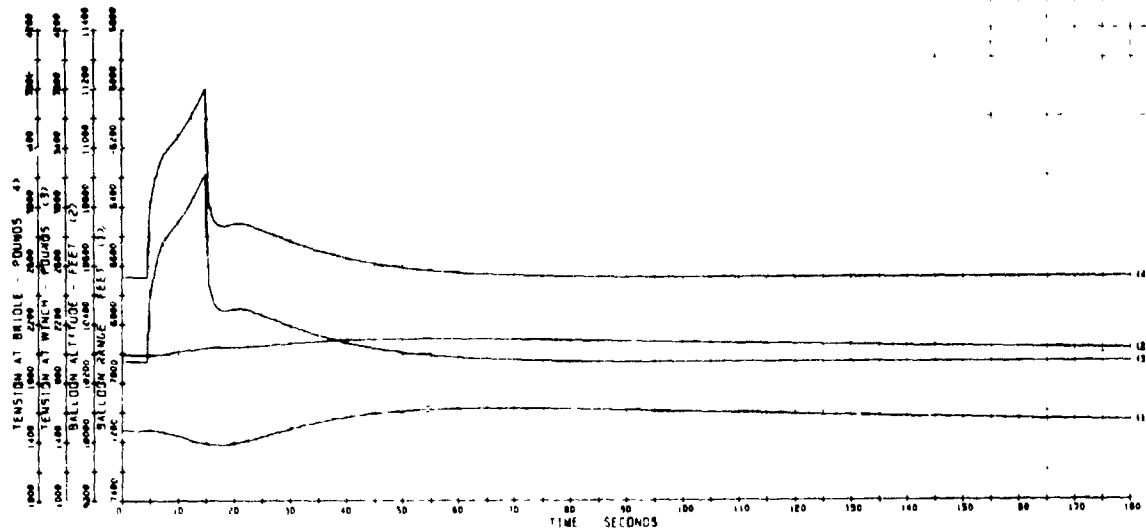
# LONGITUDINAL DYNAMICS OF TETHERED BALLOON

B.1 ALP=10.5 - 10 SEC. GUST (?)



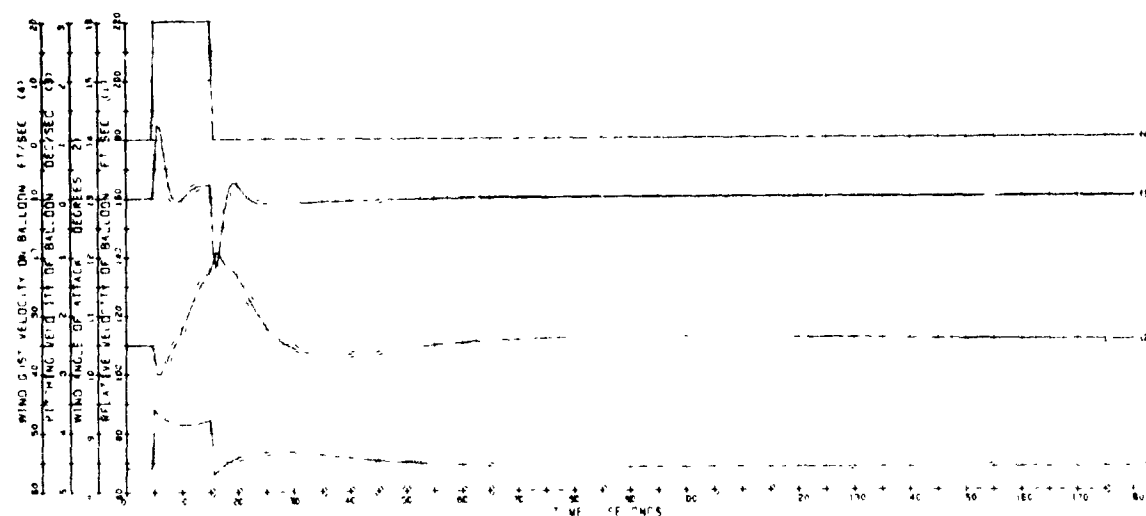
# LONGITUDINAL DYNAMICS OF TETHERED BALLOON

B.1 ALP=10.5 - 10 SEC. GUST (?)



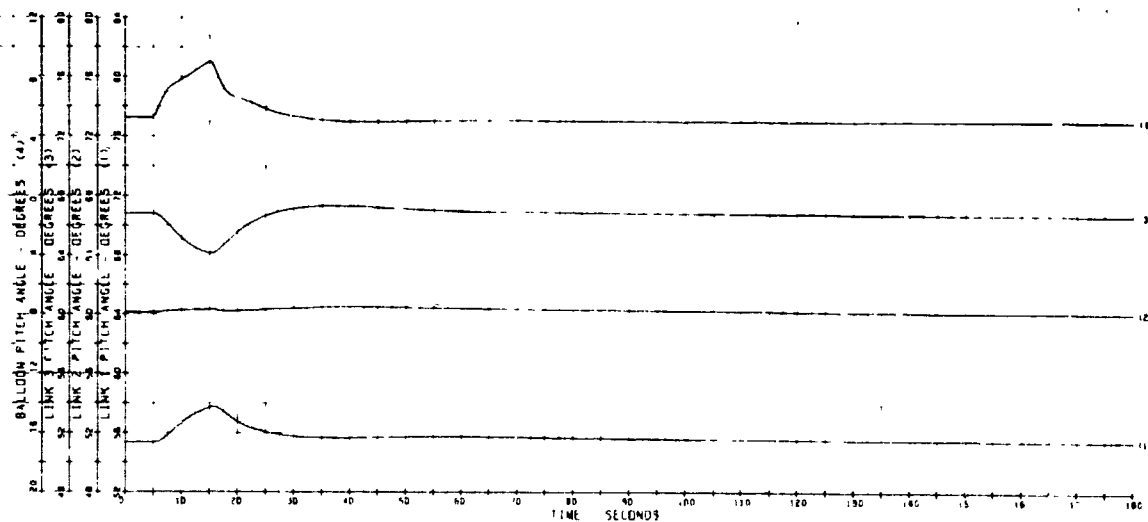
# LONGITUDINAL DYNAMICS OF TETHERED BALLOON

B. ALP=10.5 - 10 SEC. GUST (?)



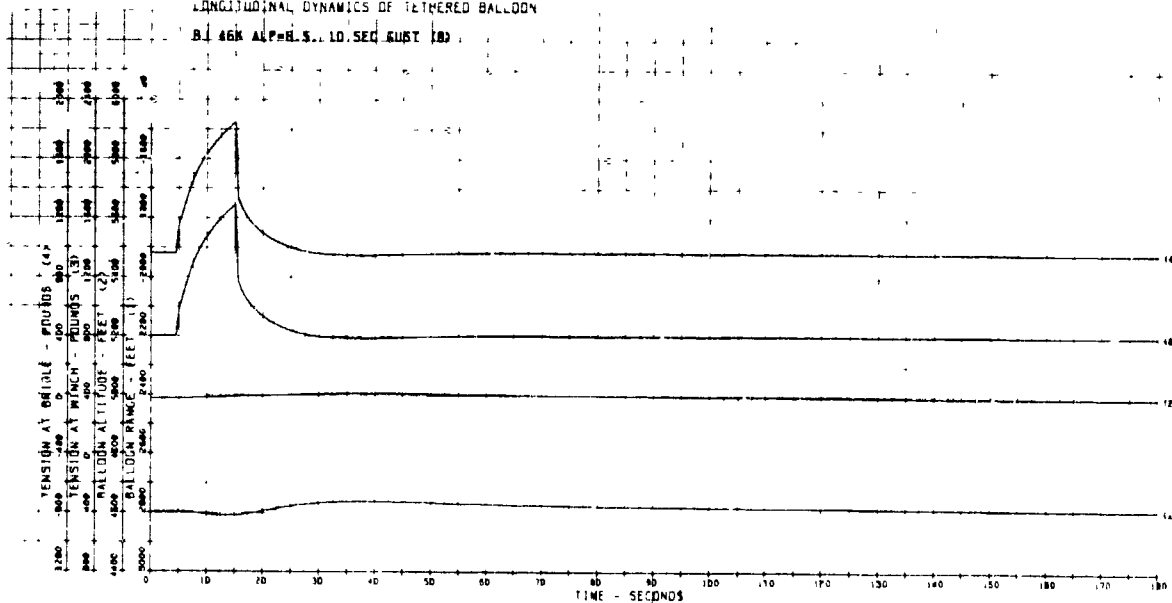
# LONGITUDINAL DYNAMICS OF TETHERED BALLOON

B.1 46K, 10 SEC GUST (8)



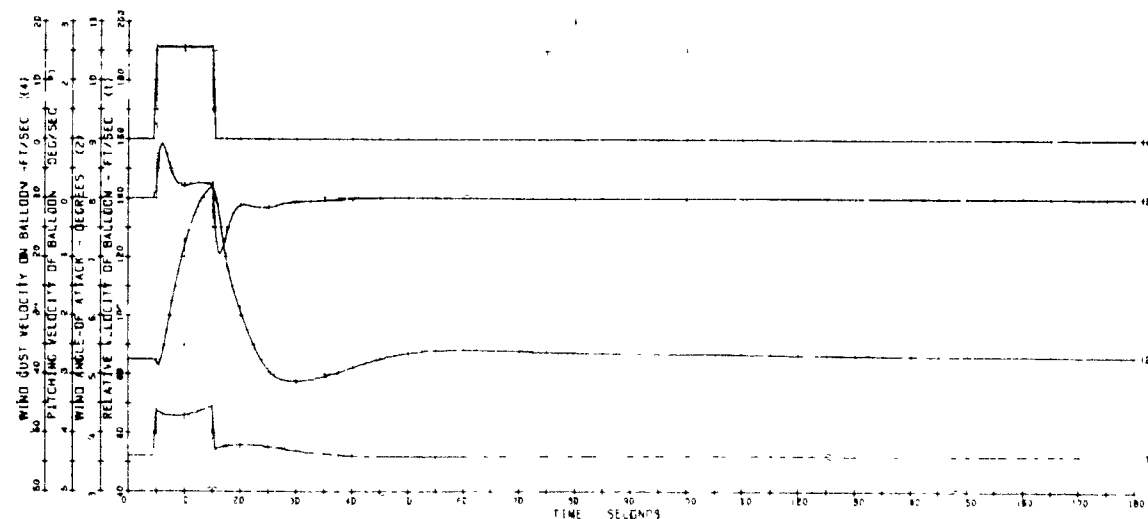
# LONGITUDINAL DYNAMICS OF TETHERED BALLOON

B.1 46K ALP=H.S., 10 SEC GUST (8)



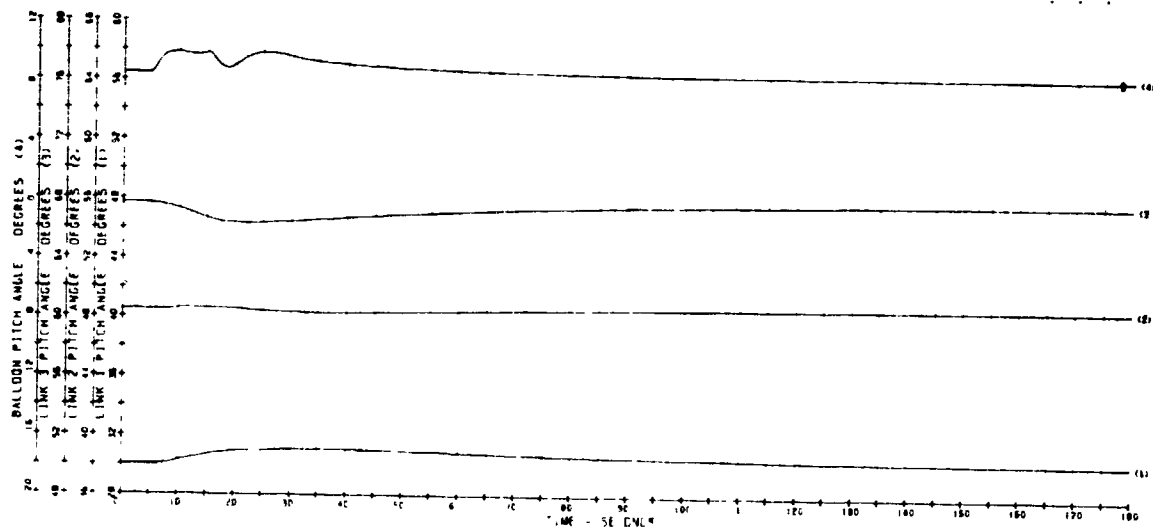
# LONGITUDINAL DYNAMICS OF TETHERED BALLOON

B.1 46K, 10 SEC, GUST (8)



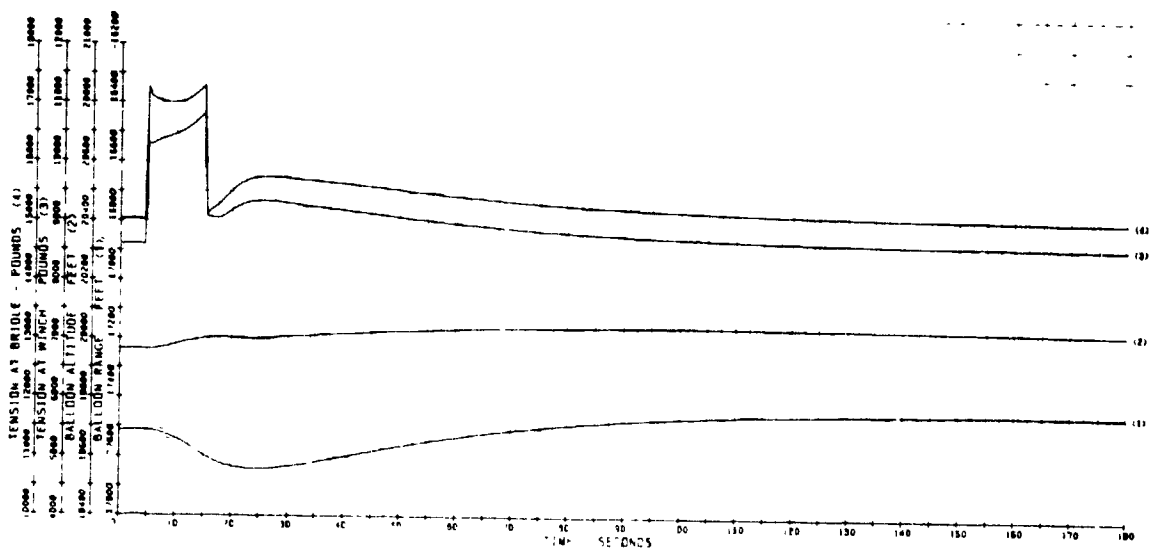
# LONGITUDINAL DYNAMICS OF TETHERED BALLOON

B.1 500K, 10 SEC GUST (A)



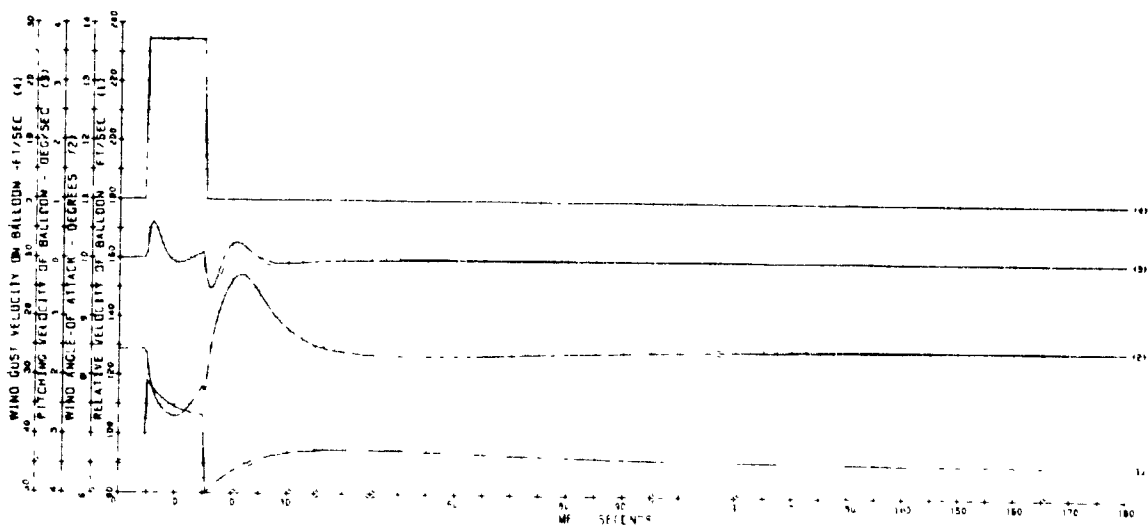
# LONGITUDINAL DYNAMICS OF TETHERED BALLOON

B.1 500K, 10 SEC GUST (B)

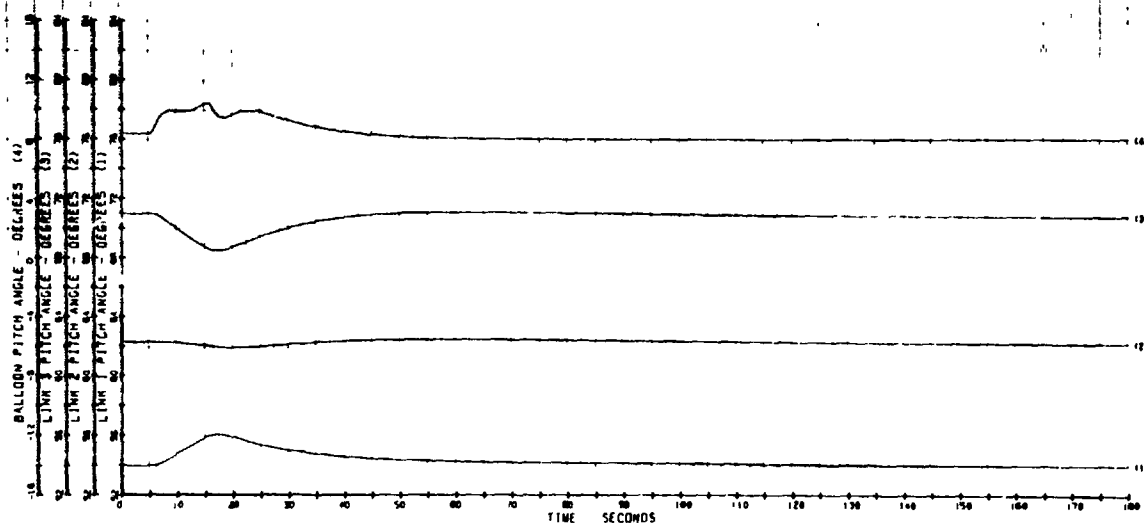


# LONGITUDINAL DYNAMICS OF TETHERED BALLOON

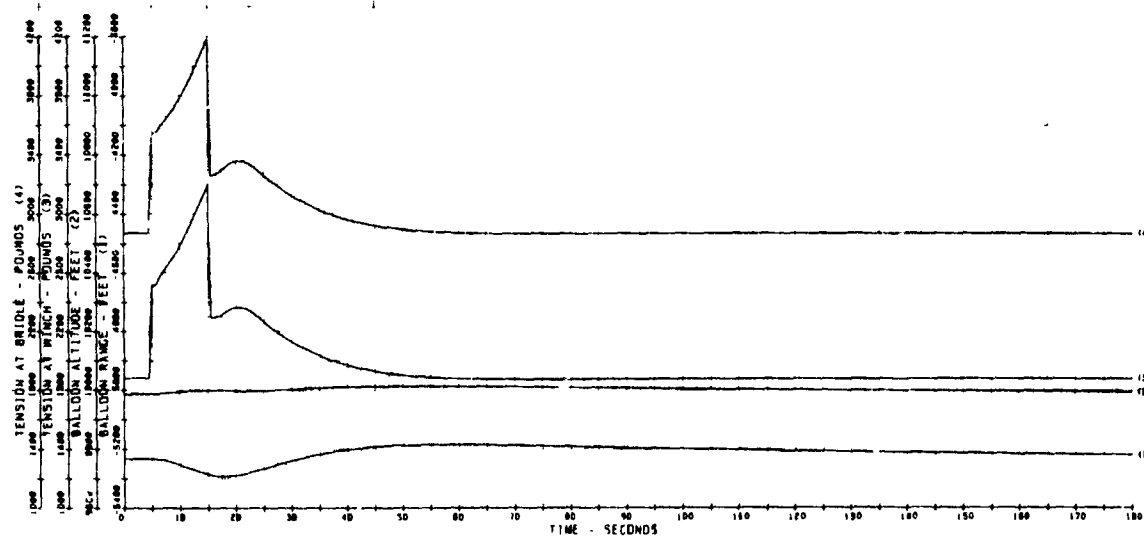
B.1 500 K, 10 SEC. GUST (B)



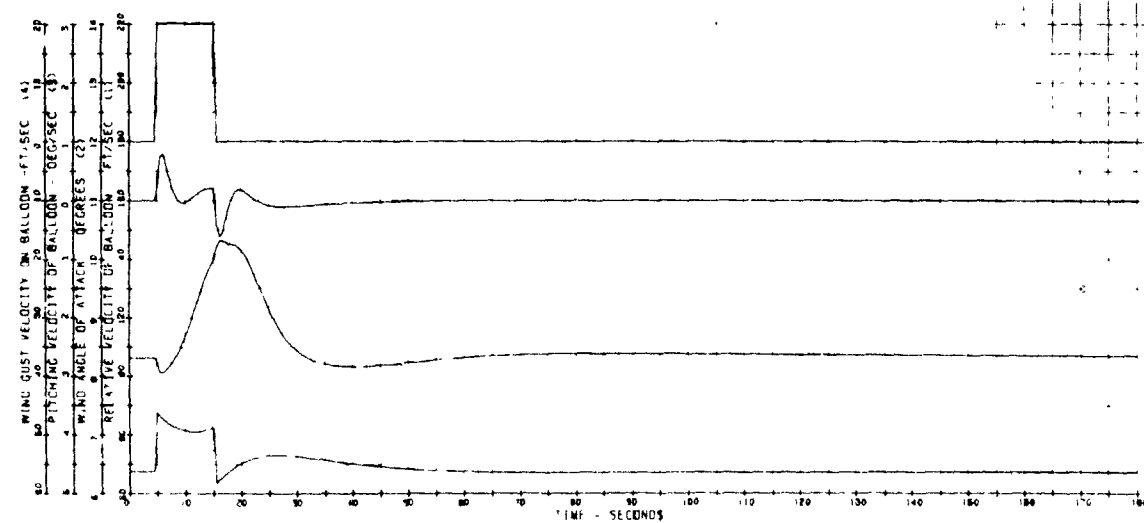
LONGITUDINAL DYNAMICS OF TETHERED BALLOON  
BJ AMCAL. 10 SEC. GUST (10)

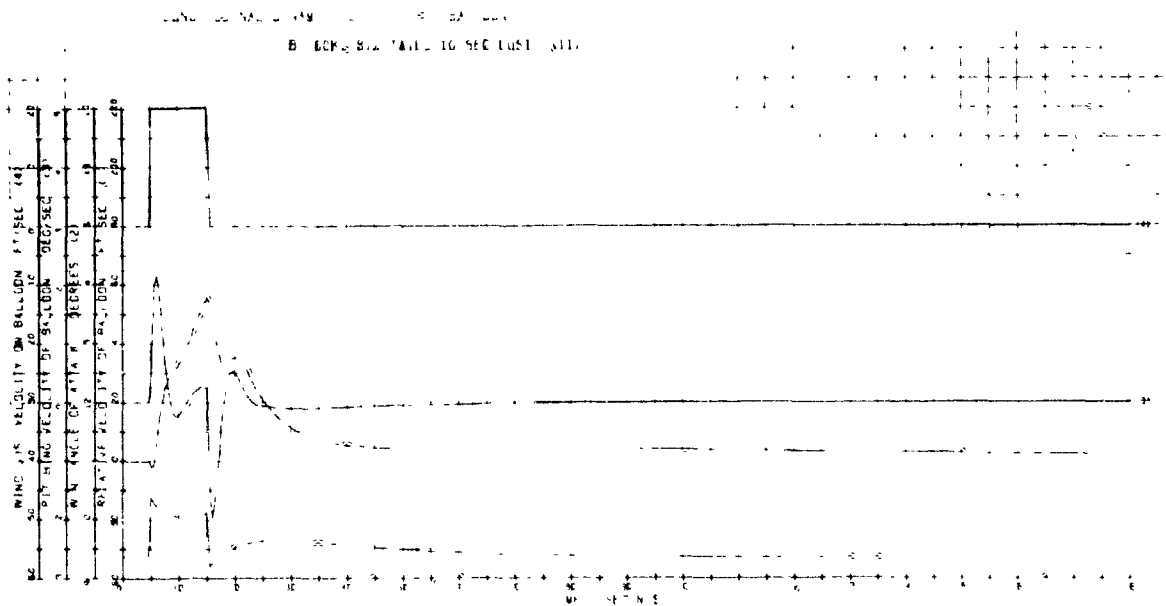
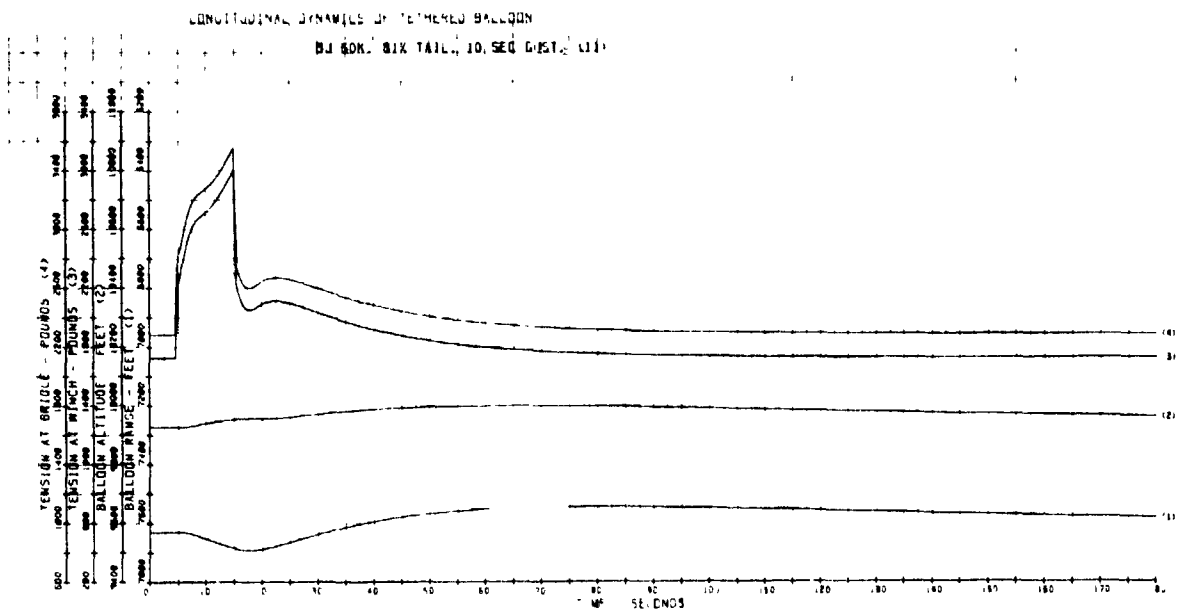
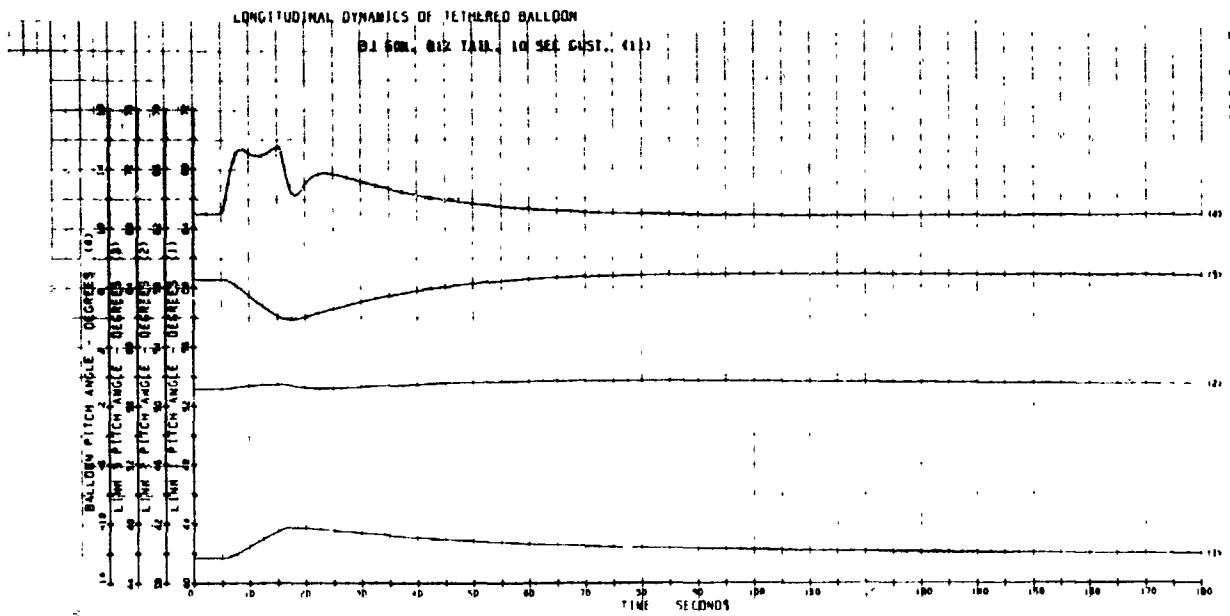


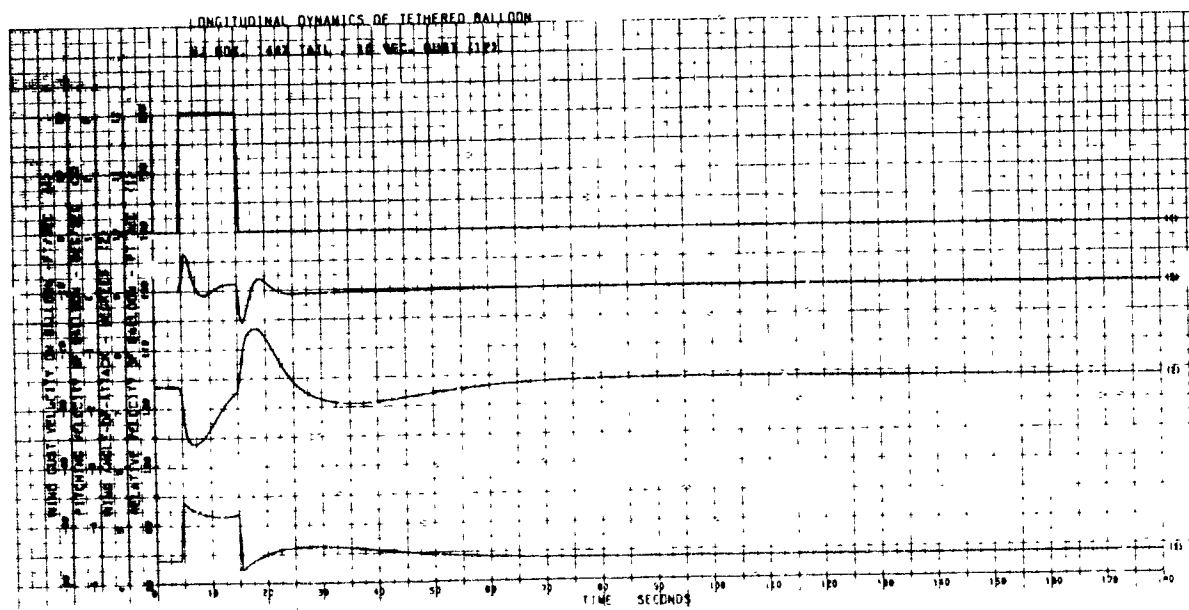
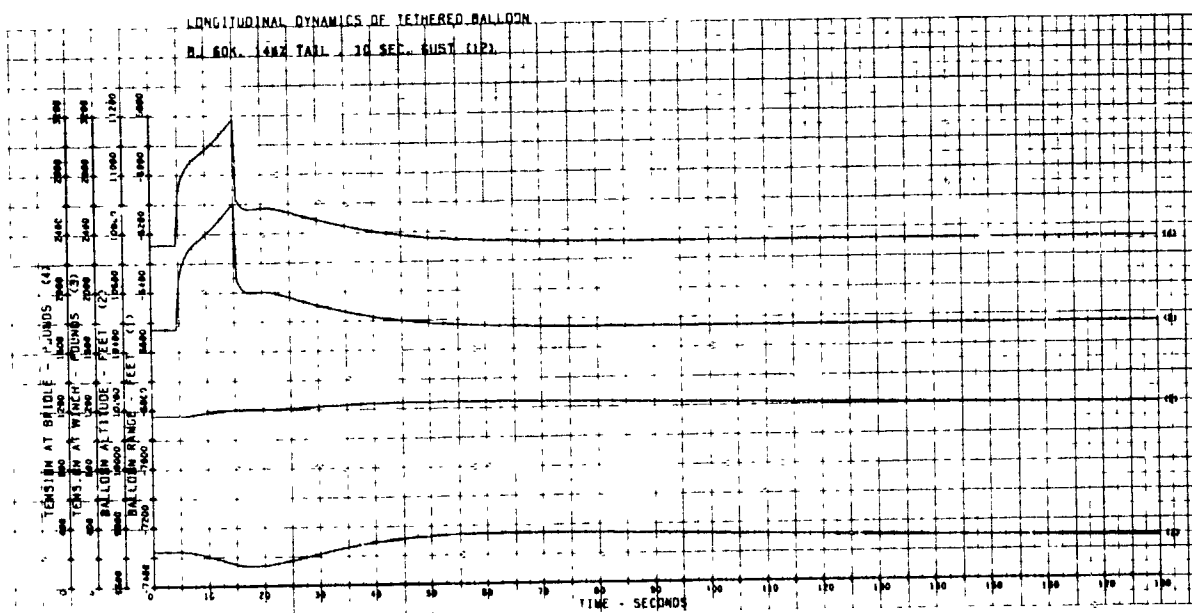
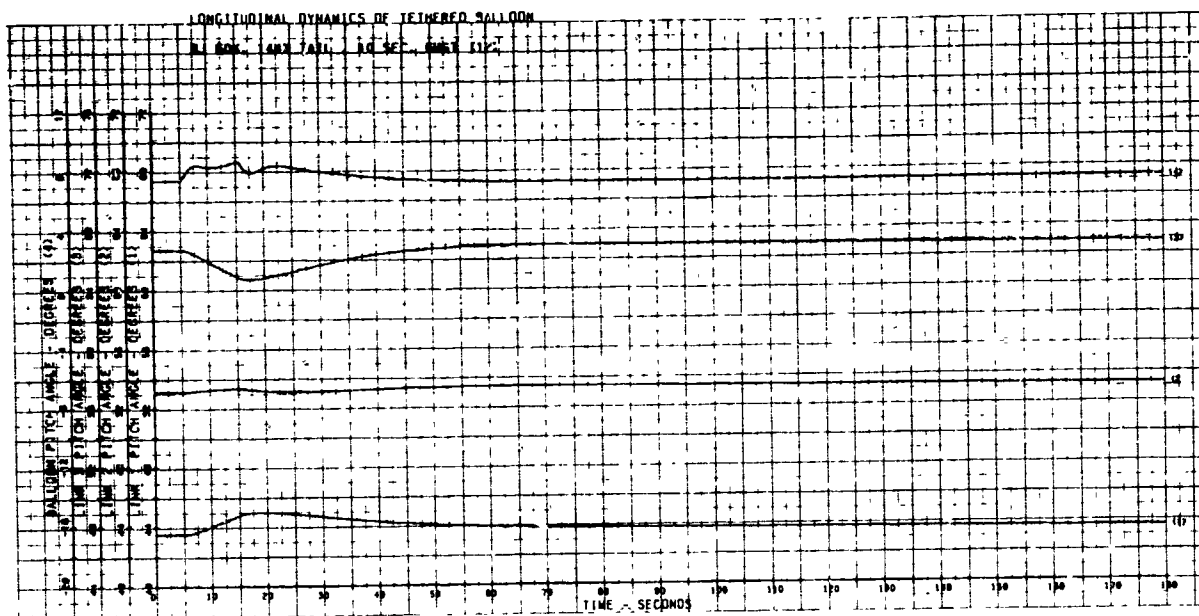
LONGITUDINAL DYNAMICS OF TETHERED BALLOON  
BJ AMCAL. 10 SEC. GUST (10)

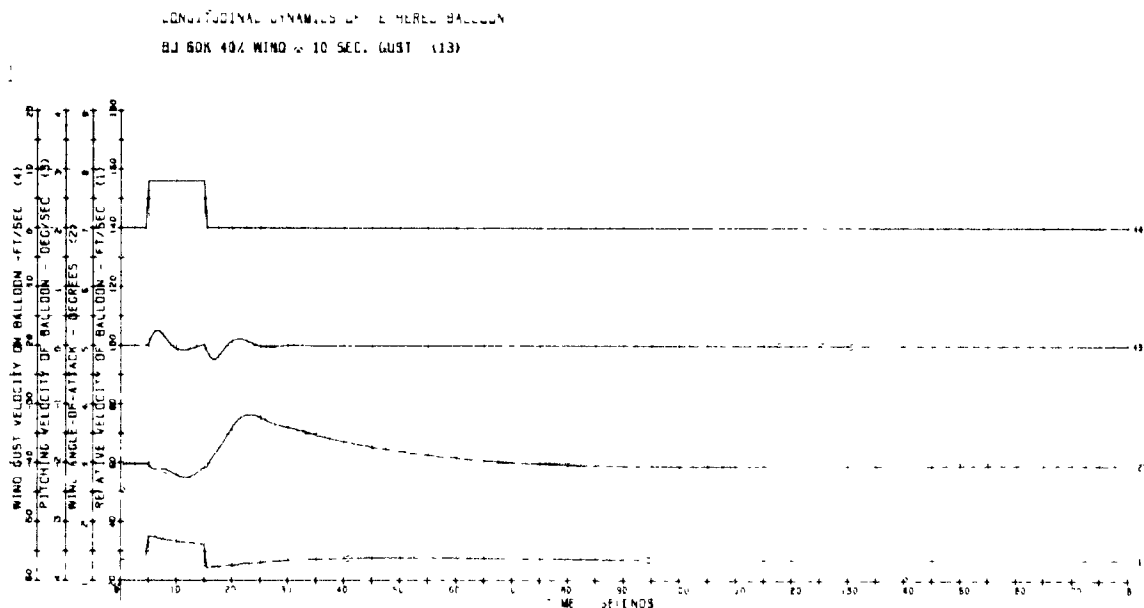
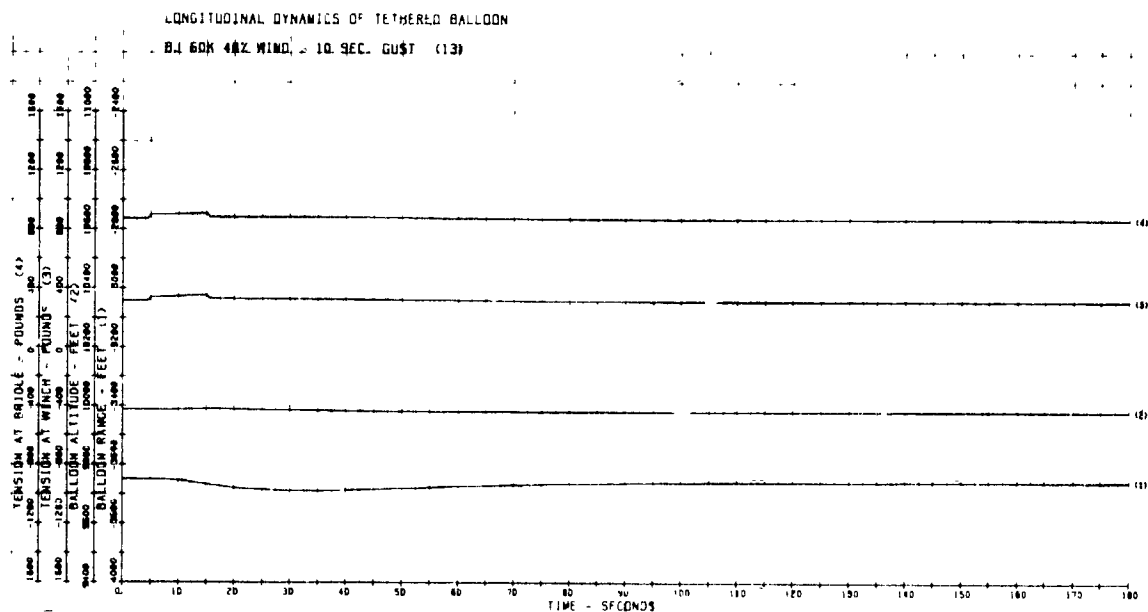
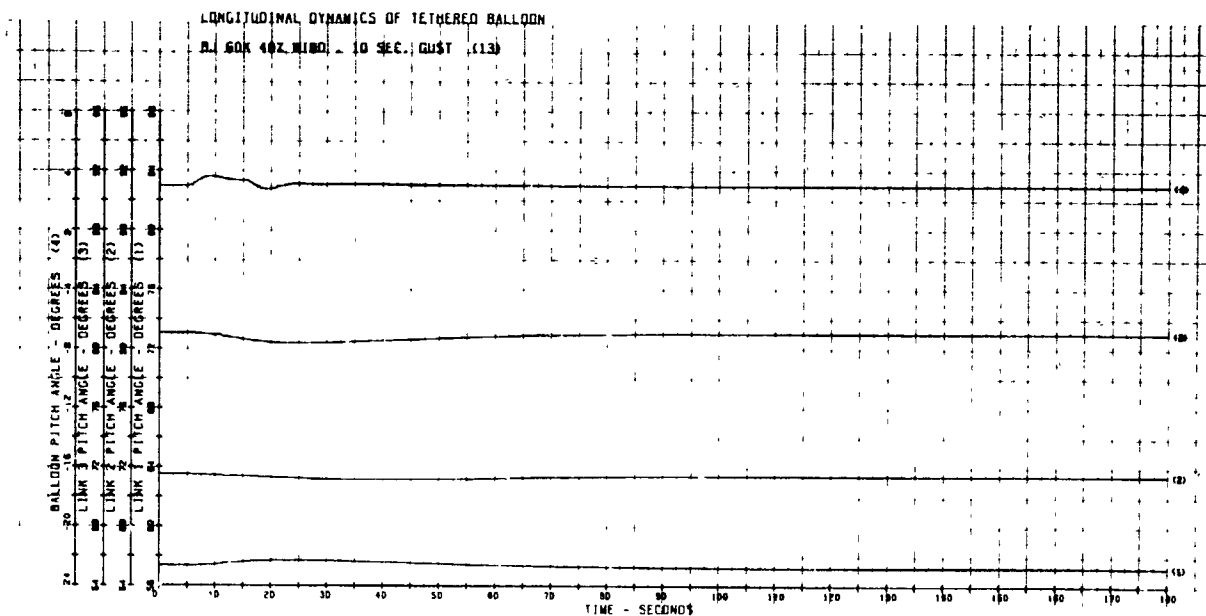


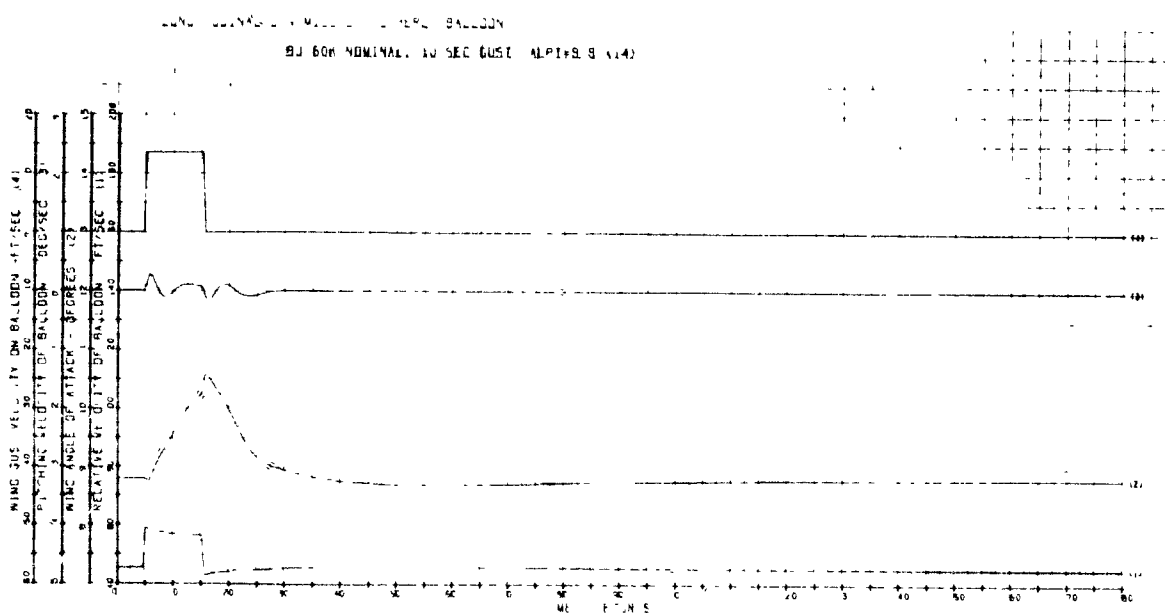
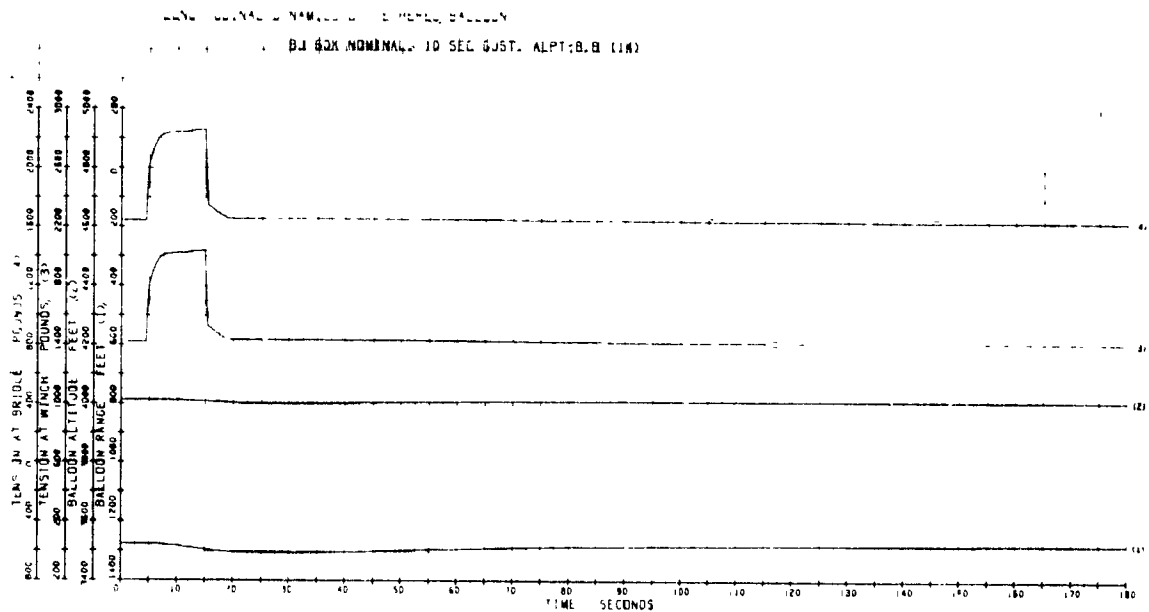
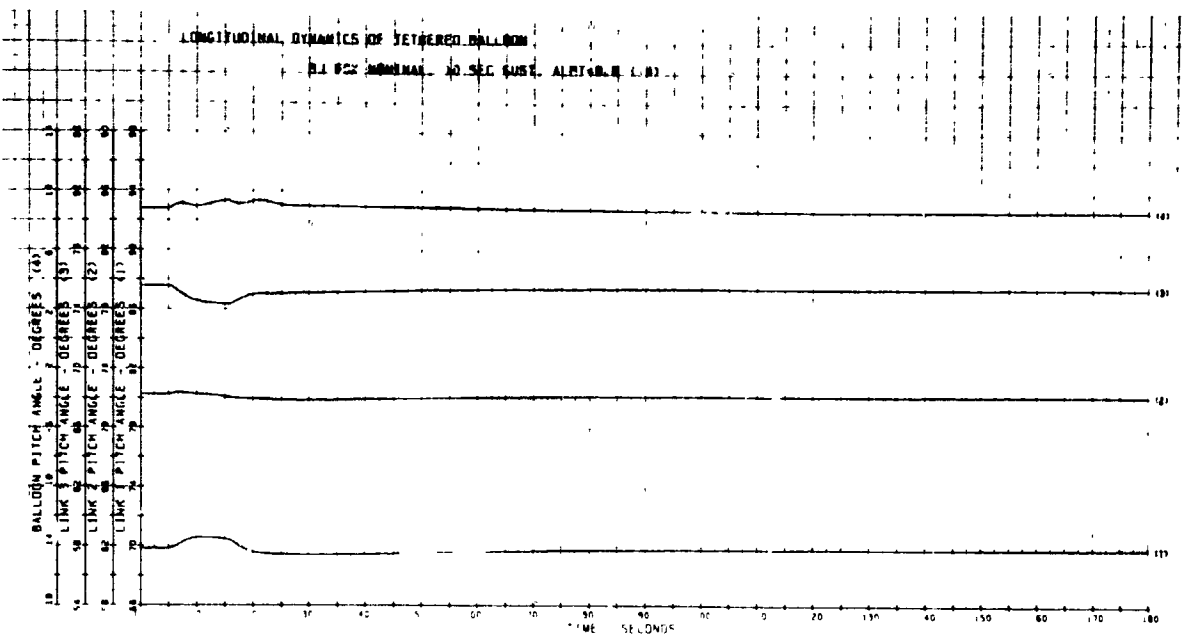
LONGITUDINAL DYNAMICS OF TETHERED BALLOON  
BJ AMCAL. 10 SEC. GUST (10)

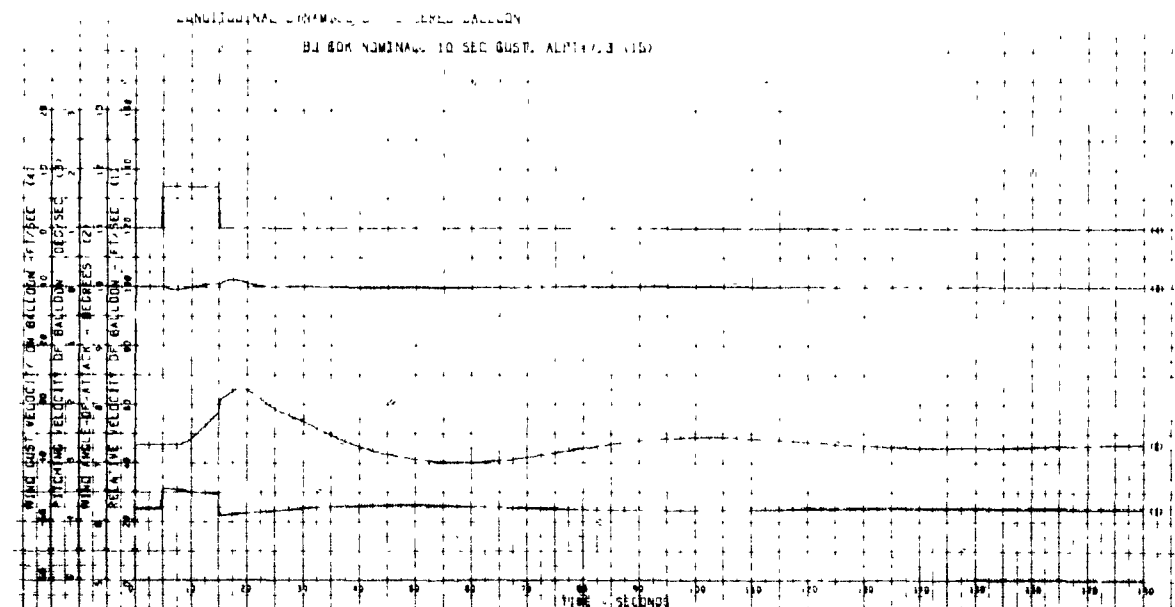
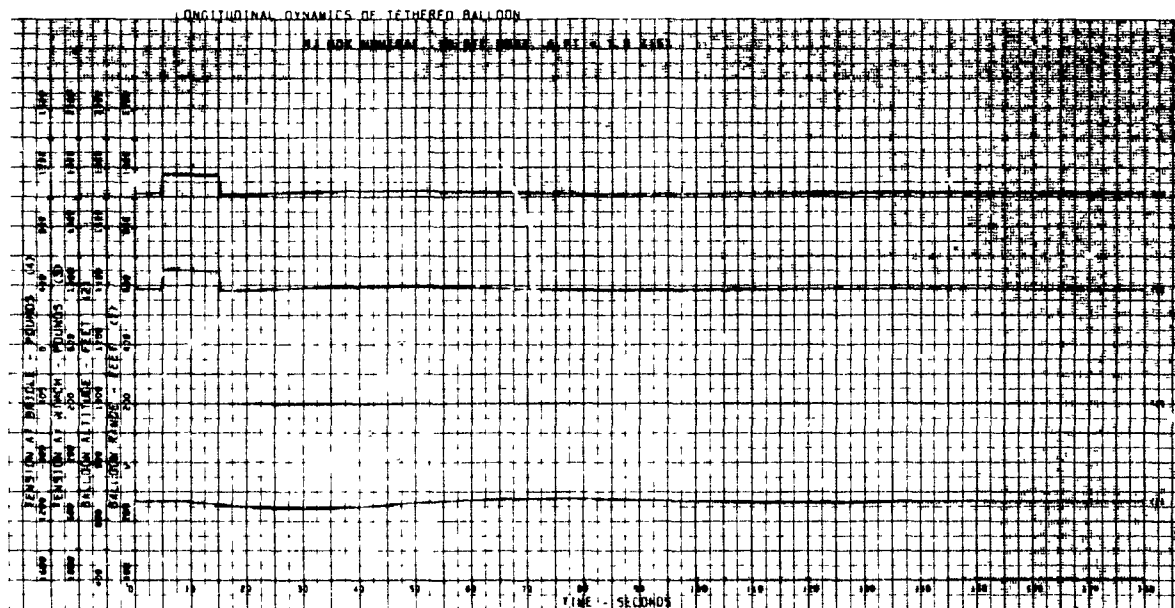
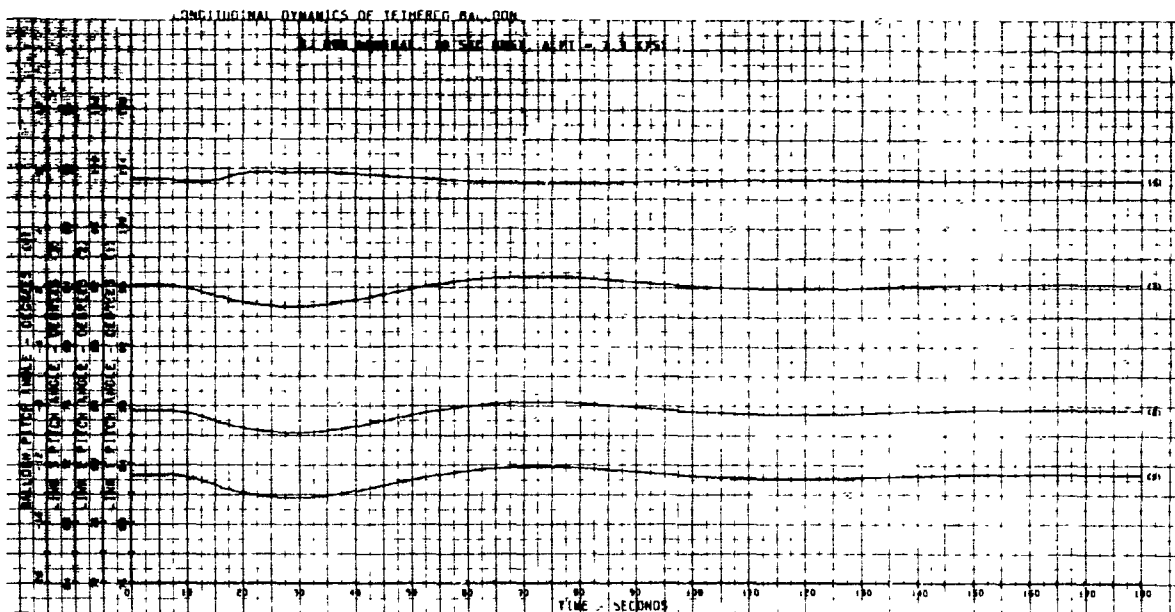






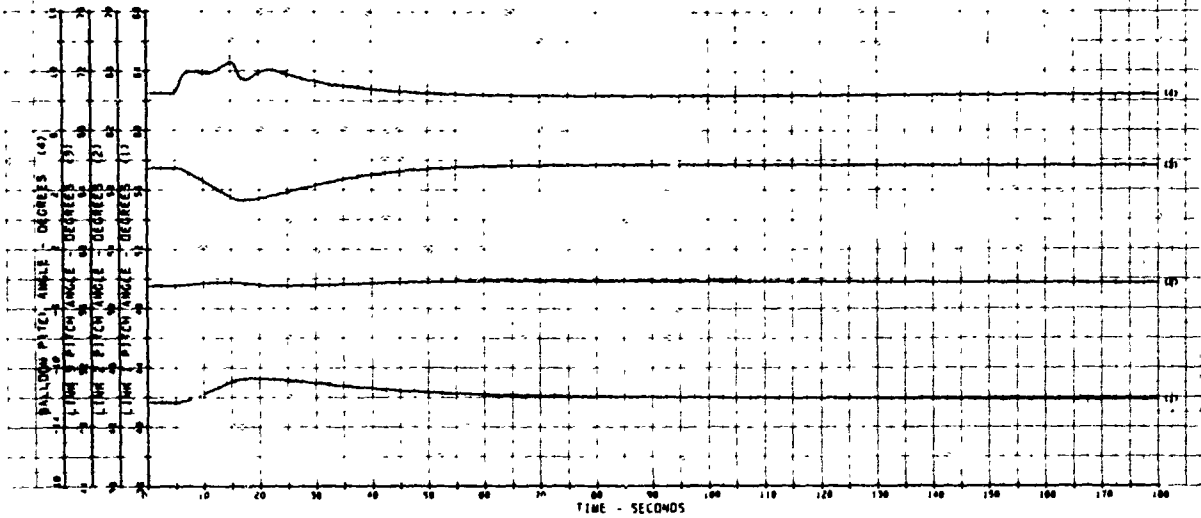






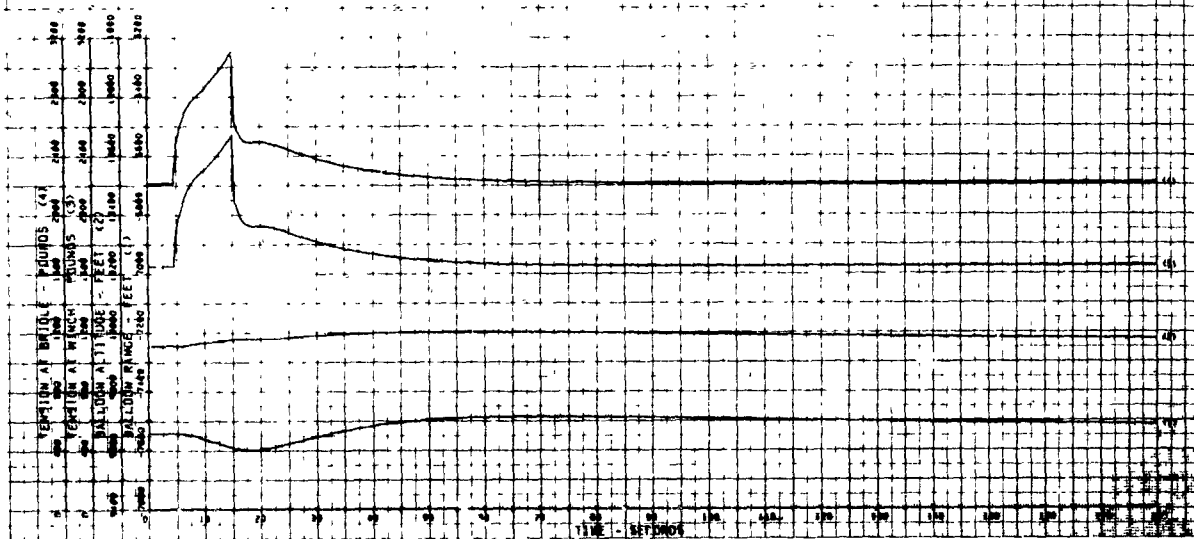
# LONGITUDINAL DYNAMICS OF TETHERED BALLOON

BJ 60K NOMINAL, 10 SEC GUST, ALPI+8.5 (15)



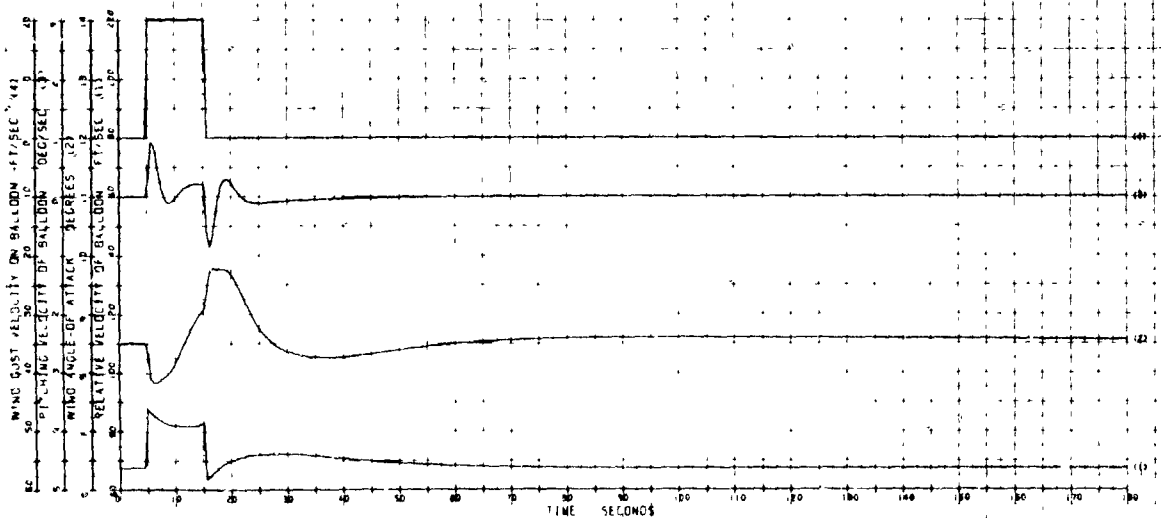
# LONGITUDINAL DYNAMICS OF TETHERED BALLOON

BJ 60K NOMINAL, 10 SEC GUST, ALPI+8.5 (16)

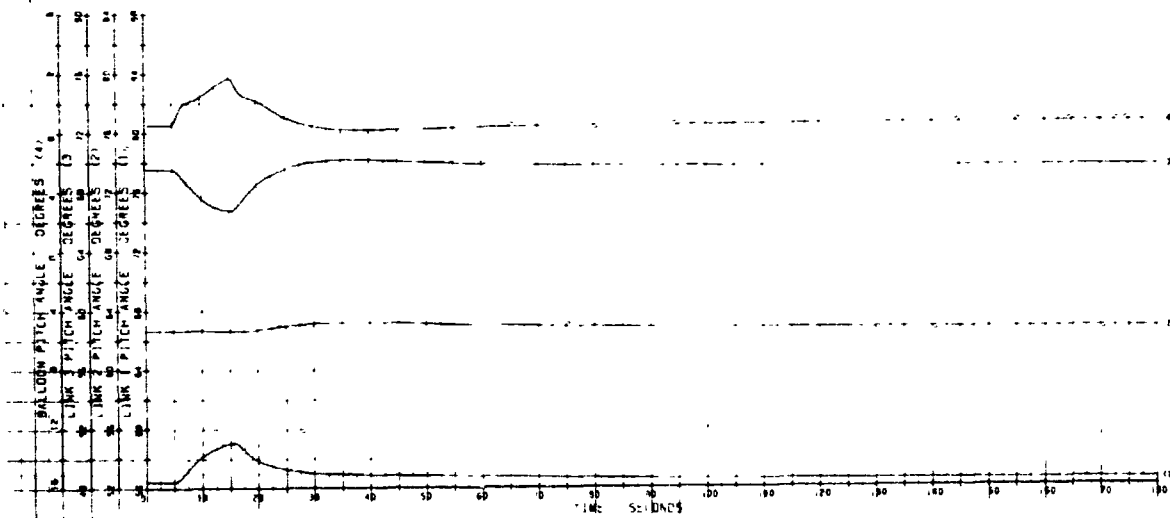


# LONGITUDINAL DYNAMICS OF TETHERED BALLOON

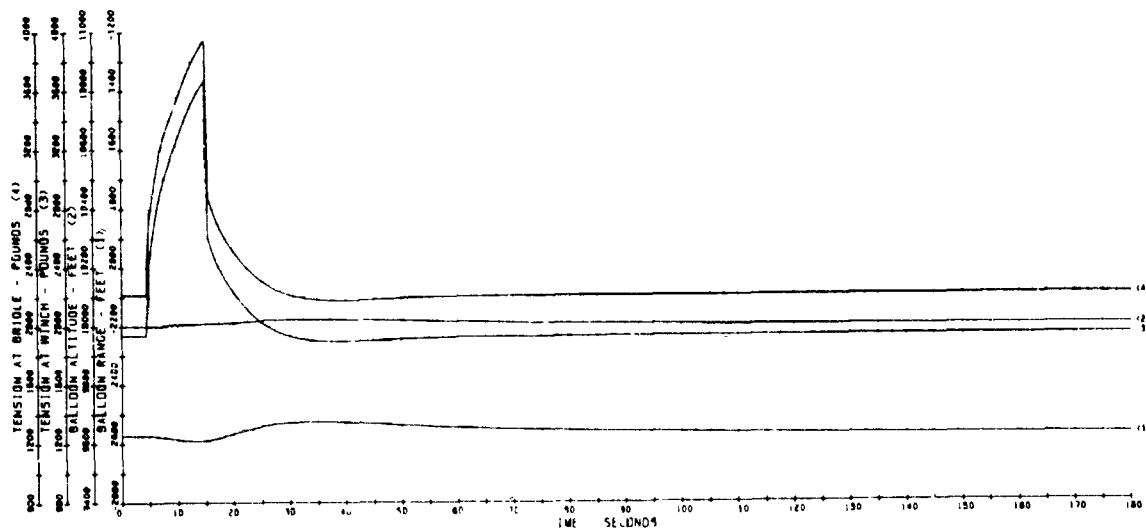
BJ 60K NOMINAL, 10 SEC GUST, ALPI+8.5 (16)



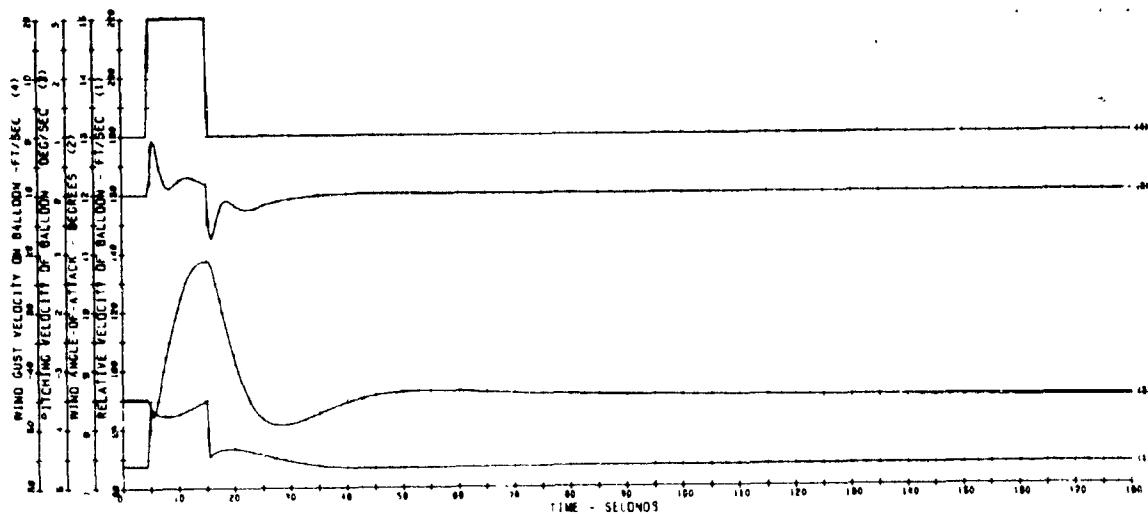
LONGITUDINAL DYNAMICS OF TETHERED BALLOON  
BJ 60K WINCH AT 5K , 10 SEC GUST (17)



LONGITUDINAL DYNAMICS OF TETHERED BALLOON  
BJ 60K WINCH AT 5K , 10 SEC GUST (17)

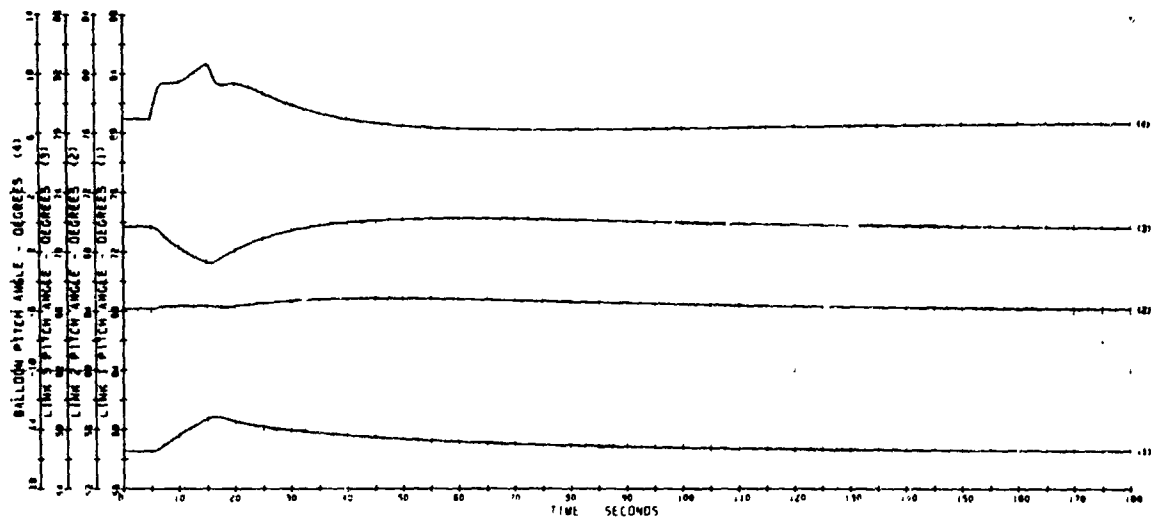


LONGITUDINAL DYNAMICS OF TETHERED BALLOON  
BJ 60K WINCH AT 5K , 10 SEC GUST (17)



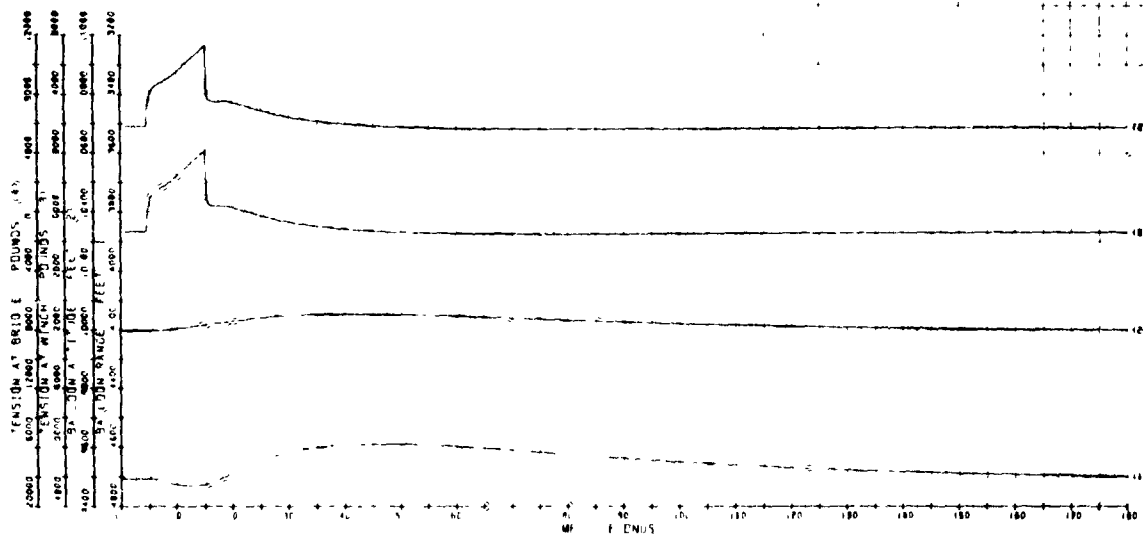
# LONGITUDINAL DYNAMICS OF TETHERED BALLOON

SEE BOM. 10 SEC GUST, ALPT=7, (18)



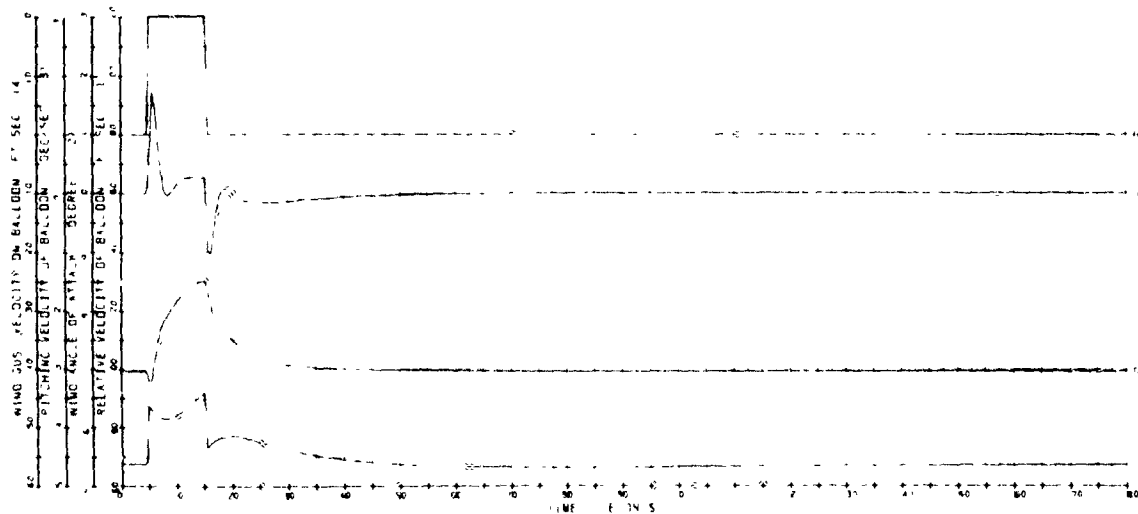
# LONGITUDINAL DYNAMICS OF TETHERED BALLOON

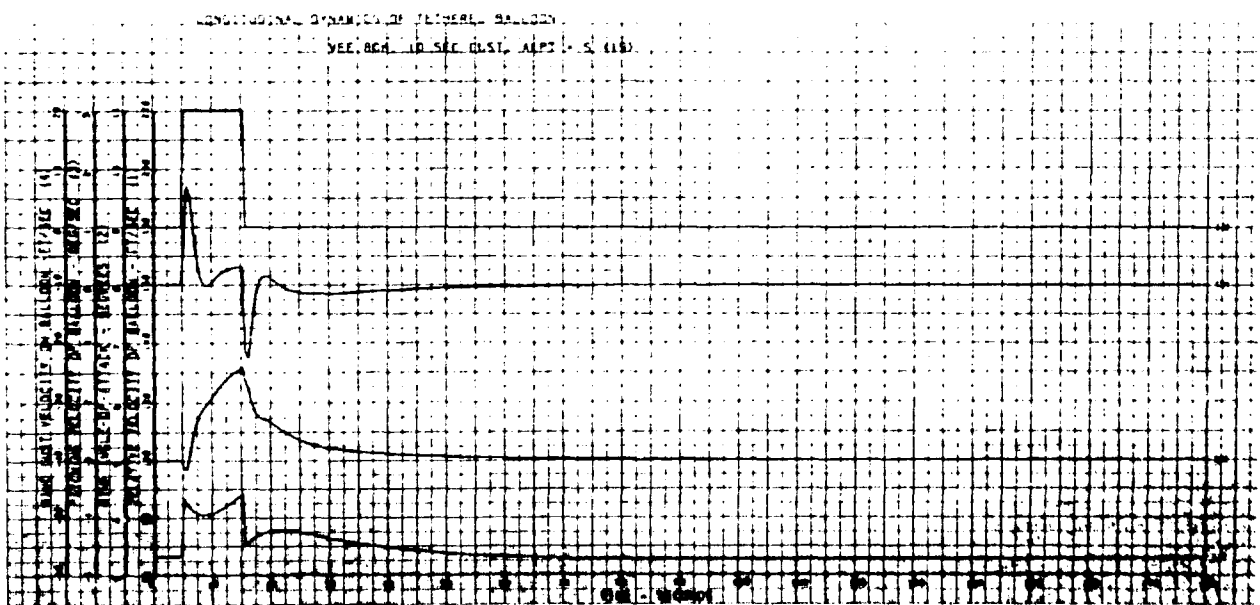
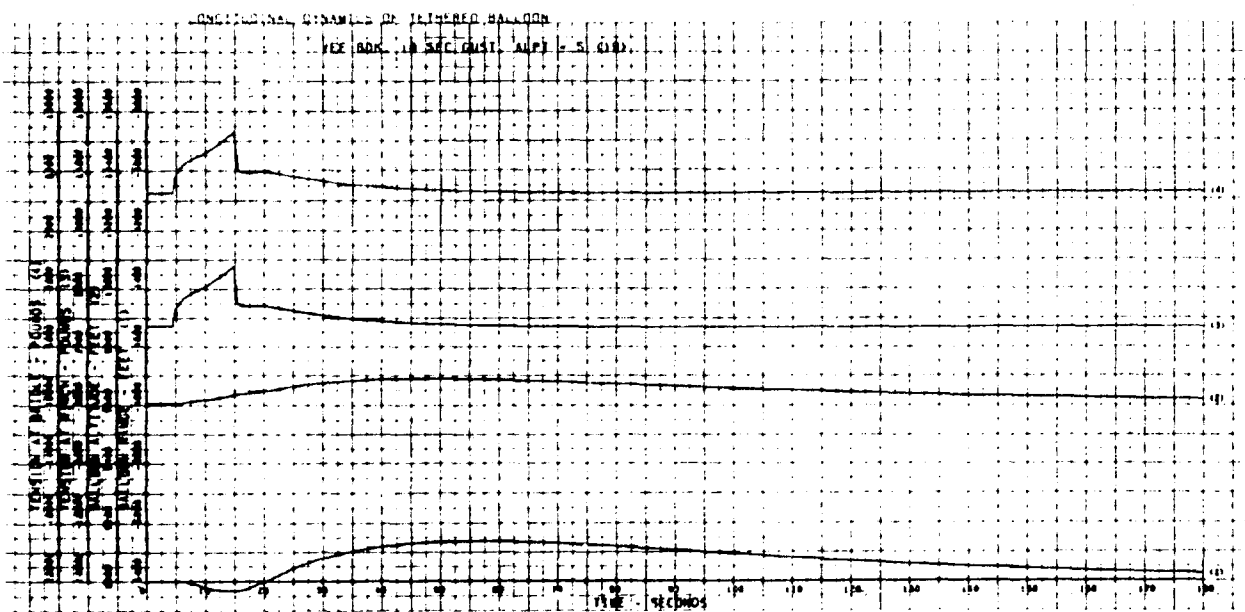
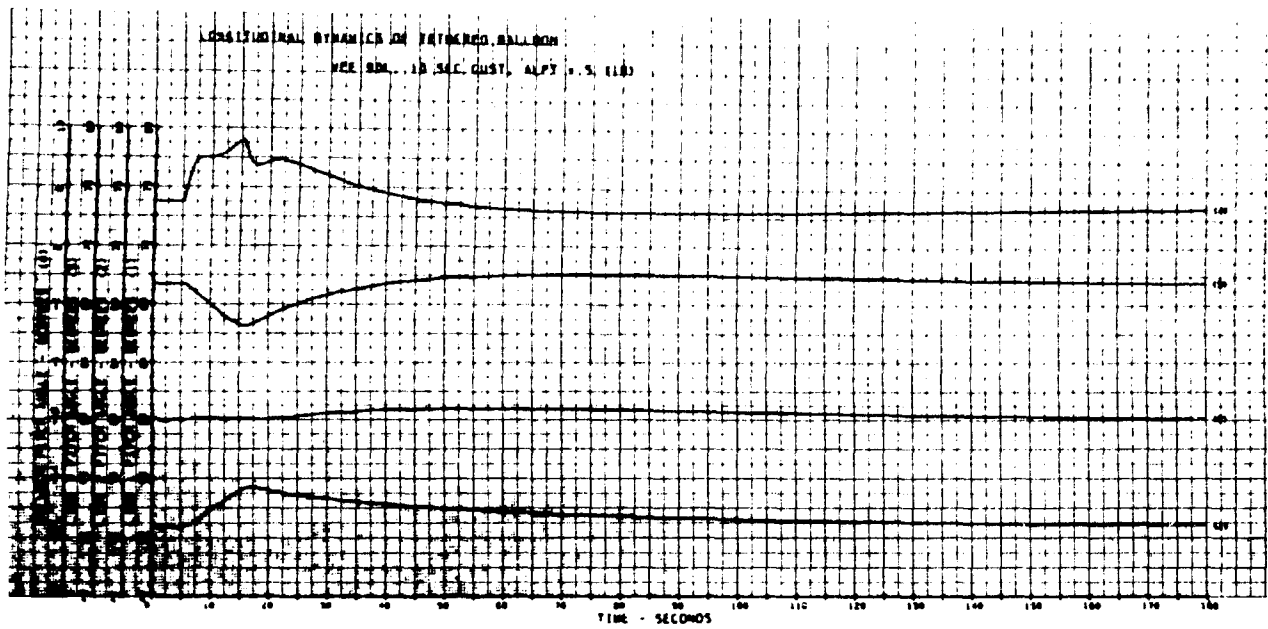
SEE BOM. 10 SEC GUST, ALPT=7, (18)

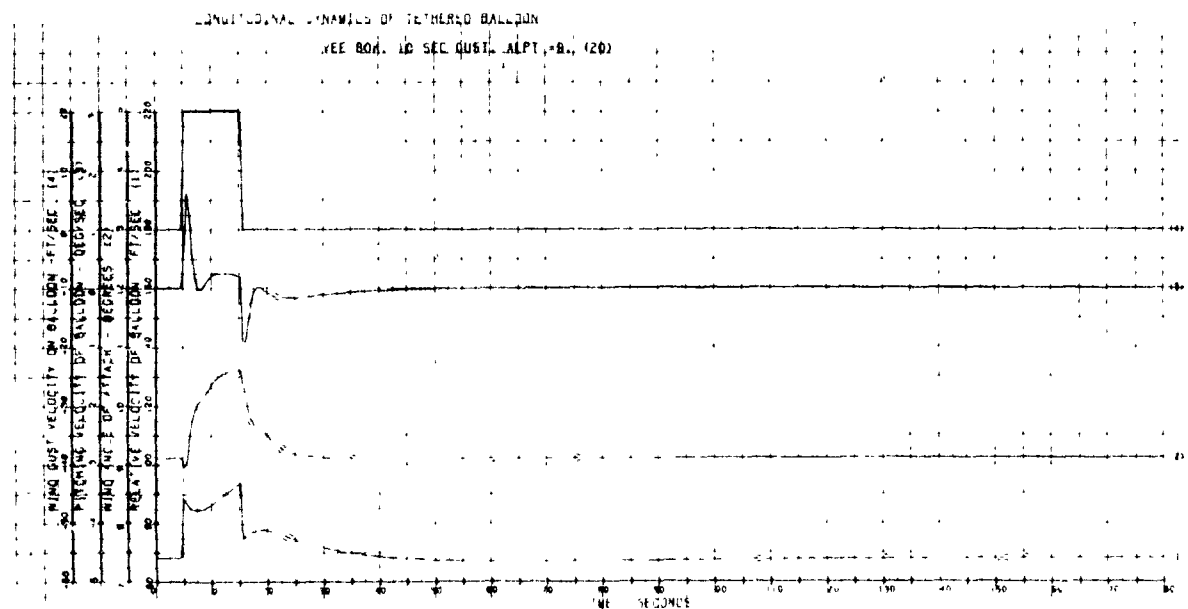
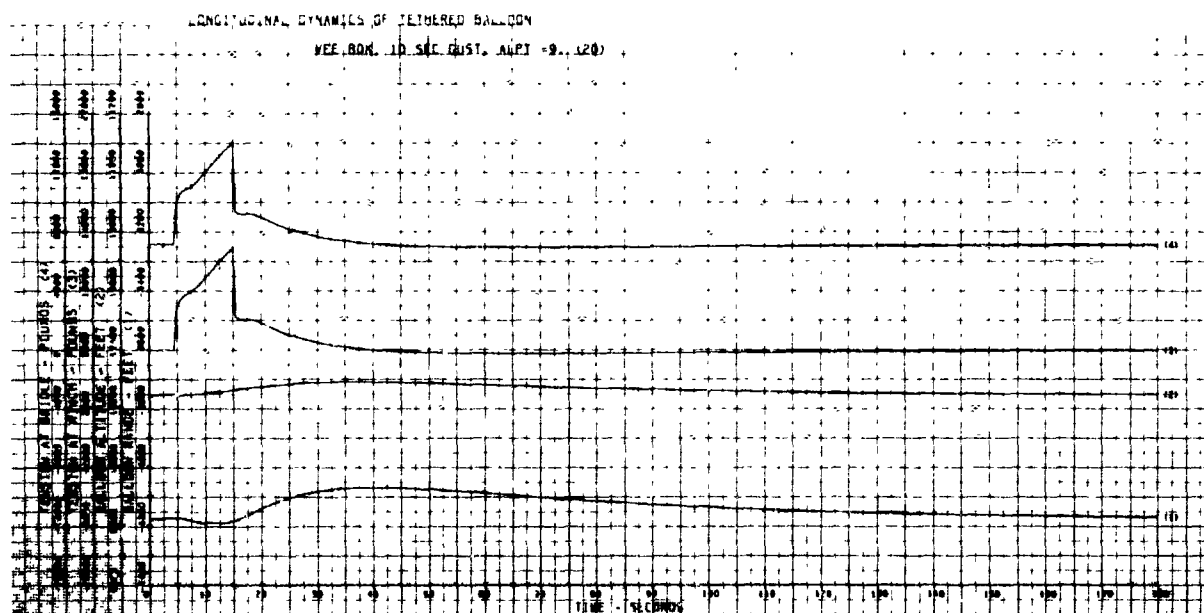
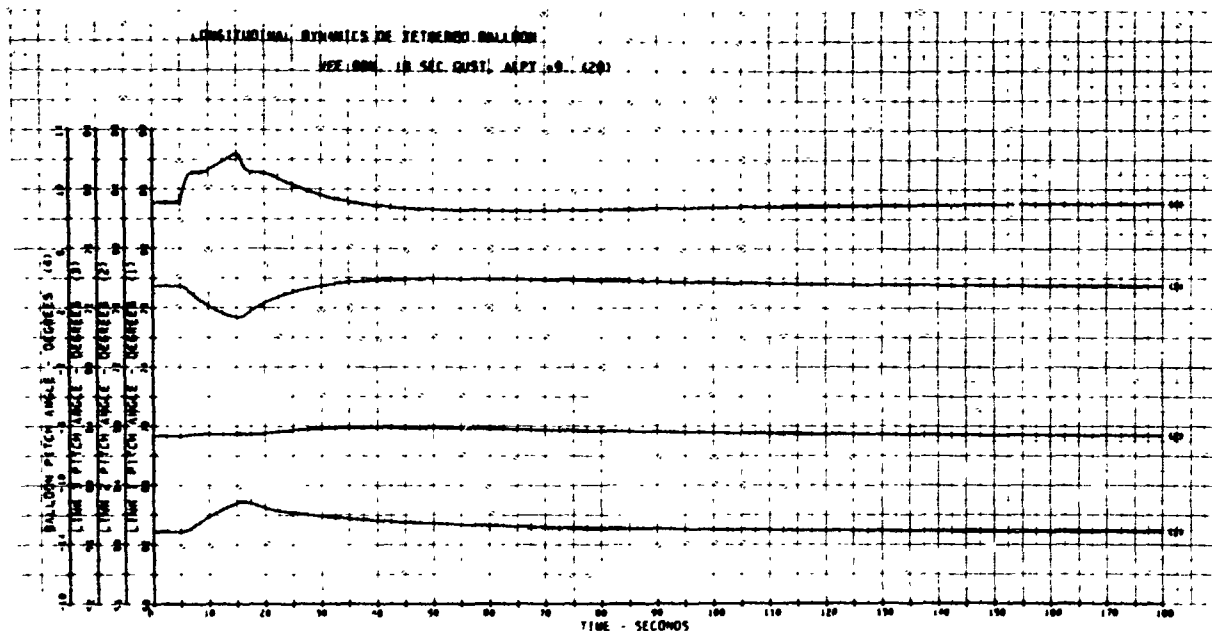


# LONGITUDINAL DYNAMICS OF TETHERED BALLOON

SEE BOM. 10 SEC GUST, ALPT=7, (18)

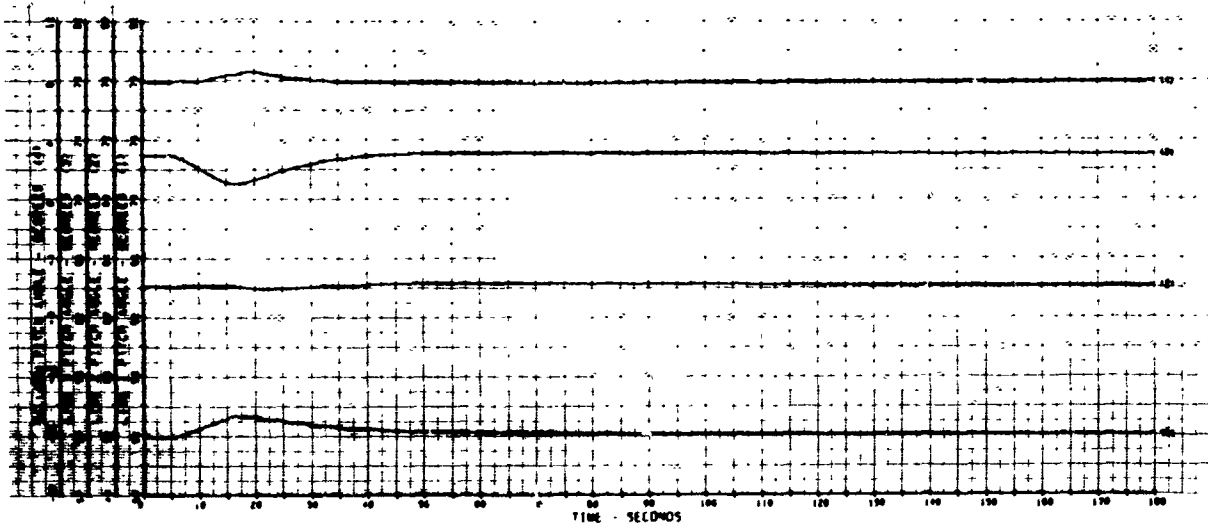






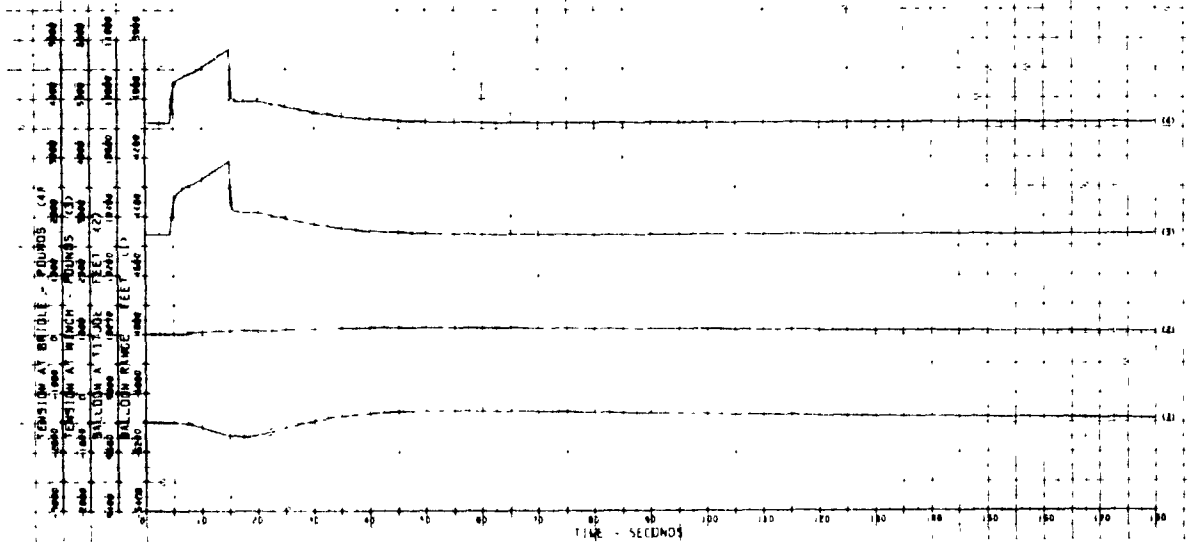
# LONGITUDINAL DYNAMICS OF TETHERED BALLOON

LAC. BOM. 10 SEC. GUST, ALPT. -8. (21)



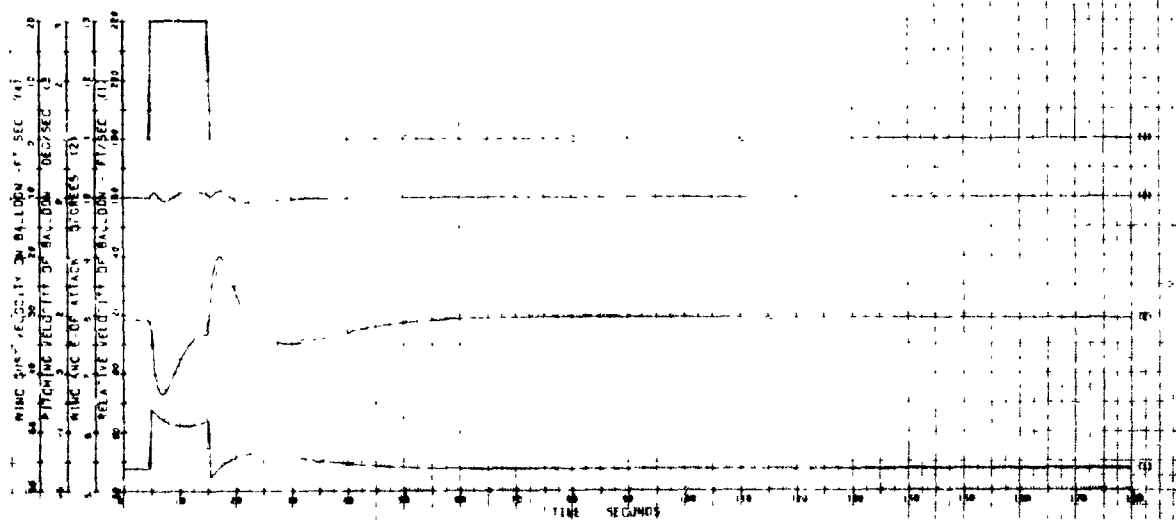
## LONGITUDINAL DYNAMICS OF TETHERED BALLOON

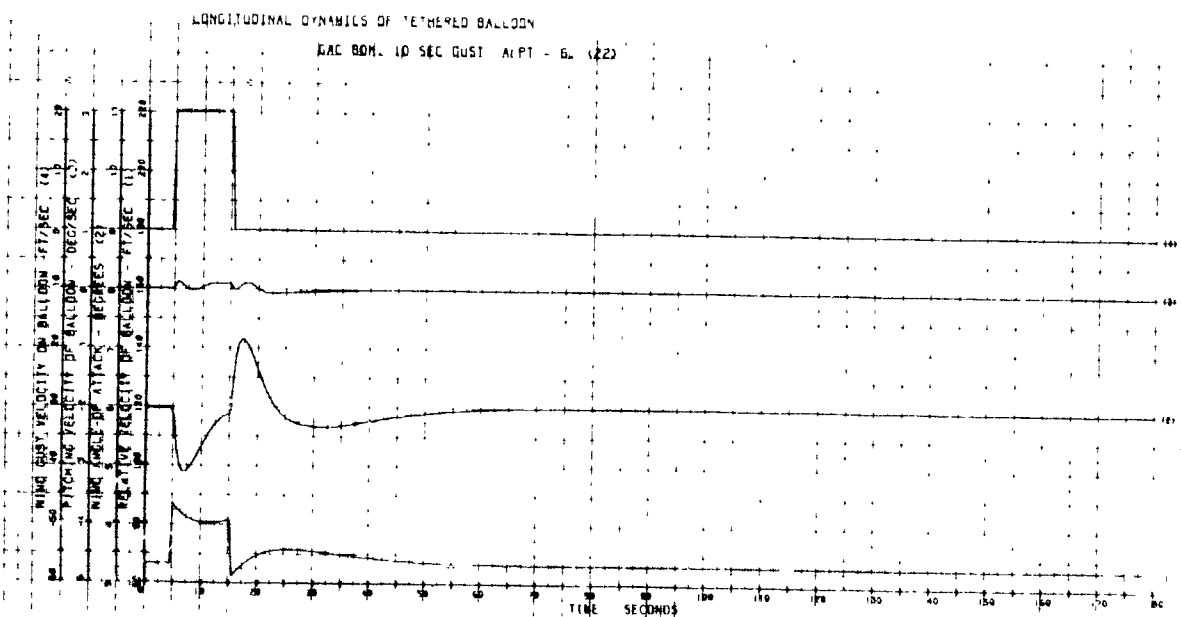
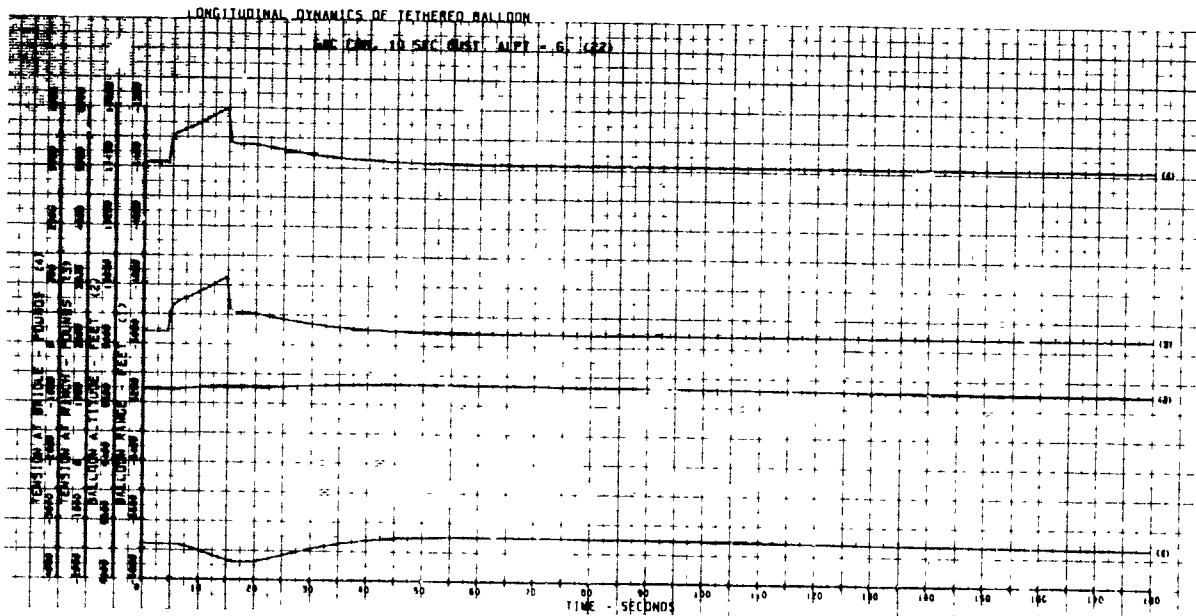
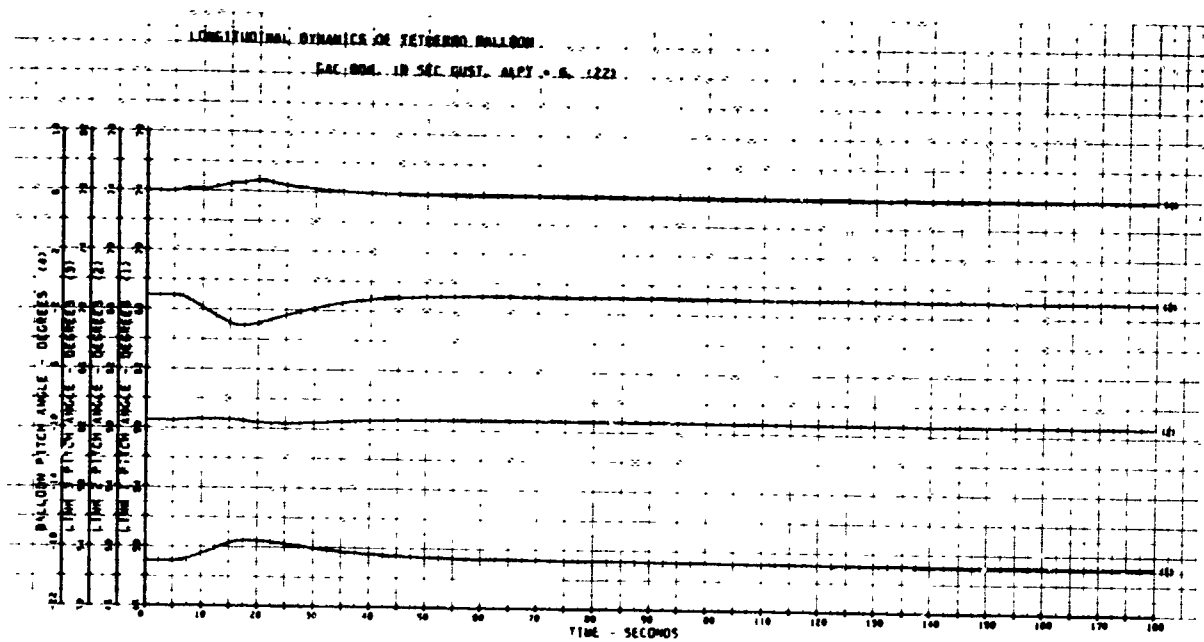
LAC. BOM. 10 SEC. GUST, ALPT. -8. (21)



## LONGITUDINAL DYNAMICS OF TETHERED BALLOON

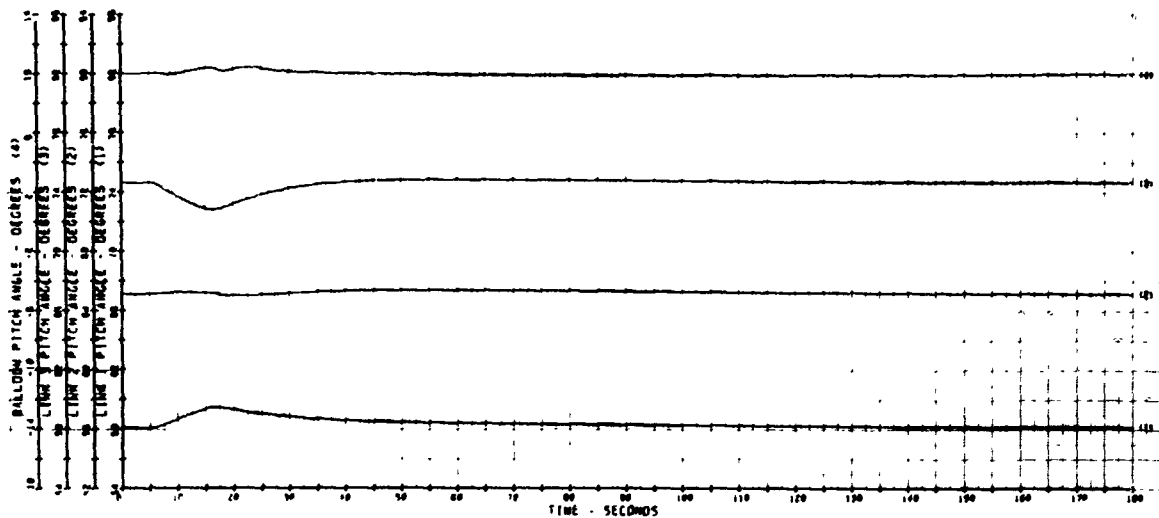
LAC. BOM. 10 SEC. GUST, ALPT. -8. (21)





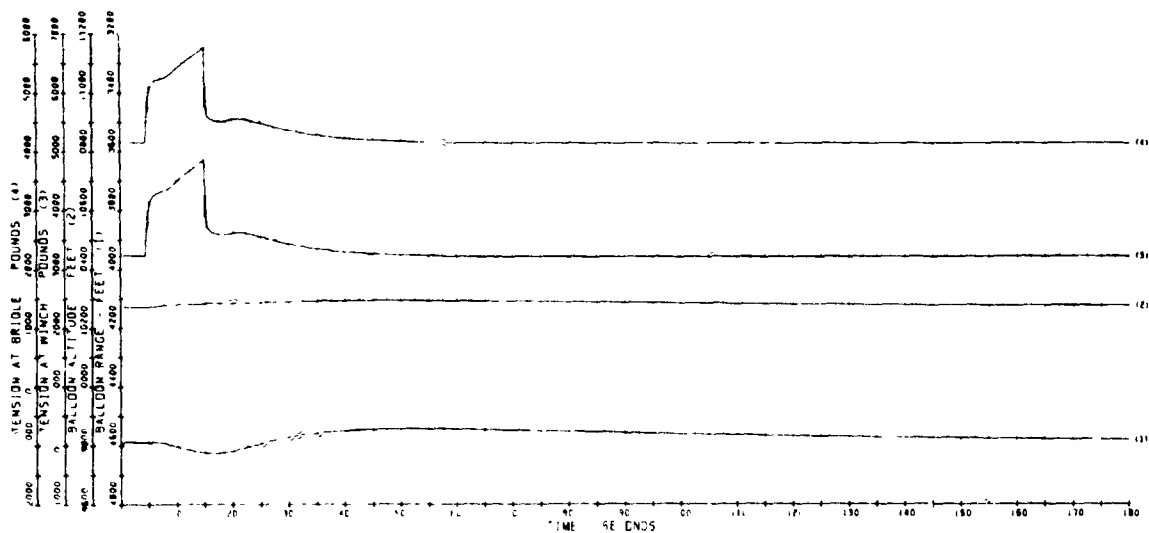
# LONGITUDINAL DYNAMICS OF TETHERED BALLOON

GAL. BOM. 10 SEC GUST, ALPT = 10. (23)



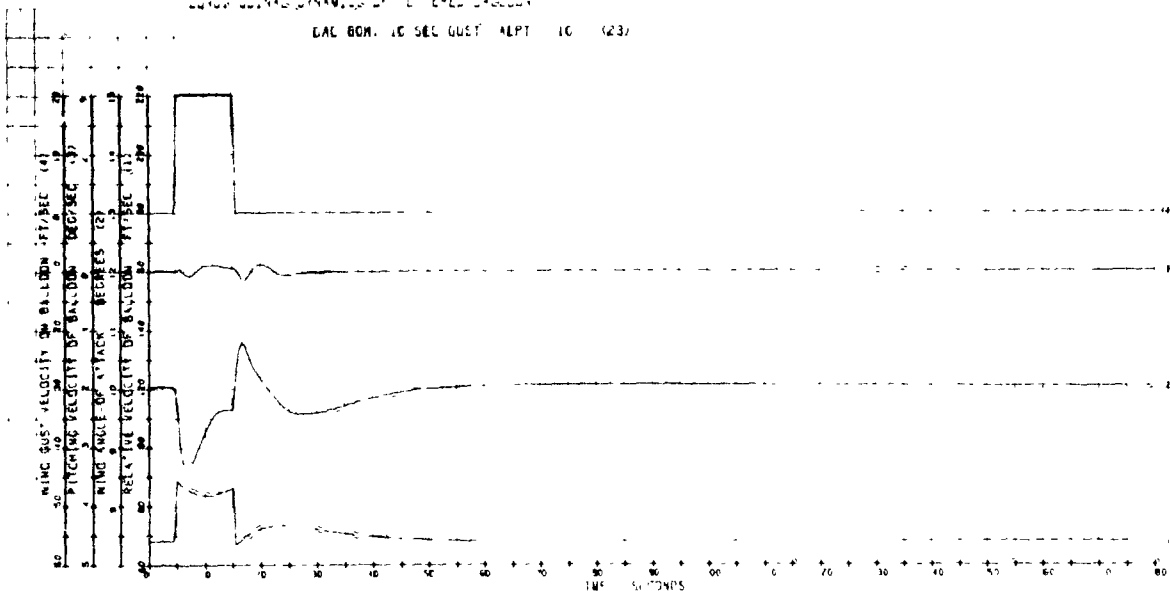
## LONGITUDINAL DYNAMICS OF TETHERED BALLOON

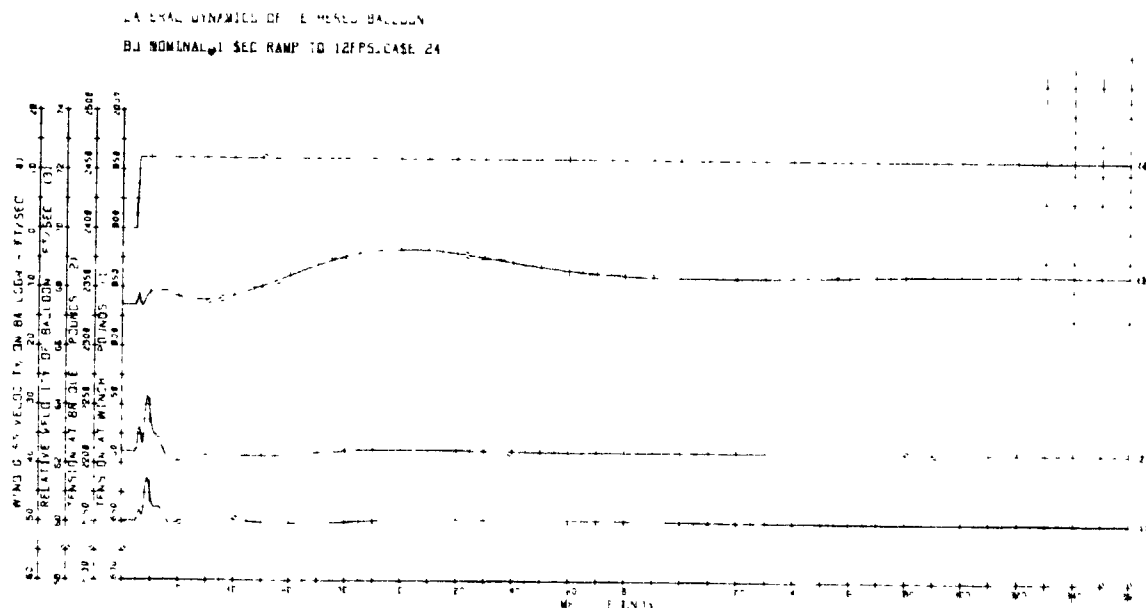
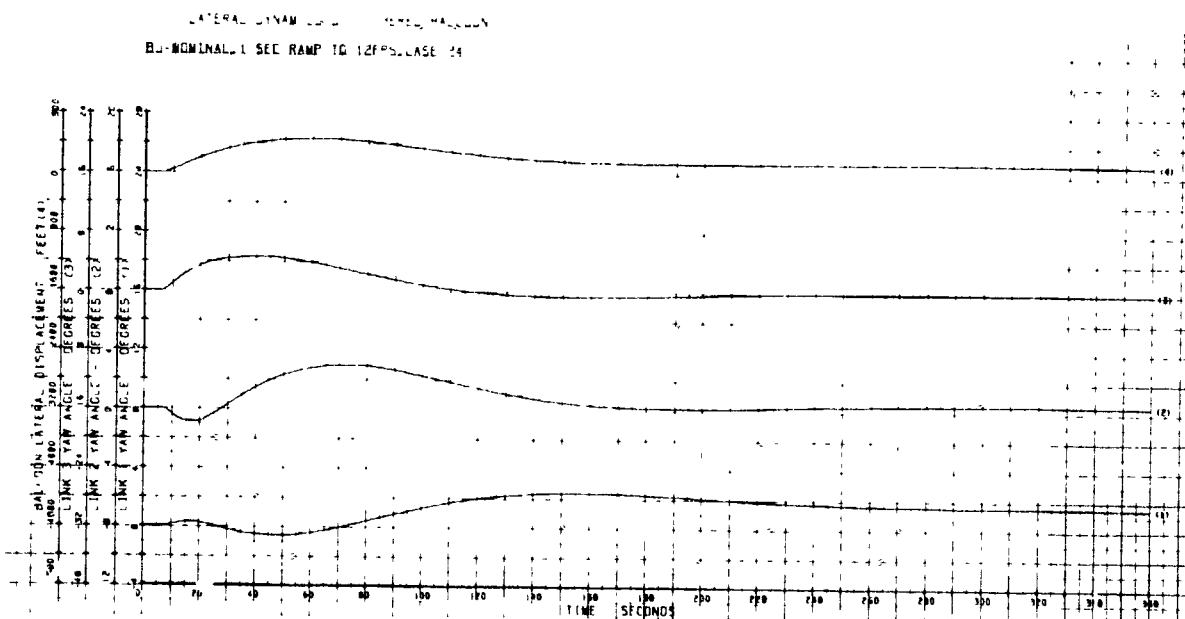
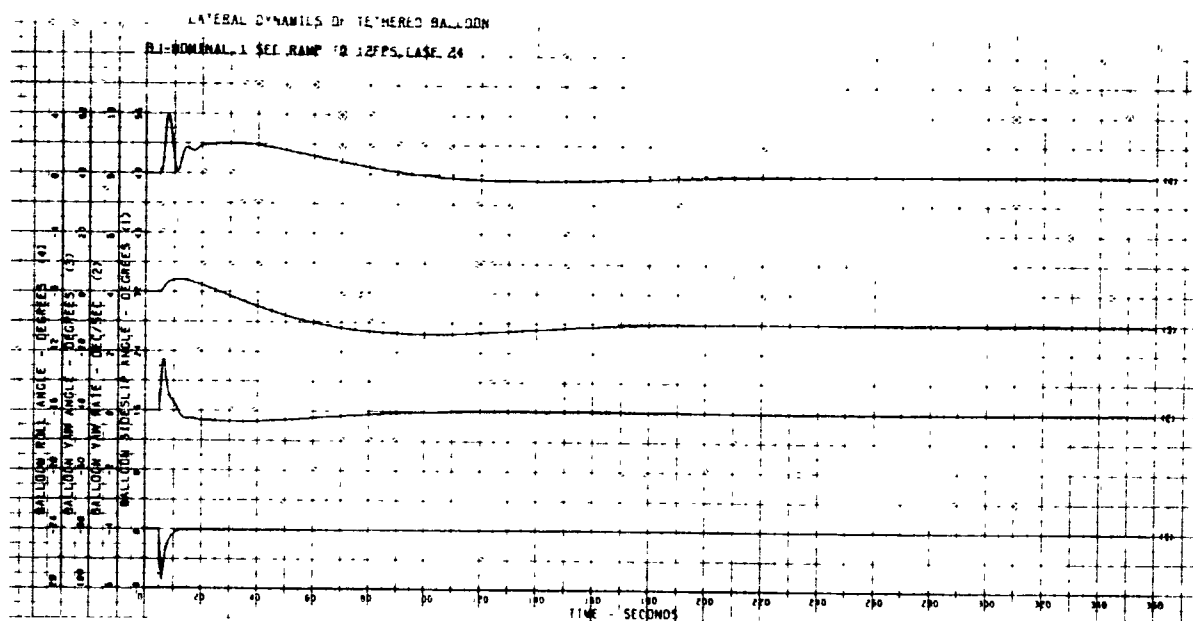
GAL. BOM. 10 SEC GUST, ALPT = 10. (23)



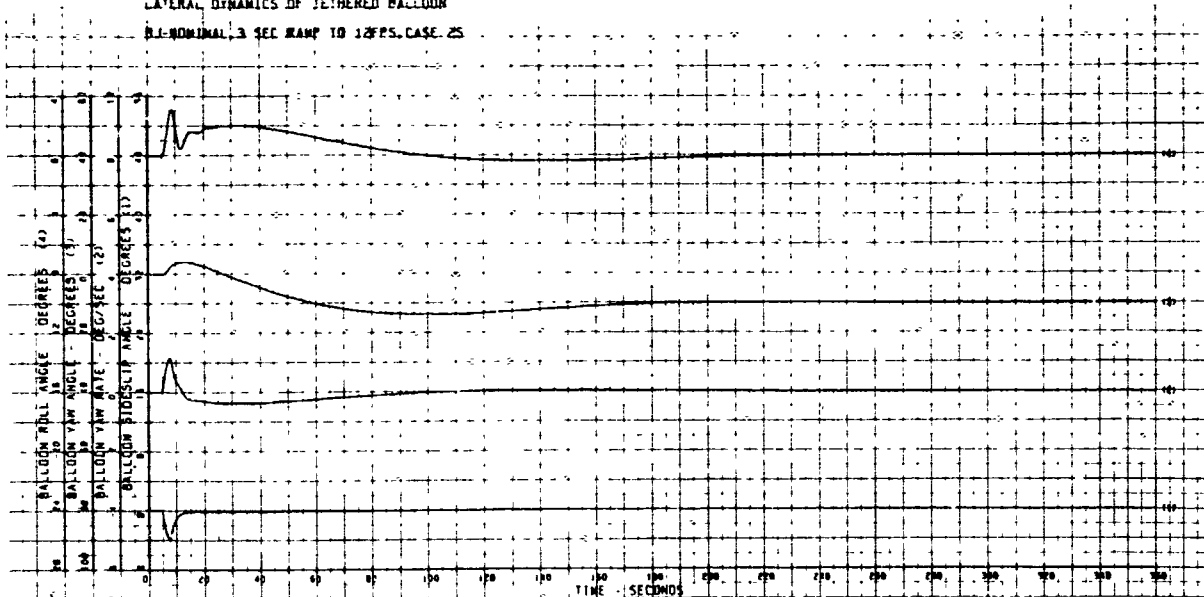
## LONGITUDINAL DYNAMICS OF TETHERED BALLOON

GAL. BOM. 10 SEC GUST, ALPT = 10. (23)

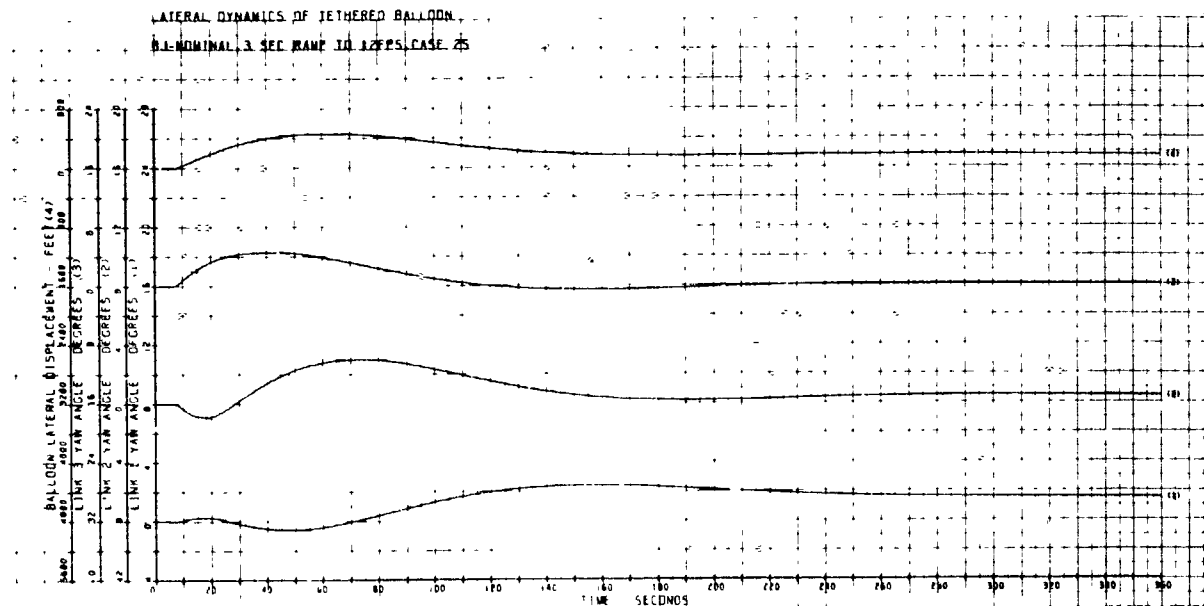




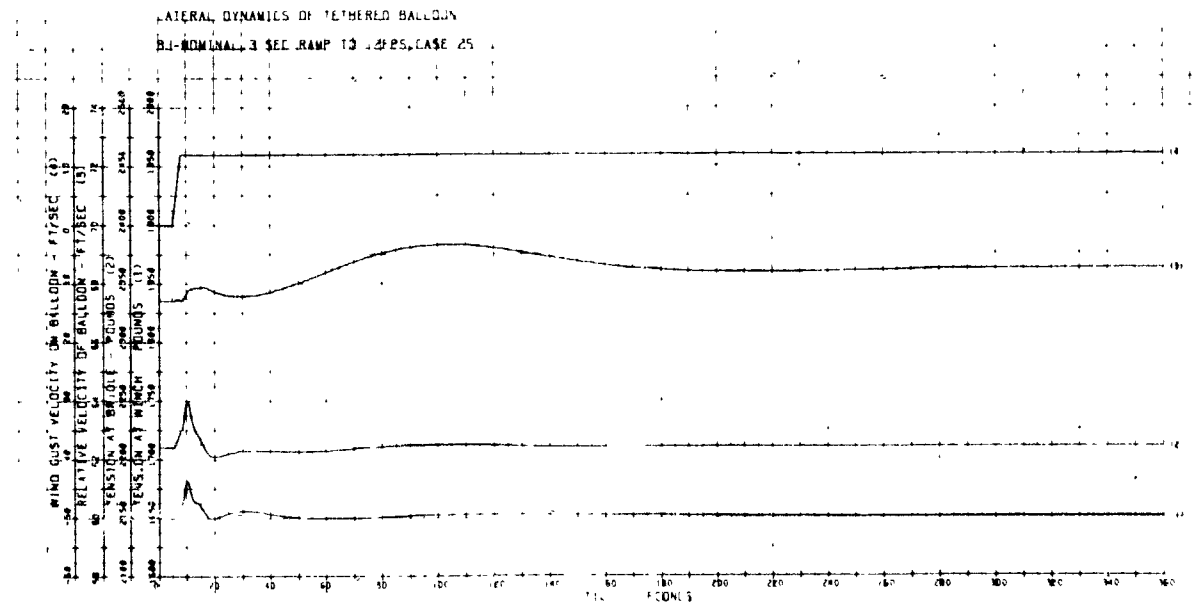
LATERAL DYNAMICS OF JETTERED BALLOON  
 BI-NOMINAL 3 SEC RAMP TO 12FPS, CASE 25

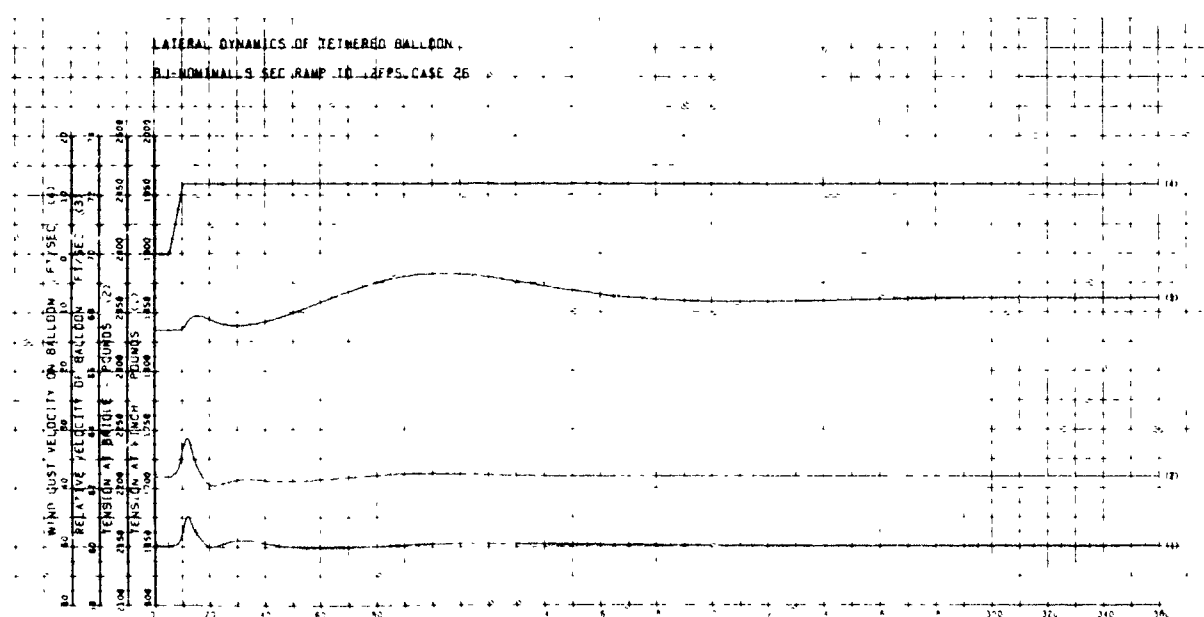
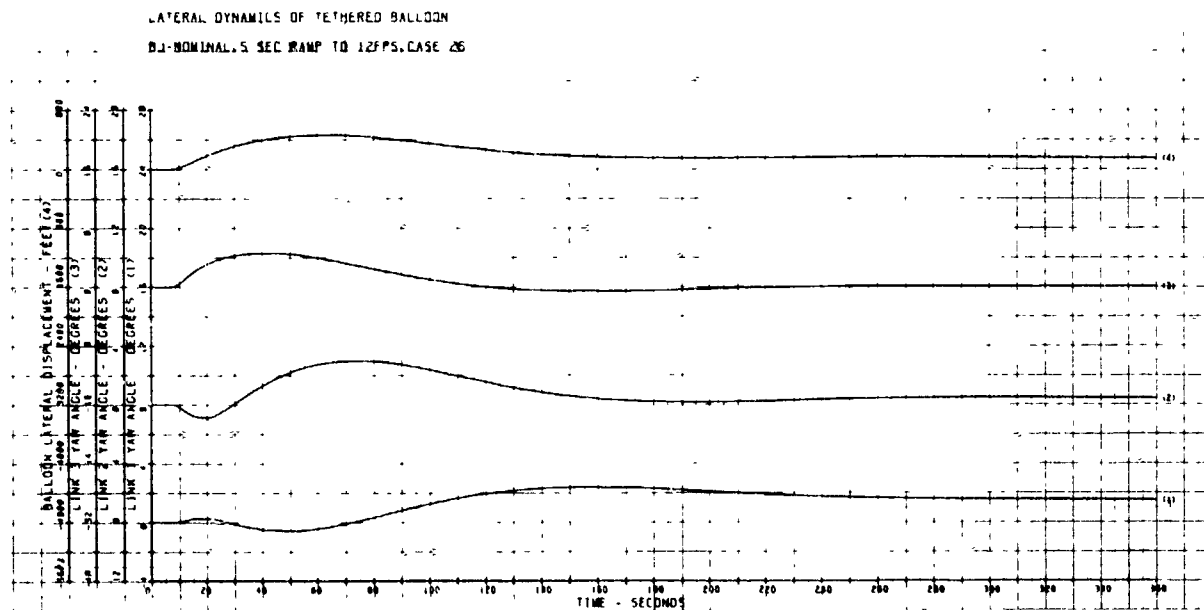
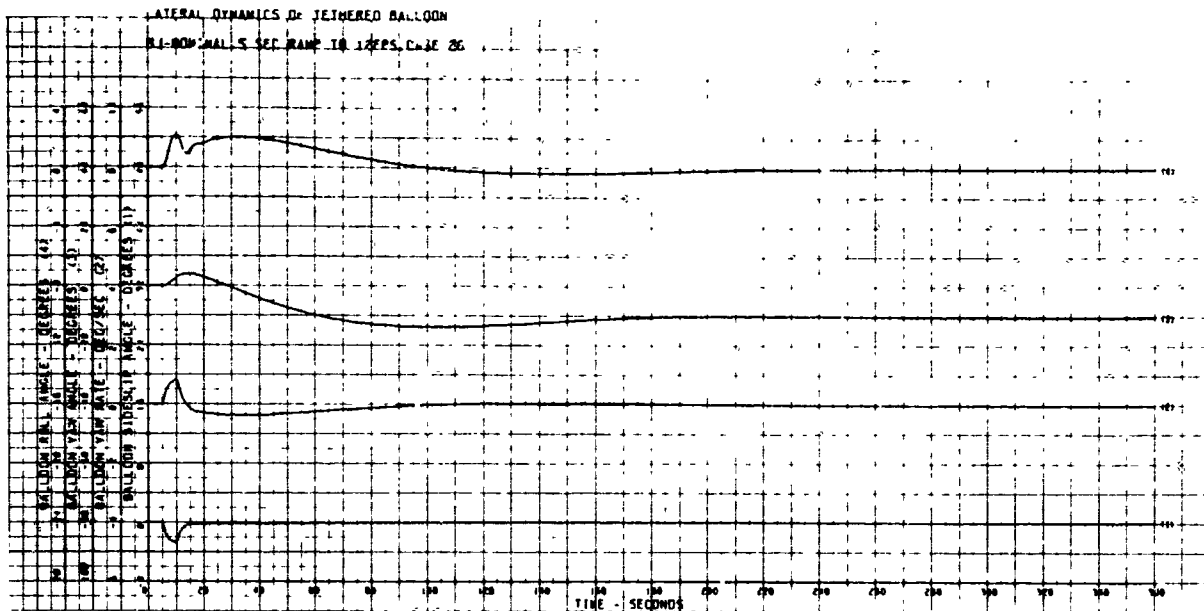


LATERAL DYNAMICS OF JETTERED BALLOON  
 BI-NOMINAL 3 SEC RAMP TO 12FPS, CASE 25

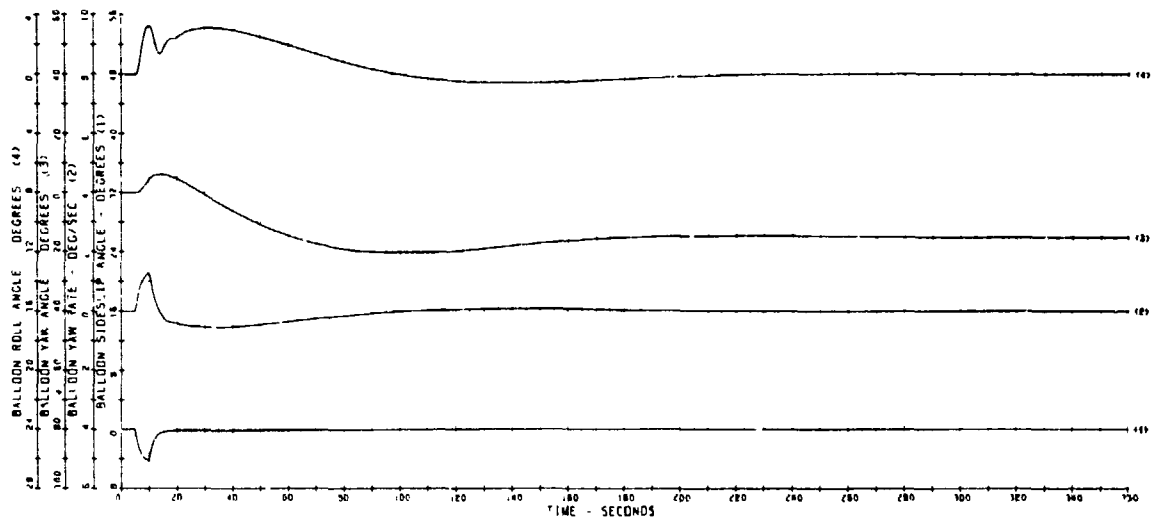


LATERAL DYNAMICS OF JETTERED BALLOON  
 BI-NOMINAL 3 SEC RAMP TO 12FPS, CASE 25

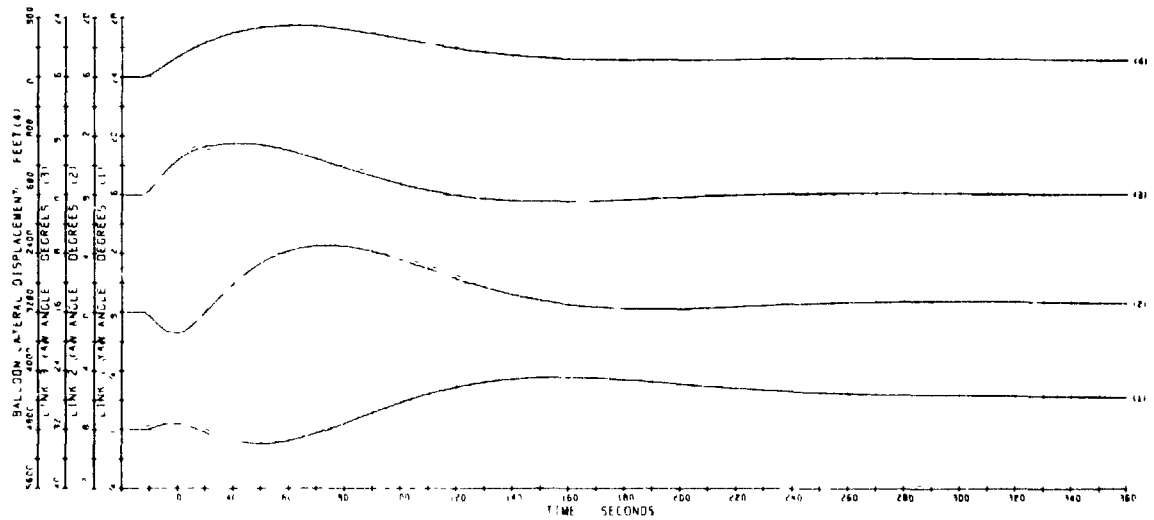




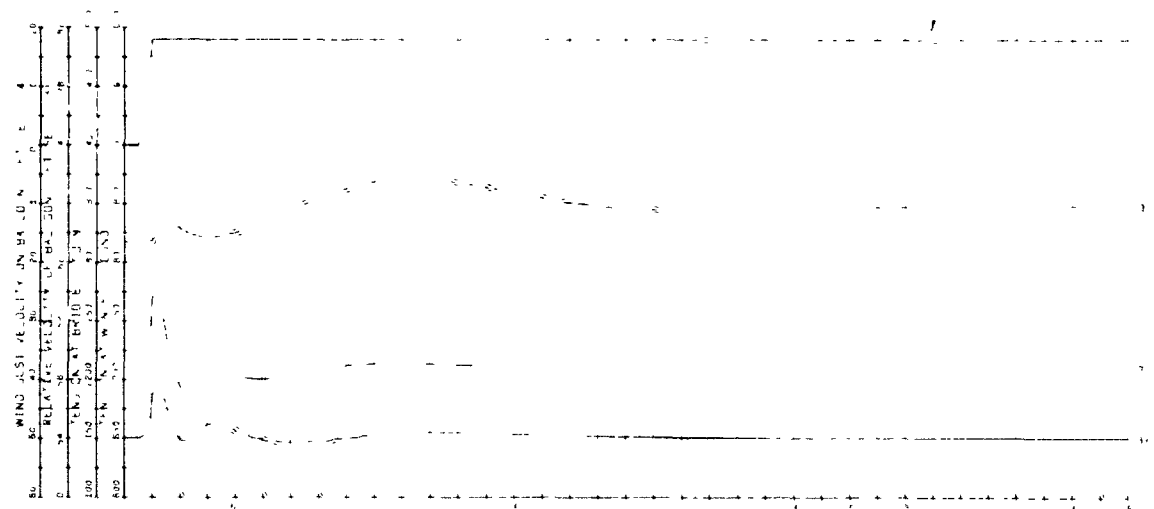
LATERAL DYNAMICS OF TETHERED BALLOON  
B1-NOMINAL 5 SEC RAMP TO 18FPS, CASE 27



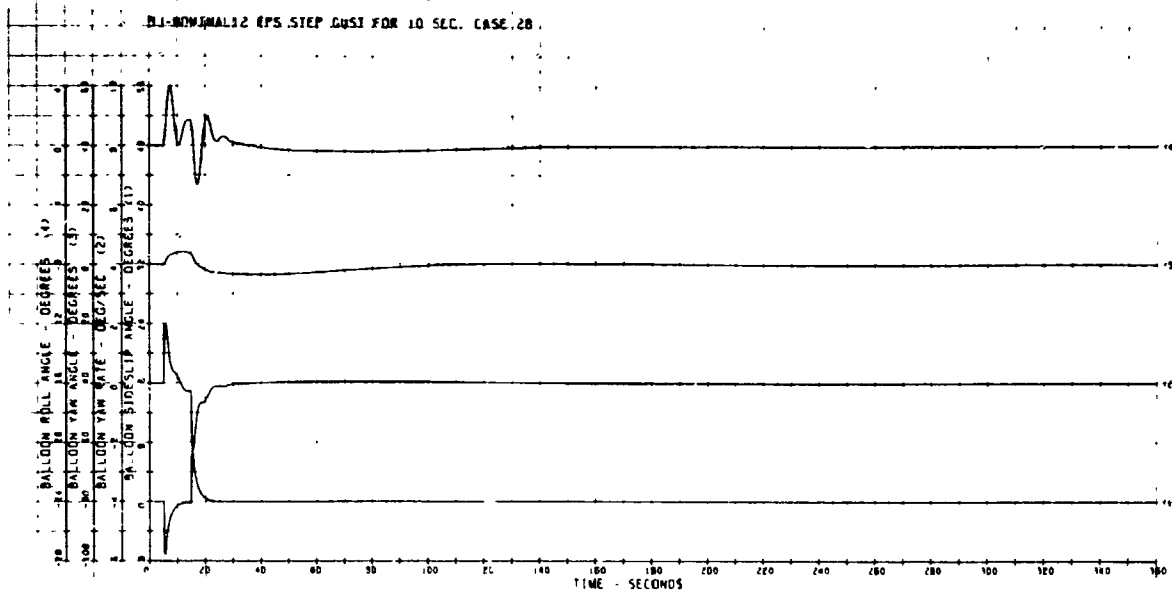
LATERAL DYNAMICS OF TETHERED BALLOON  
B1-NOMINAL 5 SEC RAMP TO 18FPS, CASE 27



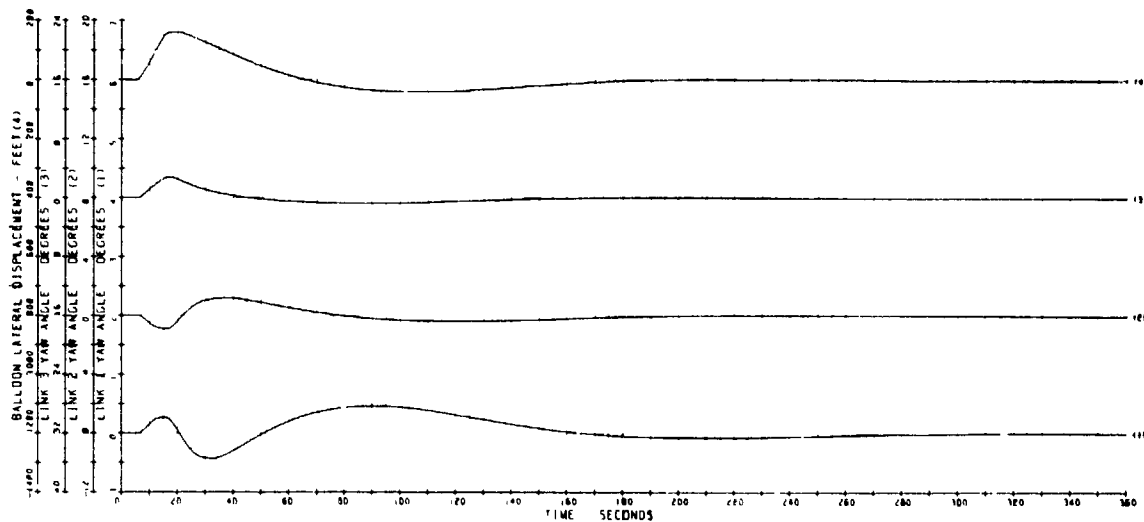
LATERAL DYNAMICS OF TETHERED BALLOON  
B1-NOMINAL 5 SEC RAMP TO 18FPS, CASE 27



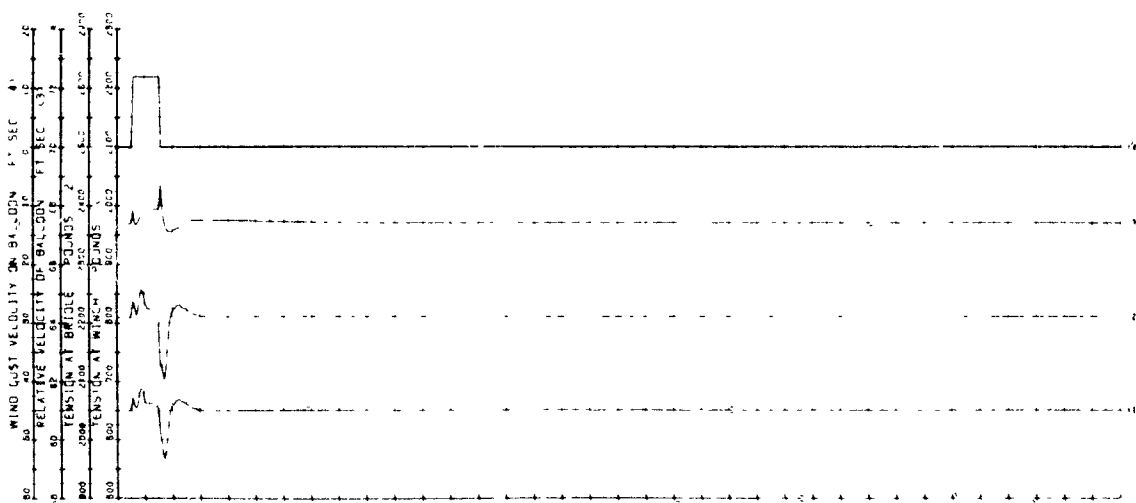
LATERAL DYNAMICS OF TETHERED BALLOON  
 B1-NOMINAL 12 FPS STEP GUST FOR 10 SEC. CASE 2B



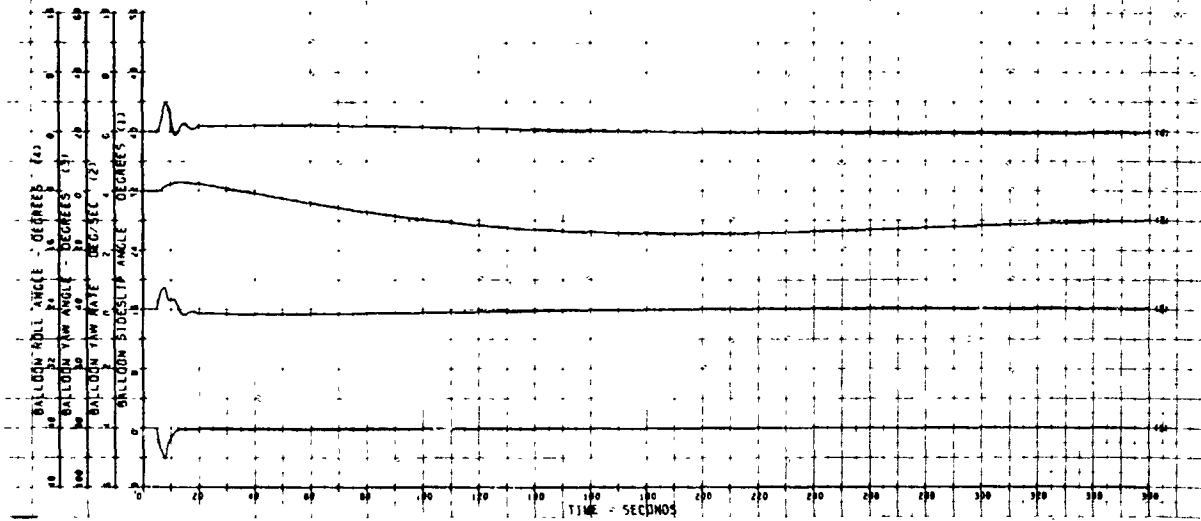
LATERAL DYNAMICS OF TETHERED BALLOON  
 B1-NOMINAL 12 FPS STEP GUST FOR 10 SEC. CASE 2B



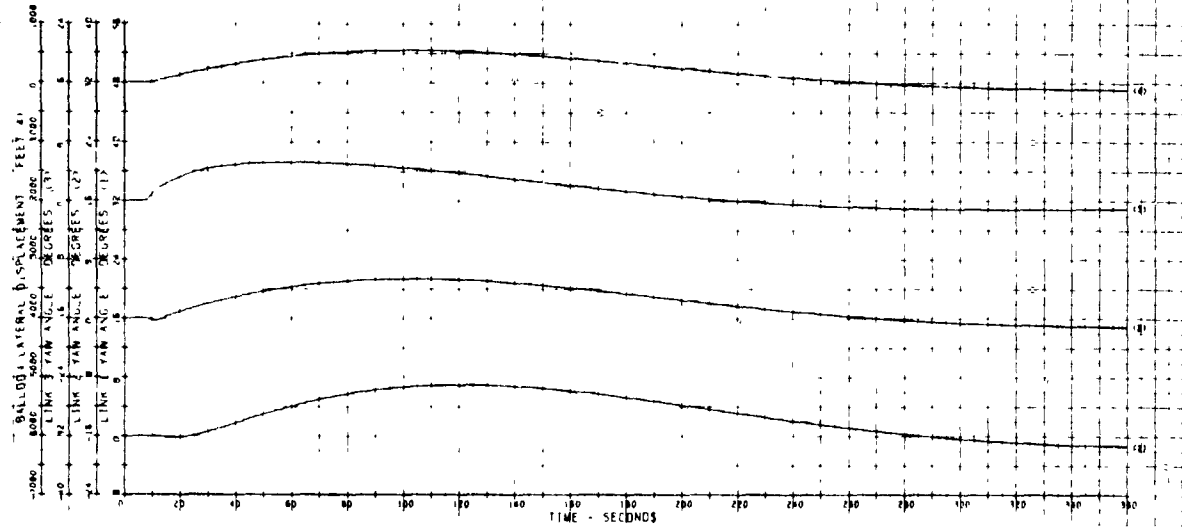
LATERAL DYNAMICS OF TETHERED BALLOON  
 B1-NOMINAL 12 FPS STEP GUST FOR 10 SEC. CASE 2B



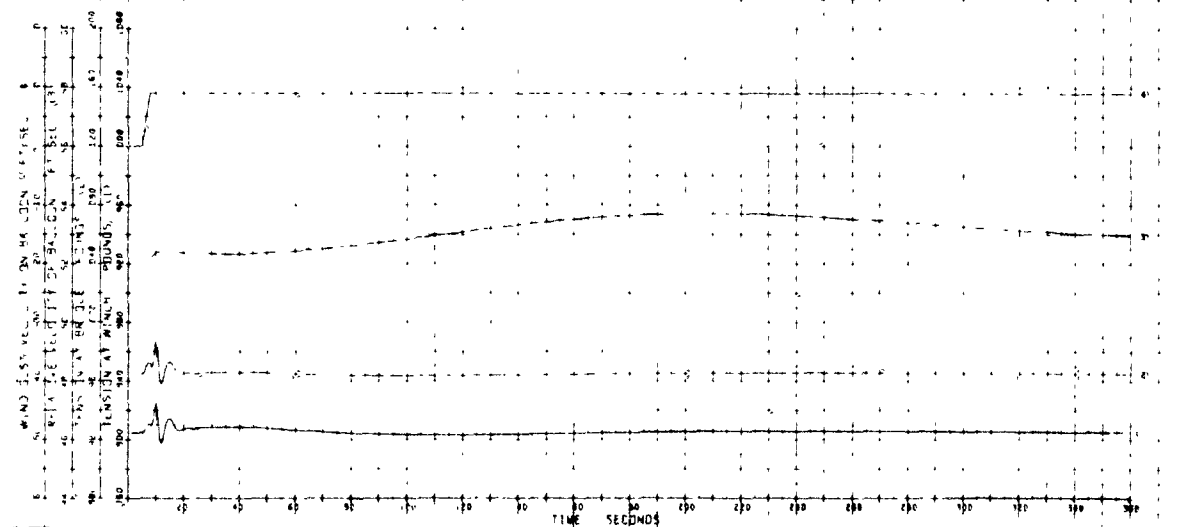
LATERAL DYNAMICS OF TETHERED BALLOON  
 BJ 46K.5K FT 3 SEC RAMP TO 3 FPS. CASE 2B

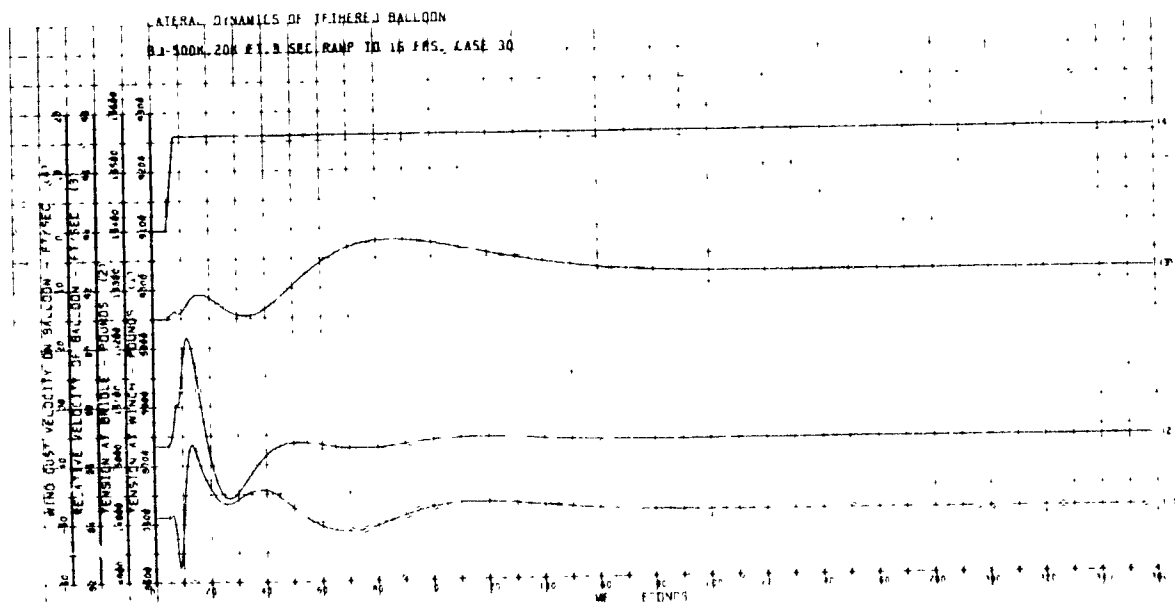
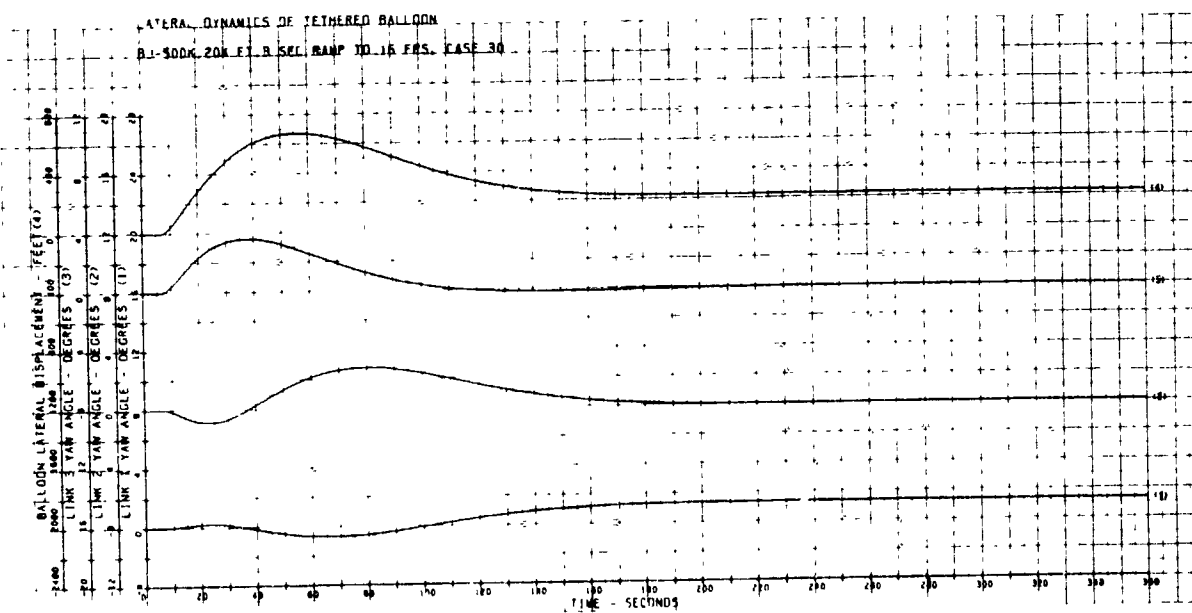
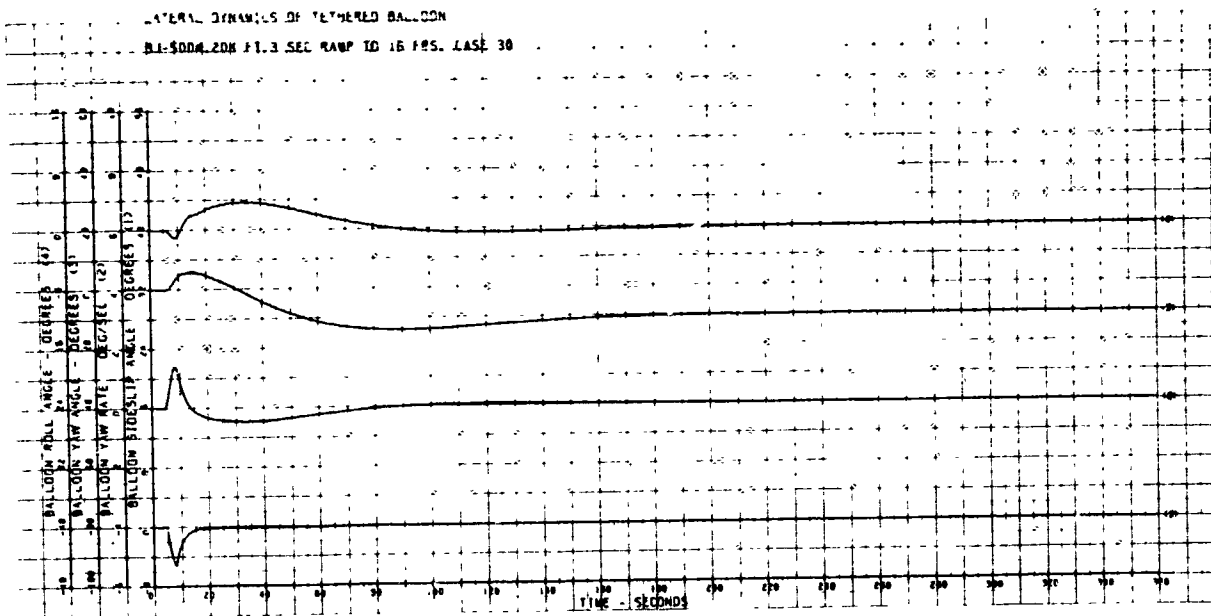


LATERAL DYNAMICS OF TETHERED BALLOON  
 BJ 46K.5K FT. 3 SEC RAMP TO 3 FPS. CASE 2B

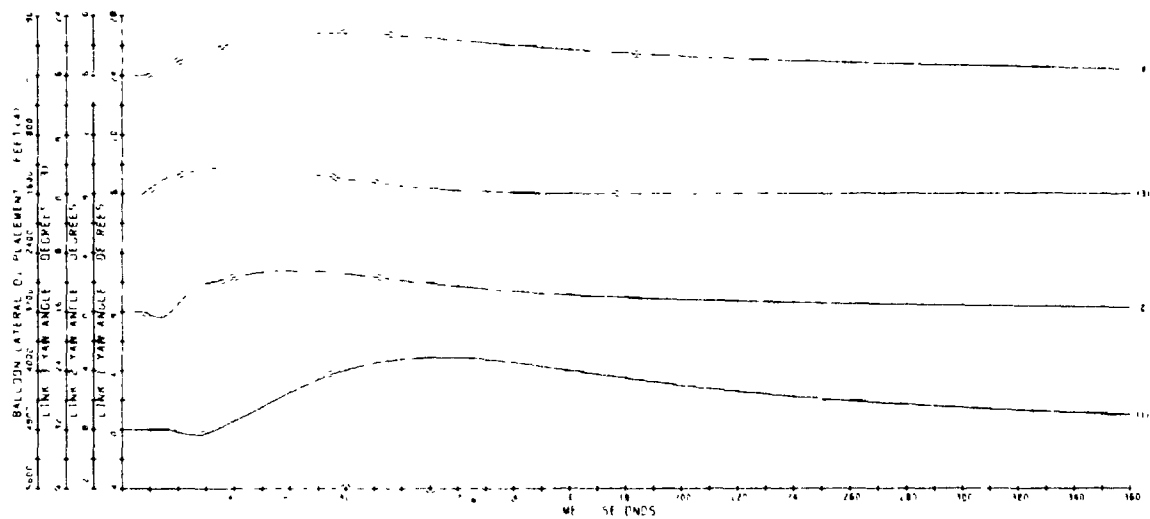


LATERAL DYNAMICS OF TETHERED BALLOON  
 BJ 46K.5K FT. 3 SEC RAMP TO 3 FPS. CASE 2B

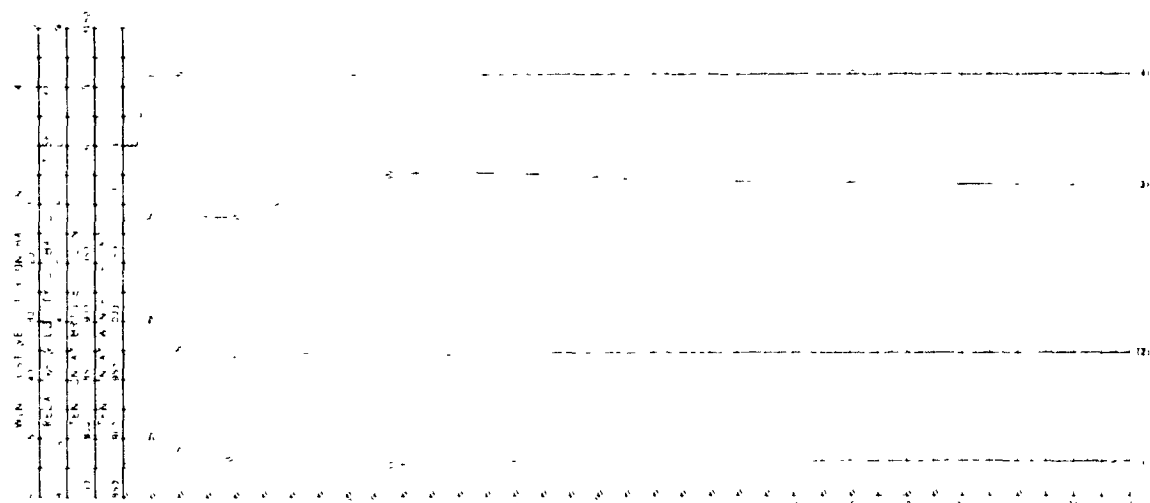


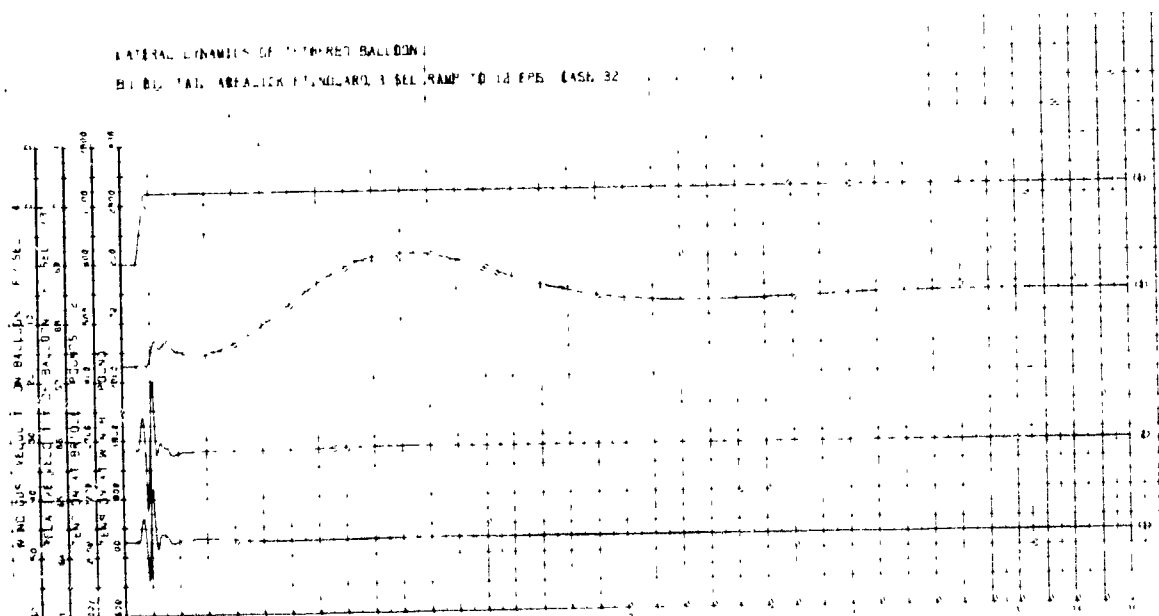
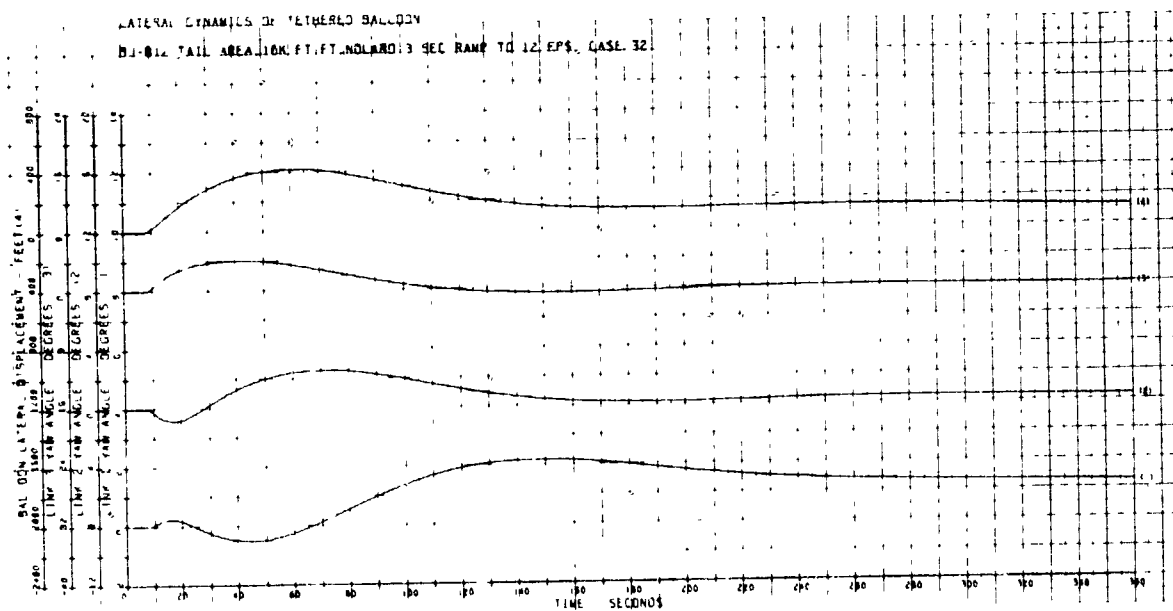
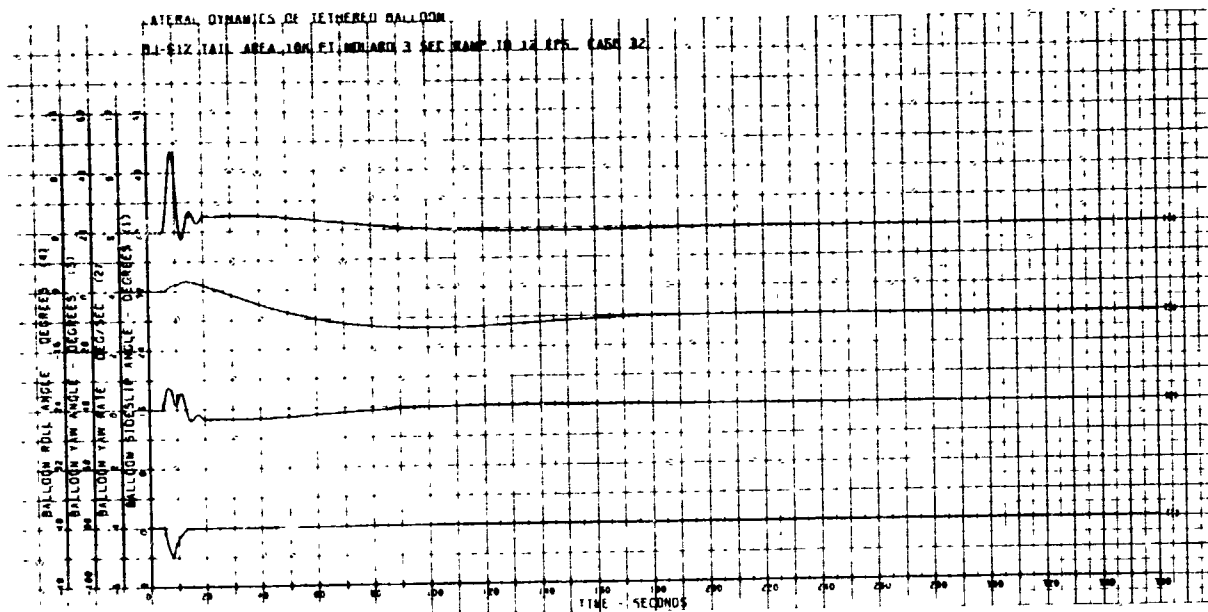


BJ NCM144.3 SLT RAMP TO 2 FPS. ANGAL. CASE 31

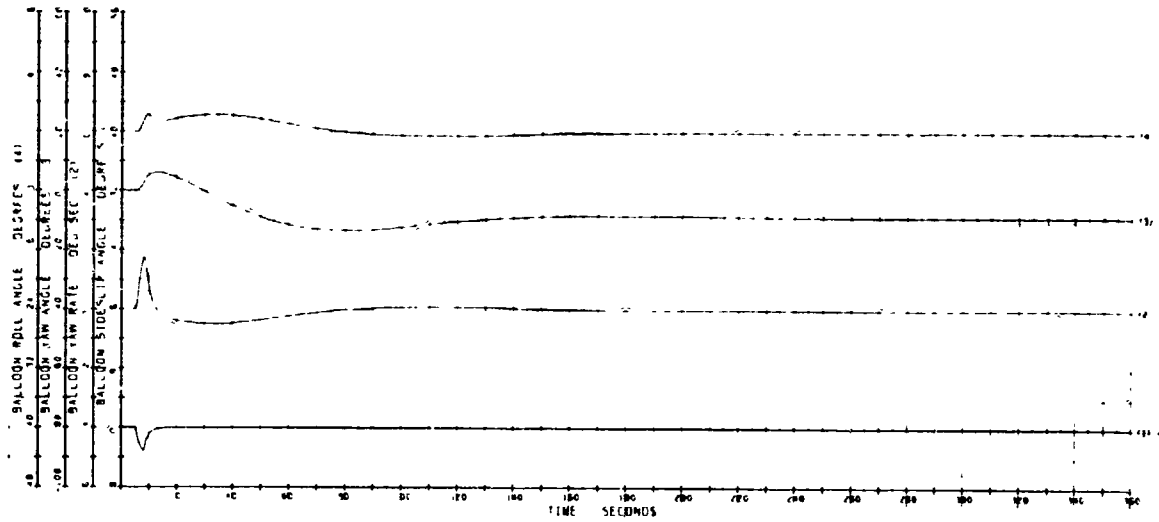


FORMINIAL J SEL NAME "U 2 F-AMAL A"

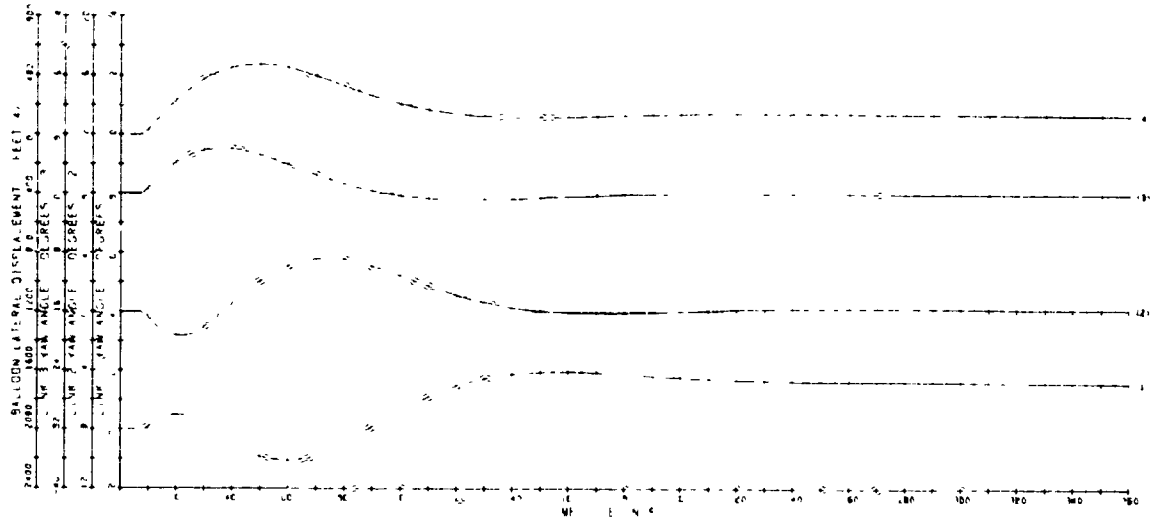




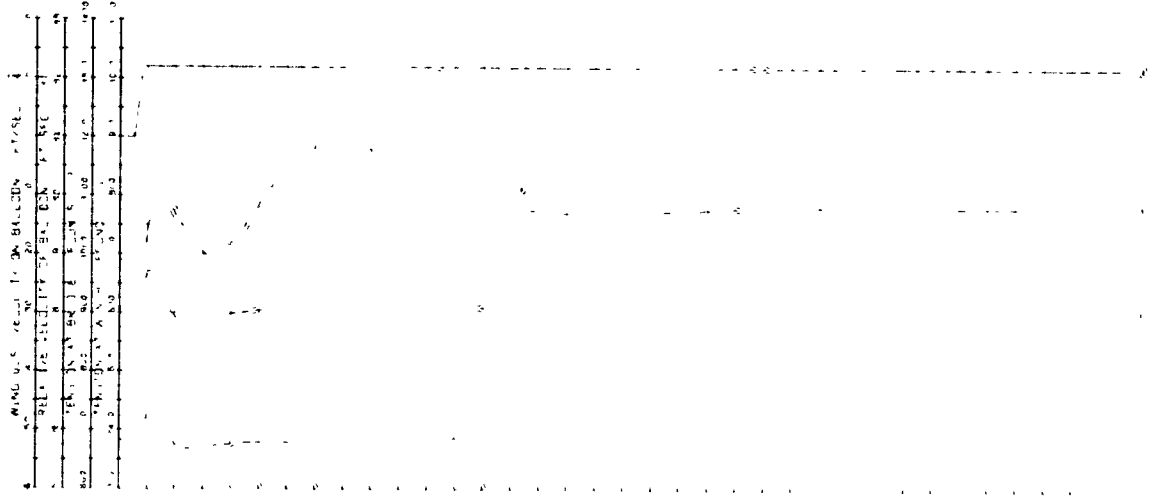
LA 144/ TAIL AREA FOR 17 INCH AND 3 SEC RAMP TO LOOPS CASE 33



LA 144/ TAIL AREA FOR 17 INCH AND 3 SEC RAMP TO LOOPS CASE 33

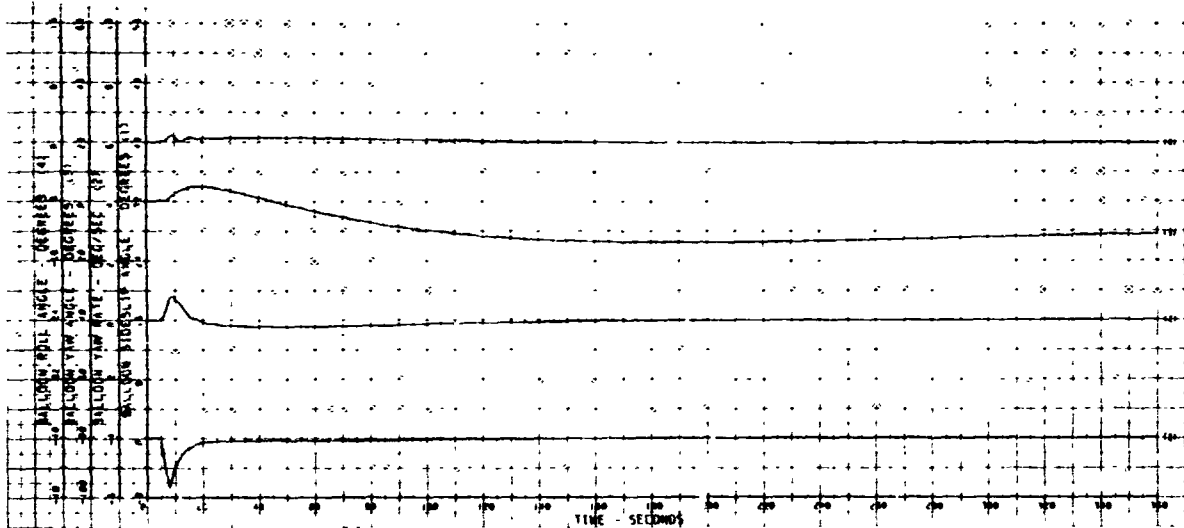


LA 144/ TAIL AREA FOR 17 INCH AND 3 SEC RAMP TO LOOPS CASE 33



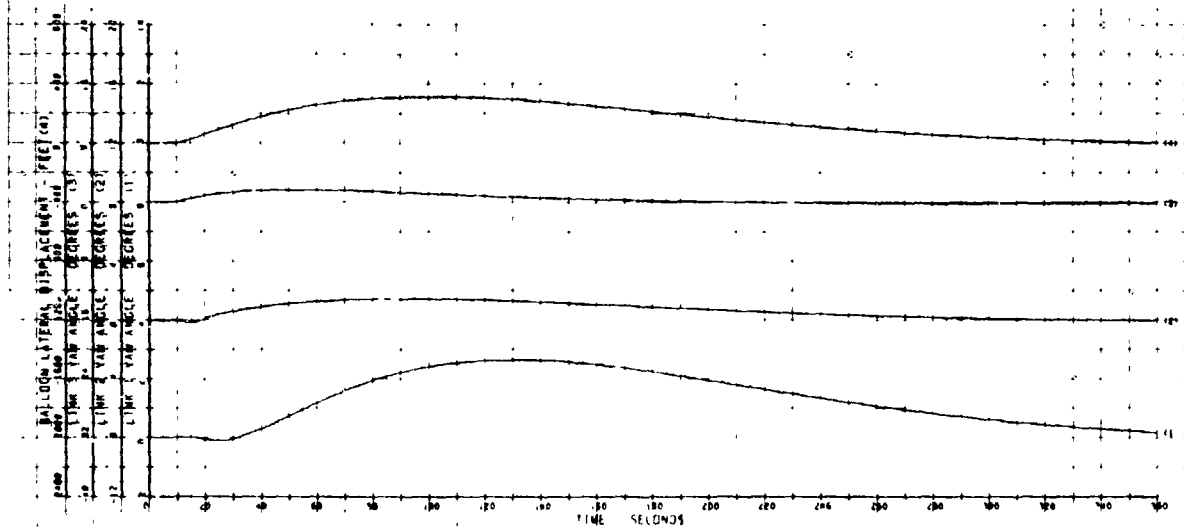
# LATERAL DYNAMICS OF TETHERED BALLOON

RI-NOM-10M, FT. 404 WIND 3 SEC RAMP TO 4.8 FPS, CASE 34.



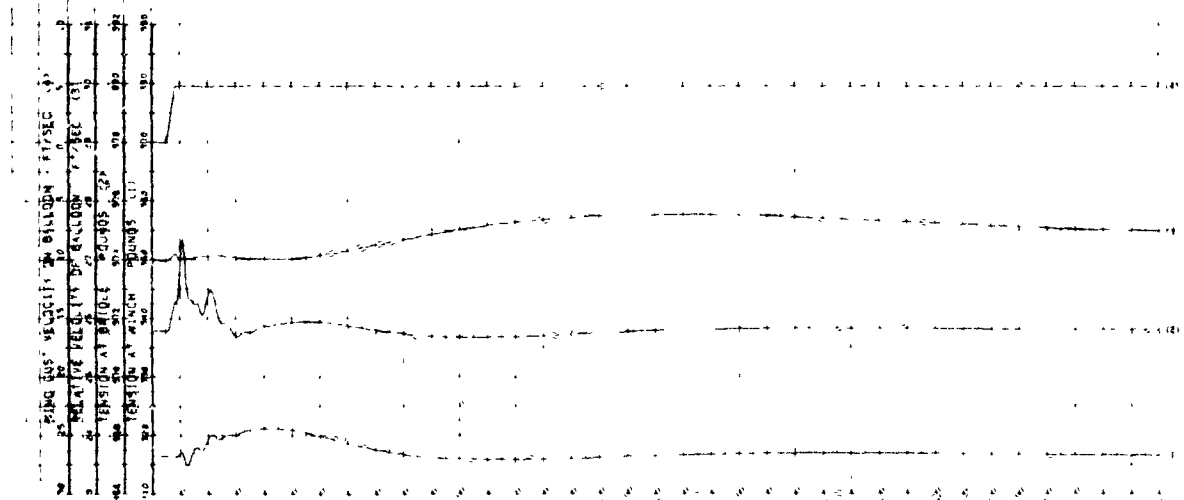
# LATERAL DYNAMICS OF TETHERED BALLOON

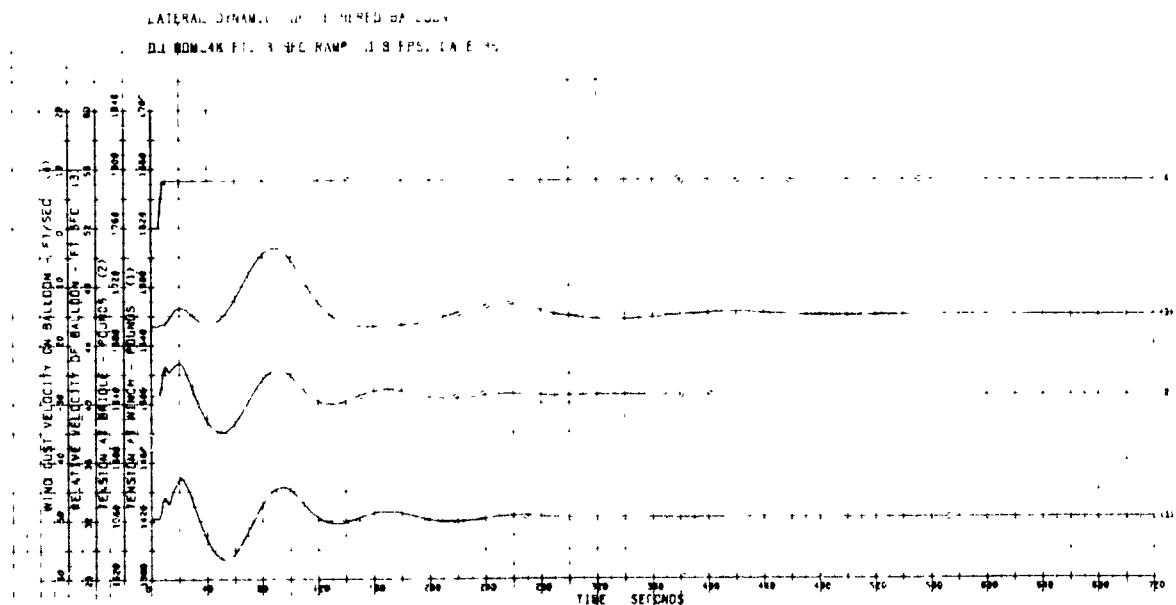
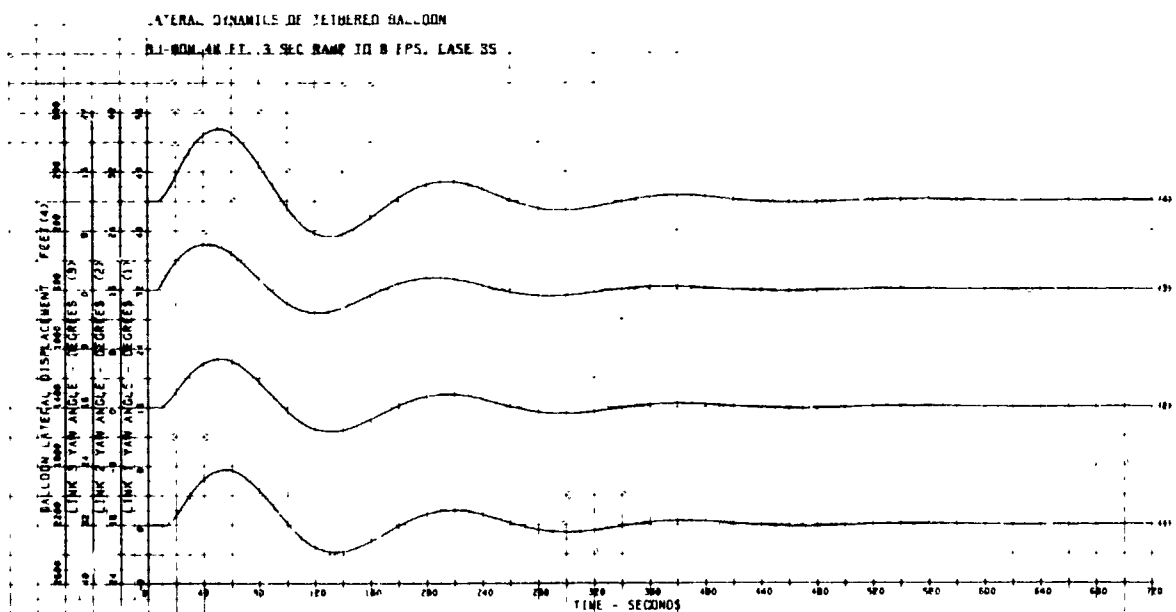
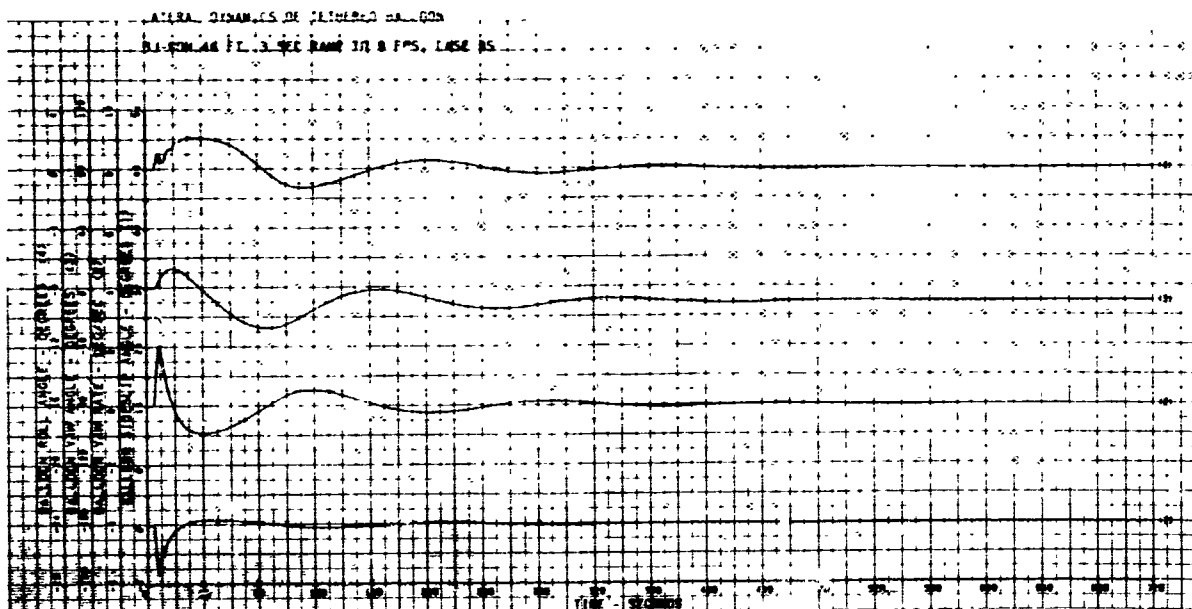
RI-NOM-10M, FT. 404 WIND 3 SEC RAMP TO 4.8 FPS, CASE 34.

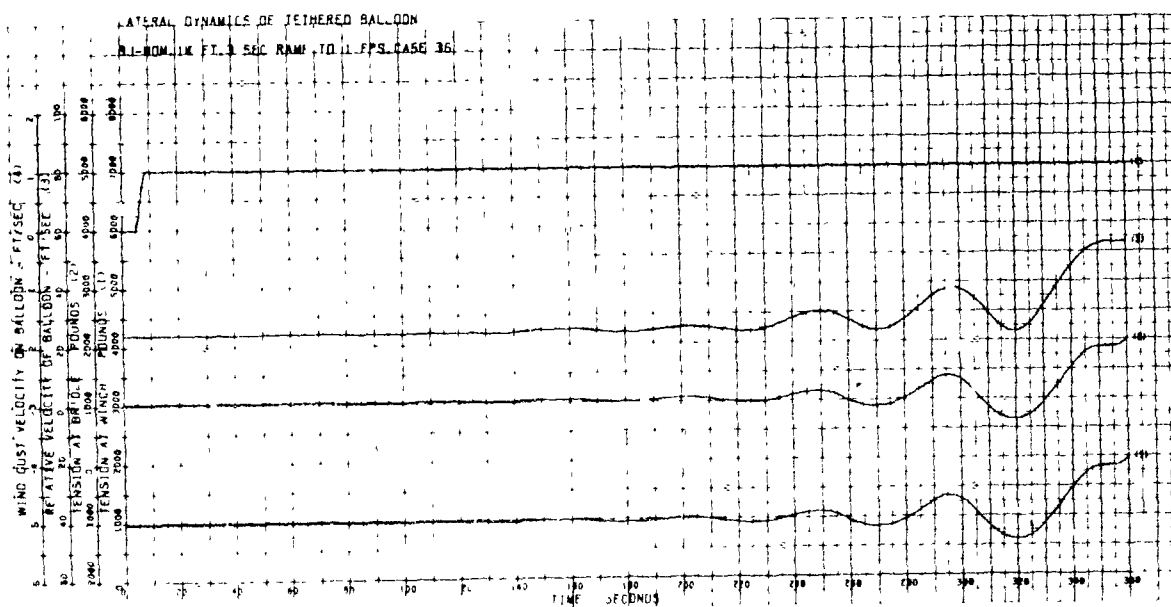
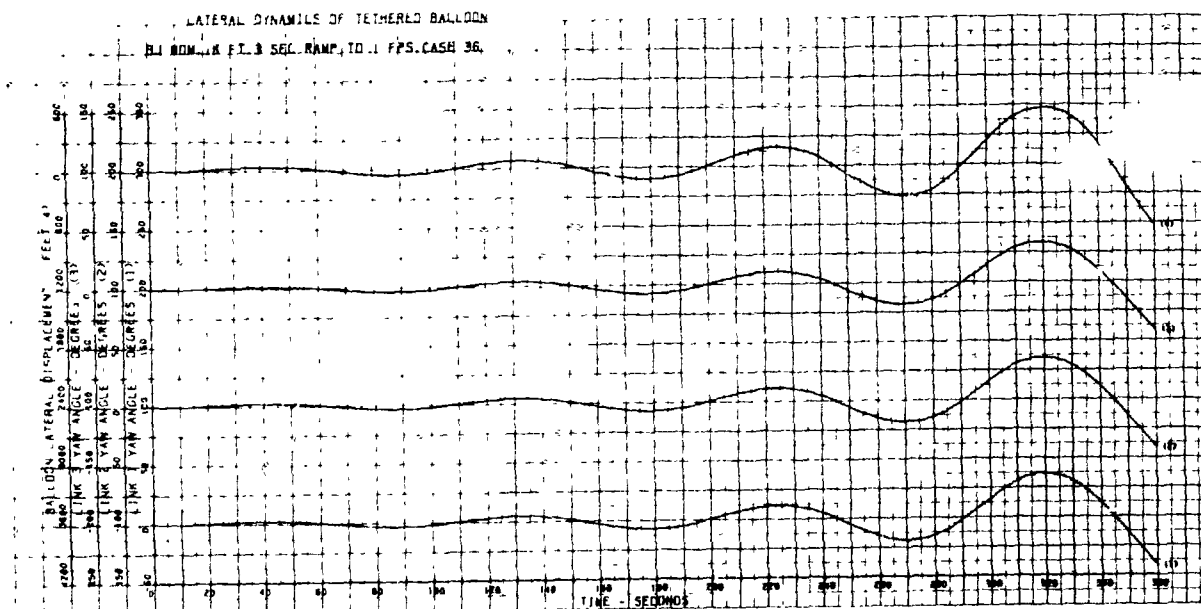
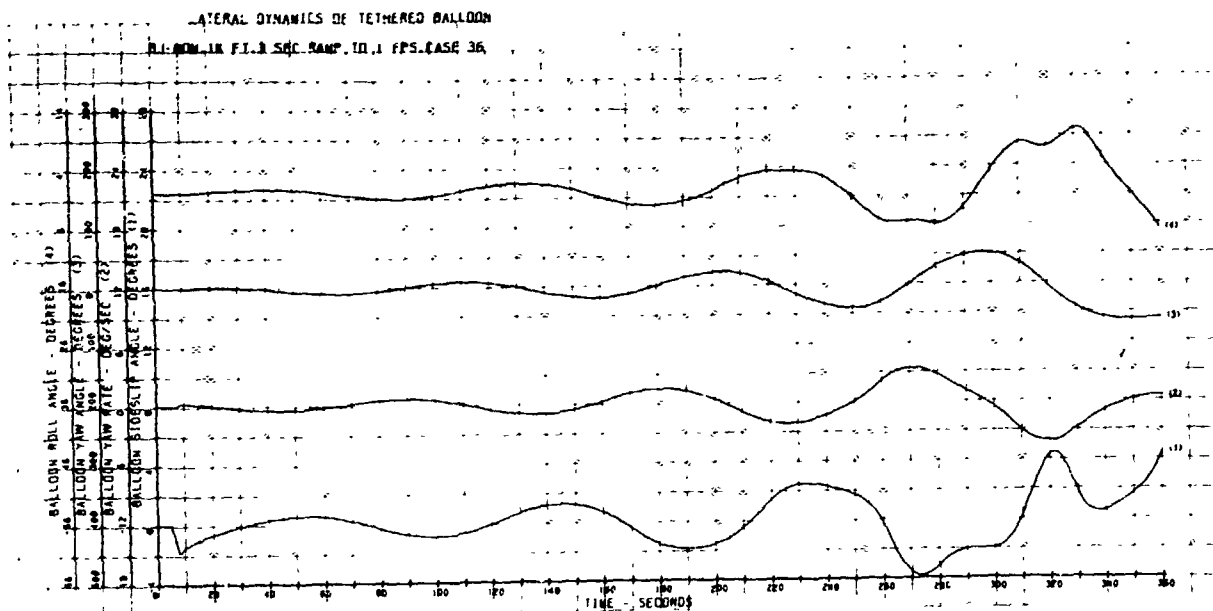


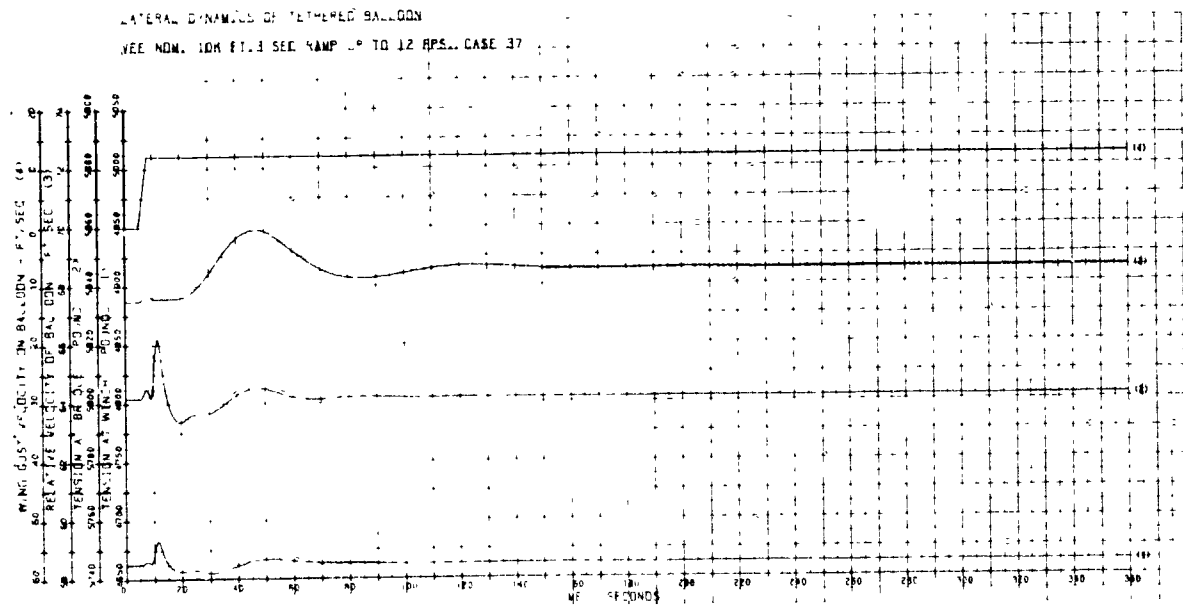
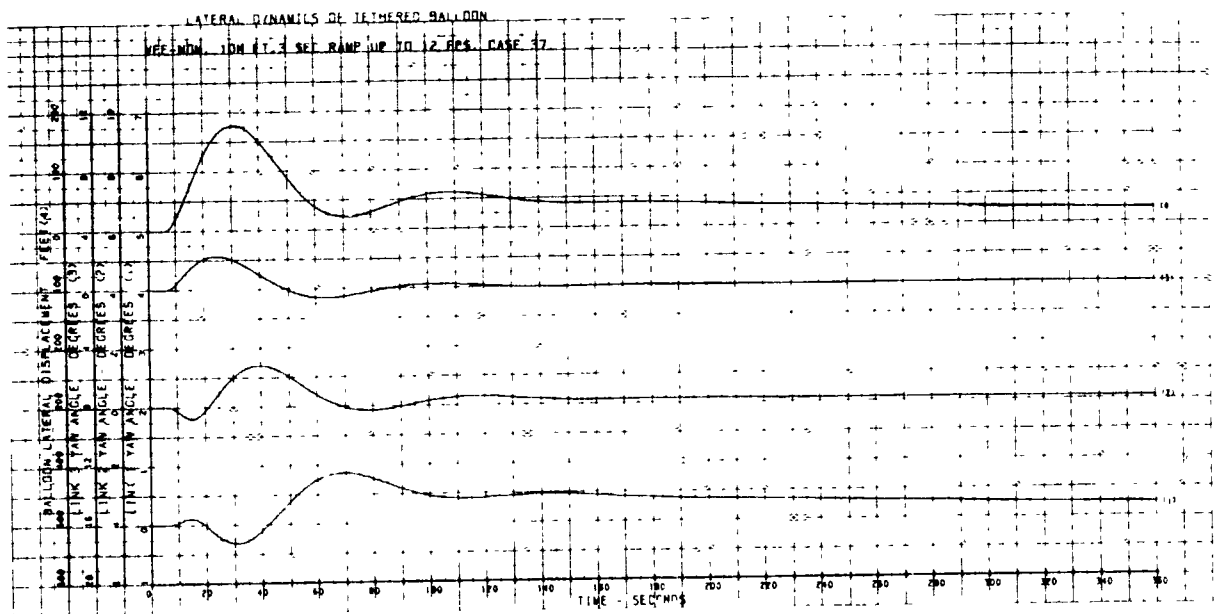
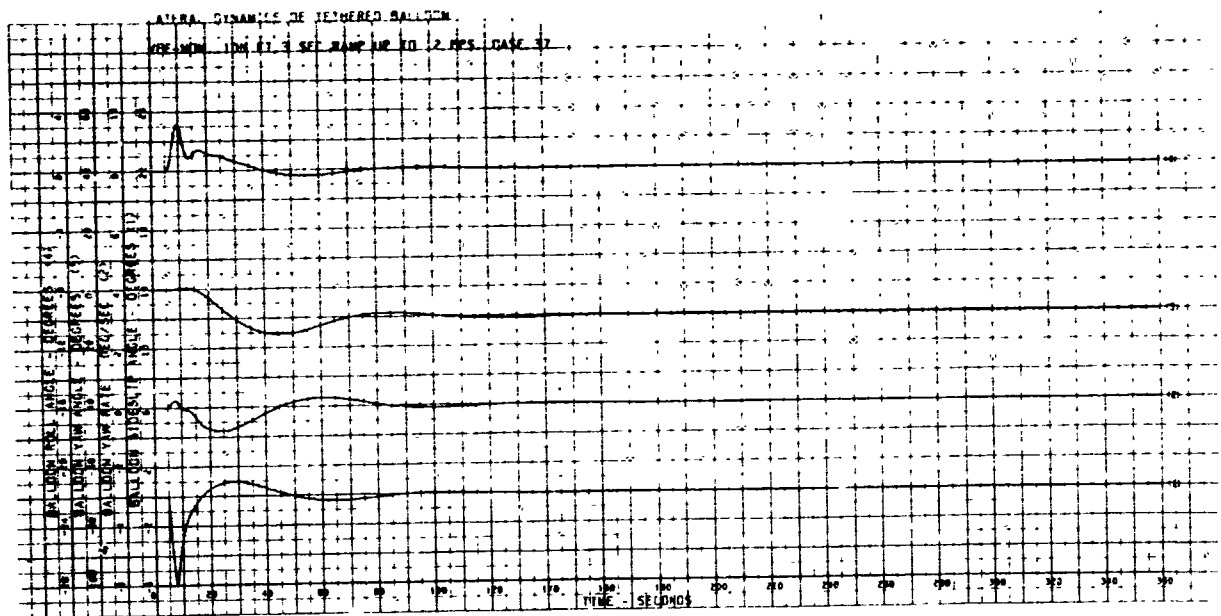
# LATERAL DYNAMICS OF TETHERED BALLOON

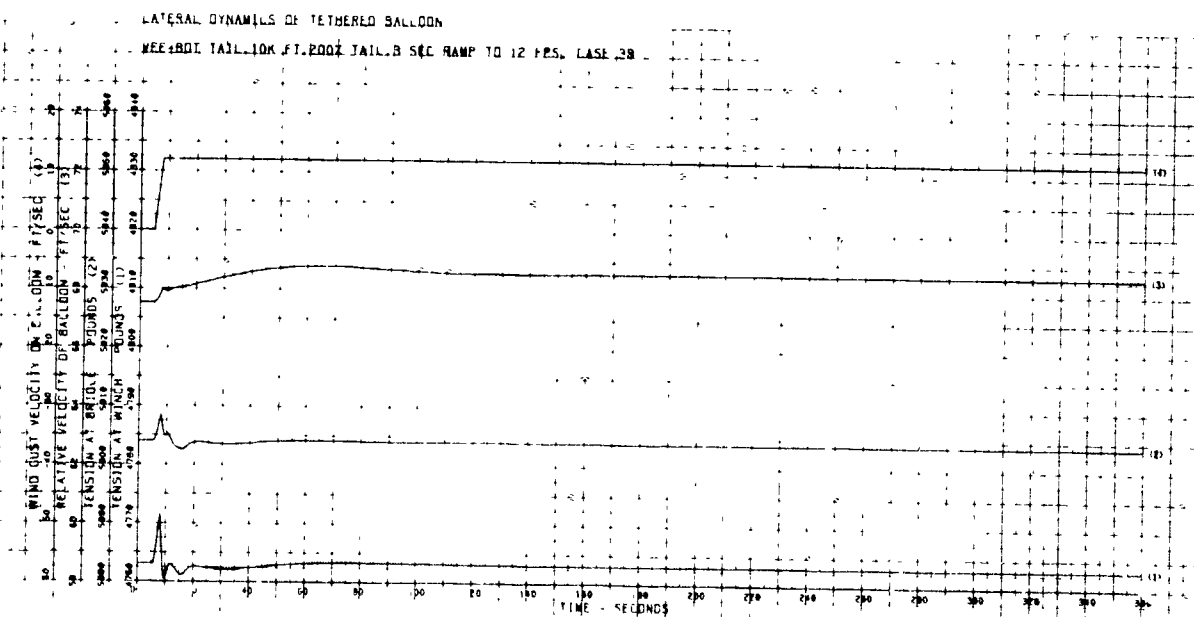
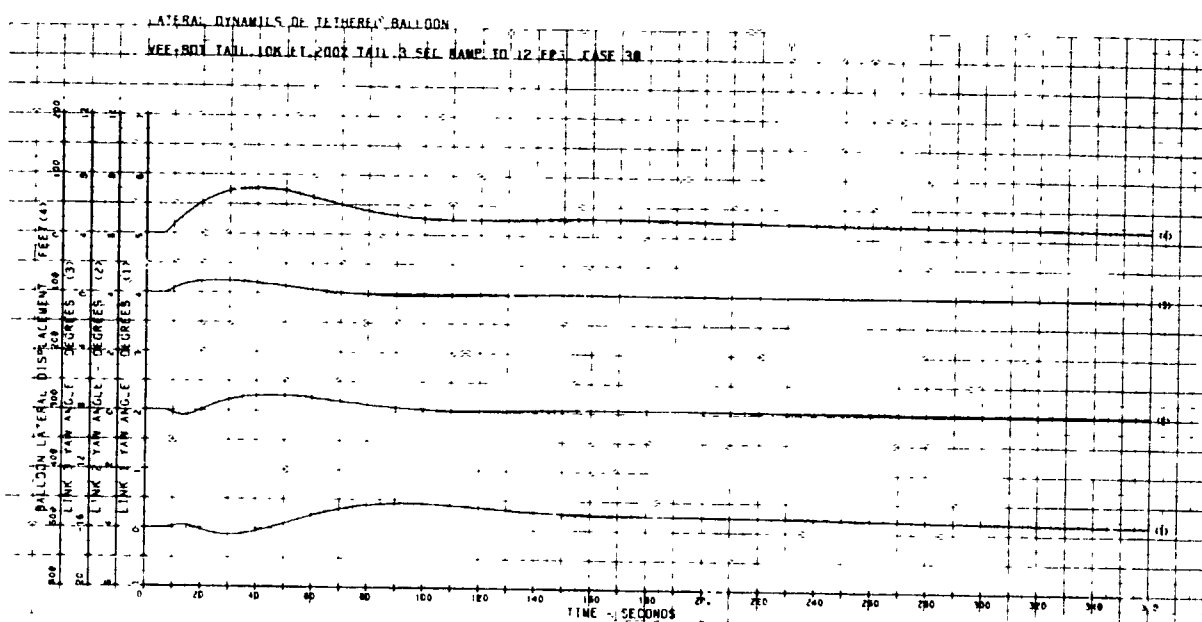
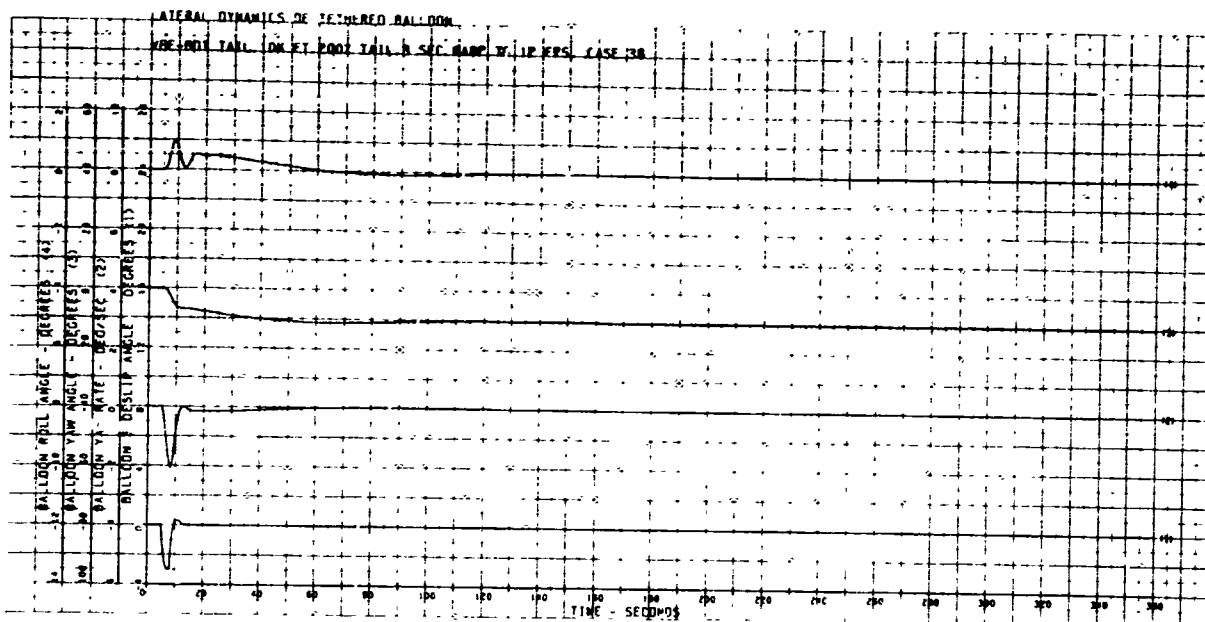
RI-NOM-10M, FT. 404 WIND 3 SEC RAMP TO 4.8 FPS, CASE 34.

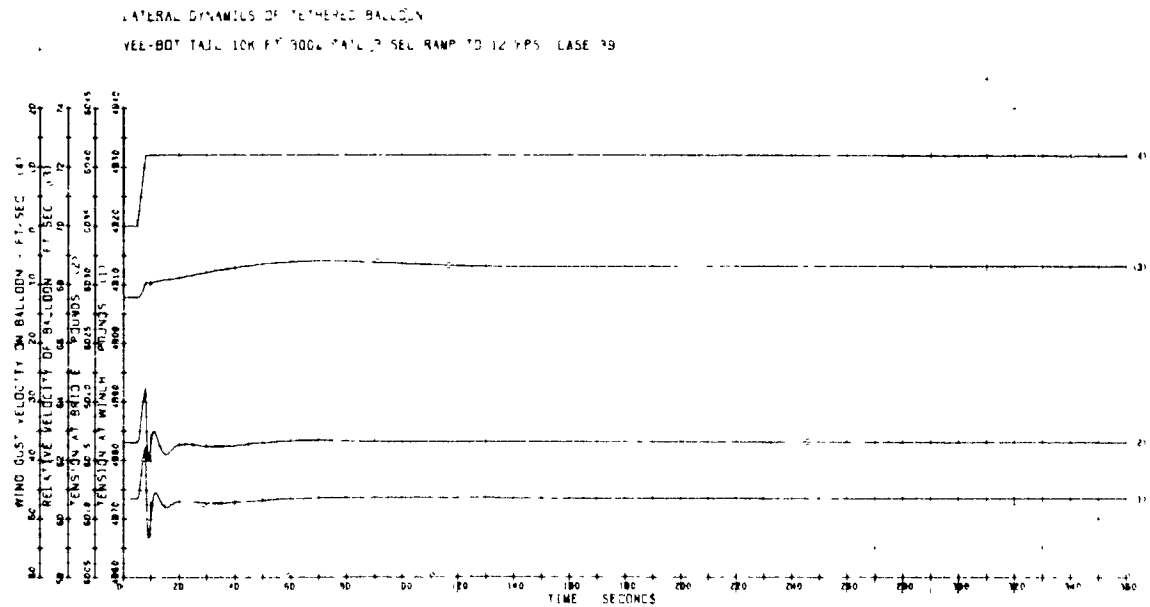
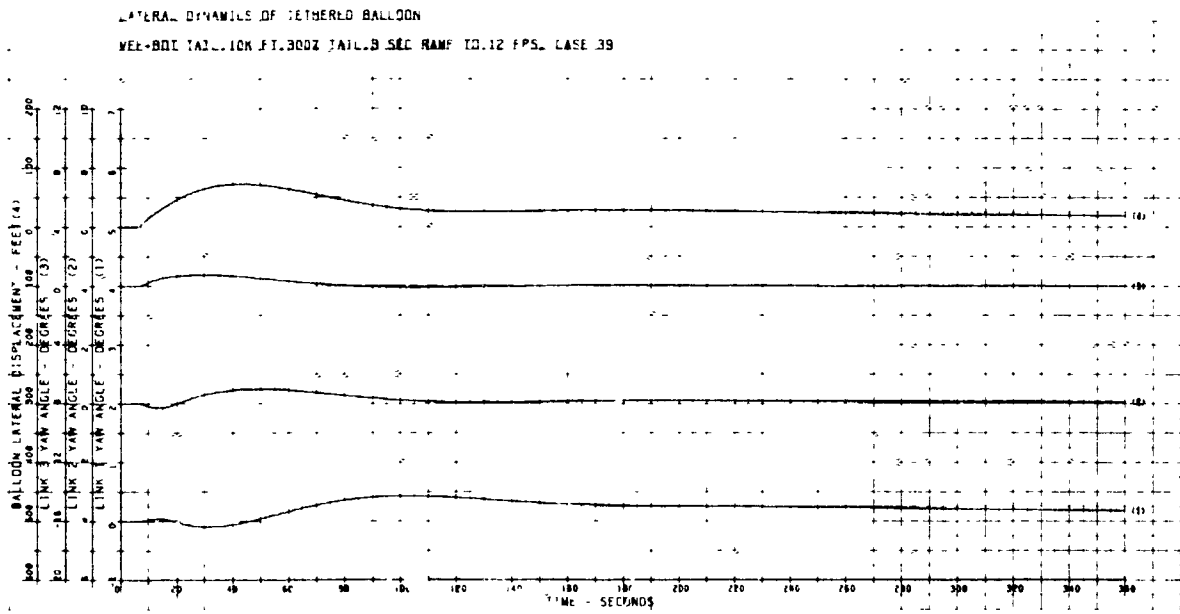
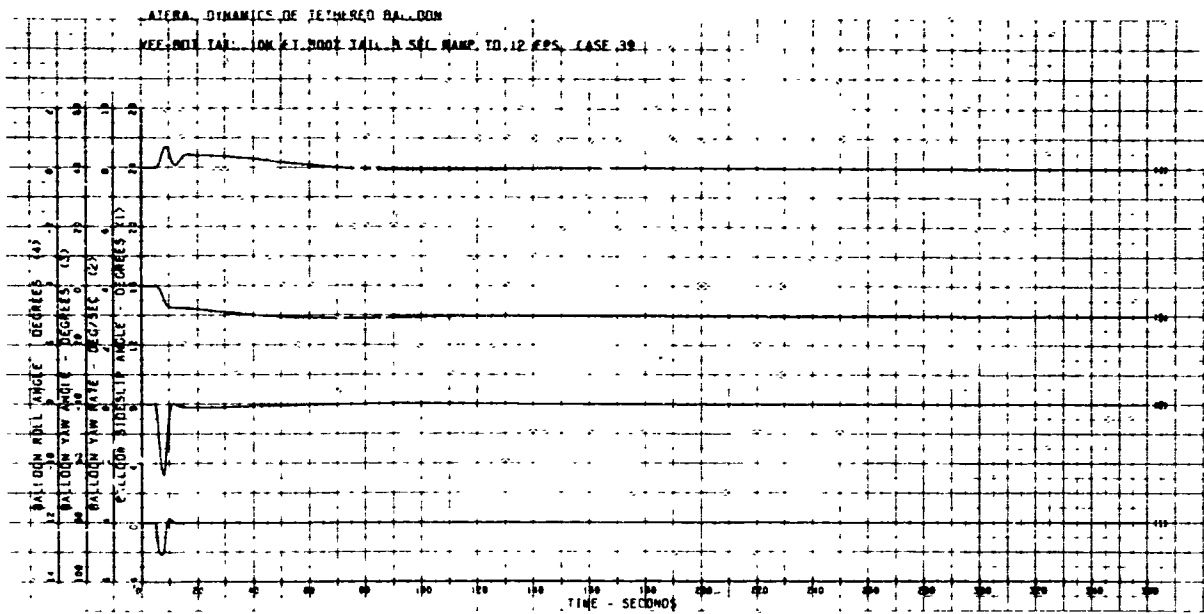


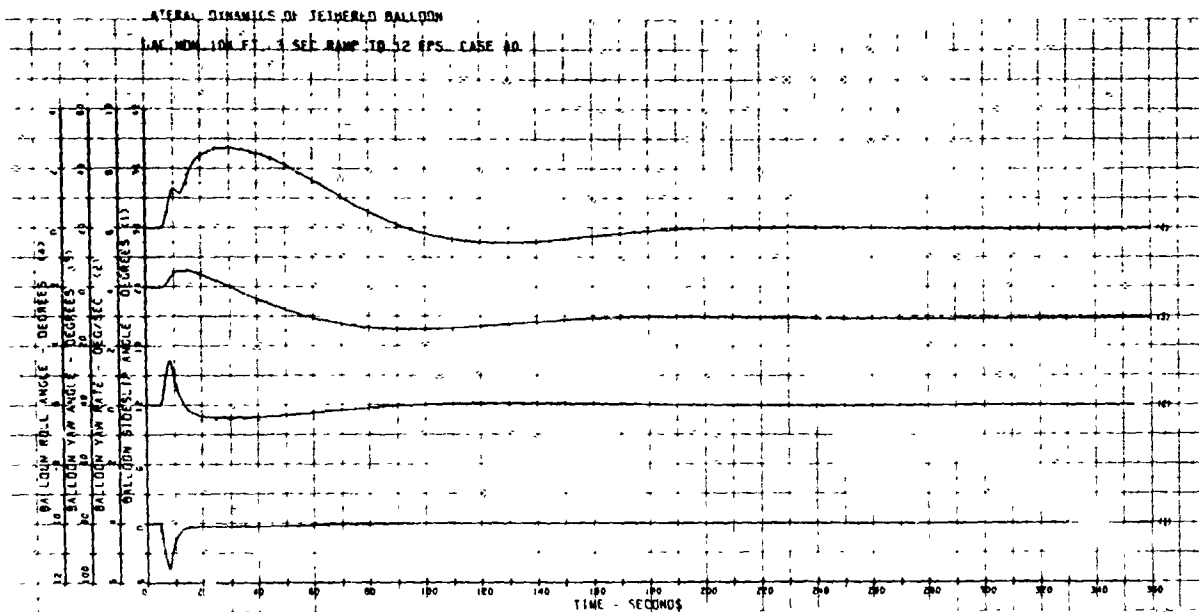




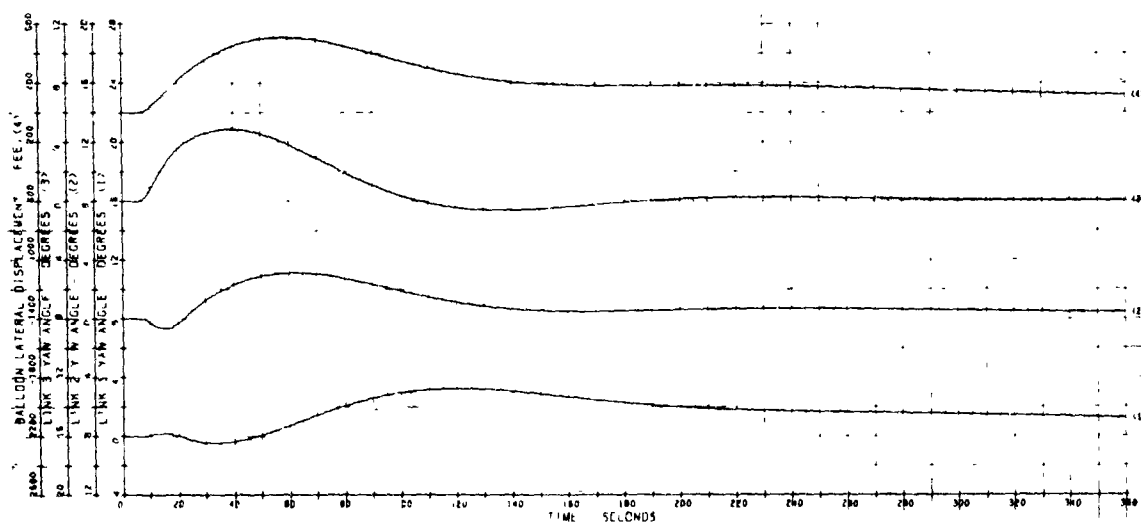








LATERAL DYNAMICS OF JETTERED BALLOON  
LAC NOM. 10K FT. 3 SEC RAMP TO 12 FPS. CASE 40



LATERAL DYNAMICS OF JETTERED BALLOON  
LAC NOM. 10K FT. 3 SEC RAMP TO 12 FPS. CASE 40

